Identification and characterization of TAT-5 interactors that regulate extracellular vesicle budding

♦♦♦♦♦

Identifizierung und Charakterisierung von TAT-5 Interaktoren, welche die Ausschüttung von Extrazellulären Vesikeln regulieren

Doctoral thesis for a doctoral degree
at the Graduate School of Life Sciences,
Julius-Maximilians-Universität Würzburg,
Section Biomedicine

submitted by

Katharina Beate Beer

From Greiz

Würzburg 2019

CC BY

Submitted on: …………………………………………………….…………………..

Office stamp

Members of the *Promotionskomitee*:

Chairperson:

Primary Supervisor: Dr. Ann Wehman

Supervisor (Second): Prof. Dr. Antje Gohla

Supervisor (Third): Dr. Eric Lambie

Date of Public Defense: ………………………………………………..…………

Date of Receipt of Certificates: ……………………………………………….

Abstract

Cells from bacteria to man release extracellular vesicles (EV) such as microvesicles (MV) that carry signaling molecules like morphogens and miRNAs to control intercellular communication during health and disease. MV release also sculpts membranes, e.g. repairing damaged membranes to avoid cell death. HIV viruses also bud from the plasma membrane in a similar fashion. In order to determine the *in vivo* functions of MVs and regulate their release, we need to understand the mechanisms of MV release by plasma membrane budding (ectocytosis).

The conserved phospholipid flippase TAT-5 maintains the asymmetric localization of phosphatidylethanolamine (PE) in the plasma membrane and was the only known inhibitor of ESCRT-mediated ectocytosis in *C. elegans*. Loss of TAT-5 lipid flipping activity increased the externalization of PE and accumulation of MVs. However, it was unclear how cells control TAT-5 activity to release the right amount of MVs at the right time, since no upstream regulators of TAT-5 were known.

To identify conserved TAT-5 regulators we looked for new proteins that inhibit MV release. To do so, we first developed a degradation-based technique to specifically label MVs. We tagged a plasma membrane reporter with the endogenous ZF1 degradation tag (degron) and expressed it in *C. elegans* embryos. This reporter is protected from degradation inside MVs, but is degraded inside the cell. Thus, the fluorescence is selectively maintained inside MVs, creating the first MV-specific reporter. We identified four MV release inhibitors associated with retrograde recycling, including the class III PI3Kinase VPS-34, Beclin1 homolog BEC-1, DnaJ protein RME-8, and the uncharacterized Dopey homolog PAD-1. We found that VPS-34, BEC-1, RME-8, and redundant sorting nexins are required for the plasma membrane localization of TAT-5, which is important to maintain PE asymmetry and inhibit MV release. Although we confirmed that PAD-1 and the GEF-like protein MON-2 are required for endosomal recycling, they only traffic TAT-5 in the absence of sorting nexin-mediated recycling. Instead, PAD-1 is specifically required for the lipid flipping activity of TAT-5 that inhibits MV release.

Thus, our work pinpoints TAT-5 and PE as key regulators of plasma membrane budding, further supporting the model that PE externalization drives ectocytosis. In addition, we uncovered redundant intracellular trafficking pathways, which affect organelle size and revealed new regulators of TAT-5 flippase activity. These newly identified ectocytosis inhibitors provide a toolkit to test the *in vivo* roles of MVs. In the long term, our work will

help to identify the mechanisms that govern MV budding, furthering our understanding of the mechanisms that regulate disease-mediated EV release, membrane sculpting and viral budding.

Zusammenfassung

Zellen von Bakterien bis zum Menschen produzieren Extrazelluläre Vesikel (EV) wie zum Beispiel Mikrovesikel (MV). MV können Signal Moleküle wie Morphogene und miRNA transportieren, welche die normale oder krankheitsbedingte interzelluläre Kommunikation kontrollieren. Bei der Produktion von MVs werden Membranen verformt, wie auch für die Reparatur von beschädigten Membranen um den Zelltod zu verhindern. Außerdem knospen HIV-Virus Partikel von der Plasma Membrane durch eine ähnliche Art und Weise. Um zu verstehen welche *in vivo* Funktion MV haben, müssen wir die Mechanismen der MV Knospung von der Plasma Membran (Ektozytose) verstehen.

Die konservierte Phospholipid Flippase TAT-5 hält die asymmetrische Verteilung von Phosphatidylethanolamine (PE) in der Plasma Membrane aufrecht und war der einzig bekannte Inhibitor der von ESCRT Proteinen durchgeführten Ektozytose in *C. elegans*. Wenn die Lipid-flippende Funktion von TAT-5 verloren geht, wird PE externalisiert und MV sammeln sich außerhalb der Zelle an. Allerdings ist es unklar mit welchen Mechanismen die Aktivität von TAT-5 reguliert wird um die richtige Menge an MV zur richtigen Zeit zu produzieren, da die vorgeschalteten Regulatoren unbekannt sind.

Um konservierte TAT-5 Regulatoren zu identifizieren suchten wir nach neuen Proteinen, die die Produktion von MV inhibieren. Dazu entwickelten wir eine Degradations-Technik um MV spezifisch zu kennzeichnen. Wir markierten einen fluoreszierenden Plasma Membran Marker mit dem endogenen ZF1 Degradations-Kennzeichen (Degron) und exprimierten es im *C. elegans* Embryo. Der Marker wird vor der Degradation geschützt, wenn er in einem MV von der Zelle ausgesondert wurde. Dadurch bleibt die Fluoreszenz speziell in MV erhalten, während sie innerhalb der Zelle abgebaut wird. Dadurch wurde die Sichtbarkeit von ausgeschütteten MV erhöht. Wir fanden vier Proteine, welche mit Protein Recycling in Verbindung gebracht werden, die die Ausschüttung von MV verhindern: Class III PI3Kiase VPS-34, Beclin1 Homolog BEC-1, DnaJ Protein RME-8 und das nicht näher charakterisierte Dopey Homolog PAD-1. Wir benutzten dieses Set an Proteinen, um zu testen ob und wie diese TAT-5 regulieren können. Wir fanden, dass Class III PI3Kinase, RME-8 und redundante Sorting Nexins für die Plasma Membran Lokalisierung von TAT-5 verantwortlich sind, was wichtig ist um die PE Asymmetrie aufrecht zu erhalten und die MV Produktion zu verhindern. Wenn auch PAD-1 und das GEF-ähnliche MON-2 für endosomales Recycling verantwortlich sind, regulieren sie die Lokalisation von TAT-5 nur in Abwesenheit von Sorting Nexins-

reguliertem Transport. Zudem scheint PAD-1 direkt für die Lipid Translokations-Aktivität von TAT-5 verantwortlich zu sein.

Demnach konnten wir zeigen, dass TAT-5 und PE Schlüsselregulatoren für MV Produktion sind, was weiterhin die Ansicht unterstützt, dass PE Externalisierung für die Ektozytose verantwortlich ist. Außerdem fanden wir, dass redundante intrazelluläre Transportwege für die Größe von Organellen verantwortlich sind und deckten neue TAT-5 Aktivitäts-Regulatoren auf. Diese neu aufgedeckten Ektozytose Inhibitoren könnten Werkzeuge sein um die *in vivo* Funktionen von MV zu testen. Längerfristig kann unsere Forschung dazu beitragen die Mechanismen der MV Produktion zu identifizieren und die Regulation während der krankheitsbedingten EV Produktion, der Membrane Reparatur und der Virus Knospung besser zu verstehen.

Table of contents

Abstract 1
Zusammenfassung 3
Table of contents 5
1. Introduction 9
- 1.1. Extracellular vesicles 9
  - 1.1.1. Extracellular vesicle subtypes: Exosomes and Microvesicles 10
- 1.2. Mechanisms of extracellular vesicle release 11
  - 1.2.1. ESCRT controls intraluminal vesicle and microvesicle budding 12
  - 1.2.2. Rab GTPases control exosome and microvesicle release 14
  - 1.2.3. SNAREs, V-ATPase and RAL-1 are only implicated in exosome formation 15
- 1.3. Membrane lipids and extracellular vesicle release 16
  - 1.3.1. Cholesterol, sphingolipids and phosphoinositides control extracellular vesicle formation 17
  - 1.3.2. Lipid asymmetry affects membrane curvature and extracellular vesicle release 19
  - 1.3.3. P4-ATPases regulate the asymmetry of specific lipids and extracellular vesicle release 20
    - 1.3.3.1. Loss of PS asymmetry does not alter extracellular vesicle release 23
    - 1.3.3.2. Loss of PE asymmetry induces microvesicle release 23
- 1.4. *C. elegans* as a genetic model organism for extracellular vesicle research 26
- 1.5. The lipid flippase TAT-5 as inhibitor of PE externalization and microvesicle release 27
- 1.6. The goal of this study 29
- 1.7. References 31

2. Materials and methods 39
- 2.1. Worm culture and strains 39
- 2.2. Worm genotyping 44
- 2.3. Plasmid construction 46
- 2.4. CRISPR/Cas9-mediated genome editing 49
- 2.5. Worm biolistic transformation 50
- 2.6. Protein knockdown by RNA interference 51
- 2.7. Immunohistochemistry of fixed worm tissues 51
- 2.8. Lipid externalization measurements 54
- 2.9. Vesicle size measurements 54
- 2.10. Colocalization measurements 54
- 2.11. Image adjustments 55
- 2.12. Statistics 55
- 2.13. TAT-5 localization and levels measurements 55
- 2.14. PAD-1 and TAT-5 antibody design 56
- 2.15. *C. elegans* protein extraction 57
- 2.16. Western Blots 57
- 2.17. Light microscopy 59
- 2.18. Electron microscopy 59

2.19. References 60

3. Degron-tagging reveals inhibitors of microvesicle release 62

3.1. Introduction: Visualizing microvesicle release using degron-mediated degradation 62

3.2. Results: Developing degron reporters to specifically label released microvesicles 66

3.2.1. Degron protection assay reveals topology of membrane-associated proteins 68

3.2.2 Identification of microvesicle release inhibitors and potential TAT-5 regulators 70

3.2.3. Only large increases in microvesicle release interrupt gastrulation 73

3.3. Discussion 74

3.3.1. Degron tagging of a PI4,5P2 reporter enables visualization of microvesicles *in vivo* 74

3.3.2. Degron tagging identifies microvesicle cargo 76

3.3.3. The class III PI3K VPS-34 and BEC-1 produce PI3P and inhibit microvesicle release 77

3.3.4. RME-8 regulates recycling from endosomes and inhibits microvesicle release 79

3.3.5. PAD-1 is likely to inhibit microvesicle release through TAT-5 81

3.3.6. Outlook 82

3.4. References 83

4. TAT-5 is trafficked by redundant sorting nexin pathways 88

4.1. Introduction: Endocytic trafficking recycles transmembrane proteins 88

4.1.1. Class III PI3K determines endosome identity 88

4.1.2. RME-8 is important for endocytosis, recycling and endosomal tubulation 90

4.1.3. Sorting nexins and Retromer are important for recycling and endosomal tubulation 90

4.2. Results: Endosomal recycling regulators control TAT-5 localization 93

4.2.1. TAT-5 antibodies to analyze endogenous TAT-5 localization 93

4.2.2. TAT-5 plasma membrane localization is altered in PI3K and RME-8 mutants 96

4.2.3. RME-8 prevents the missorting of TAT-5 into late endosomes 98

4.2.4. TAT-5 PE flipping activity depends on RME-8 100

4.2.5. PI3Kinase, RME-8, and sorting nexins control TAT-5 localization independent of the core retromer 101

4.2.6. SNX-3 regulates TAT-5 localization independent of binding to retromer 104

4.2.7. SNX-6 is not required for TAT-5 activity 105

4.2.8. SNX-1/-6 and SNX-3 redundantly inhibit extracellular vesicle release 106

4.2.9. SNX-1/-6 and SNX-3 redundantly regulate intracellular TAT-5 trafficking 108

4.2.10. Retromer proteins do not redundantly control TAT-5 plasma membrane localization or extracellular release 110

4.2.12. Testing SNX-binding motifs in TAT-5 116

4.2.12.1. Potential SNX-1/-6 binding sites 117

4.2.12.2. Potential SNX-3 binding sites 121

4.3. Discussion: Redundant trafficking pathways control TAT-5 localization and extracellular vesicle release 126

4.3.1. The class III PI3K is required for TAT-5 trafficking 128

4.3.2. RME-8 sorts TAT-5 away from the degradative pathway 129

4.3.3. SNX-1, SNX-6 and SNX-3 redundantly traffic TAT-5 to the plasma membrane 130

4.3.4. SNX-1/-6 and SNX-3 act independent of Retromer to traffic TAT-5 131
4.3.5. SNX-17 and SNX-27 inhibit microvesicle release when SNX-1/-6 or SNX-3 are absent 132
4.3.6. The search for SNX binding sites in TAT-5 133
4.3.7. TAT-5 localization and activity depend on the conserved ILYVFPF motif 134
4.4. References 136
5. PAD-1 and MON-2 control TAT-5 localization and activity 140
5.1. Introduction: TAT-5 orthologs form a complex with PAD-1 and MON-2 orthologs 140
5.1.1. The Dopey domain-containing protein PAD-1 140
5.1.2. The GEF-like protein MON-2 142
5.2. Results: PAD-1 and MON-2 have separable roles in regulating TAT-5 144
5.2.1. PAD-1 inhibits microvesicle release, but MON-2 and ARL-1 do not 144
5.2.2. Loss of PAD-1 causes sterility 145
5.2.3. Generating peptide antibodies to analyze endogenous PAD-1 localization 151
5.2.4. PAD-1 and MON-2 localize to domains of the plasma membrane 156
5.2.5. PAD-1 and MON-2 appear enriched in the midbody remnant 160
5.2.6. PAD-1 and MON-2 do not regulate TAT-5 localization 162
5.2.7. TAT-5, PAD-1 and MON-2 are trafficked into microvesicles 164
5.2.8. A subset of cortical proteins are released in microvesicles 165
5.2.9. MON-2 and PAD-1 regulate endosomal trafficking 169
5.2.10. MON-2, PAD-1, and TAT-5 regulate multivesicular endosome size 175
5.2.11. MON-2 and SNX prevent the missorting of TAT-5 into late endosomes 176
5.2.12. TAT-5 cannot maintain PE asymmetry on the plasma membrane when mislocalized to enlarged late endosomes 180
5.2.13. PAD-1 is specifically necessary to maintain PE asymmetry 181
5.2.14. PAD-1 inhibits microvesicle release through the same pathway as TAT-5 183
5.3. Discussion 184
5.3.1. The ubiquitous localization of PAD-1 suggests important functions in many cells 185
5.3.2. Potential conserved neural functions of PAD-1 and TAT-5 orthologs 186
5.3.3. TAT-5, PAD-1, and MON-2 are likely to form a complex in *C. elegans* 187
5.3.4. PAD-1 likely maintains PE asymmetry and microvesicle release through TAT-5 188
5.3.5. MON-2 could disrupt PE asymmetry to induce microvesicle release 190
5.3.6. Molecular interactions of PAD-1 191
5.3.7. Potential mechanisms of PAD-1 localization to membranes 193
5.3.8. PAD-1 and MON-2 as endosomal trafficking regulators 194
5.3.9. PAD-1, MON-2 and TAT-5 in regulating late endosome size 196
5.3.10. Potential cargoes of MON-2/PAD-1/TAT-5-dependent endosomal trafficking 198
5.3.11. PAD-1 as scaffold for MON-2 release in microvesicles 201
5.4. References 202
6. Concluding discussion 209
6.1. Summary of major findings 209

6.2. Multiple trafficking pathways regulate TAT-5 localization ... 209
6.3. TAT-5 PE flipping activity and endosomal trafficking ... 211
6.4. Identifying more regulators of TAT-5 activity and microvesicle release ... 213
6.5. Outlook ... 214
6.6. References ... 215
Abbreviations ... **217**
Acknowledgements ... **223**
Curriculum Vitae ... **224**
Affidavit ... **227**

1. Introduction

1.1. Extracellular vesicles

Extracellular vesicles (EVs) are released fragments of cells wrapped in a lipid bilayer membrane. They are released by all cell types examined so far from archaea, bacteria, protists, fungi, plants and animals[1–6]. EVs contain different cargo molecules like proteins, microRNAs, non-coding RNAs, and mRNAs, which can be internal cargo or exposed on the EV surface[7]. Consequently, there are a variety of EVs released by cells with numerous potential functions. EVs can transfer signals between cells and have important functions during intercellular or even interspecies communication[8–13]. For example, EVs released from *C. elegans* neurons induce male mating behaviors[12], while male flies release EVs that reduce female re-mating behavior in *Drosophila*[13]. This shows EVs can carry signals from one animal to the other *in vivo*. EVs can mediate intercellular communication to influence development, homeostasis and disease[7,14,15], including cancer and infections[16–19]. EVs were also found in the interface of plants and symbiotic fungi where photosynthates and minerals are exchanged[5,11,20], suggesting that EVs transfer molecules between different species. EV release can also be used to remove and repair membrane damage or to remove toxic aggregates to avoid cell death[21–24]. Because of these diverse functions in cell signaling and beyond, EVs are of broad interest.

In addition to their physiological roles, EVs are also appreciated in the clinic as new diagnostic and therapeutic tools. EVs represent a new source of clinical biomarkers that can provide information on the disease state of the patient[25–28]. EVs are present in easily extracted human biofluids, including blood, spinal fluid, or urine. These EVs can be enriched in disease-specific markers and may enable cancer detection or disease monitoring[26]. As EVs can transmit signals by presenting a signal molecule on the cell surface or after endocytic uptake by a target cell[7,10,14], EVs are also being developed as a new drug delivery system[29]. In contrast to the previously used vesicle delivery systems that contain artificial membranes (liposomes), the use of extracted EVs opens up the possibility to develop vesicles with a membrane content closer to the native membrane of the patient[30]. This may enhance the efficiency of providing drugs to a specific subset of cells or modulating the immune response. Given these diagnostic and therapeutic potentials of EVs, understanding how they are produced and how they interact with cells is of great clinical interest.

1.1.1. Extracellular vesicle subtypes: Exosomes and Microvesicles

EVs are broadly separated into two classes based on their organelle of origin[7,14]. The first class are exosomes, which are derived from endosomes. Inward budding of the limiting endosomal membrane results in the formation of internal intraluminal vesicles (ILV) (Fig. 1). An endosome with multiple ILVs is called a multivesicular body (MVB). Fusion of an MVB with the plasma membrane (i.e. exocytosis) releases ILVs, which are then called exosomes (Fig. 1). Both ILVs and exosomes typically range from 30-100 nm in diameter. As ILVs are found in different types of endosomes, lysosomes, and lysosome-related organelles, which can all fuse with the plasma membrane, there are multiple types of exosomes released by cells[7].

The second class of EVs, microvesicles (MVs), form by direct budding of the plasma membrane into the extracellular space (Fig. 1), a process called ectocytosis. For this reason, MVs are also known as ectosomes, but have also been given a variety of names, including microparticles and blebbing vesicles[7]. MVs were originally described as blebs released from activated platelets that promote coagulation[31]. Migrasomes are a class of MVs released during cell migration that are large enough to transport internal vesicles[32]. Similarly, apoptotic bodies released from dying cells are also large MVs (up to 5 µm) that are released due to altered membrane tension[33]. In contrast, Arrestin-domain-containing protein 1 (ARRDC1)-mediated MVs (ARMMs) are the size of exosomes (~50 nm in diameter), but still bud directly from the plasma membrane[34,35]. Thus, although MVs tend to be bigger than exosomes, MVs vary in size (30 nm-5 µm) and are a particularly diverse group of plasma-membrane derived EVs with many specialized MV subtypes[7,14,35].

Differential centrifugation protocols and size measurements are the popular way to separate exosomes from MVs[36]. However, it is difficult to distinguish exosomes from MVs once they are released from a cell due to their heterogeneity in size and content[7]. Furthermore, the markers used for their identification are heterogeneous among exosomes and MVs. For example, exosomes are typically detected *in vivo* by the tetraspanin proteins on their surface, but tetraspanins are also found on the plasma membrane and on MVs[31]. Thus, exosomes and MVs can be similar in size and content, and current methods cannot fully separate the two types once they are released from cells[10]. For this reason, it is not uncommon to see EVs referred to as exosomes when the authors are studying a mixed population of small EVs[7,37]. This is also the reason why it is not clear in most studies whether a certain effect is caused by exosomes or MVs. Thus, the development of specific markers for exosomes or MVs is important to clarify the functional differences between exosomes and MVs.

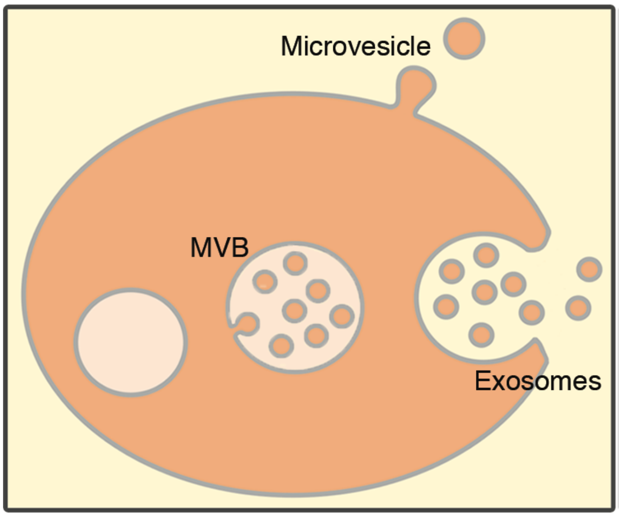

Fig. 1: The two types of extracellular vesicles. EVs released by direct budding of the plasma membrane are called microvesicles. EVs released by the fusion of a multivesicular body (MVB) with the plasma membrane are called exosomes. To form MVBs, endosomes must first bud vesicles into their lumen, called intraluminal vesicles (ILVs). Image modified from Beer and Wehman, Cell Adh Migr 2017 [15].

1.2. Mechanisms of extracellular vesicle release

To examine the functions of EVs *in vivo*, it is important to expeimentally control the formation of EVs. To finally tell apart the functions of exosomes versus MVs, it is important to alter the formation of just one of the two subtypes *in vivo*. Thus, it is important to understand which mechanisms are used to release exosomes and MVs. Many reviews have focused on the biogenesis pathways that govern the various steps of exosome formation[7,33,38], building on decades of studies on the mechanisms of MVB formation or regulated exocytosis[39–42]. In contrast, the mechanisms of MV release are much less understood, with insights coming from studies on viruses, which can also bud from the plasma membrane[43].

The release of exosomes and MVs is regulated by common and distinct molecules. The initial vesicle formation process occurs with the same topology (budding away from the cytoplasm) for both ILVs and MVs (Fig. 2A), suggesting that similar mechanisms are required for the formation of both exosomes and MVs. To initially form a vesicle, membrane-sculpting proteins like the ESCRT complex are required to induce membrane curvature either at the endosomal membrane for ILV budding or to curve the plasma membrane for MV budding (Fig. 2B-C). After the formation of a curved membrane, ESCRT proteins are also needed for scission to release ILVs into the endosome lumen or to release MV outside the cell. Protein regulators that are more likely to be specific for exosome release include proteins required to traffic MVBs to the plasma membrane, to tether MVBs to the plasma membrane, and to fuse MVBs with the plasma membrane (**Fig. 2**D). The following sections contain a summary of proteins known to be involved in EV formation.

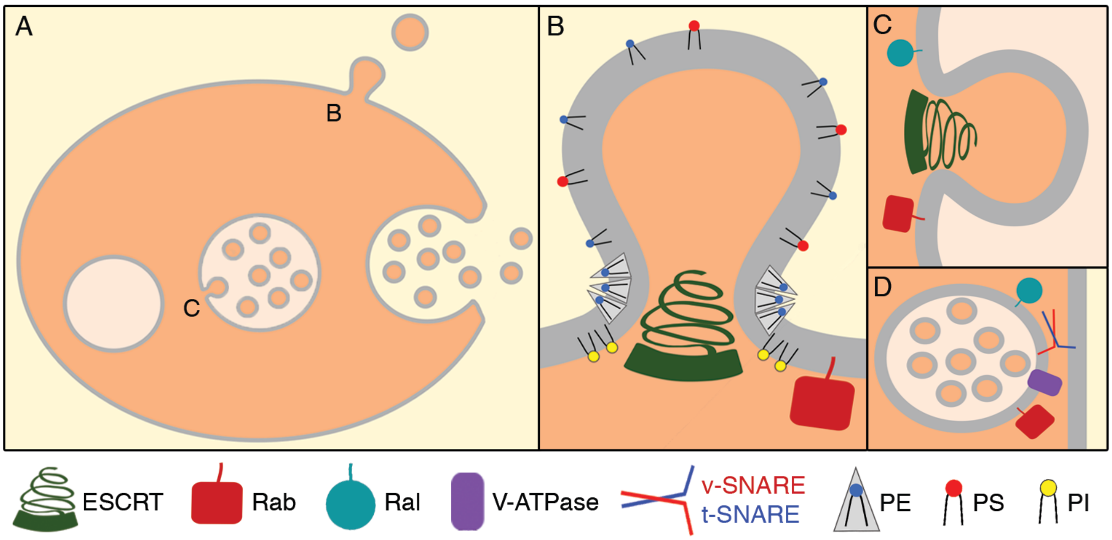

Fig. 2: Mechanisms of MV release. A) Both types of EVs use the same budding topology, e.g. budding away from the cytoplasm on the plasma membrane for MVs (B), or on endosomes to form ILVs for exosomes (C). B) Plasma membrane budding away from the cytoplasm to form MVs requires the ESCRT complex and Rab GTPases. Lipids also play an important role in microvesicle budding, with phosphatidylinositols in the cytosolic leaflet recruiting membrane-sculpting proteins and cone-shaped phosphatidylethanolamine in the extracellular leaflet inducing membrane curvature. C) The budding of ILVs into MVBs also requires Rab and Ral family GTPases, as well as the ESCRT complex. C) MVBs fuse with the plasma membrane to release exosomes with the help of Rab and Ral GTPases, SNARE proteins and the V-ATPase. Image from Beer and Wehman, Cell Adh Migr 2017[15].

1.2.1. ESCRT controls intraluminal vesicle and microvesicle budding

The Endosomal Sorting Complex Required for Transport (ESCRT) is one of the few membrane-sculpting complexes that bends membranes away from the cytoplasm[44], the topology needed for EV release. ESCRT-0 engages and clusters ubiquitinated cargo and recruits ESCRT-I and ESCRT-II to the bud site. ESCRT-I and ESCRT-II curve membranes and recruit ESCRT-III. Finally, the ESCRT-III complex forms a coil that is thought to pull the bud neck together, leading to scission and release of the vesicle (Fig. 2B-C). The disassembly factor VPS4 is an ATPase that is also responsible for the collapse of ESCRT-III coils to promote scission and to disassociate the ESCRT subcomplexes from the membrane[45,46]. Some ESCRT proteins are also found in released EVs[14], suggesting that ESCRTs are trapped in EVs after scission and implicating ESCRT in EV release.

ESCRT was first discovered for its role in forming ILVs, the precursors to exosomes (Fig. 2C). Consistently, a *C. elegans* screen identified 10 ESCRT proteins important for exosome biogenesis[47], based on defects in alae formation, a process which requires exosome secretion from seam cells[48]. These include an ESCRT-0 subunit (HGRS-1), ESCRT-I subunits (VPS-32, VPS-25, VPS-36), ESCRT-II subunits (VPS-22, VPS-25, VPS-36), ESCRT-III subunits (VPS-20, VPS-32), and the ATPase VPS-4[47]. These findings support the role of all ESCRT subcomplexes in exosome biogenesis. ESCRT components also have important functions in exosome biogenesis in flies and mammalian cells[7,49,50], consistent with a conserved role of ESCRT in exosome biogenesis.

In addition to ILV budding, the ESCRT machinery also has a conserved role at the plasma membrane to orchestrate MV budding (Fig. 2B). All ESCRT subcomplexes are required for the release of MVs from *Drosophila*, while VPS4 and the ESCRT-I subunit TSG101 have been shown to be required for MV budding from cultured mammalian cells[35,44,51]. In *C. elegans* embryos, ESCRT proteins are recruited to the plasma membrane and mediate the release of MVs[52]. This study showed that ESCRT-I (TSG-101) and ESCRT-III (VPS-32) were increased at the plasma membrane when MV budding was increased. Depleting proteins from the ESCRT-0 (HGRS-1, STAM-1) or ESCRT-I (TSG-101, VPS-28) subcomplexes significantly suppressed MV release, demonstrating that ESCRT proteins are required for plasma membrane budding in *C. elegans* embryos. Thus, the ESCRT pathway has conserved functions in plasma membrane budding to release MVs.

Viruses can hijack the ESCRT complex to produce virions by budding from the endosome membrane like an ILV or from the plasma membrane like MVs(reviewed in[43,53]). Gag proteins from different viruses directly recruit the ESCRT-I subunit TSG101 and ESCRT accessory factor Alix to the site of virus formation. ESCRT-III and VPS4 are also recruited to the virus bud site prior to virus release. Thus, viruses can hijack mechanisms used for exosome and MV formation, which suggests that identifying the mechanisms of EV release will also provide insights into the mechanisms of virus particle formation.

Although the ESCRT machinery plays a significant role in EV release, there is also evidence that both exosomes and MVs can be formed by ESCRT-independent mechanisms. In *C. elegans* embryos or *Drosophila* gland cells, depletion of ESCRT proteins did not completely suppress MV or exosome release [13,52]. Thus, additional mechanisms must exist to bud ILVs and MVs independent of ESCRT proteins. Because of these redundancies, depletion of ESCRT subunits is unlikely to completely block EV formation. Furthermore, ESCRT depletion is likely to disrupt exosome and MV release, making it impossible to differentiate the *in vivo* roles of MV from exosomes. Thus, it is important to identify new upstream regulators that specifically control the formation of MVs.

1.2.2. Rab GTPases control exosome and microvesicle release

Several Rab family GTPases have been implicated in EV release, including Rab2, Rab7, Rab11, Rab27, or Rab35. The Rab family of small GTPases are universal vesicle trafficking regulators acting at multiple steps of membrane trafficking like vesicle formation, motility and fusion[54]. Rabs are attached to membranes of distinct organelles[55], where they interact with different proteins. Rabs are activated by guanine nucleotide exchange factors (GEFs) that switch GDP for GTP, forming distinct domains of activated Rabs that can then recruit other effectors[54,56]. Thus, Rab proteins are often known to be required for the maturation of endosomes or phagosomes[56,57]. For example Rab5 localizes to early endosomes and recruits the Phophatidylinositol-3-kinases, which in turn produces PI3P on endosomal membranes that is required for early endosome fusion and the recruitment of many more effectors[54,58]. Due to their diverse functions, Rabs are likely to affect many steps of EV formation.

Rab2 acts on the Golgi and endosomal membranes and is required for endosomal trafficking pathways[59–61]. Rab2 activity promotes the fusion of lysosomes with late endosomes and is therefore required for endosomal maturation and degradation[62,63]. Thus, Rab2 is normally required for the degradation of MVBs. Knocking down Rab2 has been shown to increase EV release in cultured mammalian cells[64]. It is proposed that disruption of lysosomal degradation of MVBs can boost MVB fusion with the plasma membrane and therefore increase exosome release[7]. However, close studies describing how Rab2 inhibits EV formation are still lacking.

Rab7 is an endosome maturation factor required for exosome release. Rab7 is involved in trafficking between early endosomes and lysosomes and is associated with late endosomes and MVBs[65]. In *Drosophila*, knocking down Rab7 or expressing a dominant-negative version of Rab7 in secretory gland cells disrupts exosome release[13]. Rab7 is also required for the secretion of microRNAs in EVs from cultured mammalian cells[66]. Thus, Rab7 plays a conserved role in exosome biogenesis in *C. elegans*, *Drosophila*, and mammals.

The small GTPase Rab11 plays an important role in both exosome and MV biogenesis[14]. Rab11 is best known for its role in trafficking membrane cargo between recycling endosomes and the plasma membrane[67,68], but Rab11 was also shown to be required for an unknown step in MVB fusion with the plasma membrane in cultured human cells [69,70]. Similarly, expressing a dominant-negative version of Rab11 disrupts exosome release from *Drosophila* gland cells[13]. Rab11 thereby regulates exosome release by promoting MVB tethering, MVB docking, or MVB fusion with the plasma membrane. Rab11 has also been implicated in plasma membrane budding. Depletion of RAB-11 in *C. elegans* embryos dramatically reduced MV release[52]. RAB-11 was also released inside MVs[52], suggesting that RAB-11 localizes to budding sites and is required for MV biogenesis. Viruses can also bud from the plasma membrane using a Rab11-binding protein[71]. Intriguingly, this occurs independent of ESCRT proteins, suggesting that Rab11 defines an ESCRT-independent budding pathway. Thus, RAB-11 is a conserved regulator of exosome, MV and viral release, although its precise role is unclear.

Rab27 is involved in exosome release through its role in MVB fusion. Rab27 localizes to late endosomes and lysosome-related organelles, including MVBs[54], and regulates the fusion of lysosome-related organelles with the plasma membrane[72]. MVB fusion and exosome release are decreased after Rab27A/B knockdown in mammalian cells and its ortholog AEX-6 in *C. elegans*[47,64]. This suggests that Rab27 has important roles in the formation of exosomes. However, Rab27 may also have a role in plasma membrane budding. Rab27 has recently been shown to regulate the trafficking of lipid regulators like PI4KIIa to the plasma membrane via endosome fusion[73], and is thereby required for viruses to assemble on the plasma membrane at phosphoinositide-rich microdomains. These data could indicate a role for Rab27 in MV budding, but to date Rab27 is only thought to regulate exosome release.

Rab35 is an endosomal recycling factor required for exosome release. Rab35 is involved in a parallel recycling pathway to Rab11 and helps traffic endosomes to the plasma membrane[74]. In *Drosophila*, Rab35 RNAi disrupted exosome release from male gland cells[13]. Similarly, expressing dominant-negative Rab35 or knocking down Rab35 levels results in decreased exosome release in cultured mammalian cells, due to failed fusion of MVBs with the plasma membrane[75]. Thus, Rab35 is likely to regulate exosome biogenesis by its role in MVB trafficking, tethering, or docking.

Taken together, different Rab proteins can control the release of exosomes and MVs at multiple steps. The precise mechanisms of how Rab proteins regulate the formation of EVs and which Rab effectors are involved in EV formation needs to be determined.

1.2.3. SNAREs, V-ATPase and RAL-1 are only implicated in exosome formation

Another class of proteins that may be preferentially required for exosome release are SNAP receptors (SNAREs). SNARE proteins mediate the tethering and fusion of vesicles[76]. They are found on endosomes and the plasma membrane and have been implicated in the release of exosomes (Fig. 2D). For example, the vesicular SNARE (v-SNARE) vesicle-associated membrane protein 7 (VAMP7) is required for MVB fusion to the plasma membrane and the release of exosomes [47,77]. The target SNARE (t-SNARE) Syntaxin5 is better known for mediating vesicle fusion in ER-Golgi trafficking[78], but in *C. elegans* syntaxin 5 (SYX-5) is also required for the fusion of MVBs with the plasma membrane to release exosomes[47]. V-SNAREs and t-SNAREs are also required for the release of exosomes in *Drosophila,* including the synaptobrevin homologue Ykt6 and the syntaxin Syx1a[49,79]. This shows that SNAREs regulate exosome release in many systems.

Furthermore, the vacuolar ATPase (V-ATPase) was shown to be required for the release of exosomes, probably by regulating MVB tethering or fusion (Fig. 2D). The V-ATPase is an ATP-dependent proton pump conserved in all eukaryotes, consisting of the transmembrane V0-complex and cytoplasmic V1 complex[80]. The V0, and maybe the V1 complex were found to be required for fusion of MVBs with the plasma membrane and exosome release[48,49]. The V-ATPase also binds to Syx1a in *Drosophila*, which is required for the release of exosomes[79,81]. Thus, the V-ATPase may also interact with SNAREs to mediate exosome release.

Lastly, the small GTPase RAL-1 is a conserved regulator of vesicle tethering and fusion[82], which was identified to be required for MVB fusion to the plasma membrane and therefore exosome release[47]. Loss of RAL-1 also resulted in fewer MVBs and fewer ILVs per MVB, in addition to reduced MVB fusion and thereby less secretion of exosomes. However, MVB tethering to the plasma membrane was not disrupted. Thus, RAL-1 is likely to act in multiple steps of exosome biogenesis.

The aforementioned proteins regulate MVB trafficking and plasma membrane fusion and are therefore known to regulate exosome release. However, membrane proteins also require vesicular trafficking from endosomes to reach the plasma membrane[83], so trafficking factors would also be expected to have a role in MV formation. Taken together, although many exosome release mechanisms are known, we still lack a mechanism that specifically controls MV release, which would allow us to study the *in vivo* roles of MVs.

1.3. Membrane lipids and extracellular vesicle release

Since EV formation involves the bending of membranes, it is not surprising that the lipid content and distribution in the membrane can also have important roles in regulating EV budding[7]. Membranes consist of a mixture of many different lipid species organized in a bilayer with the hydrophilic headgroup facing the cytosol and the hydrophobic acyl chains facing the center of the bilayer. Due to their different shapes and charges, different lipids can also form nanodomains that change the biophysical and biochemical properties of a membrane[84,85]. Such lipid domains are implicated in the formation of ILVs on endosomes as well as MV budding from the plasma membrane[31,86]. Different lipids also have different binding partners[87], and can therefore be involved in the recruitment of sculpting proteins to membrane budding sites[88]. Thus, lipid content and distribution are also likely to regulate EV release.

Eukaryotic membranes consist of three major lipid classes: glycerophospholipids, sphingolipids and sterols[84]. Glycerophospholipids are the major structural lipids in eukaryotic membranes. Glycerophospholipids are amphipathic, containing a hydrophilic headgroup that consists of a glycerol and phosphate as well as a tail that typically consists of two hydrophobic fatty acyl chains, which vary in length and saturation. Glycerophospholipids with only one acyl chain occur less frequently and are called lysophospholipids. The major glycerophospholipids in biological membranes are phosphatidylcholine (PC), phosphatidylethanolamine (PE), phosphatidylserine (PS), phosphatidic acid (PA) and phosphatidylinositol (PI). Sphingolipids are another class of structural membrane lipid with a ceramide as their hydrophobic backbone. The two major types of sphingolipids in addition to ceramide are sphingomyelins (SM) and glycosphingolipids. Sterols are relatively non-polar lipids, with cholesterol predominant in animals. While glycerophospholipid species are present in all organelles, cholesterols and sphingolipids are predominantly localized to the plasma membrane to resist mechanical stress[84]. Consequently, there is a variety of lipids that can impact the formation of EVs.

Alterations in lipid composition is a broadly discussed model for regulating membrane curvature[89,90]. One hypothesis about how lipids can cause membrane curvature directly, is by selectively increasing the amount of lipids in one monolayer which creates an overhang in one bilayer[90]. Additionally, lipids can come in different shapes which also have an impact on membrane curvature. Cylindrical lipids like PS and PC form a flat bilayer[85,89], while conical lipids like PE and PA have a small headgroup that can move closer together, which creates a negative curvature in a microdomain enriched in conical lipids. Inverted conical lipids like PI species have bigger headgroups that move more apart and promote a positive curvature. As a consequence, conical and inverted-conical lipids are the most effective to deform membranes[85]. In this section, we will discuss how different lipids are thought to control EV formation.

1.3.1. Cholesterol, sphingolipids and phosphoinositides control extracellular vesicle formation

Cholesterols are enriched in the plasma membrane and in the membranes of ILVs and EVs[84,91,92], suggesting that cholesterols could have important functions in both exosome and

MV formation. Pharmacological depletion of cholesterol in neutrophils decreases the formation of MVs[93], while loading human monocytes with cholesterol accelerates MV release[94]. This demonstrates that cholesterol has an important role in MV release, but whether cholesterol also functions in exosome release remains to be determined.

Ceramide is one of the main sphingolipids in the plasma membrane and intracellular membranes[95]. The enzyme neutral sphingomyelinase (nSMase) hydrolyzes cone-shaped sphingomyelin lipids to a conical ceramide, which is thought to induce membrane curvature for vesicle biogenesis[96]. Indeed, ceramide produced by nSMase is required for ILV budding independent of the ESCRT complex in mouse cell culture[97]. Inhibitors of ceramide biosynthesis are therefore commonly used to inhibit exosome biogenesis in numerous systems[95]. Thus, the turnover of sphingomyelin to ceramide is a mechanism that induces membrane budding on endosomes.

Sphingolipids are also implicated in MV release. Formation of ceramide on the outer layer of the plasma membrane causes increased MV budding from glia cells[98]. Knockdown of the secreted acid SMase (aSMase) in fly wing discs also caused increased EV release and Hh signaling *in vivo*[79]. However, increased MV shedding from epithelial cells was also seen after pharmacological inhibition of nSMase that inhibited exosome release, suggesting that inhibition of nSMase can have opposite effects on exosome and MV release[99]. However, it is not clear whether this is a direct cause of nSMase depletion or compensation for decreased exosome release. Thus, sphingomyelinases and sphingolipids can regulate ILV budding from the cytosol or MV release when they are found in the endosomal lumen or on the outer surface of the plasma membrane, hinting that asymmetric changes to lipids are a key regulator of EV release.

PIs are a minor lipid species with major roles in intracellular signaling and vesicular trafficking[100,101]. PI can be phosphorylated on three different positions, leading to an array of different binding partners[87]. Specific kinases and phosphatases alter the phosphorylation of PI species and thereby help mature endosomes[102]. The localization of different PI species denotes the identity of organelles, helping to recruit the right proteins to the right organelle at the right time. For example, the FYVE domain of Hrs recognizes PI3P and recruits ESCRT-0 and ESCRT-I to endosomal membranes for ILV formation[103], which influences exosome biogenesis. The ESCRT proteins are also required for MV budding in *C. elegans*[52], which is also likely depend on their recruitment by PI species. Thus, PI species generally regulate EV release by recruitment of budding regulators like the ESCRT complex.

1.3.2. Lipid asymmetry affects membrane curvature and extracellular vesicle release

Lipids are asymmetrically distributed between the two membrane layers[104]. In eukaryotic cells, PC, SM and glycosphingolipids are mostly present in the exoplasmic leaflet of the plasma membrane. In contrast, PE, PS, PI (and its derivatives) and PA are mostly found on the cytoplasmic layer of the membrane bilayer. Cholesterol is the only lipid that is relatively symmetrically distributed[105]. By local concentration of cone-shaped phospholipids in one bilayer, negative membrane curvature can be induced[89]. Thus, the regulation of lipids in membrane bilayers can induce vesicle formation. Indeed, EVs are associated with a loss of lipid asymmetry. MVs have altered lipid asymmetry, where PS and PE are often externalized and found on the outer surface of the vesicle bilayer (Fig. 2B)[106,107]. This observation suggested that either budding disrupts lipid asymmetry or that lipid asymmetry plays a role in MV release. Some exosomes also externalize PS[108,109], suggesting that lipid asymmetry is also regulated on the MVB during ILV formation. Thus, the regulation of lipid asymmetry is likely to be important for EV biogenesis or function.

While cholesterol can translocate between bilayers rapidly[110], phospholipid translocation can take hours or even days to occur spontaneously[84]. Three classes of transporters are known to accelerate lipid translocation: scramblases, floppases, and flippases (reviewed in [111–114]). Examples of these transporters have also been linked to EV release.

Scramblases are bidirectional lipid transporters that destroy membrane asymmetry. They are activated by high Ca^{2+} concentrations and are energy-independent[115]. Several families of transmembrane proteins have been proposed to be a scramblase responsible for randomizing phospholipids, including GPCRs, SCRM, and XKR proteins, and anoctamins[116–118]. However, it is not yet clear how these proteins scramble lipids, also called lipid flip-flop[112]. The anoctamin TMEM16F is of particular interest, because it responds to calcium by initiating PS and PE exposure, inducing MV budding, and promoting platelet coagulation[119]. Humans with mutations in TMEM16F develop Scott syndrome, which causes defects in platelet coagulation, disrupts PS & PE externalization, and reduces MV release[120,121]. Thus, scramblases disrupt lipid asymmetry, which is associated with MV release. However, due to the large number of scramblases, it is not known whether the activity of a specific scramblase regulates EV release or whether the activity of many scramblases contributes to the disruption of lipid asymmetry. Alternatively, it is also discussed that all transmembrane proteins have the potential to cause lipid flip-flop[122–124], emphasizing the need to counteract non-specific movement to maintain the asymmetric distribution of lipids.

There are two classes of energy-dependent proteins involved in establishing and maintaining lipid asymmetry against the concentration gradient, flippases and floppases. These transporters first establish lipid asymmetry in the ER and Golgi, which are the major source of the different lipid species, but can also regulate lipid asymmetry directly in the plasma membrane[84]. It is proposed that flippases and floppases therefore balance the asymmetry disruption activity of scramblases both on the cellular and organellular level.

Floppases hydrolyze ATP to mediate the translocation of phospholipids from the cytoplasmic face of the membrane to the exoplasmic leaflet. Floppases have been identified from the ABC transporter family. For example, ABCA1 translocates cholesterol and PS to the outer surface of the cell[125,126]. ABCB4 on the other hand is thought to selectively translocate PC[127]. However, there are no reports to date that floppases are involved in EV formation.

Flippases hydrolyze ATP in order to translocate lipids from the exoplasmic leaflet to the cytoplasmic leaflet, a process often called "flipping". Flippases belong to a single family of transporters, the P4-type ATPases, whose transport mechanism has been well studied (discussed below). Intriguingly, the activity of the conserved PE flippase TAT-5 was found to inhibit MV release in *C. elegans* embryos[52], showing that flippases can have fundamental roles in the release of EVs.

1.3.3. P4-ATPases regulate the asymmetry of specific lipids and extracellular vesicle release

Loss of P4-ATPase activity leads to disruption of phospholipid asymmetry, which often affects membrane curvature for vesicle budding and membrane trafficking [88,111]. Flippases also prevent PS exposure during phagocytosis of living cells and are thought to counteract scramblases to inhibit blood coagulation[111,128,129]. Since activated platelets and dying cells release EVs with disrupted PS asymmetry[108,130,131], flippases are likely to have roles in inhibiting EV formation.

Flippases arose from the conserved family of P-type ATPases, which are transporters conserved from prokaryotes and archaea[111]. The family contains five main classes with a diverse range of substrates. The first class, P1-ATPases, contain K^+ and heavy metal ion transporters. P2-ATPases are Ca2+ and Mn2+ and monovalent ion transporters (Na+/ K+, H+/K+), while P3-ATPases transport Mg2+. Only the P4-ATPases are reported to transport lipids as substrates, but the cargo of P5-ATPases is not identified yet.

All P-type ATPases have in common that a conserved aspartic acid undergoes transient phosphorylation, which leads to conformational changes in specific transmembrane (TM) domains promoting the movement of a substrate. The first six transmembrane domains TM1-6 form the principle unit required for transport, but the total number of TM domains is variable between different P-ATPase classes. P-ATPases have three cytoplasmic domains (N, P, A) involved in the ATPase catalytic cycle known as the Post-Albers cycle[111,132]. The nucleotide-binding (N) domain facilitates ATP binding to initiate the phosphorylation cycle. The phosphorylation (P) domain facilitates transient phosphorylation of Aspartic Acid (D) in the conserved DKTGT motif. At the E1 state, ATP and the substrate can bind, which induces aspartyl phosphorylation to the E1P state and the release of ADP. Movement of the P domain stretches the link between TM domain 3 and the actuator (A) domain to the E2P state. The A domain contains the conserved TGES or DGET motif and facilitates dephosphorylation of the phosphorylated intermediate to create the E2 state, where the A domain returns to its original position, the substrate is transported, and the reaction cycle can begin again.

P4-ATPases only evolved in eukaryotes, where multiple members exist that can traffic a variety of phospholipids[114]. The yeast *Sacchromyces cerevisiae* has five P4-ATPases: Drs2, Dnf1, Dnf2, Dnf3 and Neo1, which have lipid flipping activities towards several phospholipids, including PC, PE, PS and their lyso derivatives (Table 1)[133]. Most mammals have fourteen P4-ATPases: ATP8A1-2, ATP8B1-4, ATP9A-B, ATP10A-D, and ATP11A-C[134], while mouse have an additional ATP8B5[135]. *C. elegans* has six P4-ATPases, which were named Transbilayer Amphipath Transporters (TAT-1 to TAT-6)[136]. The specificity of most of the animal P4-ATPases has not been thoroughly tested (Table 1), but at least PC, PE, and PS can be flipped by specific proteins. For example, TAT-1 is required to maintain PS asymmetry in the *C. elegans* plasma membrane, while TAT-5 is required to maintain PE asymmetry in the plasma membrane[52,137,138], but it has not been tested whether these flippases also have weaker activity to translocate other phospholipids or whether they can flip lysophospholipids.

Organism	Subclass	Name	Substrate
Saccharomyces cerevisiae	1	Drs2	PS, PE
	2	Neo1	PS, PE
	3	Dnf1	PC, PE, PS, LPC, LPE, LPS
	3	Dnf2	PC, PE, PS, LPC, LPE
	4	Dnf3	PC, PE
Caenorhabditis elegans	1a	TAT-1	PS
	1b	TAT-2	-
	5	TAT-3	-
	5	TAT-4	-
	2	TAT-5	PE
	2	TAT-6	-
Homo sapiens	1a	ATP8A1	PS, PE
	1a	ATP8A2	PS, PE
	1b	ATP8B1	PC, PS, PE
	1b	ATP8B2	PC
	1b	ATP8B3	PS
	1b	ATP8B4	-
	1b	ATP8B5	-
	2	ATP9A	-
	2	ATP9B	-
	5	ATP10A	PC
	5	ATP10B	-
	5	ATP10D	-
	6	ATP11A	PS, PE
	6	ATP11B	PS, PE
	6	ATP11C	PS, PE

Table 1: Flippases from yeast, nematodes and humans. The P4-ATPase subclass, the name of the flippase and the reported lipid substrates are indicated. Data about lipid flipping was collected from two reviews: Shin and Takatsu 2018[134] and López-Marqués et al. 2015[133]. In some cases, the subclass was derived from a phylogenetic tree from the review by van der Mark *et al.* 2013[114]. That Neo1 traffics PE in addition to PS is from Takar *et al.* 2016[139]. Abbreviations: PS: Phosphatidylserine; PE: Phosphatidylethanolamine; PC: Phosphatidylcholine; LPS, LPE, LPC: lyso-derivatives of PS, PE or PC.

1.3.3.1. Loss of PS asymmetry does not alter extracellular vesicle release

Exosomes and MVs derived from platelets or dying cells often have PS exposed on their surface[108,130,131,140], suggesting that PS could have an important function in EV formation or function. The anionic phospholipid PS has a cylindrical shape and is found in all eukaryotic membranes[89,116]. Disruption of PS membrane asymmetry is physiologically relevant, since PS exposure on the plasma membrane of blood cells promotes platelet activation and blood coagulation[116]. Furthermore, PS exposure on apoptotic cells is a signal for recognition and phagocytosis of dying cells. PS externalization also promotes cell-cell fusion, such as between myocytes or sperm-oocyte fusion, which is necessary for fertilization[141,142]. Thus, the asymmetric distribution of PS needs to be tightly regulated during many cellular processes.

PS is well-studied mainly because many specific PS probes are available[143]. The protein Annexin A5 was first identified to bind PS and several Annexin A5 mimicking peptides were developed and are widely used as probes to detect PS[143,144]. The C-terminal C2 domain of lactadherin (MFGE8) is also used to selectively bind PS[145]. The PS-binding consensus sequence of PS decarboxylase PSD or protein kinase C (PKC) were also used to develop PS-binding peptide probes called PSBP[143,146]. Thus, there are many probes that can be used to specifically label PS, making it easy to analyze the subcellular distribution of PS.

In *C. elegans*, the P4-ATPase responsible for flipping PS in the plasma membrane and endolysosomal membranes is TAT-1, the homolog of human ATP8A1/2[138,147]. TAT-1 is required for endocytosis and endolysosomal trafficking and *tat-1* mutants display severe MVB accumulation. However, alae formation, which requires exosome release from MVBs, occurs normally in *tat-1* mutants[147], suggesting that MVB biogenesis and MVB fusion with the plasma membrane for exosome secretion are not affected in *tat-1* mutants. Furthermore, *tat-1* mutants do not have increased MV release[52], suggesting that PS exposure does not induce MV budding. Thus, PS asymmetry does not seem to have a role in EV release.

However, as PS exposure is an important signal for phagocytosis[142,148], PS exposure on EVs could be important for EV signaling or uptake[7]. Alternatively, as PS exposure is important for cell-cell fusion, PS exposure could be important for the fusion of EVs with cells. Thus, PS asymmetry could alter EV biology in addition to its important roles on endolysosomes, but its precise role remains to be determined.

1.3.3.2. Loss of PE asymmetry induces microvesicle release

PE was also found to be externalized on MVs[107], and PE microdomains have been linked to viral budding[149], suggesting that PE could have an important function during plasma membrane budding. The abundant phospholipid PE has a small headgroup and conical shape that induces negative curvature[89]. PE microdomains are thought to physically bend membranes by driving steric pressure that causes negative membrane curvature (Fig. 2B)[89]. Thus, PE microdomains in the extracellular leaflet would be predicted to cause budding away from the cytoplasm (Fig. 2B).

In addition to a direct role for externalized PE in driving membrane curvature, PE externalization could also be sensed by proteins. For example, negative membrane curvature is necessary for ESCRT-III assembly at bud necks[150], which can be caused by PE microdomains. Furthermore, the movement of uncharged PE could result in a higher relative density of anionic lipids like PS and PI species in the cytoplasmic face of the plasma membrane, resulting in more negatively charged microdomains. Mammalian Hrs, an ESCRT-0 component, binds anionic lipids like PI3P via its FYVE domain[45]. Thus, the ESCRT complex important for EV budding would be expected to be recruited to membranes where PE asymmetry is lost.

PE localization is less studied than PS, mostly due to a scarcity of tools. Until now, there are no identified PE-binding domains, which makes it hard to label PE *in vivo*. Two lantibiotics from *S. cinnamoneus* bacteria, duramycin and cinnamycin, have been found to exclusively bind PE and have been used for specific PE labeling[151–153], but fluorescently or biotin-labeled versions of these peptides are not commercially available. Furthermore, these probes are toxic and have been proposed to induce PE externalization[151,152,154]. In addition, fluorescently-labeled lipids (NBD) are used to analyze lipid asymmetry[155–158], but the fluorophore changes the structure of the lipid, making it unclear whether NBD-PE lipids mirror the behavior of endogenous PE lipids. Thus, the field currently lacks good tools to investigate PE localization during membrane dynamics.

Like PS, PE is exposed on the plasma membrane of activated platelets and platelet EVs[107]. PE is exposed on apoptotic cells together with PS[159]. PE and PS externalization is also induced by multiple viruses that bud from the plasma membrane[160], promoting viral particle uptake into neighboring cells. Thus, by externalizing PE and PS, the viruses mimic MVs to escape the immune response and promote virus spreading[161]. PE is also exposed on the plasma membrane during cytokinesis and must be flipped back to the cytoplasmic leaflet for the plasma membrane to fuse during abscission[162]. Thus, the asymmetric distribution of PE needs to be tightly regulated, to control membrane curvature formation at the right space and time during many cellular processes.

To externalize a lipid that is normally maintained in the cytosolic face of the plasma membrane, both inhibition of flippase activity and induction of scramblase activity must occur[116]. HIV and hepatitis C viruses induce lipid externalization by inducing a Ca^{2+} influx[159], which is known to activate scramblases[111]. However, whether and how these viruses inactivate PE flippases was not yet tested, but this would be predicted for PE externalization. Thus, it is important to determine how PE flippases are regulated during normal physiology and viral infection.

Strong evidence for a role for PE in MV budding comes from studies in *C. elegans* on the P4-ATPase TAT-5[52]. Loss of TAT-5 flippase activity results in a dramatic increase in PE externalization, but not in PS externalization[52], suggesting that TAT-5 is the major PE flippase in the plasma membrane. Knocking down TAT-5 also causes an increase in plasma membrane budding and a massive accumulation of MVs in embryos. Thus, TAT-5 is predicted to flip PE from the extracellular face of the plasma membrane to the cytoplasmic face of the plasma membrane in order to maintain PE asymmetry and inhibit MV budding (Fig. 3). Naik *et al.* recently reported that the mammalian TAT-5 ortholog ATP9A inhibits EV release from cultured cancer cells[163], suggesting that the EV-inhibiting function of TAT-5 is conserved in humans. Thus, loss of PE asymmetry is consistently correlated with EV release, making this an important area for further research.

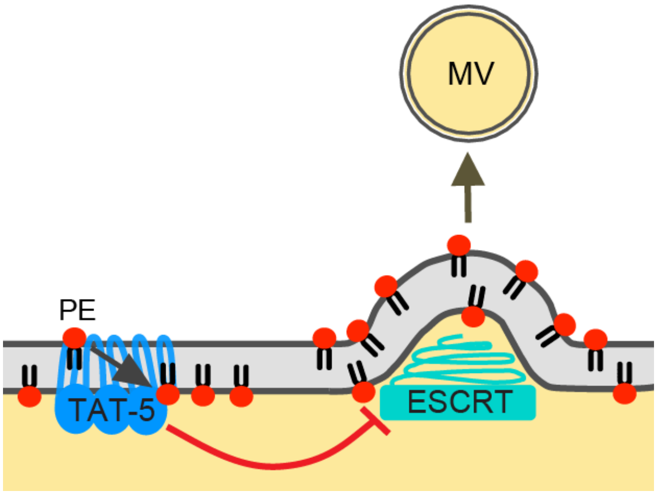

Fig. 3: TAT-5 PE flipping activity inhibits MV budding. The ATPase TAT-5 flips PE and therefore maintains the PE asymmetry at the plasma membrane. Maintaining PE asymmetry inhibits the externalization of PE, which causes membrane curvature, recruitment of the ESCRT complex and release of MVs. Image modified from Beer *et al.*, PNAS 2018[164].

1.4. *C. elegans* as a genetic model organism for extracellular vesicle research

To understand the *in vivo* roles of EVs, invertebrate genetic model organisms like the nematode *Caenorhabditis elegans* can serve as invaluable model systems. *C. elegans* has a rapid life cycle of three days from embryo to egg-laying, making it easy to examine every step of animal development. Embryogenesis follows a defined pattern of asymmetric cell divisions resulting in an invariant number of 959 somatic cells that can be easily followed live through the transparent worm using time-lapse microscopy[165]. Additionally, genetic approaches, such as transgenesis, knockdown, or knock out are well established in *C. elegans*, allowing the *in vivo* study of molecular function and localization[166,167].

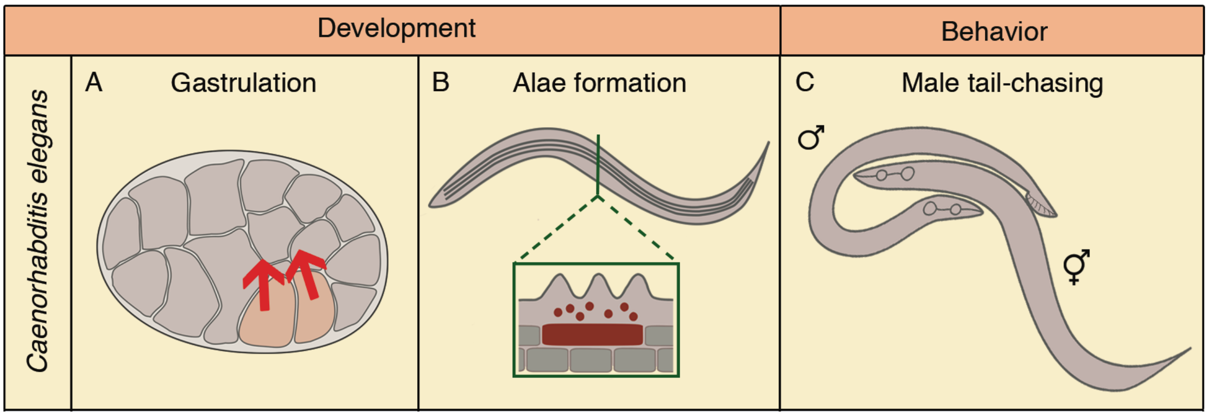

Fig. 4: *In vivo* functions of EVs in *C. elegans*. A) Excessive MV release disrupts gastrulation movements in embryos. B) In larvae and adults, seam cells (brown rectangle) release exosomes (brown circles) to build the alae, which are longitudinal ridges on the cuticle. C) In adults, EVs important for male mating behavior are released from ciliated neurons. Image modified from Beer and Wehman, Cell Adh Migr 2017[15].

C. elegans cells also release EVs under physiological conditions, making it possible to study the physiological relevance of EV release *in vivo*. For example, *C. elegans* embryos release MVs during development[52]. However, when too many MVs accumulate between cells, cell morphology and movement is disrupted. During embryogenesis, cells divide, change their shapes, and migrate to attain their proper location in the body (Fig. 4A). When MVs are overproduced, gastrulation fails and cells that normally migrate inside the embryo remain at the surface of the embryo, ultimately causing embryonic lethality. This suggests that EV overproduction can be disadvantageous for the development of an animal.

Too little EV release is also counterproductive for normal *C. elegans* development. For example, when exosome release from seam cells was blocked (Fig. 4B), the formation of longitudinal ridges called alae on the larval and adult cuticles was disrupted [48]. Thus, EVs play a role in normal *C. elegans* development.

EV release also influences *C. elegans* behavior. Ciliated sensory neurons release EVs carrying transmembrane proteins that modulate male mating behavior (Fig. 4C)[12,168]. The EVs are produced outside the base of the cilia and are released into the environment via an opening in the worm's cuticle. The released EVs contain polycystin proteins known to be responsible for male mating behaviors[169,170]. If polycystins are no longer trafficked into EVs, male tail-chasing behavior is disrupted[12]. These findings suggest that the proteins presented by ciliary EVs are able to influence the behavior of worms.

EV release also plays a role in physiology. *C. elegans* neurons are able to expel protein aggregates and defective mitochondria into large MVs called exophers[23]. Exophers are then taken up by neighboring epidermal cells or by coelomocytes, scavenger cells specialized in clearing material from the fluid in the body cavity[171]. Interestingly, exopher release helps neurons survive stressful conditions like proteotoxic or mitochondrial stress[23], suggesting that EV release is advantageous for the long-term survival of the animal.

These examples show that EVs can change the development, behavior, or disease state of *C. elegans*, establishing an invaluable *in vivo* system to study their functional roles. Furthermore, these studies establish that EVs have immense signaling potential in animals, but that there can also be too much of a good thing. This suggests that animals have developed mechanisms to control the timing and amount of EV release. As the groundbreaking study on the role of PE externalization in MV budding was also performed in *C. elegans*[52], we decided to develop new transgenic tools to visualize MVs in embryos and to determine the mechanisms that control TAT-5 activity and MV release *in vivo*.

1.5. The lipid flippase TAT-5 as inhibitor of PE externalization and microvesicle release

Using TAT-5 as a starting point to understand the mechanisms of MV release has already proven fruitful. The massive accumulation of MVs in *tat-5* embryos is visible by light microscopy using fluorescent plasma membrane reporters[52], which allowed the identification of proteins important for MV budding by suppressing this phenotype. MV production in *tat-5* mutants was shown to depend on the plasma membrane recruitment of ESCRTs (Fig. 3), similar to ESCRT function in ectocytosis in mammalian cells and HIV virus budding from infected cells[35,172]. Since increased plasma membrane budding was observed by electron tomography and the EVs released from *tat-5* mutants are larger than ILVs, TAT-5 is thought to specifically inhibit MV formation, not exosome release. Thus, TAT-5 is a regulator of ectocytosis that inhibits MV release upstream of the ESCRT complex.

TAT-5 has also provided insight into the importance of regulating MV release. TAT-5 is an essential gene and ortholog of the essential PE/PS flippase Neo1 in yeast[136]. Although *tat-5* mutant cells differentiate in terms of gene expression, they fail to move to their right position in the developing embryo or take on their normal shape and stay rounded, which ultimately causes embryonic lethality. Thus, the inhibition of MV production by TAT-5 is necessary for normal embryogenesis, showing the need to tightly control the amount of released MVs.

To date, it is unclear whether TAT-5 activity is regulated to control MV release or how the activity of TAT-5 or its orthologs in other species are regulated. Controlling MV release could be accomplished by regulating the PE translocation activity of TAT-5 or its subcellular localization. Accessory factors are required for the localization and function of many P4-ATPases[111], such as the conserved cell division cycle protein 50(CDC50)/Ligand Effect Modulator(LEM3) family of accessory β-subunits. CDC50 proteins are small glycoproteins with two TM domains that are joined by a large exoplasmic domain. Three CDC50 family proteins exist in yeast (Cdc50, Lem3, Crf1), *C. elegans* (CHAT-1, F20C5.4, W03G11.2) and mammals (CDC50A, CDC50B and CDC50C, also known as TMEM30A-C). In yeast and mammalian CDC50 mutants, P4-ATPases fail to exit the ER and lack flippase activity. However, the essential P4-ATPases Neo1, ATP9A and ATP9B do not need CDC50 or Lem3 for their activity or to exit the ER[173,174]. Similarly, TAT-5 does not need CDC50 subunits for its localization, since double knock down of the CDC50 family proteins F20C5.4 and W03G11.2 in *chat-1* mutants did not disrupt TAT-5 exit from the ER or MV release[164]. Thus, TAT-5 and its orthologs are unique among the P4-ATPases in that they do not use a CDC50 family proteins as a β-subunit. Thus, it remains elusive how TAT-5 localization and activity could be regulated by the cell to control the release of the right amount of MVs at the correct time.

The TAT-5 orthologs ATP9A and ATP9B in mammals primarily localize to the Golgi, but ATP9A is additionally found on endosomes[173]. A minimal sequence in the N-term of ATP9B is required for the Golgi localization[173], suggesting sequence-dependent regulation of the subcellular localization of ATP9B. In contrast, TAT-5 primarily localizes to the plasma membrane, but is also found on internal membranes[52,164], suggesting that there could be mechanisms that control TAT-5 trafficking. For example, GFP::TAT-5 is found on endocytic vesicles, colocalizing with the clathrin adaptor AP2, which shows that TAT-5 is endocytosed. GFP::TAT-5 also traffics through endosomes that are positive for various endosome markers, including the PI3P-binding early endosome protein EEA-1 and the recycling endosome-associated protein RME-8. Furthermore, GFP::TAT-5 was found on degradative endosomes and lysosomes positive for the ESCRT-III component VPS-32 and the lysosome-associated membrane protein LMP-1[164]. This suggests that TAT-5 gets endocytosed and can either be recycled to the plasma membrane or be degraded. However, until the point that we started this work, no regulators of TAT-5 trafficking were known.

Interestingly, the yeast and mammalian TAT-5 orthologs, Neo1 and ATP9A, form a complex with orthologs of the large Dopey-domain containing protein PAD-1, Dop1 and Dopey2, as well as a large GEF-like protein Mon2[175,176]. Thus, it is possible that MON-2 and PAD-1 are involved in regulating TAT-5 localization or activity. Loss of the yeast PAD-1 ortholog Dop1 and the MON-2 ortholog Mon2 causes reduced Neo1 levels in yeast[175], suggesting that Dop1 can control Mon2 stability. However, it is unclear how these two proteins regulate Neo1. PAD-1, MON-2 and their yeast orthologs have been implicated in vacuolar and retrograde trafficking[175,177–182], suggesting that PAD-1 and MON2 could regulate TAT-5 localization. Thus, it is worth testing whether PAD-1 and MON-2 are novel trafficking regulators of TAT-5 that thereby affect TAT-5 PE flipping activity and MV budding.

1.6. The goal of this study

As cells regulate PE asymmetry and EV release during cell division, cell fusion, and cell death[162,183,184], it is important to determine how TAT-5 flippase activity is regulated to inhibit the outward budding of the plasma membrane and the release of MVs. The goal of this thesis was to find the regulatory factors that are required for TAT-5 activity. To shed light on this issue, our lab conducted a candidate RNAi screen to look for proteins required for TAT-5 activity. Because TAT-5 PE flipping activity inhibits MV release, we designed a screen to look for proteins whose depletion causes increased MV release, similar to TAT-5 depletion.

First, we had to overcome the challenge to visualize MVs *in vivo* because MVs are small, carry the same reporters as the releasing cell and no specific markers exist that differentiate between exosomes and MVs. These issues make it hard to specifically visualize released MVs *in vivo* using bright field light microscopy. In chapter 3, we describe how we increased the visibility of released MVs for the screen by designing a membrane reporter fused with a degradation tag. The degron tag causes removal of the reporter from the cytosol by the proteasome, but retains the reporter fluorescence in the released vesicles. This trick enabled us to identify four proteins that inhibit MV release: the PI3K complex subunits VPS-34 and BEC-1, the DNAJ-domain protein RME-8 and the Dopey-domain protein and potential TAT-5 regulator PAD-1. Thus, our degron-tagging approach can help to visualize MVs *in vivo* and can uncover proteins involved in MV formation.

Next, we wanted to understand if the identified MV inhibitors are TAT-5 regulators. In chapter 4, we determined the TAT-5 regulatory function of PI3K and RME-8, which function in endosomal trafficking pathways. We found that PI3K and RME-8 are required for TAT-5 plasma membrane localization and that TAT-5 is recycled through endosomes by specific sorting nexin-dependent pathways. We found that RME-8 inhibits TAT-5 missorting to the degradative pathway, which is required to maintain TAT-5 PE flipping activity. We also identified redundant sorting nexin-depended TAT-5 trafficking pathways, which are required for TAT-5 plasma membrane localization. This shows that controlling the localization of TAT-5 can affect TAT-5 PE flipping activity to mediate MV release.

The last chapter 5 is devoted to the potential TAT-5 regulators PAD-1 and MON-2, where we wanted to know if they are regulators of TAT-5 levels, localization and/or activity. We found that PAD-1 is required for TAT-5 PE flipping activity, making PAD-1 a likely candidate to regulate MV release through regulating TAT-5 activity. We also discovered that PAD-1 and the GEF-like protein MON-2 are required for endolysosomal trafficking, which can prevent TAT-5 localization to the degradative pathway when its trafficking by sorting nexins is disrupted. This again supports the hypothesis that TAT-5 PE flipping activity needs to be maintained to inhibit ectocytosis.

In the end, we show that TAT-5 localization is regulated by several redundant pathways, which are likely to be conserved in higher organisms. We also provide a first candidate, namely PAD-1, that could be directly required for TAT-5 flipping activity. Thus, our findings provide a first look into the mechanism of how TAT-5 can be regulated to inhibit MV release. Since these proteins are conserved in humans, our findings are likely to contribute to the understanding of MV budding mechanisms during health and disease.

1.7. References

1. Budnik, V., Ruiz-Cañada, C. & Wendler, F. Extracellular vesicles round off communication in the nervous system. *Nat. Rev. Neurosci.* **17**, 160–172 (2016).
2. Tannetta, D., Dragovic, R., Alyahyaei, Z. & Southcombe, J. Extracellular vesicles and reproduction-promotion of successful pregnancy. *Cellular and Molecular Immunology* **11**, 548–563 (2014).
3. Deatherage, B. L. & Cookson, B. T. Membrane vesicle release in bacteria, eukaryotes, and archaea: a conserved yet underappreciated aspect of microbial life. *Infect. Immun.* **80**, 1948–57 (2012).
4. Schwechheimer, C. & Kuehn, M. J. Outer-membrane vesicles from Gram-negative bacteria: biogenesis and functions. *Nat. Rev. Microbiol.* **13**, 605–619 (2015).
5. Cui, Y., Gao, J., He, Y. & Jiang, L. Plant extracellular vesicles. *Protoplasma* 1–10 (2019). doi:10.1007/s00709-019-01435-6
6. Gill, S., Catchpole, R. & Forterre, P. Extracellular membrane vesicles in the three domains of life and beyond. *FEMS Microbiol. Rev.* **43**, 273–303 (2019).
7. Van Niel, G., D'Angelo, G. & Raposo, G. Shedding light on the cell biology of extracellular vesicles. *Nat. Rev. Mol. Cell Biol.* **19**, 213–228 (2018).
8. Ratajczak, J. *et al.* Embryonic stem cell-derived microvesicles reprogram hematopoietic progenitors: evidence for horizontal transfer of mRNA and protein delivery. *Leukemia* **20**, 847–856 (2006).
9. Skog, J. *et al.* Glioblastoma microvesicles transport RNA and proteins that promote tumour growth and provide diagnostic biomarkers. *Nat. Cell Biol.* **10**, 1470–6 (2008).
10. Mathieu, M., Martin-Jaular, L., Lavieu, G. & Théry, C. Specificities of secretion and uptake of exosomes and other extracellular vesicles for cell-to-cell communication. *Nat. Cell Biol.* **21**, 9–17 (2019).
11. Roth, R. *et al.* Arbuscular cell invasion coincides with extracellular vesicles and membrane tubules. *Nat. Plants* **5**, 204–211 (2019).
12. Wang, J. *et al.* C. elegans ciliated sensory neurons release extracellular vesicles that function in animal communication. *Curr. Biol.* **24**, 519–525 (2014).
13. Corrigan, L. *et al.* BMP-regulated exosomes from Drosophila male reproductive glands reprogram female behavior. *J. Cell Biol.* **206**, 671–88 (2014).
14. Colombo, M., Raposo, G. & Théry, C. Biogenesis, Secretion, and Intercellular Interactions of Exosomes and Other Extracellular Vesicles. *Annu. Rev. Cell Dev. Biol.* **30**, 255–289 (2014).
15. Beer, K. B. & Wehman, A. M. Mechanisms and functions of extracellular vesicle release in vivo —What we can learn from flies and worms. *Cell Adh. Migr.* **11**, 135–150 (2017).
16. Robbins, P. D. & Morelli, A. E. Regulation of immune responses by extracellular vesicles. *Nat. Rev. Immunol.* **14**, 195–208 (2014).
17. Desrochers, L. M., Antonyak, M. A. & Cerione, R. A. Extracellular Vesicles: Satellites of Information Transfer in Cancer and Stem Cell Biology. *Dev. Cell* **37**, 301–309 (2016).
18. Iraci, N. *et al.* Focus on Extracellular Vesicles: Physiological Role and Signalling Properties of Extracellular Membrane Vesicles. *Int. J. Mol. Sci.* **17**, 171 (2016).
19. Altan-Bonnet, N. Extracellular vesicles are the Trojan horses of viral infection. *Curr. Opin. Microbiol.* **32**, 77–81 (2016).
20. Ivanov, S., Austin, J., Berg, R. H. & Harrison, M. J. Extensive membrane systems at the host–arbuscular mycorrhizal fungus interface. *Nat. Plants* **5**, 194–203 (2019).
21. Gong, Y. N. *et al.* ESCRT-III Acts Downstream of MLKL to Regulate Necroptotic Cell Death and Its Consequences. *Cell* **169**, 286-300.e16 (2017).
22. Jimenez, A. J. *et al.* ESCRT machinery is required for plasma membrane repair. *Science* **343**, (2014).
23. Melentijevic, I. *et al.* C. elegans neurons jettison protein aggregates and mitochondria under neurotoxic stress. (2017). doi:10.1038/nature21362
24. Yoon, S., Kovalenko, A., Bogdanov, K. & Wallach, D. MLKL, the Protein that Mediates Necroptosis, Also Regulates Endosomal Trafficking and Extracellular Vesicle Generation. *Immunity* **47**, 51-65.e7 (2017).

25. Gong, J., Jaiswal, R., Dalla, P., Luk, F. & Bebawy, M. Microparticles in cancer: A review of recent developments and the potential for clinical application. *Seminars in Cell and Developmental Biology* **40**, 35–40 (2015).
26. Torrano, V. *et al.* Vesicle-MaNiA: Extracellular vesicles in liquid biopsy and cancer. *Current Opinion in Pharmacology* **29**, 47–53 (2016).
27. De Palma, G., Sallustio, F. & Schena, F. P. Clinical application of human urinary extracellular vesicles in kidney and urologic diseases. *International Journal of Molecular Sciences* **17**, 1043 (2016).
28. Cocucci, E. & Meldolesi, J. Ectosomes and exosomes: shedding the confusion between extracellular vesicles. *Trends Cell Biol.* **25**, 364–372 (2015).
29. El Andaloussi, S., Mäger, I., Breakefield, X. O. & Wood, M. J. A. Extracellular vesicles: Biology and emerging therapeutic opportunities. *Nat. Rev. Drug Discov.* **12**, 347–357 (2013).
30. Ohno, S. I., Drummen, G. P. C. & Kuroda, M. Focus on extracellular vesicles: Development of extracellular vesicle-based therapeutic systems. *International Journal of Molecular Sciences* **17**, 172 (2016).
31. Pollet, H., Conrard, L., Cloos, A. S. & Tyteca, D. *Plasma membrane lipid domains as platforms for vesicle biogenesis and shedding? Biomolecules* **8**, (2018).
32. Ma, L. *et al.* Discovery of the migrasome, an organelle mediating release of cytoplasmic contents during cell migration. *Cell Res.* **25**, 24–38 (2015).
33. Kalra, H., Drummen, G. P. C. & Mathivanan, S. Focus on extracellular vesicles: Introducing the next small big thing. *International Journal of Molecular Sciences* **17**, 170 (2016).
34. Wang, Q. & Lu, Q. Plasma membrane-derived extracellular microvesicles mediate non-canonical intercellular NOTCH signaling. *Nat. Commun.* **8**, 709 (2017).
35. Nabhan, J. F., Hu, R., Oh, R. S., Cohen, S. N. & Lu, Q. Formation and release of arrestin domain-containing protein 1-mediated microvesicles (ARMMs) at plasma membrane by recruitment of TSG101 protein. *Proc. Natl. Acad. Sci. U. S. A.* **109**, 4146–4151 (2012).
36. Ramirez, M. I. *et al.* Technical challenges of working with extracellular vesicles. *Nanoscale* **10**, 881–906 (2018).
37. Théry, C. *et al.* Minimal information for studies of extracellular vesicles 2018 (MISEV2018): a position statement of the International Society for Extracellular Vesicles and update of the MISEV2014 guidelines. *J. Extracell. Vesicles* **7**, 1535750 (2018).
38. Raposo, G. & Stoorvogel, W. Extracellular vesicles: Exosomes, microvesicles, and friends. *J. Cell Biol.* **200**, 373–383 (2013).
39. Piper, R. C. & Luzio, J. P. Late Endosomes: Sorting and Partitioning in Multivesicular Bodies. *Traffic* **2**, 612–621 (2001).
40. Stahl, P. D. & Barbieri, M. A. Multivesicular bodies and multivesicular endosomes: the 'ins and outs' of endosomal traffic. *Science's STKE : signal transduction knowledge environment* **2002**, pe32 (2002).
41. Sugita, S. Mechanisms of exocytosis. *Acta Physiol.* **192**, 185–193 (2007).
42. Gerber, S. H. & Südhof, T. C. Molecular determinants of regulated exocytosis. in *Diabetes* **51**, S3–S11 (2002).
43. Votteler, J. & Sundquist, W. I. Virus budding and the ESCRT pathway. *Cell Host and Microbe* **14**, 232–241 (2013).
44. Hurley, J. H. ESCRTs are everywhere. *EMBO J.* **34**, 2398–2407 (2015).
45. Henne, W. M., Stenmark, H. & Emr, S. D. Molecular mechanisms of the membrane sculpting ESCRT pathway. *Cold Spring Harb. Perspect. Med.* **3**, a016766 (2013).
46. Alonso Y Adell, M., Migliano, S. M. & Teis, D. ESCRT-III and Vps4: a dynamic multipurpose tool for membrane budding and scission. *FEBS J.* **283**, 3288–3302 (2016).
47. Hyenne, V. *et al.* RAL-1 controls multivesicular body biogenesis and exosome secretion. *J. Cell Biol.* **211**, 27–37 (2015).
48. Liégeois, S., Benedetto, A., Garnier, J.-M., Schwab, Y. & Labouesse, M. The V0-ATPase mediates apical secretion of exosomes containing Hedgehog-related proteins in Caenorhabditis elegans. *J. Cell Biol.* **173**, 949–61 (2006).
49. Gross, J. C., Chaudhary, V., Bartscherer, K. & Boutros, M. Active Wnt proteins are secreted on exosomes. *Nat. Cell Biol.* **14**, 1036–1045 (2012).
50. Tamai, K. *et al.* Exosome secretion of dendritic cells is regulated by Hrs, an ESCRT-0 protein.

Biochem. Biophys. Res. Commun. **399**, 384–390 (2010).

51. Matusek, T. *et al.* The ESCRT machinery regulates the secretion and long-range activity of Hedgehog. *Nature* **516**, 99–103 (2014).
52. Wehman, A. M., Poggioli, C., Schweinsberg, P., Grant, B. D. & Nance, J. The P4-ATPase TAT-5 inhibits the budding of extracellular vesicles in C. elegans embryos. *Curr. Biol.* **21**, 1951–1959 (2011).
53. Von Schwedler, U. K. *et al.* The protein network of HIV budding. *Cell* **114**, 701–713 (2003).
54. Stenmark, H. Rab GTPases as coordinators of vesicle traffic. *Nat. Rev. Mol. Cell Biol.* **10**, 513–525 (2009).
55. Miyashita, Y. *et al.* A dileucine motif in its cytoplasmic domain directs -catenin-uncoupled E-cadherin to the lysosome. *J. Cell Sci.* **120**, 4395–4406 (2007).
56. Grosshans, B. L., Ortiz, D. & Novick, P. Rabs and their effectors: Achieving specificity in membrane traffic. *Proc. Natl. Acad. Sci.* **103**, 11821–11827 (2006).
57. Levin, R., Grinstein, S. & Canton, J. The life cycle of phagosomes: formation, maturation, and resolution. *Immunol. Rev.* **273**, 156–179 (2016).
58. Bilanges, B., Posor, Y. & Vanhaesebroeck, B. PI3K isoforms in cell signalling and vesicle trafficking. *Nat. Rev. Mol. Cell Biol.* **20**, 515–534 (2019).
59. Sumakovic, M. *et al.* UNC-108/RAB-2 and its effector RIC-19 are involved in dense core vesicle maturation in Caenorhabditis elegans. *J. Cell Biol.* **186**, 897–914 (2009).
60. Lu, Q. *et al.* C. elegans Rab GTPase 2 is required for the degradation of apoptotic cells. *Development* **135**, 1069–1080 (2008).
61. Ueda, N., Tomita, T., Yanagisawa, K. & Kimura, N. Retromer and Rab2-dependent trafficking mediate PS1 degradation by proteasomes in endocytic disturbance. *J. Neurochem.* **137**, 647–658 (2016).
62. Lörincz, P. *et al.* Rab2 promotes autophagic and endocytic lysosomal degradation. *J. Cell Biol.* **216**, 1937–1947 (2017).
63. Lund, V. K., Madsen, K. L. & Kjaerulff, O. Drosophila Rab2 controls endosome-lysosome fusion and LAMP delivery to late endosomes. *Autophagy* **14**, 1520–1542 (2018).
64. Ostrowski, M. *et al.* Rab27a and Rab27b control different steps of the exosome secretion pathway. *Nat. Cell Biol.* **12**, 19–30 (2010).
65. Zhang, M., Chen, L., Wang, S. & Wang, T. Rab7: roles in membrane trafficking and disease. *Biosci. Rep.* **29**, 193–209 (2009).
66. Jaé, N., McEwan, D. G., Manavski, Y., Boon, R. A. & Dimmeler, S. Rab7a and Rab27b control secretion of endothelial microRNA through extracellular vesicles. *FEBS Lett.* **589**, 3182–3188 (2015).
67. Sato, M., Grant, B. D., Harada, A. & Sato, K. Rab11 is required for synchronous secretion of chondroitin proteoglycans after fertilization in Caenorhabditis elegans. *J. Cell Sci.* **121**, 3177–3186 (2008).
68. Takahashi, S. *et al. Rab11 regulates exocytosis of recycling vesicles at the plasma membrane. Journal of Cell Science* **125**, (2012).
69. Savina, A., Vidal, M. & Colombo, M. I. The exosome pathway in K562 cells is regulated by Rab11. *J. Cell Sci.* **115**, 2505–15 (2002).
70. Savina, A., Fader, C. M., Damiani, M. T. & Colombo, M. I. Rab11 Promotes Docking and Fusion of Multivesicular Bodies in a Calcium-Dependent Manner. *Traffic* **6**, 131–143 (2005).
71. Utley, T. J. *et al.* Respiratory syncytial virus uses a Vps4-independent budding mechanism controlled by Rab11-FIP2. *Proc. Natl. Acad. Sci. U. S. A.* **105**, 10209–14 (2008).
72. Raposo, G., Marks, M. S. & Cutler, D. F. Lysosome-related organelles: driving post-Golgi compartments into specialisation. *Curr. Opin. Cell Biol.* **19**, 394–401 (2007).
73. Perez, C. *et al.* Structure and mechanism of an active lipid-linked oligosaccharide flippase. *Nature* **524**, 433–438 (2015).
74. Klinkert, K. & Echard, A. Rab35 GTPase: A Central Regulator of Phosphoinositides and F-actin in Endocytic Recycling and Beyond. *Traffic* **17**, 1063–1077 (2016).
75. Hsu, C. *et al.* Regulation of exosome secretion by Rab35 and its GTPase-activating proteins TBC1D10A-C. *J. Cell Biol.* **189**, 223–32 (2010).
76. Bombardier, J. P. & Munson, M. Three steps forward, two steps back: mechanistic insights into the assembly and disassembly of the SNARE complex. *Curr. Opin. Chem. Biol.* **29**, 66–71

(2015).

77. Fader, C. M., Sánchez, D. G., Mestre, M. B. & Colombo, M. I. TI-VAMP/VAMP7 and VAMP3/cellubrevin: two v-SNARE proteins involved in specific steps of the autophagy/multivesicular body pathways. *Biochim. Biophys. Acta* **1793**, 1901–16 (2009).
78. Jahn, R., Lang, T. & Südhof, T. C. Membrane Fusion. *Cell* **112**, 519–533 (2003).
79. Koles, K. *et al.* Mechanism of evenness interrupted (Evi)-exosome release at synaptic boutons. *J. Biol. Chem.* **287**, 16820–34 (2012).
80. Marshansky, V., Rubinstein, J. L. & Grüber, G. Eukaryotic V-ATPase: novel structural findings and functional insights. *Biochim. Biophys. Acta* **1837**, 857–79 (2014).
81. Wang, D. *et al.* Ca2+-Calmodulin regulates SNARE assembly and spontaneous neurotransmitter release via v-ATPase subunit V0a1. *J. Cell Biol.* **205**, 21–31 (2014).
82. Armenti, S. T., Chan, E. & Nance, J. Polarized exocyst-mediated vesicle fusion directs intracellular lumenogenesis within the C. elegans excretory cell. *Dev. Biol.* **394**, 110–21 (2014).
83. Naslavsky, N. & Caplan, S. The enigmatic endosome – sorting the ins and outs of endocytic trafficking. *J. Cell Sci.* **131**, jcs216499 (2018).
84. Van Meer, G., Voelker, D. R. & Feigenson, G. W. Membrane lipids: Where they are and how they behave. *Nat. Rev. Mol. Cell Biol.* **9**, 112–124 (2008).
85. Suetsugu, S., Kurisu, S. & Takenawa, T. Dynamic shaping of cellular membranes by phospholipids and membrane-deforming proteins. *Physiological reviews* **94**, 1219–1248 (2014).
86. Skotland, T., Hessvik, N. P., Sandvig, K. & Llorente, A. Exosomal lipid composition and the role of ether lipids and phosphoinositides in exosome biology. *J. Lipid Res.* **60**, 9–18 (2019).
87. Lemmon, M. A. Membrane recognition by phospholipid-binding domains. *Nature Reviews Molecular Cell Biology* **9**, 99–111 (2008).
88. McMahon, H. T. & Gallop, J. L. Membrane curvature and mechanisms of dynamic cell membrane remodelling. *Nature* **438**, 590–596 (2005).
89. McMahon, H. T. & Boucrot, E. Membrane curvature at a glance. *J. Cell Sci.* **128**, 1065–1070 (2015).
90. Graham, T. R. & Kozlov, M. M. Interplay of proteins and lipids in generating membrane curvature. *Curr. Opin. Cell Biol.* **22**, 430–436 (2010).
91. Möbius, W. *et al.* Recycling Compartments and the Internal Vesicles of Multivesicular Bodies Harbor Most of the Cholesterol Found in the Endocytic Pathway. *Traffic* **4**, 222–231 (2003).
92. Möbius, W. *et al.* Immunoelectron Microscopic Localization of Cholesterol Using Biotinylated and Non-cytolytic Perfringolysin O. *J. Histochem. Cytochem.* **50**, 43–55 (2002).
93. Del Conde, I., Shrimpton, C. N., Thiagarajan, P. & López, J. A. Tissue-factor-bearing microvesicles arise from lipid rafts and fuse with activated platelets to initiate coagulation. *Blood* **106**, 1604–1611 (2005).
94. Liu, M. L., Reilly, M. P., Casasanto, P., McKenzie, S. E. & Williams, K. J. Cholesterol enrichment of human monocyte/macrophages induces surface exposure of phosphatidylserine and the release of biologically-active tissue factor-positive microvesicles. *Arterioscler. Thromb. Vasc. Biol.* **27**, 430–435 (2007).
95. Verderio, C., Gabrielli, M. & Giussani, P. Role of sphingolipids in the biogenesis and biological activity of extracellular vesicles. *J. Lipid Res.* **59**, 1325–1340 (2018).
96. Clarke, C. J. *et al.* The Extended Family of Neutral Sphingomyelinases. *Biochemistry* **45**, 11247–11256 (2006).
97. Trajkovic, K. *et al.* Ceramide triggers budding of exosome vesicles into multivesicular endosomes. *Science* **319**, 1244–7 (2008).
98. Bianco, F. *et al.* Acid sphingomyelinase activity triggers microparticle release from glial cells. *EMBO J.* **28**, 1043–1054 (2009).
99. Menck, K. *et al.* Neutral sphingomyelinases control extracellular vesicles budding from the plasma membrane. *J. Extracell. Vesicles* **6**, (2017).
100. Posor, Y., Eichhorn-Grünig, M. & Haucke, V. Phosphoinositides in endocytosis. *Biochimica et Biophysica Acta - Molecular and Cell Biology of Lipids* **1851**, 794–804 (2015).
101. Viaud, J. *et al.* Phosphoinositides: Important lipids in the coordination of cell dynamics. *Biochimie* **125**, 250–258 (2016).
102. Balla, T. Phosphoinositides: Tiny lipids with giant impact on cell regulation. *Physiological Reviews* **93**, 1019–1137 (2013).

103. Hurley, J. H. & Hanson, P. I. Membrane budding and scission by the ESCRT machinery: it's all in the neck. *Nat. Rev. Mol. Cell Biol.* **11**, 556–566 (2010).
104. van Meer, G. Dynamic transbilayer lipid asymmetry. *Cold Spring Harb. Perspect. Biol.* **3**, 1–11 (2011).
105. Marquardt, D., Geier, B. & Pabst, G. Asymmetric lipid membranes: Towards more realistic model systems. *Membranes (Basel).* **5**, 180–196 (2015).
106. Basse, F., Gaffet, P., Rendu, F. & Bienvenue, A. Translocation of spin-labeled phospholipids through plasma membrane during thrombin- and ionophore A23187-induced platelet activation. *Biochemistry* **32**, 2337–2344 (1993).
107. Larson, M. C., Woodliff, J. E., Hillery, C. A., Kearl, T. J. & Zhao, M. Phosphatidylethanolamine is externalized at the surface of microparticles. *Biochim. Biophys. Acta - Mol. Cell Biol. Lipids* **1821**, 1501–1507 (2012).
108. Heijnen, H. F., Schiel, A. E., Fijnheer, R., Geuze, H. J. & Sixma, J. J. Activated platelets release two types of membrane vesicles: microvesicles by surface shedding and exosomes derived from exocytosis of multivesicular bodies and alpha-granules. *Blood* **94**, 3791–9 (1999).
109. Arraud, N. *et al.* Extracellular vesicles from blood plasma: Determination of their morphology, size, phenotype and concentration. *J. Thromb. Haemost.* **12**, 614–627 (2014).
110. Maxfield, F. R. & van Meer, G. Cholesterol, the central lipid of mammalian cells. *Curr. Opin. Cell Biol.* **22**, 422–429 (2010).
111. Andersen, J. P. *et al.* P4-ATPases as phospholipid flippases-structure, function, and enigmas. *Front. Physiol.* **7**, 1–23 (2016).
112. Montigny, C., Lyons, J., Champeil, P., Nissen, P. & Lenoir, G. On the molecular mechanism of flippase- and scramblase-mediated phospholipid transport. *Biochim. Biophys. Acta - Mol. Cell Biol. Lipids* **1861**, 767–783 (2016).
113. Daleke, D. L. Regulation of transbilayer plasma membrane phospholipid asymmetry. *Journal of Lipid Research* **44**, 233–242 (2003).
114. van der Mark, V. A., Oude Elferink, R. P. J. & Paulusma, C. C. P4 ATPases: Flippases in health and disease. *Int. J. Mol. Sci.* **14**, 7897–7922 (2013).
115. Williamson, P. Phospholipid Scramblases. *Lipid Insights* **8s1**, LPI.S31785 (2015).
116. Leventis, P. A. & Grinstein, S. The Distribution and Function of Phosphatidylserine in Cellular Membranes. *Annu. Rev. Biophys.* **39**, 407–427 (2010).
117. Ernst, O. P. & Menon, A. K. Phospholipid scrambling by rhodopsin. *Photochem. Photobiol. Sci.* **14**, 1922–31 (2015).
118. Kodigepalli, K. M., Bowers, K., Sharp, A. & Nanjundan, M. Roles and regulation of phospholipid scramblases. *FEBS Lett.* **589**, 3–14 (2015).
119. Fujii, T., Sakata, A., Nishimura, S., Eto, K. & Nagata, S. TMEM16F is required for phosphatidylserine exposure and microparticle release in activated mouse platelets. *Proc. Natl. Acad. Sci. U. S. A.* **112**, 12800–12805 (2015).
120. Suzuki, J., Umeda, M., Sims, P. J. & Nagata, S. Calcium-dependent phospholipid scrambling by TMEM16F. *Nature* **468**, 834–838 (2010).
121. Castoldi, E., Collins, P. W., Williamson, P. L. & Bevers, E. M. Compound heterozygosity for 2 novel TMEM16F mutations in a patient with Scott syndrome. *Blood* **117**, 4399–400 (2011).
122. Nakao, H., Ikeda, K., Ishihama, Y. & Nakano, M. Membrane-Spanning Sequences in Endoplasmic Reticulum Proteins Promote Phospholipid Flip-Flop. *Biophys. J.* **110**, 2689–2697 (2016).
123. Anglin, T. C., Brown, K. L. & Conboy, J. C. Phospholipid flip-flop modulated by transmembrane peptides WALP and melittin. *J. Struct. Biol.* **168**, 37–52 (2009).
124. Fattal, E., Nir, S., Parente, R. A. & Szoka, F. C. Pore-Forming Peptides Induce Rapid Phospholipid Flip-Flop in Membranes. *Biochemistry* **33**, 6721–6731 (1994).
125. Smith, J. D., Waelde, C., Horwitz, A. & Zheng, P. Evaluation of the role of phosphatidylserine translocase activity in ABCA1-mediated lipid efflux. *J. Biol. Chem.* **277**, 17797–17803 (2002).
126. Oram, J. F. & Lawn, R. M. ABCA1: The gatekeeper for eliminating excess tissue cholesterol. *Journal of Lipid Research* **42**, 1173–1179 (2001).
127. van Helvoort, A. *et al.* MDR1 P-glycoprotein is a lipid translocase of broad specificity, while MDR3 P-glycoprotein specifically translocates phosphatidylcholine. *Cell* **87**, 507–17 (1996).
128. Segawa, K., Kurata, S. & Nagata, S. Human type IV P-type ATPases that work as plasma

membrane phospholipid flippases and their regulation by caspase and calcium. *J. Biol. Chem.* **291**, 762–772 (2016).

129. Segawa, K. *et al.* Caspase-mediated cleavage of phospholipid flippase for apoptotic phosphatidylserine exposure. *Science* **344**, 1164–8 (2014).
130. Stuart, M. C. *et al.* Ultrastructural detection of surface exposed phosphatidylserine on activated blood platelets. *Thromb. Haemost.* **74**, 1145–51 (1995).
131. Nagata, S. Apoptosis and Clearance of Apoptotic Cells. *Annu. Rev. Immunol.* **36**, 489–517 (2018).
132. Apell, H.-J. How do P-Type ATPases transport ions? *Bioelectrochemistry* **63**, 149–156 (2004).
133. López-Marqués, R. L. *et al.* Structure and mechanism of ATP-dependent phospholipid transporters. *Biochim. Biophys. Acta - Gen. Subj.* **1850**, 461–475 (2015).
134. Shin, H.-W. & Takatsu, H. Substrates of P4-ATPases: beyond aminophospholipids (phosphatidylserine and phosphatidylethanolamine). *FASEB J.* **33**, 3087–3096 (2018).
135. Xu, P. *et al.* Identification of a novel mouse P4-ATPase family member highly expressed during spermatogenesis. *J. Cell Sci.* **122**, 2866–2876 (2009).
136. Lyssenko, N. N., Miteva, Y., Gilroy, S., Hanna-Rose, W. & Schlegel, R. A. An unexpectedly high degree of specialization and a widespread involvement in sterol metabolism among the C. elegans putative aminophospholipid translocases. *BMC Dev. Biol.* **8**, 1–17 (2008).
137. Züllig, S. *et al.* Aminophospholipid Translocase TAT-1 Promotes Phosphatidylserine Exposure during C. elegans Apoptosis. *Curr. Biol.* **17**, 994–999 (2007).
138. Darland-Ransom, M. *et al.* Role of C. elegans TAT-1 Protein in Maintaining Plasma Membrane Phosphatidylserine Asymmetry. *Science* **320**, 528–531 (2008).
139. Takar, M., Wu, Y. & Graham, T. R. The essential Neo1 protein from budding yeast plays a role in establishing aminophospholipid asymmetry of the plasma membrane. *J. Biol. Chem.* **291**, 15727–15739 (2016).
140. Zargarian, S. *et al.* Phosphatidylserine externalization, &quot;necroptotic bodies&quot; release, and phagocytosis during necroptosis. *PLoS Biol.* **15**, e2002711 (2017).
141. Rival, C. M. *et al.* Phosphatidylserine on viable sperm and phagocytic machinery in oocytes regulate mammalian fertilization. *Nat. Commun.* **10**, 4456 (2019).
142. Zhou, X. & Platt, J. L. Molecular and Cellular Mechanisms of Mammalian Cell Fusion. in *Advances in Experimental Medicine and Biology* **713**, 33–64 (Springer, Dordrecht, 2011).
143. Gao, J. & Zheng, H. Illuminating the lipidome to advance biomedical research: Peptide-based probes of membrane lipids. *Future Medicinal Chemistry* **5**, 947–959 (2013).
144. Tait, J. F. & Gibson, D. Phospholipid binding of annexin V: Effects of calcium and membrane phosphatidylserine content. *Arch. Biochem. Biophys.* **298**, 187–191 (1992).
145. Shi, J., Heegaard, C. W., Rasmussen, J. T. & Gilbert, G. E. Lactadherin binds selectively to membranes containing phosphatidyl-l-serine and increased curvature. *Biochim. Biophys. Acta - Biomembr.* **1667**, 82–90 (2004).
146. Igarashi, K. *et al.* A novel phosphatidylserine-binding peptide motif defined by an anti- idiotypic monoclonal antibody. Localization of phosphatidylserine-specific binding sites on protein kinase C and phosphatidylserine decarboxylase. *J. Biol. Chem.* **270**, 29075–29078 (1995).
147. Ruaud, A. F. *et al.* The C. elegans P4-ATPase TAT-1 regulates lysosome biogenesis and endocytosis. *Traffic* **10**, 88–100 (2009).
148. Li, Z. *et al.* Necrotic Cells Actively Attract Phagocytes through the Collaborative Action of Two Distinct PS-Exposure Mechanisms. *PLOS Genet.* **11**, e1005285 (2015).
149. Booth, A. M. *et al.* Exosomes and HIV Gag bud from endosome-like domains of the T cell plasma membrane. *J. Cell Biol.* **172**, 923–935 (2006).
150. Lee, I.-H., Kai, H., Carlson, L.-A., Groves, J. T. & Hurley, J. H. Negative membrane curvature catalyzes nucleation of endosomal sorting complex required for transport (ESCRT)-III assembly. *Proc. Natl. Acad. Sci.* **112**, 15892–15897 (2015).
151. Hullin-Matsuda, F., Makino, A., Murate, M. & Kobayashi, T. Probing phosphoethanolamine-containing lipids in membranes with duramycin/cinnamycin and aegerolysin proteins. *Biochimie* **130**, 81–90 (2016).
152. Hou, S., Johnson, S. E. & Zhao, M. A One-Step Staining Probe for Phosphatidylethanolamine. *ChemBioChem* **16**, 1955–1960 (2015).
153. Stafford, J. H. & Thorpe, P. E. Increased exposure of phosphatidylethanolamine on the surface

of tumor vascular endothelium. *Neoplasia* **13**, 299–308 (2011).

154. Iwamoto, K. *et al.* Curvature-dependent recognition of ethanolamine phospholipids by duramycin and cinnamycin. *Biophys. J.* **93**, 1608–1619 (2007).
155. Sleight, R. G. & Pagano, R. E. Transbilayer movement of a fluorescent phosphatidylethanolamine analogue across the plasma membranes of cultured mammalian cells. *J. Biol. Chem.* **260**, 1146–54 (1985).
156. Kihara, A. & Igarashi, Y. Cross talk between sphingolipids and glycerophospholipids in the establishment of plasma membrane asymmetry. *Mol. Biol. Cell* **15**, 4949–4959 (2004).
157. Rimon, G., Meyerstein, N. & Henis, Y. I. Lateral mobility of phospholipids in the external and internal leaflets of normal and hereditary spherocytic human erythrocytes. *Biochim. Biophys. Acta - Biomembr.* **775**, 283–290 (1984).
158. Julien, M., Tournier, J.-F. & Tocanne, J.-F. Differences in the Transbilayer and Lateral Motions of Fluorescent Analogs of Phosphatidylcholine and Phosphatidylethanolamine in the Apical Plasma Membrane of Bovine Aortic Endothelial Cells. *Exp. Cell Res.* **208**, 387–397 (1993).
159. Zenarruzabeitia, O., Vitallé, J., Eguizabal, C., Simhadri, V. R. & Borrego, F. The Biology and Disease Relevance of CD300a, an Inhibitory Receptor for Phosphatidylserine and Phosphatidylethanolamine. *J. Immunol.* **194**, 5053–5060 (2015).
160. Moller-Tank, S. & Maury, W. Phosphatidylserine receptors: Enhancers of enveloped virus entry and infection. *Virology* **468**, 565–580 (2014).
161. Soares, M. M., King, S. W. & Thorpe, P. E. Targeting inside-out phosphatidylserine as a therapeutic strategy for viral diseases. *Nat. Med.* **14**, 1357–1362 (2008).
162. Emoto, K. *et al.* Redistribution of phosphatidylethanolamine at the cleavage furrow of dividing cells during cytokinesis. *Proc. Natl. Acad. Sci. U. S. A.* **93**, 12867–12872 (1996).
163. Naik, J. *et al.* The P4-ATPase ATP9A is a novel determinant of exosome release. *PLoS One* **14**, e0213069 (2019).
164. Beer, K. B. *et al.* Extracellular vesicle budding is inhibited by redundant regulators of TAT-5 flippase localization and phospholipid asymmetry. *Proc. Natl. Acad. Sci.* **115**, E1127–E1136 (2018).
165. Sulston, J. E., Schierenberg, E., White, J. G. & Thomson, J. N. The embryonic cell lineage of the nematode Caenorhabditis elegans. *Dev. Biol.* **100**, 64–119 (1983).
166. Boulin, T. & Hobert, O. From genes to function: the C. elegans genetic toolbox. *Wiley Interdiscip. Rev. Dev. Biol.* **1**, 114–137 (2012).
167. Sugi, T. Genome Editing in C. elegans and Other Nematode Species. *Int. J. Mol. Sci.* **17**, 295 (2016).
168. Maguire, J. E. *et al.* Myristoylated CIL-7 regulates ciliary extracellular vesicle biogenesis. *Mol. Biol. Cell* **26**, 2823–2832 (2015).
169. Barr, M. M. *et al.* The Caenorhabditis elegans autosomal dominant polycystic kidney disease gene homologs lov-1 and pkd-2 act in the same pathway. *Curr. Biol.* **11**, 1341–1346 (2001).
170. Barr, M. M. & Sternberg, P. W. A polycystic kidney-disease gene homologue required for male mating behaviour in C. elegans. *Nature* **401**, 386–389 (1999).
171. Sato, K., Norris, A., Sato, M. & Grant, B. D. C. elegans as a model for membrane traffic. *WormBook* 1–47 (2014).
172. Nolte-‘t Hoen, E., Cremer, T., Gallo, R. C. & Margolis, L. B. Extracellular vesicles and viruses: Are they close relatives? *Proc. Natl. Acad. Sci.* **113**, 9155–9161 (2016).
173. Takatsu, H. *et al.* ATP9B, a P4-ATPase (a putative aminophospholipid translocase), localizes to the trans-Golgi network in a CDC50 protein-independent manner. *J. Biol. Chem.* **286**, 38159–38167 (2011).
174. Saito, K. *et al.* Cdc50p, a Protein Required for Polarized Growth, Associates with the Drs2p P-Type ATPase Implicated in Phospholipid Translocation in *Saccharomyces cerevisiae*. *Mol. Biol. Cell* **15**, 3418–3432 (2004).
175. Barbosa, S., Pratte, D., Schwarz, H., Pipkorn, R. & Singer-Krüger, B. Oligomeric Dop1p is part of the endosomal Neo1p-Ysl2p-Arl1p membrane remodeling complex. *Traffic* **11**, 1092–1106 (2010).
176. McGough, I. J. *et al.* SNX3-retromer requires an evolutionary conserved MON2:DOPEY2:ATP9A complex to mediate Wntless sorting and Wnt secretion. *Nat. Commun.* **9**, 3737 (2018).

177. Gillingham, A. K., Whyte, J. R. C., Panic, B. & Munro, S. Mon2, a relative of large Arf exchange factors, recruits Dop1 to the Golgi apparatus. *J. Biol. Chem.* **281**, 2273–2280 (2006).
178. Kanamori, T. *et al.* β-Catenin asymmetry is regulated by PLA1and retrograde traffic in C. elegans stem cell divisions. *EMBO J.* **27**, 1647–1657 (2008).
179. Bonangelino, C. J., Chavez, E. M. & Bonifacino, J. S. Genomic Screen for Vacuolar Protein Sorting Genes in *Saccharomyces cerevisiae*. *Mol. Biol. Cell* **13**, 2486–2501 (2002).
180. Avaro, S., Belgareh-Touzé, N., Sibella-Argüelles, C., Volland, C. & Haguenauer-Tsapis, R. Mutants defective in secretory/vacuolar pathways in the EUROFAN collection of yeast disruptants. *Yeast* **19**, 351–371 (2002).
181. Jochum, A., Jackson, D., Schwarz, H., Pipkorn, R. & Singer-Krüger, B. Yeast Ysl2p, homologous to Sec7 domain guanine nucleotide exchange factors, functions in endocytosis and maintenance of vacuole integrity and interacts with the Arf-Like small GTPase Arl1p. *Mol. Cell. Biol.* **22**, 4914–28 (2002).
182. Efe, J. A. *et al.* Yeast Mon2p is a highly conserved protein that functions in the cytoplasm-to-vacuole transport pathway and is required for Golgi homeostasis. *J. Cell Sci.* **118**, 4751–4764 (2005).
183. Emoto, K., Toyama-Sorimachi, N., Karasuyama, H., Inoue, K. & Umeda, M. Exposure of phosphatidylethanolamine on the surface of apoptotic cells. *Exp. Cell Res.* **232**, 430–434 (1997).
184. Irie, A., Yamamoto, K., Miki, Y. & Murakami, M. Phosphatidylethanolamine dynamics are required for osteoclast fusion. *Sci. Rep.* **7**, 46715 (2017).

2. Materials and methods

2.1. Worm culture and strains

Worms where kept in petri dishes at room temperature (22-24°C) on Nematode Growth Media (NGM) seeded with OP50 bacteria using the standard protocols[1]. The temperature-sensitive *rme-8(b1023)* mutants DH1206 and WEH226 were kept in a 15°C incubator. The *unc-119(ed3)* mutant HT1593 was kept in an 18°C incubator on peptone-rich plates before biolistic transformation. After biolistic transformation, the potential transformants were kept at room temperature[2]. To cross worm strains, male *C. elegans* worms were induced by heat shock. For this, worms were incubated at larval stage L3 and/or L4 for three to four hours at 33°C in an incubator. Male worms were crossed to hermaphrodites in a ratio of 4 to 1. F1 hermaphrodites were separated from male siblings at L3 and/or L4 to avoid re-mating. F1-F3 hermaphrodites where genotyped using primers listed in Table 2 and/or analyzed for fluorescence on an Olympus SZX16 or a Leica DM5500 to identify homozygous worms. Maternal-zygotic *bec-1* and *vps-34* mutant embryos were isolated as described[3]. As *vps-34* mutants arrest as larvae, they are rescued by an extrachromosomal array carrying a wild-type copy of the *vps-34* gene[4].

Lethal and sterile mutants were maintained as heterozygotes by crossing to a “balancer” strain. Balancers are chromosome rearrangements that prevent meiotic recombination over large regions[5]. In this study we mostly used the translocation rearrangements nT1 or hT2. The balancer *hT2[bli-4(e937) let-?(q782) pIs48]* has a chromosome translocation at chromosome I and III and was used to maintain sterile and lethal mutants on chromosome I and III. The translocation *nT1[qIs51]* was used to maintain mutants on chromosome IV and V.

Strains used in this study are listed in Table 1. Some worm strains were obtained from Jeremy Nance, Julie Ahringer, Bruce Bowerman, Barth Grant, Zheng Zhou, Zhirong Bao, the National Bioresource Project for the Nematode *C. elegans* (Japan), the *C. elegans* Gene Knockout Project at the Oklahoma Medical Research Foundation, the *C. elegans* Reverse Genetics Core Facility at the University of British Columbia, and the *Caenorhabditis* Genetics Center.

Strain	**Genotype**	**Source**
N2	wild type	Brenner[1]
BV76	*nmy-2::NMY-2::GFP;* *mCherry::PH(PLC1delta1)*	Gift of Zhirong Bao
DH1206	*rme-8(b1023) I*	Zhang[6]
EW0015	*tat-1(kr15:Mos) III*	Ruaud[7]
FT47	*xnIs3[par-6::gfp, unc-119(+)];* *unc-119(ed3) III;* *xnIs8[nmy-2::mCherry, unc-119(+)]*	Gift of Jeremy Nance[8,9]
FT207	*tat-5(tm1741) I / hT2[bli-4(e937) let-?(q782) qIs48] (I; III)*	Wehman[10]
FT598	*xnSi1[mex-5::GFP::PH::nos-2 3'UTR, unc-119] II;* *unc-119(ed3) III;* *xnIs91[pDC05: end-1::mCherry::PH(PLC1delta1)]* *pJN254[unc-119(+)]*	Chihara[11]
FT1091	*unc-119(ed3) III;* *xnIs390 [pie-1::GFP::ZF1::PH(PLC1delta1), unc-119(+)]*	Bombardment
FT1182	*bec-1(ok691) IV / nT1[qIs51] (IV; V)*	Outcrossed from VC517
FT1217	*chc-1(ok2369) III / hT2[bli-4(e937) let-?(q782) qIs48] (I; III);* *xnIs388[pJN578: chc-1p::ZF1::mCh::chc-1, unc-119(+)]*	Gift of Jeremy Nance
FX00847	*snx-1(tm847) X*	Shi[12]
FX01595	*snx-3(tm1595) I*	Harterink[13]
FX02423	*lst-4(tm2423) IV*	Chen[14]
FX14884	*vps-26(tm1523) IV / nT1[qIs51] (IV; V)*	Chen[14]
FX168114	*snx-6(tm3790) V*	Chen[14]
HT1593	*unc-119(ed3) III*	Dickinson[15]
KN555	*vps-35(hu68) II*	Harterink[13]
KN2761	*snx-3(hu256[Y22A]) I; muIs32[pmec-7::GFP + lin-15(+)] II*	McGough[16]
MAD3	*unc-119(-) III;* *dqIs3[pYN08: pie-1::dyn-1b-gfp::pie-1 3' UTR, unc-119(+)]*	Skop[17]
MCP6	*pad-1(babIs1[GFP]) I*	CRISPR/Cas9
OD58	*unc-119(ed3) III;* *ltIs38[pie-1::GFP::PH(PLC1delta1), unc-119(+)]*	Audhya[18]
OD70	*unc-119(ed3) III;* *ltIs44[pie-1p::mCherry::PH(PLC1delta1), unc-119(+)] V*	Kachur[19]
OD178	*unc-119(ed3) III;* *ltIs105[pAA280: pie-1::GFPLAP::MVB-12, unc-119(+)]*	Audhya[20]
PF100	*pie-1::gfp-moesin*	Motegi[21]
RT2277	*unc-119(ed3) III; pwIs834[pID3.01-tat-5a: pie-1::gfp::tat-5a, unc-119(+)] V*	Wehman[10]
RT1952	*pie-1::GFP-snx-1[pID3.01-snx-1]*	Gift of Barth Grant
VC1258	*chat-1(ok1681) IV / nT1[qIs51(myo-2::GFP; pes-10::GFP; F22B7.9::GFP)](IV;V)*	*C. elegans* Gene KO Consortium
WEH02	*ltIs38[pie-1::GFP::PH(PLC1∂1), unc-119(+)]* *xnIs8[pJN343: nmy-2::NMY-2::mCherry, unc-119(+)]* *unc-119(ed3) III*	Fazeli[4]
WEH03	*ltIs38[pie-1::GFP::PH(PLC1∂1), unc-119(+)]* *xnIs8[pJN343: nmy-2::NMY-2::mCherry, unc-119(+)]* *unc-119(ed3) III; bec-1(ok691) IV / nT1[qIs51] (IV; V)*	Fazeli[4]
WEH14	*unc-119(ed3) III;* *wurIs09[mon-2::TY1::GFP::3xFLAG fosmid WRM06 12A_D10]*	Bombardment
WEH51	*unc-119(ed3) III;*	Fazeli[4]

	xnIs65[nmy-2::gfp::zf1, unc-119(+)] IV; *ltIs44[pie1p::mCherry::PH(PLC1∂1), unc-119(+)] V*	
WEH62	*unc-119(ed3) III;* *wurIs45[pie-1::GFP::tat-5 cDNA, unc-119(+)]*	Bombardment
WEH63	*unc-119(ed3) III;* *wurIs46[pie-1::GFP::tat-5c cDNA, unc-119(+)]*	Bombardment
WEH68	*tat-5(tm1741)/hT2[bli-4(e937) let-?(q782) qIs48] I; unc-119(ed3)/hT2 III; wurIs45[pID3.01-tat-5c: pie-1::GFP::tat-5c cDNA, unc-119(+)]*	Crossed WEH62 to FT207
WEH69	*bec-1(ok691) xnIs65[nmy-2::gfp::zf1, unc-119(+)] / nT1 IV;* *ltIs44 [pie-1p::mCherry::PH(PLC1delta1)] / nT1[qIs51] V*	Fazeli[4]
WEH73	*vps-34(h510) dpy-5(e61) I;* *unc-119(ed3) III;* *xnIs65[nmy-2::gfp::zf1, unc-119(+)] IV;* *ltIs44[pie-1p::mCherry::PH(PLC1delta1)] V;* *enEx441[vps-34(+), ced-1C::mRFP]*	Fazeli[4]
WEH95	*unc-119(ed3) III;* *pie-1::mCherry-HistoneH2B;* *xnIs390[pie-1::GFP::ZF1::PH(PLC1delta1), unc-119(+)]*	Crossed EU1436 and FT1091
WEH106	*zbIs2[pie-1::LifeAct::RFP, unc-119(+)] I;* *bec-1(ok691) zuIs45[nmy-2::NMY-2::GFP, unc-119(+)] IV / nT1[qIs51] (IV; V)*	Fazeli[4]
WEH126	*+ / hT2[bli-4(e937) let-?(q782) qIs48] (I;III)*	Crossed FT207 and N2
WEH159	*pad-1(wur02) I / hT2[bli-4(e937) let-?(q782) qIs48] (I; III)*	CRISPR/Cas9
WEH192	*pad-1(wur02) I / hT2[bli-4(e937) let-?(q782) qIs48] (I; III);* *pwIs834[pID3.01-tat-5a: pie-1::gfp::tat-5a, unc-119(+)] V*	Crossed RT2277 and WEH159
WEH222	*unc-119(ed3) III (?);* *bec-1(ok691) / nT1[qIs51] IV; pwIs834[pID3.01-tat-5a: pie-1::gfp-tat-5a, unc-119(+)] / nT1 V*	Crossed RT2277 and FT1182
WEH226	*rme-8(b1023) I;* *pwIs834[pID3.01-tat-5a: pie-1::gfp::tat-5a, unc-119(+)] V*	Crossed DH1206 and RT2277
WEH228	*pad-1(wur04) I*	CRISPR/Cas9
WEH229	*pad-1(wur05) I*	CRISPR/Cas9
WEH238	*pad-1(wur06) I*	CRISPR/Cas9
WEH244	*unc-119(ed3) III;* *mon-2(xh22) IV;* *wurIs09[mon-2::TY1:: GFP::3xFLAG fosmid WRM06 12A_D10]*	Crossed WEH14 and XH2006
WEH254	*pad-1(wur07) I / hT2[bli-4(e937) let-?(q782) qIs48] (I; III)*	CRISPR/Cas9
WEH255	*pad-1(wur07) I / hT2[bli-4(e937) let-?(q782) qIs48] (I; III)*	CRISPR/Cas9
WEH260	*unc-119(ed3) III;* *wurIs90 [pGF7:pie-1::mCh::PH::ZF1, unc-119(+)] V*	Bombardment
WEH263	*unc-119(ed3) III; mon-2(xh22) IV;* *ltIs44[pie-1p::mCherry::PH(PLC1delta1), unc-119(+)] V*	Crossed OD70 and XH2006
WEH264	*pad-1(wur08)/+ I*	CRISPR/Cas9
WEH265	*pad-1(wur09)/+ I*	CRISPR/Cas9
WEH266	*pad-1(wur10)/+ I*	CRISPR/Cas9
WEH280	*vps-26(tm1523) IV;* *pwIs834[pID3.01-tat-5a: pie-1::gfp::tat-5a, unc-119(+)] V*	Crossed FX14884 and RT2277
WEH281	*unc-119(ed3) III; mon-2(xh22) IV;* *pwIs834[pID3.01-tat-5a: pie-1::gfp::tat-5a, unc-119(+)] V*	Crossed RT2277 and XH2006
WEH287	*pad-1(wur12) I*	CRISPR/Cas9
WEH288	*pad-1(wur13) I*	CRISPR/Cas9
WEH289	*pad-1(wur14)/+ I*	CRISPR/Cas9

WEH290	*pad-1(wur15)/+ I*	CRISPR/Cas9
WEH291	*pad-1(wur16)/+ I*	CRISPR/Cas9
WEH293	*unc-119(ed3) III;* *dqIs3[pYN08: pie-1::dyn-1b-gfp::pie-1 3' UTR, unc-119(+)];* *wurIs90[pGF7:pie-1::mCh::PH::ZF1, unc-119(+)] V*	Crossed WEH260 and MAD3
WEH310	*unc-119(ed3) III;* *pwls834[pID3.01-tat-5a: pie-1::gfp::tat-5a, unc-119(+)] V;* *snx-1(tm847) X*	Crossed RT2277 and FX00847
WEH315	*unc-119(ed3) III;* *wurIs111[pGF14: pie-1p::mCherry::unc-108, unc-119(+)]*	Bombardment
WEH316	*snx-3(tm1595) I;* *unc-119(ed3) III;* *wurIs90[pGF7: pie-1::mCh::PH::ZF1, unc-119(+)] V*	Crossed FX01595 and WEH260
WEH318	*unc-119(ed3) III;* *pwIs834[pID3.01-tat-5a: pie-1::gfp-tat-5a, unc-119(+)] V;* *snx-17(tm3779) X*	Crossed FX03779 to RT2277
WEH319	*unc-119(ed3) III;* *snx-17(tm3779) X;* *wurIs90[pGF7:pie-1::mCh::PH::ZF1, unc-119(+)] V*	Crossed FX03779 to WEH260
WEH327	*unc-119(ed3) III;* *wurIs117[pie-1::mCh::2xFYVE, unc-119(+)]*	Bombardment
WEH329	*unc-119(ed3) III;* *pwIs834[pID3.01-tat-5a: pie-1::gfp::tat-5a, unc-119(+)] V;* *wurIs111[pGF14: pie-1p::mCherry::unc-108, unc-119(+)]*	Crossed WEH315 and RT2277
WEH330	*unc-119(ed3) III;* *pwIs834[pID3.01-tat-5a: pie-1::gfp::tat-5a, unc-119(+)] V;* *wurIs117[pie-1::mCh::2xFYVE, unc-119(+)]*	Crossed WEH327 and RT2277
WEH332	*snx-3(tm1595) I, unc-119(ed3) III;* *pwIs834[pID3.01-tat-5a: pie-1::gfp::tat-5a, unc-119(+)] V*	Crossed FX01595 and RT2277
WEH334	*unc-119(ed3) III;* *mon-2(xh22) IV;* *pwIs834[pID3.01-tat-5a: pie-1::gfp::tat-5a, unc-119(+)] V;* *wurIs111[pGF14: pie-1p::mCherry::unc-108, unc-119(+)]*	Crossed WEH281 and WEH315
WEH397	*unc-119(ed3) III;* *wurIs142[pID3.01-tat-5a: pie-1::GFP::tat-5 (W609A), unc-119(+)]*	Bombardment
WEH401	*unc-119(ed3) III;* *wurIs142[pID3.01-tat-5a: pie-1::GFP::tat-5 (W411A), unc-119(+)]*	Bombardment
WEH411	*snx-3(hu256[Y22A]) I;* *wurIs90[pGF7:pie-1::mCh::PH::ZF1, unc-119(+)] V*	crossed KN2761 to WEH269
WEH426	*unc-119(ed3) III;* *wurEx22[pID3.01-tat-5a: pie-1::GFP::tat-5 (Y566D), unc-119(+)]*	Bombardment
WEH427	*unc-119(ed3) III;* *wurEx23[pID3.01-tat-5a: pie-1::GFP::tat-5 (F115A); unc-119(+)]*	Bombardment
WEH428	*unc-119(ed3) wurIs154[pID3.01-tat-5a: pie-1::GFP::tat-5 (Y566D); unc-119(+)] III*	Bombardment
WEH435	*unc-119(ed3) III;* *wurIs156[pID3.01-tat-5a: pie-1::GFP::tat-5 (Y566D), unc-119(+)]*	Bombardment
WEH439	*unc-119(ed3) III;* *xnIs388[pJN578: chc-1p::ZF1::mCh::chc-1, unc-119(+)];* *xnIs390[pie-1::GFP::ZF1::PH(PLC1delta1), unc-119(+)]*	crossed FT1217 to FT1091

WEH452	*tat-5(tm1741) / hT2[bli-4(e937) let-?(q782) qIs48] I;* *unc-119(ed3) wurIs154[pID3.01-tat-5a(Y566D): pie-1::GFP::tat-5(Y566D), unc-119(+)] / hT2 III*	Crossed WEH428 to FT207
WEH453	*unc-119(ed3) III;* *wurIs165[pID3.01-tat-5a F115A: pie-1::GFP::tat-5(F115A), unc-119(+)]*	Bombardment
WEH469	*unc-119(ed3) III;* *wurIs168[pID3.01-tat-5a F570A: pie-1::GFP::tat-5(F570A), unc-119(+)]*	Bombardment
WEH470	*unc-119(ed3) III;* *wurIs169[pID3.01-tat-5a F570A: pie-1::GFP::tat-5(F570A), unc-119(+)]*	Bombardment
WEH471	*unc-119(ed3) III;* *wurIs170[pID3.01-tat-5a F570A: pie-1::GFP::tat-5(F570A), unc-119(+)]*	Bombardment
WEH472	*tat-5(tm1741) / hT2[bli-4(e937) let-?(q782) qIs48] I;* *unc-119(ed3) wurIs156[pID3.01-tat-5a Y566D: pie-1::GFP::tat-5(Y566D), unc-119(+)] / hT2 III*	Crossed FT207, to WEH435
WEH473	*unc-119(ed3) III;* *wurIs171[pID3.01-tat-5a F570D: pie-1::GFP::tat-5(F570D), unc-119(+)]*	Bombardment
WEH474	*unc-119(ed3) III;* *wurIs172[pID3.01-tat-5a F570D: pie-1::GFP::tat-5(F570D), unc-119(+)]*	Bombardment
WEH475	*unc-119(ed3) III;* *wurIs173[pID3.01-tat-5a F570D: pie-1::GFP::tat-5(F570D), unc-119(+)]*	Bombardment
WEH476	*unc-119(ed3) III;* *wurEx31[pID3.01-tat-5a I564D: pie-1::GFP::tat-5(I564D), unc-119(+)]*	Bombardment
WEH477	*unc-119(ed3) III;* *wurIs167[pID3.01-tat-5a Y566Q: pie-1::GFP::tat-5(Y566Q), unc-119(+)]*	Bombardment
WEH478	*unc-119(ed3) III;* *wurIs174[pID3.01-tat-5a Y566Q: pie-1::GFP::tat-5(Y566Q), unc-119(+)]*	Bombardment
WEH479	*tat-5(tm1741) / hT2[bli-4(e937) let-?(q782) qIs48] I;* *unc-119(ed3)? / hT2 III;* *wurIs146[pID3.01-tat-5a W411A: pie-1::GFP::tat-5(W411A); unc-119(+)]*	Crossed FT207 and WEH401
WEH480	*tat-5(tm1741) / hT2[bli-4(e937) let-?(q782) qIs48] I;* *unc-119(ed3) wurIs168[pID3.01-tat-5a F570A: pie-1::GFP::tat-5(F570A); unc-119(+)] / hT2 III*	Crossed FT207 to WEH469
WEH481	*tat-5(tm1741) / hT2[bli-4(e937) let-?(q782) qIs48] I;* *unc-119(ed3) wurIs168[pID3.01-tat-5a F570A: pie-1::GFP::tat-5(F570A); unc-119(+)] / hT2 III*	Crossed FT207 to WEH469
WEH482	*tat-5(tm1741) / hT2[bli-4(e937) let-?(q782) qIs48] I;* *unc-119(ed3 or +) / hT2 III;* *wurIs169[pID3.01-tat-5a F570A: pie-1::GFP::tat-5(F570A); unc-119(+)]*	Crossed FT207 to WEH470
WEH483	*tat-5(tm1741) I;* *unc-119(ed3)? III;* *wurIs146[pID3.01-tat-5a W411A: pie-1::GFP::tat-5(W411A); unc-119(+)]*	Crossed FT207 and WEH401

WEH484	*tat-5(tm1741) / hT2[bli-4(e937) let-?(q782) qIs48] I;* *unc-119(ed3) / hT2 III;* *wurIs169[pID3.01-tat-5a F570A: pie-1::GFP::tat-5(F570A); unc-119(+)]*	Crossed FT207 to WEH470
WEH485	*tat-5(tm1741) / hT2[bli-4(e937) let-?(q782) qIs48] I;* *unc-119(ed3 or +) / hT2 III;* *wurIs170[pID3.01-tat-5a F570A: pie-1::GFP::tat-5(F570A); unc-119(+)]*	Crossed FT207, to WEH471
WEH488	*unc-119(ed3) III;* *wurEx32[pID3.01-tat-5a I564D: pie-1::GFP::tat-5(I564D), unc-119(+)]*	Bombardment
WEH489	*unc-119(ed3) III;* *wurEx33[pID3.01-tat-5a I564D: pie-1::GFP::tat-5(I564D), unc-119(+)]*	Bombardment
XH2006	*mon-2(xh22) IV;* *wIs51[scm::gfp] V*	Kanamori[22]

Table 1: Worm strains used in this study: Strain name, genotype and source are given. Strains that were created for this study were either created using gene bombardment (biolistic transformation), strain crossing or CRISPR/Cas9.

2.2. Worm genotyping

To genotype worms, hermaphrodites were lysed for 1h at 60°C and 15 min for 95°C using single worm lysis buffer and used in a polymerase chain reaction (PCR) to amplify the region of interest with the respective primers.

Single worm lysis buffer:
500 µl 1M KCl
100 µl 1M Tris, pH 8.3
250 µl 100 mM $MgCl_2$
45 µl NP-40
45 µl Tween-20
1 ml 0.1% gelatin
60 µl proteinase K (10 mg/ml)
8 ml ddH_2O

Primers used to genotype worm strains from crosses in this study are listed in Table 2. If necessary, PCR products were digested with restriction enzymes to visualize specific transgenes. The *rme-8* mutation *b1023* was digested with BclI (NEB), the *mon-2* mutation *xh22* with BstXI (Thermo Fisher Scientific), the *snx-3* mutation *hu256* with NdeI (NEB).

Primer name	**Sequence**	**Transgenes genotyped**
bec-1ok691 internal B+	CGGTATTTCCCAACTCCTCAAGT	*ok691*
bec-1 ok691 external F	ACGTAATCGCTCAGTGCC TT	*ok691*
bec-1 exon 6 F	GGCGTACAACATCACGAACTG A	*ok691*
mCherry exon 1R	GCGGTTTGTGTTCCCTCATA	*wurIs111*
mon-2 ex7BstX1F	CACTTTCATTGATGAGACTTCCAGTA	*xh22*
mon-2 intron 7R	CTGTCATGACAATTGCCGGAAA	*xh22*
oJN437	GTTTGAAGGTGATACCCTTG	*pwIs834*
oJN753	GCATTGAACACCATAACAGAAAGTAG	*babIs1*
oKate R1	CGTCTTGGAGGGAGGTGTCTT	*wur08-11*
pad-1 promoter F1	GGCCGAAAATTGAGCCAATCTAGC	*wur02, wur03*
pad-1 promoter F2	TCGAGGTTATTCATGCAATGCGGA	*wur02, wur03*
pad-1 promoter F4	CCGTAACATTTCTCAACTTTCTGCT	*babIs1, wur01-17*
pad-1 promoter F3	TTCACGCTCTTTCCCCCATT	*babIs1*
pad-1 exon 1R	TCCGAGTGCCGAAATGAGAT	*babIs1, wur01-17*
pad-1 exon 2R	GCTGGATGAAGGCATTGTGACA	*wur02, wur03*
pad-1 exon 12F	CGATAGTGAAGCTGACGATGAA	*wur02, wur03*
pad-1 exon 12R	GAATCGCTCGAACATGCCGA	*wur02, wur03*
pad-1 downstream R	TCGCCATTTTCTTGCCAGTTGT	*wur02, wur03*
rme-8 exon 9F	GCGATGAAGGAGAAGTTTGACCA	*b1023*
rme-8 exon 10R	CCTGTATTAATCTCGTTCGGCTGAT	*b1023*
snx-1 exon 1F	GCGATGAGATCAACTTGGGGAA	*tm847*
snx-1 exon 5R	GTCAACTTCGGCTTGTTTCCCA	*tm847*
snx-1 exon 4F	TGGAGAGCAATTGGGGAAGGT	*tm847*
snx-3 exon 1F	CAACTCAGCGGATCCCTTCAAAAC	*tm1595*
snx-3 exon 3R	CATCGGATCGGAATGGCAGTT	*tm1595*
snx-3 downstream R	CGCATTTTGGTGGAGGGATG	*tm1595, hu256*
snx-3 ex1 ATGF	CAGTGCAAATGGCATCCG	*hu256*
snx-6 exon 2F	CAGACGAAGCGATTTGTGTTGA	*tm3790*
snx-6 exon 5R	GCATTGCGACAGTCTTCTTGAA	*tm3790*
snx-6 exon 4R	GTAGCTTCACCTTCACCGAGTT	*tm3790*
snx-17 ex 2F	TGACCCAGCGGATAAGACAAC	*tm3779*
snx-17 ex 3R	CGGGTCCCTTATATCGTTGTGA	*tm3779*
snx-17 ex 6R	CACGTCCTTTTGCCATGAACAA	*tm3779*
snx-27 promoter F	TGTTTCCATCCGTTTGCCTCTT	*tm5678*
snx-27 intron 1R	GTTGTGCAGTTCTAGTTGGGAGT	*tm5678*
snx-27 exon 2R	CCTCCTTCGCTCACTTGTCCTT	*tm5678*
tat-5 geno F	TGCTCCAATCACTTACTGGGGAC	*tm1741*
tat-5 geno R	TACGCGGAGTGAAATTGGAATAA	*tm1741*
tat-5 SL1 exon 1R	AACATGCCTCCCTTGGCAGCAG	*pwIs834*
vps-26 exon 1F	GCTTTGGCCAATCAGCAGAAA	*tm1523*
vps-26 exon 2R	GTCTCCGCGTGCTTTTACAATCT	*tm1523*
vps-26 exon 3R	GACGAGCCAGTTCACGAGTCAA	*tm1523*

Table 2: Primers used to genotype worm strains: Name of the primers, primer sequence and genotyped transgene with the respective primers are listed.

2.3. Plasmid construction

The sgRNA plasmids *pKB03, pKB04* and *pKB06* for CRISPR/Cas9 experiments were amplified from pDD122 with the sgRNA primers listed below (Table 3) in addition to the pDD122 sgRNA R primer using the Q5 site-directed mutagenesis Kit (New England Biolabs), according to Dickinson[15]. The *pie-1::GFP::ZF1::PH* plasmid was constructed by moving the PH domain of rat PLCδ1 from the PH entry vector pJN415 to the *pie-1::GFP::ZF1::Gateway* destination vector pJN371 using Gateway cloning (Invitrogen). The plasmids pGF7 (*pie-1::mCh::PH::ZF1*) and pGF14 (*pie-1::mCh::UNC-108*) were created by Gholamreza Fazeli[23]. The *pie-1::mCh::2xFYVE* plasmid was constructed by amplifying two tandem FYVE domains of EEA-1 from the plasmid pRA017 (gift of Julie Ahringer) using a two-step PCR with primers attB MCS 2xFYVE and attB Stop 2xFYVE, followed by attB1 and attB2 primers. The PCR fragment was then introduced into pDonor221 and pAZ132-*mCh::Gateway* using Gateway cloning. The *pie-1::GFP::TAT-5 cDNA* plasmid was constructed by amplifying whole worm cDNA using the primers tat-5af_nostart and tat-5r_withstop. Using Gateway cloning, the construct was introduced into pDonr221 and pID3.01. All plasmids were cloned using DH5alpha or NEB-alpha cells.

TA cloning was used to construct plasmids for RNAi experiments. For the *rme-8* RNAi plasmid, the *rme-8* primers below were used to clone a 1 kb fragment of *rme-8* from cDNA into the pPD129.36 vector. The resulting plasmid was then transformed into HT115 bacteria for RNAi experiments by Kenneth Kuhn. Primer sequences used to generate plasmids are given in Table 3.

Experiment	**Primer name**	**Sequence**
pKB3(ATG2)	*pad-1 ATG sgRNA2*	AAATGGCATCAGCATCAGGgttttagagctagaaatagcaagt
pKB4(Stop1)	*pad-1 Stop sgRNA1*	GCCGTGGCCCGACTCGAATgttttagagctagaaatagcaagt
pKB6(Stop6)	*pad-1 Stop sgRNA6*	CTCGAATCGGCTCTCTACGgttttagagctagaaatagcaagt
pie-1::mCh::2xFYVE	*attB MCS 2xFYVE*	aaaaagcaggcttcAGCCCACAAGCTTTGGAATTCA
	attB Stop 2xFYVE	agaaagctgggttaGTATGGCCGGCTAGCTTTCT
pie-1::mCh::2xFYVE	*attB1*	ggggacaagtttgtacaaaaaagcaggct
	attB2	ggggaccactttgtacaagaaagctgggt
pie-1::GFP::TAT-5 cDNA	*tat5af_nostart*	ggggacaactttgtacaaaaaagttgTGGGCAAACGGAAGAAGAACGAC
	tat5r_withstop	ggggacaactttgtacaaaaaagttgTCAGTTGACTTTCGCGTAGCTTG
pPD129.36-rme-8	*rme-8 F*	GCGATGAAGGAGAAGTTTGACCA
	rme-8 R	CCTGTATTAATCTCGTTCGGCTGAT
CRISPR/Cas9 Homology repair template I	*hdr5'Kate2 pad-1*	tgctcaaattcaaagaaaaattgcagaaagaaataagaaATGGTCTCCGAGCTCATTAAAGAAAAC
	hdr3'Kate2 pad-1	ctatctttttctcgacccgctggtacatctg**c**ACCTGATGCTGATGCCTCACGGTGTCCGAGCTTGGA T
CRISPR/Cas9 Homology repair template II	*Kate pad-1 F3*	caaagaaaaattgcagaaagaaataagaaatggcatcagcatcaGTCTCCGAGCTCATTAAAGAAAACA
	Kate pad-1 R3	gcacgatatttactatctttttctcgacccgctggtacatctccacctGCACGGTGTCCGAGCTTGGAT
GFP::PAD-1 knock-in homology repair template	*oMCP039F*	aaagaaaaattgcagaaagaaataagaaATGAGTAAAGGAGAAGAACTTTTC
	oMCP040R	gccgctggtacatctgcacctgatgctgatgcTTTGTATAGTTCATCCATGC
	oMCP041R	gtatgcacgatatttactatctttttctcgagccgctggtacatctgcacc
Amplify RNAi Inserts	*T7*	GTAATACGACTCACTATAGGGC

Table 3: Primers used to construct plasmids and DNA templates. The purpose of the plasmid is noted in Experiment. F at the end of the primer name indicates forward, R indicates reverse primer. Primer sequence homologous to the transgene is in capital, lower case indicates DNA sequence homologous to the plasmid backbone. Substitutions are bold and underlined.

To mutate potential SNX-binding sites of GFP::TAT-5, potential SNX-3 and SNX-6 binding sites were identified by sequence homology and listed in Table 4. Q5-site directed mutagenesis was used to introduce substitution in the *tat-5* DNA sequence to mutate potential sorting nexin binding motifs. The genomic sequence was either substituted to “gcc”, the codon used for Alanine (A), “gac” or “gat” for Aspartic Acid (D) or “caa” for Glutamine (Q). Substitutions are numbered according to *tat-5* isoform a. Substitutions were introduced in the forward primer and used with a back-to-back reverse primer to amplify and mutate *tat-5* from the plasmid pDonr221-*tat-5a* using around the world PCR (Table 4). All exons of the *tat-5* plasmids were sequenced. If the correct substitution were detected and no other exons were mutated, the constructs were moved into pID3.01-*pie-1::GFP::Gateway* destination vector and used for biolistic transformation.

Construct name	Motif	Primer name	Sequence
pID3.01 tat-5a F115A	FS**F**	*tat-5 F115A F5*	TAACATTTTCAGTgccGTGCCAATTGTAAGTGA
		tat-5 F115A R5	TATTTCTGATTGCACACTGTGTTTGGTGT
pID3.01 tat-5a W411A	YS**W**	*tat-5 W930A F*	CTTCTACTCGgccCAAATTGGTCGTGAC
		tat-5 W411A R2	GAGTTTAGCCATGTCGAGATTTAC
pID3.01 tat-5a I564D	**I**LYVF	*tat-5 I564D F*	ACAATTCCAGgaTCTTTATGTATTCCCAT
		tat-5 I564 R	TTCATCAATGTCTGTCCATTTGG
pID3.01 tat-5a Y566D	IL**Y**VF	*tat-5 Y562D F*	CCAGATTCTTgacGTATTCCCATTTACATCAGAAAC
		tat-5 Y566Q F	CCAGATTCTTcaaGTATTCCCATTTACatcaga
		tat-5 Y562D R	AATTGTTTCATCAATGTCTGTCCATTTGG
pID3.01 tat-5a F568D	ILYV**F**	*tat-5 F568D F*	ATTCCAGATTCTTTATGTAgacCCATTTACATCAGAAAC
		tat-5 F568D R	TGTTTCATCAATGTCTGTCCATTTG
pID3.01 tat-5a F570A	FP**F**	*tat-5 F1512A F*	TGTATTCCCAgccACATCAGAAACAAAAC
		tat-5 F570D F	TGTATTCCCAgaTACATCAGAAACAAAACGAA
		tat-5 F1512 R	TAAAGAATCTGGAATTGTTTC
pID3.01 tat-5aW609A	WL**D**	*tat-5 W609A F3*	ATATAATGATgccTTAGATGAAGAATGTAGTAATATGGC
		tat-5 W609A R3	TGAACCATTCCACTCATTAC

Table 4: Plasmids for mutating TAT-5 sorting nexin binding motifs. Amino acids that are mutated in the indicated motifs are in bold. The primer name indicates the original amino acid of the motif, the position in the protein sequence followed by the amino acid it will be mutated to. F at the end of the primer name indicates the forward primer, R indicates the reverse primer followed by the primer number. Lower case in the DNA sequence indicates the mutated sequence region, upper case indicates the wild type *tat-5* sequence.

2.4. CRISPR/Cas9-mediated genome editing

The *pad-1* deletion allele *wur02* and *wur03* were obtained by injecting 50 ng/µl of each of the three Cas9 + sgRNA plasmids pKB3(ATG2), pKB04(Stop1) and pKB06(Stop6) (see Table 3) as well as the pRF4[*rol-6(su1006d)*] marker into N2 young adults to delete 24 kb of *pad-1* genomic sequence. For *wur02*, a 23.6 kb deletion was verified by sequencing and includes the following 21 bp insertion (capital letters) between the break sites (lowercase):

gaaagaaataagaaatggcatcagcGTGGATTAGGCATCAGCGTGGcgtggatttttctgaacatttgcaa

The heterozygous *wur02* deletion strain was crossed with WEH126 to balance the sterile mutant and generate the WEH159 strain. The *wur03* allele had a 23.3 kb deletion verified by sequencing. 238 bp of the last intron and the complete last exon of *pad-1* remained. Lowercase represents the *pad-1* sequences between the break sites, capital letters indicate the remaining *pad-1* sequence after the break point:

aataagaaatggcatcagcTTCGAGACCCATTCGAGTAATTCCGTGCGCCTTTAGGAAGAAA
ATTAAGGAAAAAGTGTTTTTTGTCGAAAAACTTGTCAAAAAACCGGAAAATTGAG
GAATTTTGAGCTAGAAAATTATAAAATTCGCTGTAAAAAAATCAGAAGTTCCCAT
AGATTTTGAAATTTTTAAGAAAAAAAGCGATTTTTATCGCGATATATCGAAAAAC
TTGCCATTTTTTAACCCAAATTTTTTCCAGAACACACTCCGCGACGCTCACGCTCT
CTCCGGAAGCCTTACCTACAAAAACGCCGTGGCCCGACTCGAATCGGCTCTCTAcg
tggatttttctgaacatttgcaa

Because homozygous *wur03* worms are sterile, the heterozygous *wur03* worms were also crossed to WEH126 to generate the balanced WEH160 strain.

To generate *wur04-wur11*, the plasmids pKB3(ATG2) and a homology template of mKate2 together with the pRF4[*rol-6(su1006d)*] marker was injected in young adult N2 worms. For *wur04-wur08*, pKB3(ATG2) and pRF4[*rol-6(su1006d)*] were each injected at 50 ng/µl and the homology template of mKate2 at 230 ng/µl. For *wur09-wur11* all constructs were injected at a concentration of 50 ng/µl. The homology template was amplified by PCR from pDD285[mKate2-C1-SEC-3xFlag][24] (derived from Addgene) using the primer *hdr5'Kate2 pad-1* and *hdr3'Kate2 pad-1* (Table 3). DNA quality of a subvolume of the amplification was tested on an agarose gel. PCRs with a single bright band were combined in one tube and extracted using the QiaQuick PCR Purification Kit (Qiagen). To create *wur12-wur16*, pKB3(ATG2) and a homology template were injected at a concentration of 50 ng/µl each together with the pRF4[*rol-6(su1006d)*] marker at 100 ng/µl. The homology template was amplified from pDD285 using the primers *Kate pad-1 F3* and *Kate pad-1 R3*. All mutant alleles were isolated and verified by sequencing (see chapter 5 Table 2). Names of the worm strains with the respective alleles are listed in Table 1. The strains of *wur04-wur06* and *wur12-wur13* were kept as homozygous lines because they are fertile. Because *wur07-wur10* and *wur14-16* worms were also mostly sterile, they were maintained as heterozygous lines or crossed to WEH126 to create balanced strains WEH254 and WEH255. The line *wur11* could not be maintained because the founder worm was sterile, but contained the same mutation as *wur10*.

The GFP::PAD-1 strain MCP6 was generated by Maïté Carre-Pierrat at the University Claude Bernard in Lyon, France using CRISPR/Cas9 to knock eGFP with introns into the N-terminus of PAD-1 as described by Paix *et al.* 2014[25]. Briefly, N2 worms were injected with *pad-1* ATG sgRNA2 and a PCR repair template amplified from pPD95.75 with the nested primers oMCP039F, oMCP040R, and oMCP041R. Correct insertion of GFP was verified by sequencing. The MCP6 strain is fertile and viable, unlike *pad-1* deletion mutants, indicating that GFP insertion does not disrupt the essential functions of PAD-1.

2.5. Worm biolistic transformation

Transgenic strains were made by biolistic transformation (Bombardment) of the HT1593 strain using a Bio-Rad PDS 1000 by standard methods[2]. Briefly, plasmids for biolistic transformation were extracted from bacteria using the Wizard MidiPrep kit (Promega). 1 mg/µl plasmid DNA was mixed with gold beads and spermidine to blast onto young adult HT1593 worms. The FT1091 strain was generated by bombardment with *pie-1p::GFP::ZF1::PH* plasmid, WEH62 and WEH63 with *pie-1::GFP::tat-5c cDNA*, and WEH327 with *pie-1p::mCh::2xFYVE,* WEH397 with *pie-1::GFP::tat-5(W609A)*, WEH401 with *pie-1::GFP::tat-5(W411A),* WEH476, WEH488 and WEH489 with *pie-1::GFP::tat-5(Y564D),* WEH428 and WEH435 with *pie-1::GFP::tat-5(Y566D),* WEH477 and WEH478 with *pie-1::GFP::tat-5(Y566Q),* WEH419 with *pie-1:GFP::tat-5(F568D)*, WEH421, WEH469, WEH470, WEH471 with *pie-1::GFP::tat-5(F570A),* WEH473, WEH474 and WEH475 with *pie-1::GFP::tat-5(F570D),* WEH427, WEH449, WEH450 and WEH453 with *pie-1::GFP::tat-5(F115A).*The WEH14 MON-2::GFP::3xFlag strain was generated by bombardment with the following GFP-tagged fosmid from the TransgenOme project[26]:

WRM06_12A_D10(pRedFlp-Hgr)
(F11A10.4[28269]::S0001_pR6K_Amp_2xTY1ce_EGFP_FRT_rpsl_neo_FRT_3xFlag)
dFRT::unc-119-Nat.

2.6. Protein knockdown by RNA interference

RNAi was performed by feeding L1 larvae through adulthood at 25°C, as described previously[27]. Control worms were fed with the empty RNAi vector pPD129.36 in HT115 bacteria. For *rme-8* RNAi, worms were treated starting at the L3 stage to avoid sterility or larval lethality. The following RNAi clones were used from available libraries (Source BioScience): *arl-1* (JA:54C9.1), *bec-1* (MV:T19E7.3) *mon-2* (JA:F11A10.4), *lst-4* (JA:Y37A1B.2 & MV:Y37A1B.2), *pad-1* (JA:Y18D10A.13 & MV:Y18D10A.15, provided by Reinoud de Groot), *pad-1*(pPD129.36-pad-1) (covers exon 20-22, made from cDNA,), *snx-1* (MV:C05D9.1), *snx-3* (JA:W06D4.5), *snx-6* (MV:Y59A8B.22), *snx-17* (JA:X-6M05), *snx-27* (MV:F25H2.10), *tat-5* (JA:F36H2.1), *vps-4* (JA:Y34D9A.152.a) *vps-26* (JA:T20D3.7), *vps-29* (JA:ZK1128.8 & MV:ZK1128.8), *vps-34* (MV:B0025.1a); *vps-35* (JA:F59G1.3).

For double RNAi, constructs were PCR amplified using T7 primers (Table 3) and then transcribed into RNA using T7 RNA Polymerase and RNase Inhibitor Ribolock (both from Thermo Fisher Scientific). DNA was removed with DNase (Thermo Fisher Scientific) and RNA was cleaned using standard Phenol Chloroform extraction. Briefly, DEPC Water and Phenol:Chloroform:Isoamyl Alcohol 15:24:1 were added to the RNA mix (Thermo Fisher Scientific). After centrifugation, the top phase was mixed with 3M potassium acetate and 100% ethanol. RNA Precipitation was done overnight at -20ºC. The centrifuged RNA pellet was cleaned using 75% ethanol and was resuspended in DEPC water. To anneal double-stranded RNA, RNA preps were boiled and slowly cooled to room temperature. For *snx-17/snx-27* double RNAi *snx-17*(JA:X-6M05) and *snx-27*(MV:F25H2.10) RNAi constructs were used to generate dsRNA (done by Jiapei Chen). For *pad-1* and *vps-4* double RNAi we used adult *pad-1*(pPD129.36-pad-1) and *vps-4*(JA:Y34D9A.152a) RNAi to generate dsRNA. Adult worms were injected with 1 µg/µl total dsRNA and incubated at room temperature for >16 hours before observation on the microscope.

2.7. Immunohistochemistry of fixed worm tissues

Embryos were extracted by cutting hermaphrodites in M9 and washed three times in M9. Embryos were freeze-fractured, fixed in methanol or methanol plus paraformaldehyde fixative, and stained as described previously[4]. Briefly, slides with fixed embryos were rinsed and washed in PBS+0.05% Triton twice for 10 min each. Incubation with the primary antibody was either 2h at room temperature or overnight at 4°C. This was followed by one rinse and three times washing in PBS+0.05% Triton for 10 min each. Incubation with the secondary antibody was also either conducted for 2h at room temperature or overnight at 4°C. This was followed by one rinse and two times washing in PBS+0.05% Triton for 10 min each and finally a 10 min wash in PBS+0.05% Triton and 3 µl of 50 µg/ml DAPI to stain DNA. Embryos were mounted in DABCO and slides were protected from evaporation by sealing with nail polish. Antibodies used in this study are listed in the following tables (Table 5 for primary antibodies, Table 6 for secondary antibodies).

Antibody Staining Buffer (ASB)
400 mg BSA
4 ml 10x PBS
4 ml Normal Donkey Serum
20 µl Triton-X
200 µl 10% NaN3
ddH2O up to 40 µl

10% Paraformaldehyde
100 mg Paraformaldehyde
40 µl NaOH
ddH_2O up to 1 ml

Fixative
100 µl 1 M EDTA
96 µl 0.5 M PIPES
50 µl 0.5 M HEPES
20 µl 100 mM $MgCl_2$
370 µl 10% Paraformaldehyde
382 µl ddH_2O

Primary Antibodies			
Antibody	**Lot Number**	**Source**	**Concentration**
chicken α-GFP	0511FP12	Aves	1:200, 1:500, 1:1000
rabbit α-GFP	ab6556	Abcam	1:200
rabbit α-VPS-32	-	gift of Renaud Legouis[28]	1:1000
mouse α-CAV-1	-	Developmental Studies Hybridoma Bank[29]	1:10
mouse α-DYN-1	-	Developmental Studies Hybridoma Bank[29]	1:10
mouse α-ERM-1	-	Developmental Studies Hybridoma Bank[29]	1:20
mouse α-LMP-1	-	Developmental Studies Hybridoma Bank[29]	1:5
mouse α-RME-1	-	Developmental Studies Hybridoma Bank[29]	1:10

Table 5: Primary Antibodies used in this study. All antibodies were diluted in ASB at the given concentrations.

Secondary Antibodies				
Antibody	**Catalog Number**	**Lot Number**	**Source**	**Concentration**
Alexa Fluor® A488 Donkey Anti-Chicken (IgG)	703-545-155	108862	Jackson ImmunoResearch	1:200
Alexa Fluor® A488 Donkey Anti-Mouse IgG	715-545-151	108424	Jackson ImmunoResearch	
Cy3™ Goat Anti-Mouse IgG	115-165-164	101114	Jackson ImmunoResearch	
Cy3 Donkey anti Rabbit	711-165-152	109623	Jackson Immuno Research	
A488 Donkey anti Rabbit	711-545-152	109117	Jackson Immuno Research	
A488 Chicken anti Rabbit	A-21441	470144	Molecular Probes	
A568 Donkey anti Rabbit	A10042	685254	Molecular Probes	

Table 6: Secondary Antibodies used in this study. All antibodies were diluted in ASB at the given concentrations.

2.8. Lipid externalization measurements

L3-L4 worms were isolated one day before lipid staining. Gonads were dissected from young adult worms in embryonic culture medium (ECM) and were washed twice in ECM. Duramycin staining was performed by incubating dissected gonads from young adult worms in 0.25 µg/mL biotinylated duramycin (gift of Philip Thorpe[30]) and 1 µg/mL Alexa488-Streptavidin (Invitrogen) in ECM for 30 min at room temperature in the dark. The gonads were then washed twice in ECM before mounting on slides in ECM. Annexin V staining was performed by incubating dissected gonads in 1:100 Alexa488-Annexin V (Invitrogen) for 30 min, washing in ECM twice and mounting on slides in ECM. Images were taken in a stereotyped manner (Fluorescence exposure time: 193.87 msec, Gain: 2, FIM: 55%). For lipid externalization measurements, membranes were chosen blindly from DIC or mCh::PH images and the mean fluorescence intensities were measured along three membranes of the same gonad using Fiji. The three measurements were averaged to obtain the final intensity. All measurements were normalized to the vector control of the OD70 strain.

ECM

12 µl	100x Penn-Strep solution
900 µl	L15 culture medium
100 µl	Fetal calf serum
50 µl	20% Sucrose

2.9. Vesicle size measurements

For the analysis of extracellular vesicle size in chapter 3 Fig.8 and multivesicular endosome and lysosome size in chapter 5 Fig.18, the perimeter of each vesicle was measured in a circle traced on TEM images using Fiji[31]. The diameter of each vesicle was calculated from the perimeter.

2.10. Colocalization measurements

To measure colocalization of GFP::TAT-5 with LMP-1 or UNC-108 in chapter 4 Fig. 4 and chapter 5 Fig. 20, deconvolved and thresholded z-stacks of stained embryos were analyzed using the colocalization tool of Imaris. Confocal images of live embryos used to measure colocalization with 2xFYVE in chapter 5 Fig.19 were not deconvolved, because of high vesicle motility. The whole embryo excluding the eggshell was defined as the region of interest from which the Pearson's coefficient and percentage of colocalized GFP::TAT-5 voxels was calculated. The background was masked in Imaris to only measure colocalization in 2- to 12-cell embryos. The line scans in chapter 4 Fig. 4 and chapter 5 Fig. 20 were measured in Fiji using Multi Plot with a one-pixel width straight or free-hand line to trace large TAT-5 vesicles. In chapter 5 Fig.19, line scans were measured using a 4-pixel width straight or freehand line. Colocalization of large GFP::TAT-5 vesicles with 2xFYVE, UNC-108 or LMP-1 puncta was counted manually per embryo from *mon-2* mutants after *snx-6* RNAi for chapter 5 Fig.20.

2.11. Image adjustments

For clarity, all images were cropped, rotated and the intensity was adjusted using Adobe Photoshop. In chapter 5 Fig. 6, Fig. 9, Z-stacks were deconvolved using 3D deconvolution in the Leica LAS AS software. Huygens Professional compute engine (version 17.04.op5 64b) was used to deconvolve Fig. 4 in chapter 4 and Fig. 19 and 20 in chapter 5. In chapter 5, several Z's were projected for Fig. 6 to span a region of approximately 600 nm, 3 z's were projected in Fig. 8 covering approximately 600 nm, 5z's were projected in Fig. 9 spanning a region of 1 µm, several Z's were projected in Fig.13: A) spans a region of 9 µm, B) 4.7 µm and C) 6.6 µm to be able to show all midbodies. Only one Z is shown in all other figures.

2.12. Statistics

Box and Whisker plots were generated using Microsoft Excel, with the lower quartile and upper quartile separated by the median. Whiskers represent the lowest and highest values, with the exception of outliers depicted with a circle. Outliers represent values above or below 1.5 times the width of the interquartile range. Error bars display standard error of the mean in chapter 4 Fig. 3F and chapter 5 Fig. 10E and standard deviation in chapter 4 Fig. 4C-D and 4G-H and in chapter 5 Fig. 19C-D and Fig. 20B-C, E-G. For statistical analyses, Student's one-tailed *t*-test or Student's two-tailed *t*-test with Bonferroni correction to adjust for multiple comparisons or 2-tailed Fisher's exact test was used. If a statistical test was used, the used test is indicated in the text and in the figure legend.

2.13. TAT-5 localization and levels measurements

Worms were dissected in M9 and mounted on an agar pad. To measure the localization of TAT-5 to the plasma membrane, images of 1z of live 2- to 4-cell embryos were taken with a

75% fluorescent lamp intensity to reduce photobleaching. The mean fluorescence intensity of GFP::TAT-5 was measured on the cell contact of 2- and 4-cell embryos in Fiji. In 4-cell embryos, the cell-cell contact with the clearest plasma membrane fluorescence was measured. If the plasma membrane was not visible due to GFP::TAT-5 mislocalization, the plasma membrane was traced using DIC. The mean intensity in the cytoplasm was then measured with the same size line three steps away from the plasma membrane in both neighboring cells. Data is presented as the ratio of the mean fluorescence on the cell contact to the average of the neighboring cytoplasm.

To measure total GFP::TAT-5 levels, one z of 2- to 4-cell embryos were thresholded in Fiji[31] to measure the integrated density in the whole embryo excluding the eggshell. As TAT-5 accumulates on EVs, all *pad-1* RNAi embryos with visibly increased EV release were excluded from quantification.

2.14. PAD-1 and TAT-5 antibody design

Peptide antibodies were designed for the N- and C-terminal regions of both TAT-5 and PAD-1 and ordered from Davids Biotechnology. For PAD-1 peptides, sequences were chosen that recognizes the conserved Dopey domain at the N-term and the disordered region at the C-term that have no similarity to other *C. elegans* proteins. For TAT-5 peptides, a N- and C-terminal sequences were chosen that should recognize all three isoforms of TAT-5 plus TAT-6, but have no homology to other P4-ATPases in worms. The peptides used for antibody synthesis are listed in Table 7. For each peptide, two animals were immunized, creating two antibodies per peptide. To analyze the binding specificity in fixed embryo tissues, antibody staining was conducted with a final concentration of 5 μg/ml of the antibodies and 1 μg/ml for western blots.

Localization	Peptide
TAT-5 N-term	RSLFSRRRVLHSRTVRVGYGP, RRRVLHSRTVRVGYGPVGHDA
TAT-5 C-term	KALRRKFSPPSYAKVN
PAD-1 N-term	GREKDSKYRAYAKAIDQALK, AKFDKLKSLDDQIHLVGDH
PAD-1 C-term	LAERLTDLLDSVSKSDEKDK, DKTEIFKPFAERINDLLAKK, RDAHALSGSLTYKNAVARLES

Table 7: PAD-1 and TAT-5 synthesized peptides for antibody generation

2.15. *C. elegans* protein extraction

Gravid worms were washed from plates using M9 buffer and were collected in protein low-bind tubes. The worms were rinsed twice in M9 to remove bacteria from the buffer. Worms were incubated for about 30 min in M9 on a rocker, to digest most intestinal bacteria. Excess M9 was removed and worms were pipetted dropwise in a liquid-nitrogen containing falcon tube. Before freezing, 100 µl of the worm pellet was pipetted onto a glass slide to count the number of worms and extrapolate the total amount of worms in the pellet. Worm pellets were stored at -80ºC. For small worm protein extracts (~ 100 µl worms), the Eppendorf protein low-bind tube containing the worms was put into liquid nitrogen and then stored at -80ºC. The weight of the pellet was measured and an equal amount of 2x Laemmli buffer was added. 2x Laemmli Buffer was diluted from 5x Laemmli Buffer (see recipe below). The worm pellets were homogenized with a clean pestle. Extracts for the cytosolic protein PAD-1 were boiled for 15 min, vortexed and centrifuged at 10000g for 5 min. Samples for the transmembrane protein TAT-5 were also centrifuged, but not boiled to avoid the formation of insoluble aggregates. The liquid phase was used to load onto a polyacrylamide gel.

5x Laemmli Buffer

1.5 ml	300 mM Tris pH 6.8
2.5 ml	40% Sodium dodecyl sulfate (SDS)
5 ml	50% glycerol
2.5 ml	25% β-Mercaptoethanol
Spatula tip	Bromophenol blue

2.16. Western Blots

8% Polyacrylamide (PAA) separating gels were poured in a Mini-PROTEAN system (Bio-Rad) and topped with 100% Isopropanol. After 30 min and completed polymerization, a 4% PAA stacking gel was poured on top of the separating gel and incubated for 30 min. The gel was put in the running chamber containing Running buffer. Approximately 10 worms worth of protein extract were loaded in each well. After separation of the proteins by electrophoresis, proteins were transferred onto a nitrocellulose membrane in 1x Transfer buffer containing methanol overnight at 4ºC. The membrane was rinsed in distilled water and stained for 3 min in Ponceau Red. The staining was washed three times in water and then documented as a protein loading control. To control for successful transfer, the gel was rinsed in water three times and stained in Coomassie for 2h. The gel was rinsed three times in 10% acetic acid, three times in water and stored at 4 ºC. The nitrocellulose membrane was cut in TBST as needed. Blots were blocked in TBST with 5% milk for 2h at room temperature. Blots were incubated with the primary antibodies in 5% milk TBST and 0.02% NaN3 overnight at 4 ºC (Table 8). Blots were rinsed and washed four times for 10 min each in TBST before incubation in secondary antibodies containing horse radish peroxidase in 5% milk TBST for 1h at room temperature. Blots were rinsed and washed three times for 10 min each in TBST before detection using Electrochemiluminescence (ECL) substrate (Bio-Rad).

100x Running Buffer
30.27 g Tris base
144 g Glycine
1L ddH$_2$O

TBST
100 ml 10x TBS
900 ml ddH$_2$O
1 ml Tween

10x Transfer Buffer
146.5 g Glycine
290.5 g Tris Base
18.75 g SDS
Methanol up to 5l

1x Transfer Buffer
100 ml 10x Transfer Buffer
700 ml ddH$_2$O
200 ml Methanol

Ponceau Red staining solution
0.1% Ponceau S
5% Acetic Acid

Coomassie staining solution

0.1%	Coomassie Brilliant Blue G-250
25%	Isopropanol
10%	Acetic Acid

	Primary Antibodies			
Antibody	**Source**	**Catalog Number**	**Lot Number**	**Dilution**
Rabbit anti GFP	Abcam	ab6556	-	1:500, 1:1000
Mouse anti actin	Sigma	A4551	122M4782	1:10000
	Secondary Antibodies			
Donkey anti rabbit HRP	Jackson ImmunoResearch	711-035-152	121911	1:5000
Sheep anti mouse HRP	GE Healthcare	UK RPN4201V	9532441	1:5000

Table 8: Antibodies used for Western Blots

2.17. Light microscopy

Most fluorescent images were taken on a Leica DM5500 wide-field fluorescence microscope with a HC PL APO 40X 1.3 NA oil objective or a HCX PL APO 63X 1.4 NA glycerol objective with a Leica DFC365 FX CCD camera controlled by LAS AF software. All immunochemistry and live images were taken with 100% fluorescent lamp intensity. For TAT-5 plasma membrane localization measurements all images were taken at 75% lamp intensity to reduce phototoxicity. Live colocalization images in chapter 5 Fig. 19A-B were collected simultaneously on a Leica SP8 confocal with a HC PL APO CS2 63X 1.2 NA water objective with HyD detectors, provided by the imaging facility of the RVZ.

2.18. Electron microscopy

Electron micrographs were obtained from high-pressure frozen, freeze-substituted, gravid adults, as described previously[10]. Tilt series were collected on a 200 kV JEM-2100 transmission electron microscope (JEOL) equipped with a TemCam F416 4k×4k camera (Tietz Video and Imaging Processing Systems) running Serial EM software[32], provided by the EM facility at the Biocenter in Würzburg. Tomograms were computed using eTomo and IMOD software[33].

2.19. References

1. Brenner, S. The genetics of Caenorhabditis elegans. *Genetics* **77**, 71–94 (1974).
2. Praitis, V., Casey, E., Collar, D. & Austin, J. Creation of low-copy integrated transgenic lines in Caenorhabditis elegans. *Genetics* **157**, 1217–1226 (2001).
3. Lu, N. *et al.* Two PI 3-Kinases and One PI 3-Phosphatase Together Establish the Cyclic Waves of Phagosomal PtdIns(3)P Critical for the Degradation of Apoptotic Cells. *PLoS Biol.* **10**, e1001245 (2012).
4. Fazeli, G., Trinkwalder, M., Irmisch, L. & Wehman, A. M. C. elegans midbodies are released, phagocytosed and undergo LC3-dependent degradation independent of macroautophagy. *J. Cell Sci.* **129**, 3721–3731 (2016).
5. Edgely, M. Genetic balancers. *WormBook* (2006). doi:10.1895/wormbook.1.89.1
6. Zhang, Y., Grant, B. & Hirsh, D. RME-8, a conserved J-domain protein, is required for endocytosis in Caenorhabditis elegans. *Mol. Biol. Cell* **12**, 2011–2021 (2001).
7. Ruaud, A. F. *et al.* The C. elegans P4-ATPase TAT-1 regulates lysosome biogenesis and endocytosis. *Traffic* **10**, 88–100 (2009).
8. Anderson, D. C., Gill, J. S., Cinalli, R. M. & Nance, J. Polarization of the C. elegans embryo by RhoGAP-mediated exclusion of PAR-6 from cell contacts. *Science* **320**, 1771–4 (2008).
9. Nelson, M. D. *et al.* A bow-tie genetic architecture for morphogenesis suggested by a genome-wide RNAi screen in Caenorhabditis elegans. *PLoS Genet.* **7**, e1002010 (2011).
10. Wehman, A. M., Poggioli, C., Schweinsberg, P., Grant, B. D. & Nance, J. The P4-ATPase TAT-5 inhibits the budding of extracellular vesicles in C. elegans embryos. *Curr. Biol.* **21**, 1951–1959 (2011).
11. Chihara, D. & Nance, J. An E-cadherin-mediated hitchhiking mechanism for C. elegans germ cell internalization during gastrulation. *Dev.* **139**, 2547–2556 (2012).
12. Shi, A. *et al.* Regulation of endosomal clathrin and retromer-mediated endosome to Golgi retrograde transport by the J-domain protein RME-8. *EMBO J.* **28**, 3290–3302 (2009).
13. Harterink, M. *et al.* A SNX3-dependent retromer pathway mediates retrograde transport of the Wnt sorting receptor Wntless and is required for Wnt secretion. *Nat. Cell Biol.* **13**, 914–923 (2011).
14. Chen, D. *et al.* Retromer is required for apoptotic cell clearance by phagocytic receptor recycling. *Science* **327**, 1261–1264 (2010).
15. Dickinson, D. J., Ward, J. D., Reiner, D. J. & Goldstein, B. Engineering the Caenorhabditis elegans genome using Cas9-triggered homologous recombination. *Nat. Methods* **10**, 1028–1034 (2013).
16. McGough, I. J. *et al.* SNX3-retromer requires an evolutionary conserved MON2:DOPEY2:ATP9A complex to mediate Wntless sorting and Wnt secretion. *Nat. Commun.* **9**, 3737 (2018).
17. Nakayama, Y. *et al.* Dynamin Participates in the Maintenance of Anterior Polarity in the Caenorhabditis elegans Embryo. *Dev. Cell* **16**, 889–900 (2009).
18. Audhya, A. *et al.* A complex containing the Sm protein CAR-1 and the RNA helicase CGH-1 is required for embryonic cytokinesis in Caenorhabditis elegans. *J. Cell Biol.* **171**, 267–279 (2005).
19. Kachur, T. M., Audhya, A. & Pilgrim, D. B. UNC-45 is required for NMY-2 contractile function in early embryonic polarity establishment and germline cellularization in C. elegans. *Dev. Biol.* **314**, 287–299 (2008).
20. Audhya, A., McLeod, I. X., Yates, J. R. & Oegema, K. MVB-12, a fourth subunit of metazoan ESCRT-I, functions in receptor downregulation. *PLoS One* **2**, e956 (2007).
21. Motegi, F., Velarde, N. V., Piano, F. & Sugimoto, A. Two Phases of Astral Microtubule Activity during Cytokinesis in C. elegans Embryos. *Dev. Cell* **10**, 509–520 (2006).
22. Kanamori, T. *et al.* β-Catenin asymmetry is regulated by PLA1and retrograde traffic in C. elegans stem cell divisions. *EMBO J.* **27**, 1647–1657 (2008).
23. Beer, K. B. *et al.* Extracellular vesicle budding is inhibited by redundant regulators of TAT-5 flippase localization and phospholipid asymmetry. *Proc. Natl. Acad. Sci.* **115**, E1127–E1136 (2018).
24. Dickinson, D. J., Pani, A. M., Heppert, J. K., Higgins, C. D. & Goldstein, B. Streamlined genome

engineering with a self-excising drug selection cassette. *Genetics* **200**, 1035–1049 (2015).
25. Paix, A. *et al.* Scalable and versatile genome editing using linear DNAs with microhomology to Cas9 sites in Caenorhabditis elegans. *Genetics* **198**, 1347–1356 (2014).
26. Sarov, M. *et al.* A genome-scale resource for in vivo tag-based protein function exploration in C. elegans. *Cell* **150**, 855–866 (2012).
27. Fraser, A. G. *et al.* Functional genomic analysis of C. elegans chromosome I by systematic RNA interference. *Nature* **408**, 325–330 (2000).
28. Michelet, X. *et al.* The ESCRT-III protein CeVPS-32 is enriched in domains distinct from CeVPS-27 and CeVPS-23 at the endosomal membrane of epithelial cells. *Biol. Cell* **101**, 599–615 (2009).
29. Hadwiger, G., Dour, S., Arur, S., Fox, P. & Nonet, M. L. A monoclonal antibody Toolkit for C. elegans. *PLoS One* **5**, (2010).
30. Stafford, J. H. & Thorpe, P. E. Increased exposure of phosphatidylethanolamine on the surface of tumor vascular endothelium. *Neoplasia* **13**, 299–308 (2011).
31. Schindelin, J. *et al.* Fiji: An open-source platform for biological-image analysis. *Nat. Methods* **9**, 676–682 (2012).
32. Mastronarde, D. N. Automated electron microscope tomography using robust prediction of specimen movements. *J. Struct. Biol.* **152**, 36–51 (2005).
33. Kremer, J. R., Mastronarde, D. N. & McIntosh, J. R. Computer visualization of three-dimensional image data using IMOD. *J. Struct. Biol.* **116**, 71–76 (1996).

3. Degron-tagging reveals inhibitors of microvesicle release

3.1. Introduction: Visualizing microvesicle release using degron-mediated degradation

Identifying the mechanisms that regulate MV release is important to analyze their *in vivo* functions. Therefore, we wanted to screen for proteins that inhibit microvesicle (MV) release like TAT-5[1]. Because the EV inhibitory function of TAT-5 is conserved in human cell culture[2], we predict that such a screen will also identify proteins that regulate ectocytosis in humans during normal physiology and disease.

Due to their small size (90 - 500 nm), it can be challenging to study the release and fate of MVs *in vivo* with normal light microscopy techniques[3]. The most specific fluorescent extracellular vesicle (EV) labelling methods are fusion proteins between fluorophores and proteins enriched in EVs[4,5]. However, due to the heterogeneity in EV content, these techniques only stain a subpopulation of EVs. For example, EVs are typically detected *in vivo* by the tetraspanin proteins on their surface, but tetraspanin content is heterogeneous among EV subpopulations[6], making it hard to exclusively screen for MVs. Alternatively, membrane-binding fluorescent dyes have been developed to label all subpopulations of EVs[7,8], which would allow screening for regulators of both exosome and MV release. However, as there was no observed effect on exosome release in *tat-5* mutants[1], we wanted to focus specifically on MVs. Therefore, we searched for general reporters of the plasma membrane to label MVs.

Fluorescent reporters binding specific phosphatidylinositol (PI) species are popular for studying membrane dynamics, because different PI species localize to different organelles[9]. For example, $PI4,5P_2$ is predominantly localized to the plasma membrane[10]. The Plekstrin homology (PH) domain of the cytosolic phospholipase C (PLC) binds $PI4,5P_2$-containing membranes and is therefore found primarily at the plasma membrane[11,12]. As MVs are derived from the plasma membrane, fluorescent $PI4,5P_2$-binding domains can label MVs[1]. However, these reporters bind to $PI4,5P_2$ both on the plasma membrane and the membrane of MVs[1,13], making it difficult to specifically visualize MVs. Electron microscopy and super-resolution light microscopy can visualize the few tens of nm that separate the plasma membrane from neighbouring MV membranes[1,14], but these techniques rely on fixation, which makes it challenging to study dynamics. Furthermore, they are time- and cost-intensive and not appropriate for a genetic screen.

To tackle these problems, we developed a system where we label the plasma membrane and MVs and then specifically remove the plasma membrane labeling by selective degradation. This approach specifically maintains the fluorescence of the reporters in MVs. Selective degradation of degron-tagged proteins is a widely used tool to study molecular processes in developing animals[15]. Degrons are degradation motifs that target proteins for ubiquitination and degradation, which has led to degron-tagging being used as an alternative loss-of-function approach to RNA interference or genetic knockouts[15]. Degrons recruit ubiquitin ligases to polyubiquitinate target proteins, resulting in the proteasomal degradation of cytosolic targets or the lysosomal degradation of transmembrane targets[16]. Rather than using degron tags for a loss-of-function technique, we used the temporally-controlled degradation of degron-tagged $PI4,5P_2$-binding reporters to specifically label MVs.

Spatiotemporal control of degron-mediated degradation has been achieved by external stimuli like temperature, drugs or light [17–21]. However, most animals are temperature- and light-sensitive and some tissues can be inaccessible to drugs. Therefore, we looked for an *in vivo* degron system that did not require temperature shifts, permeabilization, or complicated imaging protocols. The first zinc finger (ZF1) domain of PIE-1 is an endogenous degron in *C. elegans* that targets PIE-1 for proteasomal degradation at specific stages[22]. The ZF1 degron is a 36 amino acid motif recognized by the SOCS-box protein ZIF-1, which binds to the elongin C subunit of an ECS ubiquitin ligase complex[23]. ZIF-1 is expressed in sequential sets of differentiating somatic cells[24], resulting in a stereotyped pattern of degradation in developing embryos (Fig. 1). Fusing the ZF1 degron to a target protein results in degradation within 30 to 45 min of ZIF-1 expression in both embryonic and adult tissues[23]. Thus, ZF1 degron tagging would enable us to screen for MV release in early *C. elegans* embryos, where TAT-5 was found to inhibit MV biogenesis[1].

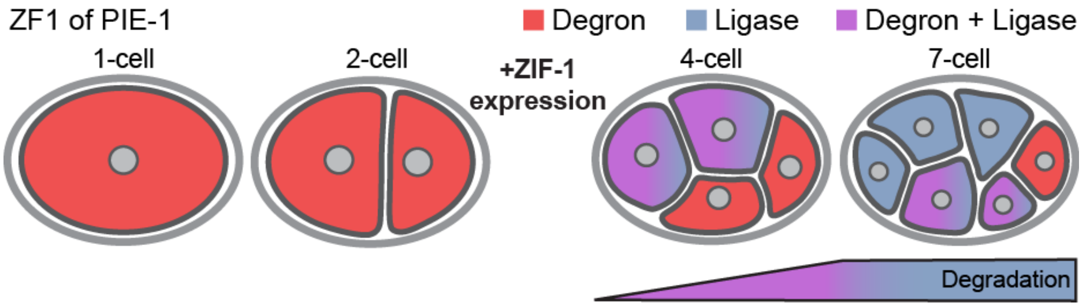

Fig. 1: ZF1 degradation pattern. Proteins with a ZF1 degron (red) are stable before expression of the ubiquitin ligase adaptor ZIF-1 (blue) in *C. elegans* embryos. ZIF-1 starts to be expressed in a stereotyped pattern of somatic cells after the 2-cell stage, starting with the anterior cells (red + blue = purple). Proteins with a ZF1 degron are degraded in somatic cells, starting with the anterior cells (purple to blue). Cells that do not express ZIF-1, such as the posterior germ cell, do not degrade proteins with a ZF1 tag (red). Image modified from Beer *et al.*, Nat. Commun. 2019[25].

Previously, a ZF1-tagged syntaxin-4 (SYX-4) was successfully used to visualize MVs in *C. elegans* embryos[1]. SYX-4 is a single-pass transmembrane protein that localizes to the plasma membrane and endocytic vesicles[26]. After ZIF-1 expression begins, ZF1-tagged SYX-4 was endocytosed from the plasma membrane and degraded (Fig. 2), but persisted on MVs that had been released before ZIF-1 expression began[1]. Thus, degron-tagged reporters separated from the ubiquitin ligase complex by intervening membranes are no longer accessible to ubiquitination and degradation.

Degradation of endosomal ZF1-tagged SYX-4 is likely to occur in lysosomes after sequestration inside intraluminal vesicles (Fig. 2), which is the typical pathway of ubiquitin-mediated degradation for transmembrane proteins[16]. However, the endolysosomal pathway of ubiquitin-mediated degradation leads to the labelling of endosomes in addition to MVs, including MVBs (Fig. 2). As the *C. elegans* embryo develops, the cells become smaller and stack in three-dimensions, making it difficult to distinguish whether labelling is at the plasma membrane in MVs or cytosolic in endosomes. Furthermore, as MVBs can fuse with the plasma membrane to release the ILVs as exosomes[27], labelling a transmembrane protein could result in labelling a mixture of MVs and exosomes. Thus, to specifically label MVs, we needed to apply the ZF1 degron approach to a plasma membrane reporter that did not include an integral membrane protein.

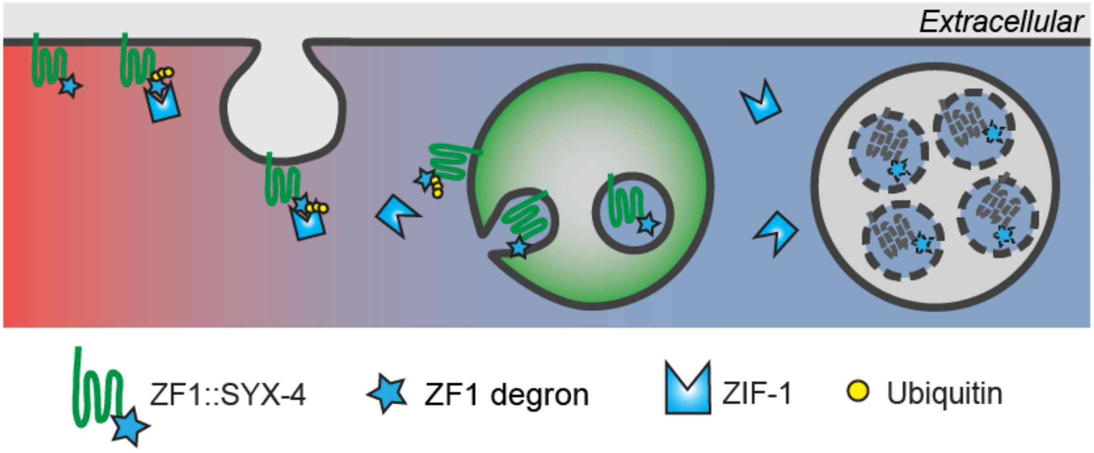

Fig. 2: Degron tags drive endocytosis and lysosomal degradation of a transmembrane reporter. A transmembrane protein tagged with the ZF1 degron is recognized by the ubiquitin ligase adaptor ZIF-1 at the plasma membrane and ubiquitinated. Polyubiquitination leads to endocytosis and degradation of degron-tagged transmembrane reporters on intraluminal vesicles within lysosomes (dotted lines). Image modified from Beer *et al.*, Nat. Commun. 2019[25].

Here, we ZF1-tagged the $PI4,5P_2$-binding PH domain of PLC1∂1 to achieve proteasomal degradation of the reporter in MV-releasing cells (Fig. 3A-B). Since intervening membranes hinder the degradation of the ZF1::SYX-4 reporter, we predicted that ZF1::PH fluorescence will be maintained in MVs released before ZIF-1 expression begins (Fig. 3B). We found that using a degron-tagged reporter improved the signal-to-noise ratio between MVs and neighboring cells, enabling the visualization of MVs. This technical advance helped us to identify new ectocytosis regulators in *C. elegans* embryos, as well as to determine the cargo of MVs *in vivo*. Since degron-mediated degradation is a widely used tool in many animal model systems[15], this technique may help to visualize and track MVs in a broad range of *in vivo* studies.

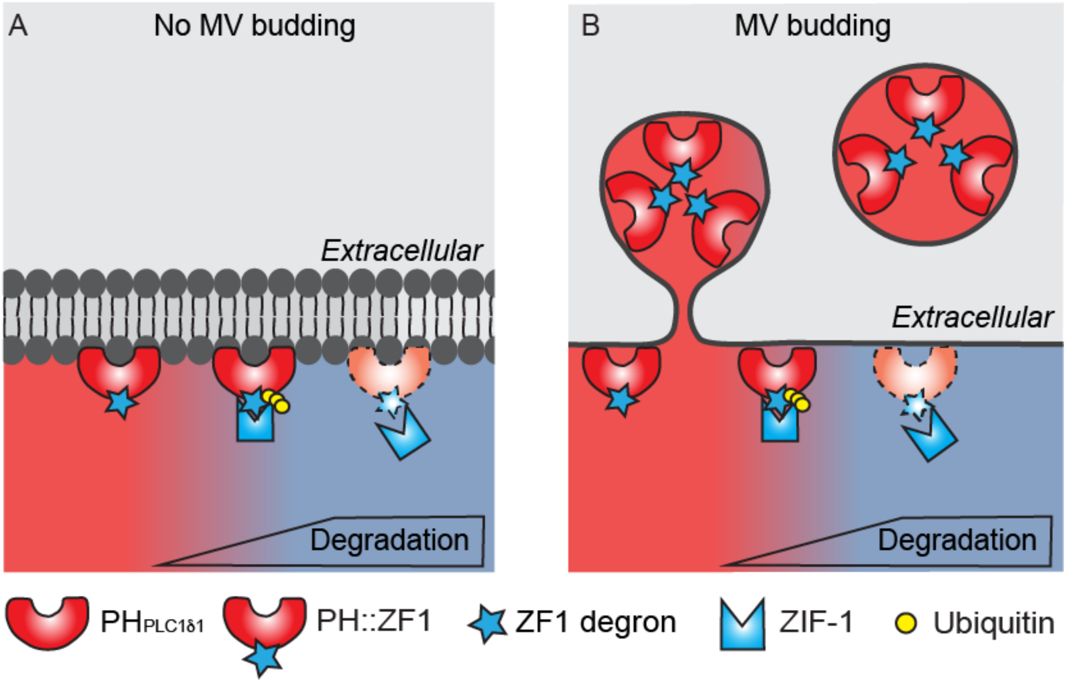

Fig. 3: Model for ZF1 degradation of a plasma membrane reporter during MV release. A) The lipid-binding cytosolic PH domain tagged with the ZF1 degron is recognized by the ubiquitin ligase adaptor ZIF-1 and ubiquitinated. Polyubiquitination leads to proteasomal degradation of degron-tagged fluorescent reporters (dotted lines). B) PH domain reporters released in MVs that bud from the plasma membrane maintain fluorescence, because ZF1-tagged reporters in vesicles released before ZIF-1 expression are not ubiquitinated or degraded. Image from Beer *et al.*, Nat. Commun. 2019[25].

3.2. Results: Developing degron reporters to specifically label released microvesicles

At first, we tested whether a degron-tagged PI4,5P$_2$-binding reporter could specifically label MVs. Therefore, we tagged the PH domain of rat PLC1∂1 with a fluorescent protein and the ZF1 degron and expressed this transgene in worm embryos. Similar to an mCherry-tagged PH reporter (Fig. 4A), the mCh::PH::ZF1 reporter localized to the plasma membrane in 4-cell embryos (Fig. 4D). Thus, the degron tag did not disrupt the normal localization of the reporter.

ZF1-mediated degradation begins in somatic cells during the 4-cell stage, due to the onset of expression of the ubiquitin ligase adapter protein ZIF-1[28]. While the fluorescence of mCh::PH persists in developing embryos (Fig. 4B-C), mCh::PH::ZF1 is progressively degraded (Fig. 4E-F), starting with the anterior and dorsal AB cells (Fig. 4E, Fig. 1). ZIF-1 is not expressed in the germ lineage, resulting in persistent fluorescence in a couple of posterior cells (Fig. 4E-F). During meiosis, the two polar bodies are born and released outside the embryo to expel extra copies of the genome[29,30]. The released polar bodies also maintain mCh::PH::ZF1 fluorescence (Fig. 4D-F arrow and arrowhead), confirming that ZF1 degradation does not occur in structures released before ZIF-1 expression begins[31]. Thus, ZF1 tagging is able to rapidly degrade a bright, exogenous reporter in cells where the reporter could be ubiquitinated.

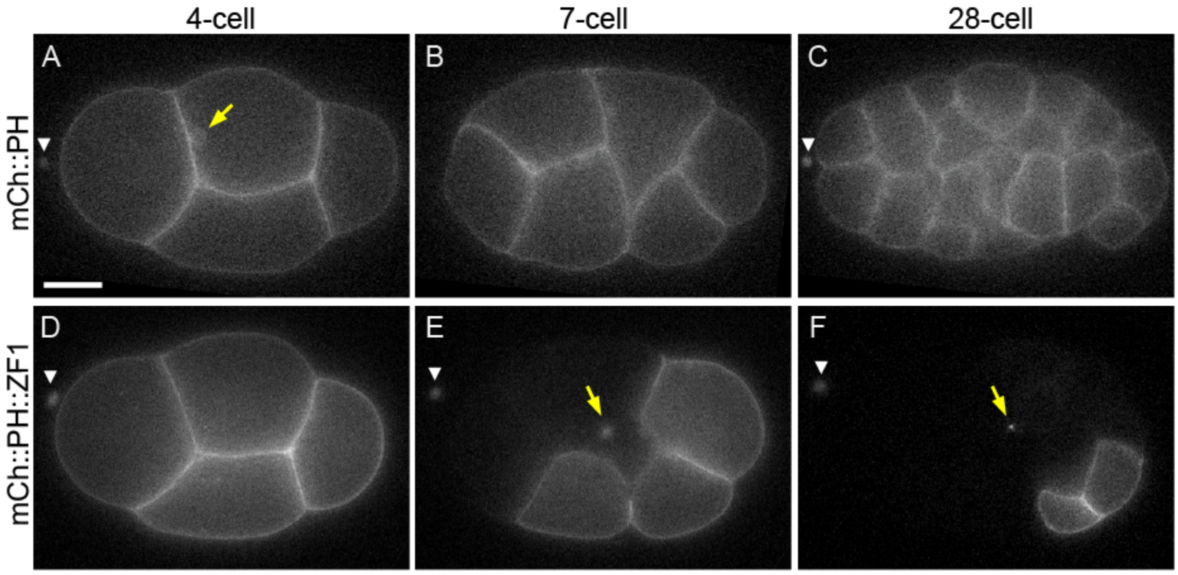

Fig. 4: The ZF1 degron enables labelling of specific cells and vesicles in *C. elegans* embryos. A-C) The lipid-binding mCh::PH$_{PLC1∂1}$ reporter localizes to the plasma membrane and endocytic vesicles (arrow) in 4-, 7-, and 28-cell embryos (n=19). D-F) ZIF-1-driven proteasomal degradation of the degron-tagged mCh::PH$_{PLC1∂1}$::ZF1 reporter starts in anterior blastomere (AB) cells during the 4-cell stage (D), leading to the absence of the mCh::PH::ZF1 fluorescence in anterior AB cells at the 7-cell stage (E) and most somatic cells at the 28-cell stage (F, n=10). The ubiquitin ligase adaptor ZIF-1 is not expressed in the posterior germ line or in anterior polar bodies (arrowhead), resulting in the persistence of

mCh::PH::ZF1 on the plasma membrane in these cells. Arrows indicate labelled intracellular vesicles, which are protected from proteasomal degradation by intervening membranes. Anterior is left, dorsal is up. Images were taken by Ann Wehman and Gholamreza Fazeli. Scale bar: 10 µm. Image from Beer *et al.*, Nat. Commun. 2019[25].

We next tested whether we could use the mCh::PH::ZF1 approach to specifically label MVs *in vivo*. In wild type embryos, MVs are difficult to detect due to their low abundance and proximity to the plasma membrane. MV budding is normally inhibited by the TAT-5 lipid flippase, resulting in increased MV release when *tat-5* is knocked down[1]. Therefore, we compared the localization of mCh::PH and mCh::PH::ZF1 after *tat-5* RNAi treatment. In mCh::PH embryos, MV release is visible as thickened membrane areas between cell contacts (Fig. 5A-C) in comparison to control embryos (Fig. 4A-C). However, small patches of MVs are difficult to detect over the background of the plasma membrane fluorescence. Therefore, we tested whether the visibility of MVs was enhanced using the degron-tagged PH-reporter. Indeed, released MVs are clearly visible after *tat-5* knockdown using the mCh::PH::ZF1 reporter (Fig. 5E-F)[32], due to proteasomal degradation of the plasma membrane label and protection in MVs (Fig. 3B). Thus, by using a general plasma membrane reporter with a degron tag, it is possible to easily observe MV release *in vivo*.

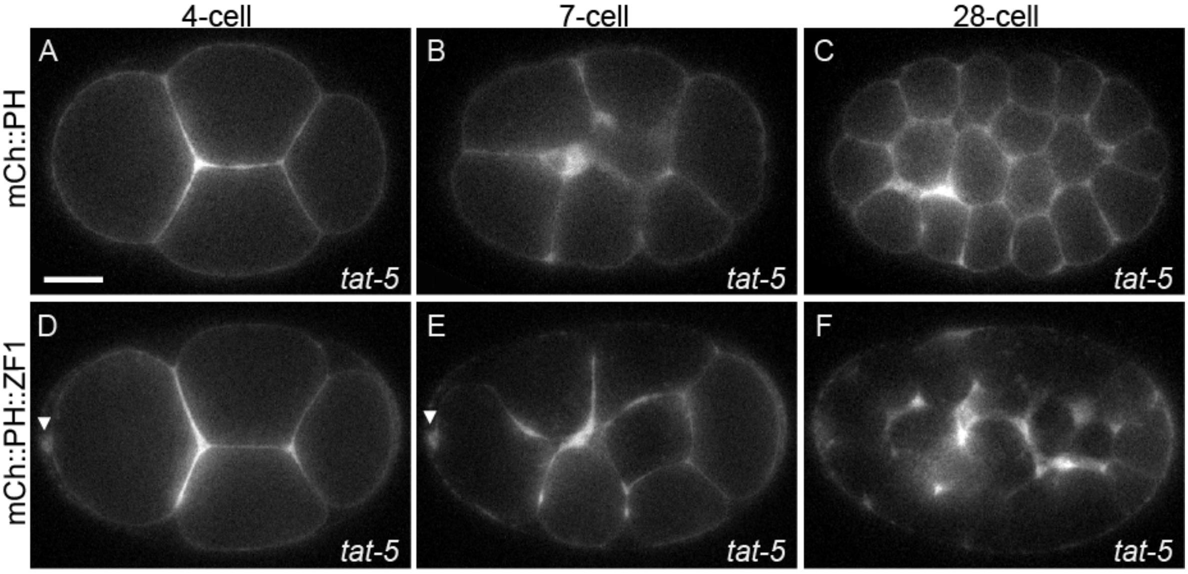

Fig. 5: Degron tags enhance the visibility of extracellular vesicles in vivo. A-C) Embryos treated with tat-5 RNAi show increased mCh::PH membrane labelling due to accumulated microvesicles (MVs) at the 4-, 7-, and 28-cell stage (n=11). D) Increased mCh::PH::ZF1 is also visible at the 4-cell stage in embryos treated with *tat-5* RNAi. E-F) Gradual degradation of mCh::PH::ZF1 in somatic cells facilitates

visualization of released MVs in a 7- and 28-cell embryo (n=22). Due to degradation of cytosolic mCh::PH::ZF1 reporter at the plasma membrane, even small amounts of released MVs are easily visible. Arrowhead marks the anterior polar body. Images were taken by Ann Wehman and Gholamreza Fazeli. Scale bar: 10 µm. Image from Beer *et al*., Nat. Commun. 2019[25].

3.2.1. Degron protection assay reveals topology of membrane-associated proteins

Given that a cytosolic factor was able to label MVs, we wondered whether any cytosolic protein recruited to the cell surface could be used to label MVs. Previously, we had observed that clathrin is enriched at the cell surface after *tat-5* knockdown[1], but it was unclear whether this was due to increased clathrin inside the plasma membrane or due to the release of clathrin in MVs that accumulated outside the plasma membrane (Fig. 6F). Both possibilities were plausible, as clathrin-binding proteins are also increased at the plasma membrane after *tat-5* knockdown, including ESCRT proteins[1]. Alternatively, clathrin was previously found in purified *Drosophila* and mammalian EVs[33,34]. Therefore, we asked whether a degron-tagged clathrin heavy chain (CHC-1) reporter would be protected from degradation inside MVs or be accessible to degradation at the cell cortex (Fig. 6F).

Consistent with previous results[1], we initially saw increased ZF1::mCh::CHC-1 and GFP::ZF1::PH labelling clathrin and membrane at cell contacts in embryos treated with *tat-5* RNAi (Fig. 6B) compared to control embryos (Fig. 6A). This increase persisted in posterior *tat-5* knockdown cells (Fig. 6E), but after ZIF-1 expression began in anterior cells, ZF1::mCh::CHC-1 disappeared from the cell surface in both control and *tat-5* RNAi-treated embryos (Fig. 6C-E), while GFP::ZF1::PH persisted in MVs after tat-5 knockdown (Fig. 6D). This demonstrates that the increased clathrin signal is due to association with the plasma membrane and not due to clathrin trapped within MVs (Fig. 6F). Thus, degron-tagging can reveal whether a protein is sorted inside MVs.

In summary, these results demonstrate that not every protein at the cell surface is released in MVs, even in *tat-5* mutants that overproduce MVs. They also demonstrate that only certain plasma membrane reporters are suited to visualize MVs and screen for new regulators of MV release.

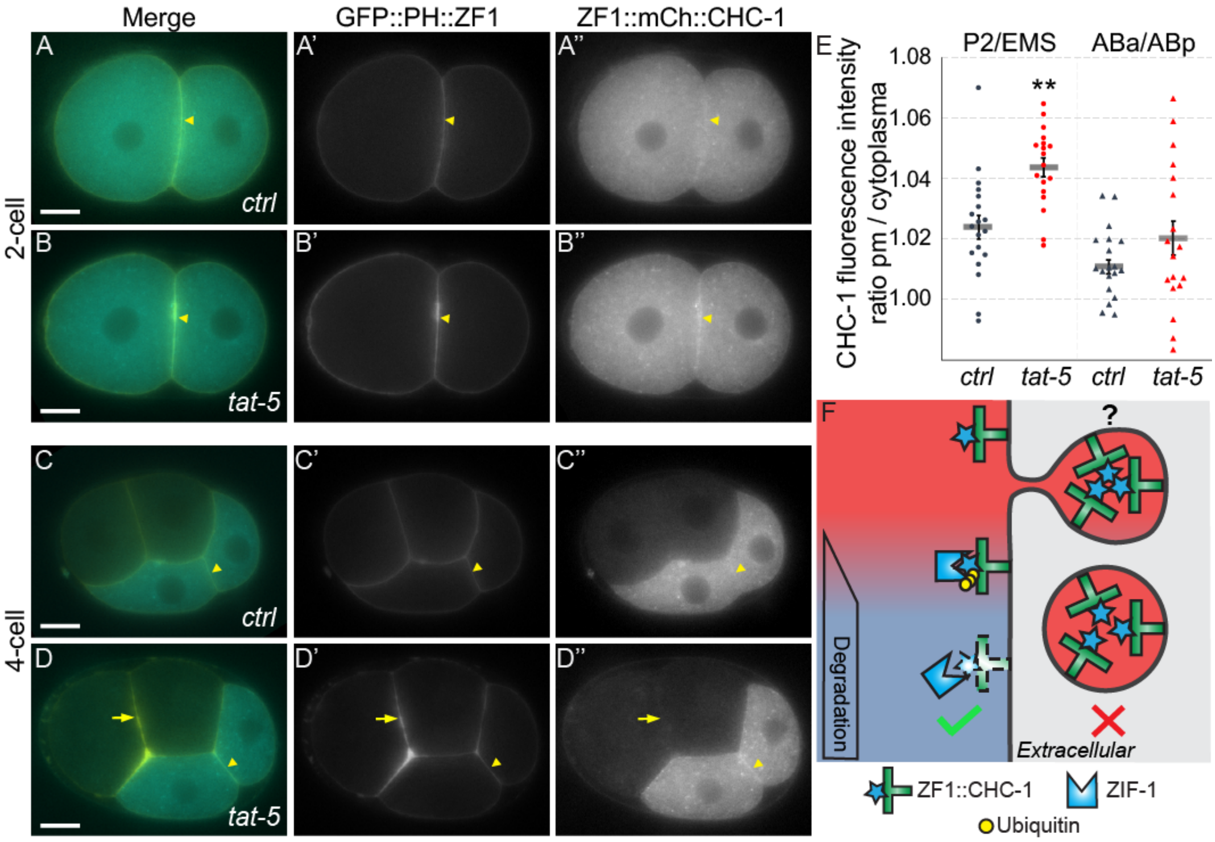
Merge
GFP::PH::ZF1
ZF1::mCh::CHC-1
A
A'
A''
2-cell
ctrl
B
B'
B''
tat-5
C
C'
C''
4-cell
ctrl
D
D'
D''
tat-5
E
P2/EMS
ABa/ABp
CHC-1 fluorescence intensity ratio pm / cytoplasma
1.08
1.06
1.04
1.02
1.00
**
ctrl
tat-5
ctrl
tat-5
F
?
Degradation
Extracellular
ZF1::CHC-1
ZIF-1
Ubiquitin

Fig. 6: Degron protection assay reveals protein topology. A) A degron-tagged clathrin reporter ZF1::mCh::CHC-1 initially localizes to the plasma membrane (arrowhead) and intracellular puncta (n=9). B) After *tat-5* knockdown, ZF1::mCh::CHC-1 is enriched at the plasma membrane (arrowhead, n=14). C) After expression of ZIF-1 begins in anterior cells, ZF1::mCh::CHC-1 is degraded throughout the anterior cells in control embryos (n=19). D) Although ZF1::mCh::CHC-1 is still enriched at the plasma membrane in posterior cells (arrowhead) in *tat-5* RNAi-treated embryos, ZF1::mCh::CHC-1 is lost from the plasma membrane in anterior cells (arrow, n=18), indicating that clathrin is accessible to ubiquitin ligases. GFP::PH::ZF1 labels the plasma membrane and extracellular vesicles. Scale bar:10 µm. E) Quantification of clathrin enrichment on a posterior cell contact (EMS:P2) or anterior cell contact (ABa:ABp) compared to the neighbouring cytoplasm at the 4- and 6-cell stage from two independent experiments. ZF1::mCh::CHC-1 fluorescence was significantly increased at the posterior EMS:P2 cell contact after *tat-5* knockdown (**$p<0.001$ using one-tailed Student's t-test with Bonferroni correction, *ctrl* n=19, *tat-5* RNAi n=18). No change was observed at anterior cell contacts ($p>0.05$). Bars represent mean ± SEM. F) If clathrin were in extracellular vesicles, ZF1::mCh::CHC-1 would be protected from ZIF-1-mediated degradation, but that did not match our observations (X). As clathrin is inside the plasma membrane (check mark), ZF1::mCh::CHC-1 is accessible to ZIF-1-mediated degradation. Image from Beer *et al*., Nat. Commun. 2019[25].

3.2.2 Identification of microvesicle release inhibitors and potential TAT-5 regulators

To identify how MV release is regulated, we first sought to identify potential TAT-5 regulators that also inhibit MV release. Therefore, an RNAi screen with 137 candidate interactors, many of which are involved in membrane trafficking and lipid biogenesis, was conducted together with Birgit Karmann[32]. We scored for proteins that caused increased MV release using the $\mathrm{PH}_{\mathrm{PLC1}\partial 1}$ plasma membrane reporter with a degron tag to label plasma-membrane-derived EVs (Fig. 3). In control embryos, no MV release is visible because of low MV abundance in wild type *C. elegans* embryos (Fig. 7A)[1]. We discovered two highly conserved proteins whose disruption appeared to cause increased MV release(Fig. 7B-C, G), based on increased labeling similar to *tat-5* mutants (Fig. 5F), namely the Dopey domain protein PAD-1 and the DnaJ domain-containing protein RME-8. This suggests that PAD-1 and RME-8 inhibit MV release.

Two additional potential MV regulators were identified by Gholamreza Fazeli while carrying out unrelated studies using the non ZF1-tagged mCh::PH strain. Maternal-zygotic mutants for the Beclin homolog BEC-1 and the class III PI3Kinase VPS-34 showed small patches of extra membrane labeling (7E-F, G) compared to control embryos (Fig. 7D). These data suggest that VPS-34 and BEC-1 inhibit MV release.

Notably, BEC-1 and VPS-34 only showed a membrane phenotype in maternal-zygotic mutants. When we treated the GFP::ZF1::PH strain with *bec-1* or *vps-34* RNAi, there was no sign of increased MV release (Fig. 7G). This suggests that we cannot rule out a role for other genes in our screen based on the lack of an RNAi phenotype.

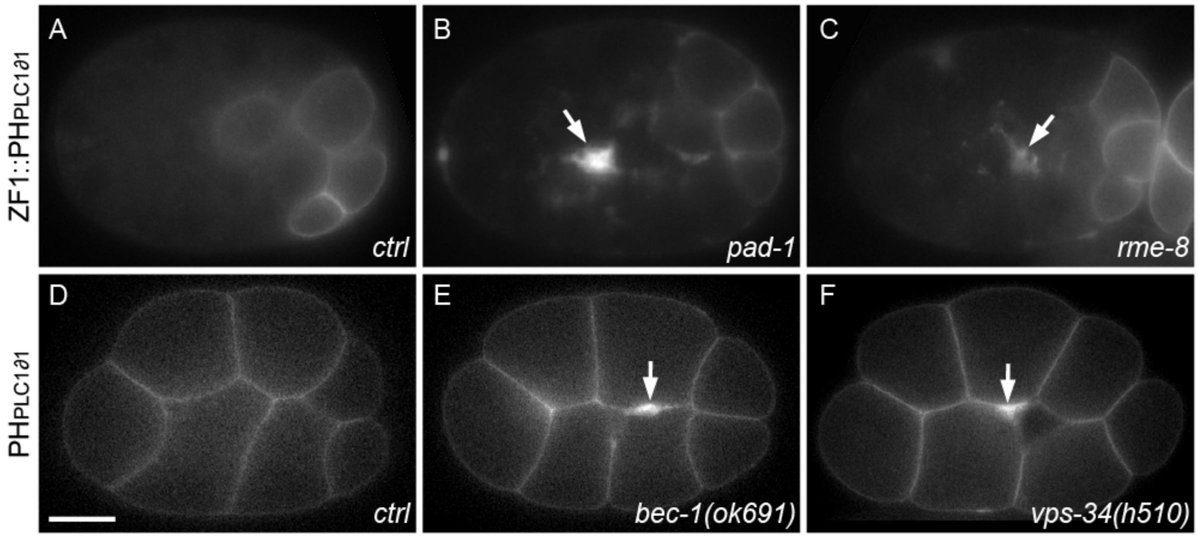

G

Genotype	RNAi	Increased EV release (thick membranes)	
		%	n
+	-	0%	119
	tat-5	90%	31
	pad-1	89%	55
	rme-8	84%	50
bec-1(ok691)	-	75%	32
+	*bec-1*	0%	20
vps-34(h510)	-	25%	28
+	*vps-34*	0%	60

Fig. 7: Identification of potential EV release inhibitors. A) In a 26-cell control embryo, GFP::ZF1::PH$_{\text{PLC1}\partial 1}$ is degraded in most somatic cells, only persisting on the plasma membrane in a few posterior cells. B-C) MVs labeled with GFP::ZF1::PH$_{\text{PLC1}\partial 1}$ (arrow) accumulate between cells in *pad-1* and *rme-8* RNAi-treated embryos. D) PH$_{\text{PLC1}\partial 1}$::mCh localizes primarily to the plasma membrane in control embryos at the 8-cell stage. E-F) PH reporters localize to thickened membranes (arrow) in *bec-1(ok691)* (PH$_{\text{PLC1}\partial 1}$::mCh) and *vps-34(h510)* (PH$_{\text{PLC1}\partial 1}$::GFP) maternal zygotic mutants (data from Gholamreza Fazeli). Scale bar: 10 µm. G) Summary of EV release phenotypes observed in this screen. Control (+) and mutant worms expressing fluorescent PH-reporters were treated with RNAi or untreated (-). The percentage of embryos showing the indicated phenotype is given. Embryos (n) from the late 4-cell to 102-cell stage were scored for thickened membrane labeling between cells, which is indicative of EV release. The *rme-8* RNAi data was collected by Kenneth Kuhn, *bec-1* and *vps-34* RNAi data was collected by Birgit Karmann. Images A-F modified from Beer *et al.*, PNAS 2018[32].

To verify that the increased plasma membrane labeling was caused by increased EV release, we used transmission electron microscopy and tomography in *bec-1(ok691)* mutants or wild type strains after *pad-1* or *rme-8* RNAi treatment. We saw areas with increased EV release between cell contacts from various embryonic stages in *bec-1* mutants, *pad-1* RNAi and *rme-8* RNAi (Fig. 8A-D). Thus, BEC-1, PAD-1 and RME-8 inhibit EV release, similar to TAT-5.

TAT-5 flippase activity only inhibited EVs formed by ectocytosis, called microvesicles (MVs)[1]. To analyze whether the identified proteins specifically regulate MV release or could also regulate exosome release from the fusion of multivesicular bodies with the plasma membrane, we measured the diameter of EVs and compared it to the size of intraluminal vesicles (ILVs) in multivesicular bodies. 98% of EVs found in *bec-1(ok691)* mutants and 97% of EVs in *pad-1* RNAi were larger than ILVs (Fig. 8E-F), consistent with the larger size of MVs (>100nm) that derive from ectocytosis after *tat-5* knockdown[1]. Thus, PAD-1 and BEC-1 inhibit microvesicle release, like TAT-5.

In contrast, *rme-8* RNAi embryos have EVs with a diameter similar to both ILVs (13% <100 nm) and MVs (87% >100 nm) (Fig. 8G). This is a statistically significant increase in small EVs in *rme-8* RNAi in comparison to *bec-1(ok691)* or *pad-1* RNAi ($p<0.01$ using 2-tailed Fisher's exact test). We conclude that *rme-8* knockdown primarily causes increased MV release, but RME-8 may also contribute to the size of MVs or additionally inhibit exosome release.

Given that BEC-1 and VPS-34 are both subunits of the class III PI3Kinase complex and show similar EV release phenotypes by light microscopy (Fig. 8E-F)[35], we predict that VPS-34 inhibits microvesicle release similar to BEC-1. Taken together, our screening approach identified four proteins that inhibit ectocytosis like TAT-5, namely BEC-1, VPS-34, RME-8, and PAD-1. This demonstrates that degron-tagged reporters can reveal MV release, enabling screens for new proteins that regulate MV budding.

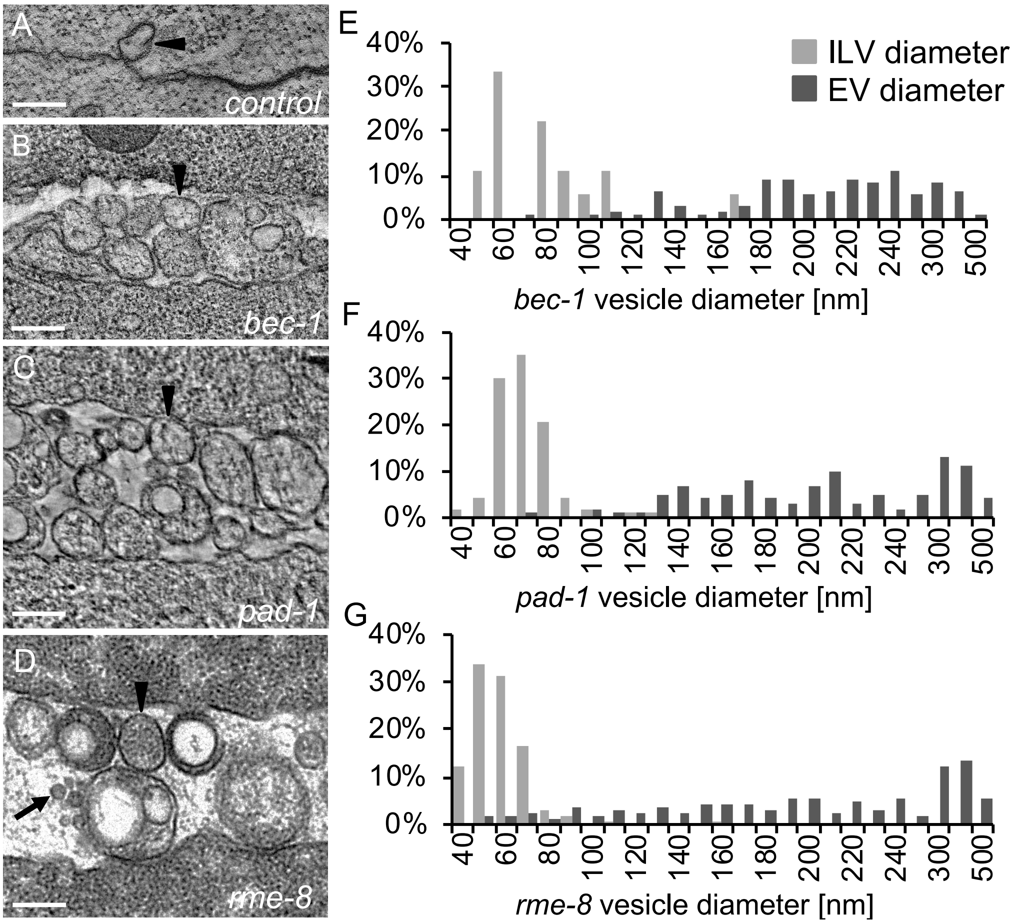

Fig. 8: Electron Microscopy of EV releasing mutants. A) EVs are infrequently observed between wild-type N2 cells in an electron tomogram from a 2-cell embryo. B-D) Released EVs accumulate between cells in a tomogram from a three-cell *bec-1* maternal-zygotic mutant, a three-cell embryo treated with *pad-1* RNAi, and a 24-cell *rme-8* RNAi embryo. Scale bar: 200 nm. Arrowheads point to MV-sized EVs, arrows point to exosome-sized EVs. E-G) Histograms of extracellular vesicle (EV) and intraluminal vesicle (ILV) diameters measured from TEM images of *bec-1* maternal-zygotic mutant embryos and *pad-1* RNAi embryos demonstrate that the majority of EVs are MVs, because they are larger than ILVs (measurements were done together with Kenneth Kuhn and Teresa Kee). In *rme-8* RNAi, EVs could be a mix of exosomes and MVs, because they are the same size (13%) or larger than ILVs (87%). Image from Beer *et al.*, PNAS 2018[32].

3.2.3. Only large increases in microvesicle release interrupt gastrulation

It was previously reported that loss of the MV release inhibitors TAT-5 and PAD-1 caused embryonic lethality due to gastrulation defects[1,36], which could result from decreased cell adhesion caused by increased numbers of MVs between cells. As *rme-8* RNAi also causes embryonic lethality[37], we wondered whether the increase in EV release in *rme-8* RNAi also disrupts gastrulation. In control embryos, germ cells and endodermal precursor cells migrated to the center of the developing embryo (Fig. 9A). In contrast, germ cells and endoderm precursor cells remain at the surface of the embryo after *pad-1* depletion (Fig. 9B), confirming that PAD-1 is required for gastrulation like TAT-5. On the other hand, depletion of RME-8 did not cause gastrulation defects, as germ cells and endoderm cells were able to migrate properly (Fig. 9C). However, EV release was much less in *rme-8* RNAi than in *tat-5* or *pad-1* RNAi (Fig. 5D-F, Fig. 7B-C). Therefore, the amount of EVs released from *rme-8* RNAi appears not to be enough to disrupt cell adhesion to an extent that alters cell migration, unlike the massive increase seen after *pad-1* or *tat-5* RNAi. Thus, small accumulations of MVs seem not to disrupt gastrulation. Furthermore, the embryonic lethality caused by *rme-8* depletion is not due to disrupted gastrulation.

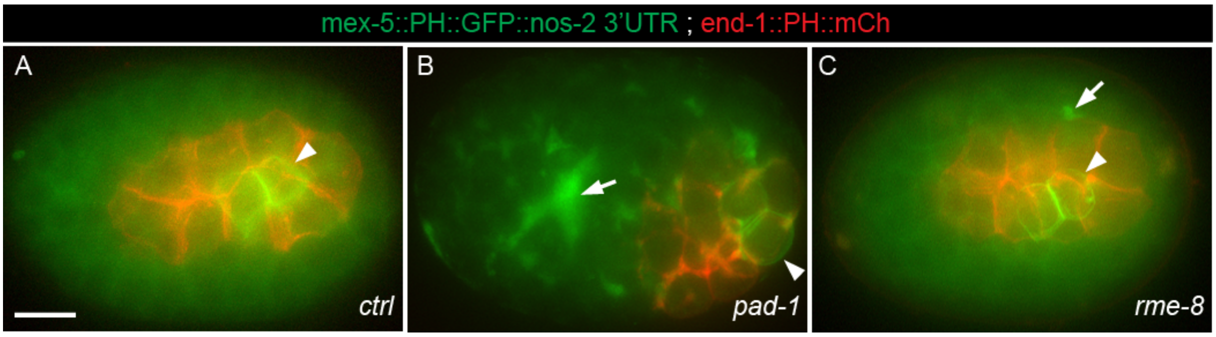

Fig. 9: RME-8 is not required for gastrulation. A) Germ cells (green) and endodermal precursor cells (red) migrate from the center of a ~200 cell *C. elegans* control embryo (n=9). Arrowheads point to the germ cells. B) Depletion of PAD-1 prevents gastrulation, probably due to increased EV release (arrow), resulting in localization of the germ cells and intestinal cells to the posterior surface (n=11). C) Gastrulation is not disrupted in *rme-8* RNAi-treated embryo(n=15), consistent with less substantial MV release than *pad-1* RNAi. Scale bar: 10 µm.

3.3. Discussion

3.3.1. Degron tagging of a PI4,5P2 reporter enables visualization of microvesicles *in vivo*

We created a general probe for plasma membrane-derived MVs by degron-tagging the PH domain of PLC, which binds to PI4,5P$_2$ [10,13]. We found that PH::ZF1 efficiently labels both MVs and the cell membrane. By removing the reporter from the cytosol, we gain the visibility of released reporters in the MV lumen. Previously, electron microscopy and super-resolution light microscopy where used to tell nanometre-sized MVs apart from cells[1,14]. Using our degron technique, we have achieved enhanced visibility of released MVs, which enabled us to screen for MVs *in vivo* on a standard epifluorescence microscope.

In this study, we focused on using membrane reporters to label MVs released from the plasma membrane, but this approach also works to enhance the visibility of any structure separated from the ubiquitin ligase by a membrane bilayer. We recently showed that degron protection assays can also be applied to nuclear, phagosomal endosomal, or endoplasmic reticulum proteins[25]. Thus, using degrons to label specific organelles is an important cell biology technique beyond understanding MVs.

As degron tags are widely used in cell extracts, cell culture and *in vivo,* this approach can be used to visualize EVs in many systems. We used an endogenous ZF1 degron in *C. elegans* embryos, because it only required expression of a degron-tagged reporter. Ectopic expression of ZIF-1 in worms or zebrafish can also degrade ZF1-tagged proteins, showing that this degradation system can be adapted to visualize EVs in more systems[23,38]. Fusing an anti-GFP nanobody to ubiquitin ligase adaptors like ZIF-1 enables degradation of GFP-tagged proteins in *C. elegans*, *Drosophila*, plants, and zebrafish[38–41], which allows existing GFP-tagged reporters to be used for degron protection assays. This could help to identify whether proteins are released in MVs using GFP-tagged proteins already available in a lab. Expression of the auxin-inducible degron (AID) and TIR1 ligase adaptor is also used in various animal models and could also help to visualize MVs in many systems[19,42,43]. Furthermore, as degradation is induced when the specimen is incubated with the plant hormone auxin, this approach enables spatial and temporal control of degradation[15,44]. Thus, degron-tagging can help to clarify EV functions and release mechanisms from many model systems.

Although our PH::ZF1 reporter is likely to favor plasma membrane-derived MVs, it is possible to target endosome-derived EVs (exosomes) by degron-tagging proteins associated with the endosome surface. Alternatively, exosomes may also be labelled by degron-tagging transmembrane proteins, given that ubiquitination drives endocytosis of transmembrane proteins and their budding into intraluminal vesicles, the precursors of exosomes[25,45]. Degron-tagging reporters found at both the plasma membrane and endosome surface, such as actin-binding domains or abundant proteins like GAPDH, should label both MVs and exosomes[46]. As other reporters are found in both the source cell and released EVs, degron-tagged reporters are uniquely able to specifically label EVs, enabling *in vivo* tracking and functional studies.

One potential caveat of using the PH domain to probe MVs is that we may miss important genes that regulate PI4,5P$_2$ biosynthesis. The role of PI kinases and phosphatases might not be possible to analyze with the PH reporter, as altering PI4,5P$_2$ levels may disrupt the localization of the PH reporter. If PI4,5P$_2$ synthesis is blocked, for example, we expect to see the reporter accumulate in the cytosol instead of on the plasma membrane. However, cytosolic proteins can also be released in EVs [47]. Thus, it is possible that the reporter could still end up in MVs. We did not observe mislocalization of the PH reporter in *vps-34* and *bec-1* PI3K mutants, which phosphorylate PI to produce PI3P (also discussed in 3.3.3.), suggesting that at least disruption of PI3P levels did not affect the PI4,5P$_2$ production. Since multiple pathways generate PI4,5P$_2$ from other PI species like PI4P, PI5P or PI3,4,5P$_3$[10], loss of one pathway may not completely block PI4,5P$_2$ production. Depleting the PI4K that produces PI4P could be especially interesting, as the flippase activity of Drs2 depends on binding to PI4P through the C-term[48,49]. Thus, it would be interesting to test whether PI4P is also required for the flippase activity of TAT-5 and its role in inhibiting MV release. Thus, we predict that it should still be possible to screen for regulators of MV release when individual PI biosynthetic pathways are disrupted.

3.3.2. Degron tagging identifies microvesicle cargo

Because of the broad potential of EVs during development and disease, the content of EVs purified from body fluids and cell culture media is extensively studied and collected in large databases like Vesiclepedia and ExoCarta[47,50,51]. In contrast, little is known about the content of EVs released in tissues, because they are challenging to extract for proteomic analysis. EVs released from *C. elegans* embryos are especially difficult to analyze, as the EVs are trapped between cells, inside the eggshell, and inside the mother worm. To overcome this challenge, we have shown that degron-tagged reporters can help to clarify which proteins are found in EVs *in situ*. We degron-tagged the potential MV cargo clathrin heavy chain (CHC-1) and could show that CHC-1 was not a MV cargo in *tat-5* mutant embryos. Thus, in addition to helping identify which proteins are required for EV release, degron-tagged reporters can also demonstrate which proteins are EV cargo *in vivo*.

We found that clathrin accumulates at the cell surface, but not in MVs after *tat-5* RNAi treatment. The reason for clathrin accumulation at the plasma membrane remains puzzling. Clathrin has been shown to be required for EV internalization by clathrin-dependent endocytosis[52]. Thus, clathrin may accumulate on the plasma membrane after *tat-5* RNAi because more MVs accumulate and present signals for endocytosis. Consistently, preliminary data from TEM images of wild type (n=1), *tat-5* (n=2) and *pad-1* (n=5) embryos show one large ILV (>100 nm) inside an endosome, which is likely to be an endocytosed MV. However, we saw persistent accumulation of MVs between cell contacts using the PH::ZF1 reporter, suggesting that more MVs are released in *tat-5* and *pad-1* mutants than are endocytosed. In this case, clathrin recruitment to the plasma membrane could be secondary to the increased MV release.

On the other hand, clathrin could be recruited to the plasma membrane for the ESCRT-mediated release of MVs. ESCRT-0 (Hrs) recruits clathrin to endosomes[53,54], where it is required for the disassembly of ESCRT-0 (Hrs) and ESCRT-I (TSG101) from ILV bud sites, effective ILV formation and correct ILV size[55]. This suggests that clathrin is required for the membrane budding function of the ESCRT complex. In addition, the clathrin adaptor complex AP1 interacts with TSG101 and is needed for HIV budding and HIV Gag shuttling to bud sites[56]. Since ESCRT-0 and ESCRT-I are enriched at the plasma membrane and required for MV release in *tat-5* mutants, it is possible that they also recruit clathrin to bud sites on the plasma membrane. However, neither AP1 nor the plasma membrane-associated clathrin adaptor complex AP2 were required for MV release in *tat-5* mutants[1], suggesting that clathrin is not essential for MV budding. Thus, it remains open whether the increased clathrin accumulation in *tat-5* mutants is because of endocytic signaling or its interaction with mislocalized proteins, such as ESCRT-0/-1.

3.3.3. The class III PI3K VPS-34 and BEC-1 produce PI3P and inhibit microvesicle release

We found that two core subunits of the class III PI3K, VPS-34 and BEC-1, inhibit MV release. The class III PI3K mediates PI3P levels on membranes, thereby controlling the recruitment and function of a large variety of trafficking proteins[57]. The catalytic subunit VPS-34 phosphorylates PI on position 3 to produce PI3P on membranes. Beclin 1 (BEC-1) forms a complex with VPS-34 and serves as a regulatory arm together with either Atg14 (complex 1 involved in autophagy) or UVRAG (complex 2 involved in endosomal trafficking) (see also chapter 4.1.)[35,58]. Thus, we predict that VPS-34 and BEC-1 act together as part of the PI3K to inhibit MV release. Jaime Lisack and Gholamreza Fazeli from our lab found that deletion mutants in the Atg14 ortholog *epg-8* do not show increased EV release using the PH::ZF1 reporter (n=19), suggesting that the autophagy-related PI3K complex is unlikely to play a role in MV budding. Therefore, the UVRAG-containing PI3K complex II on endosomes is more likely to be important for MV release. To confirm which class III PI3K complex is specifically regulating EV release, it will be necessary to generate mutants for the *C. elegans* UVRAG ortholog, Y34B4A.2, and then examine EV release. However, based on the identification of other genes involved in endosomal trafficking in our screen for MV release inhibitors, we predict that the endosomal functions of PI3K will be most relevant.

The function of PI3K complex II is required to determine endosome identity and is a prerequisite for the recruitment of many PI3P-binding endosomal proteins. For example, recruitment of the ESCRT-0 protein Hrs depends on PI3P, which is required for protein sorting into intraluminal vesicles (ILV), as well as the formation of ILVs (also discussed in 1.X.) [52,58]. Thus, PI3K is required for the lysosomal degradation of transmembrane proteins. Proper PI3P levels are also required for the endosomal localization of some sorting nexins (SNX) like SNX1, SNX3, SNX17 and SNX27[59–63], which control cargo sorting and recycling from endosomes[64]. Thus, PI3K is also required for the recycling of transmembrane proteins away from the degradative pathway.

Most interestingly, PI3K has been shown to regulate endosomal trafficking of the TAT-5 ortholog Neo1p in yeast[65]. In yeast, Neo1p normally traffics between endosomes and the Golgi[66]. Dalton *et al.* found that Neo1 accumulated at endosomes in *vps30* (beclin 1) mutants, suggesting that Neo1 could no longer undergo retrograde trafficking from endosomes to the Golgi. They also found that PI3K acts in conjunction with the conserved sorting nexin Snx3p[65], which is also important for endosome to Golgi trafficking. Neo1 accumulated in the vacuole in *snx3* mutants, suggesting that Snx3p is required to recycle Neo1 away from the degradative pathway. These findings lead us to hypothesize that the class III PI3K is required for TAT-5 trafficking and suggest a role for SNX-3 in TAT-5 trafficking and MV release. However, we did not find a role for SNX-3 in our PH::ZF1 screen for increased MV release (see also chapter 4), suggesting that the class III PI3K regulates TAT-5 differently from SNX-3. In the following chapter 4, we characterize whether and how the class III PI3K and SNX-3 have a role in TAT-5 trafficking.

Because of the general function of class III PI3K to create PI3P, which is required for endosome organelle identity and protein trafficking[57,67], it is possible that PI3K also regulates MV release independent of TAT-5 trafficking. MV release caused by loss of VPS-34 and BEC-1 was less prominent in comparison to *tat-5, pad-1* or *rme-8* mutants. This could be caused by the combined mislocalization of MV inhibitors and MV activators. Thus, PI3K mutants may disrupt both the activation of MV release through an unknown factor and the inhibition of MV release through TAT-5 trafficking. While flippases like TAT-5 can translocate phospholipids (PLs) from the extracellular face of the lipid bilayer to the cytoplasmic layer, floppases can translocate PLs in the opposite direction and scramblases can randomly translocate phospholipids in both directions[68]. Thus, floppases or scramblases are likely transmembrane proteins to induce PE externalization and activate MV budding. Thus, endosomal trafficking regulation of floppases and scramblases by PI3K may cause reduction of the MV budding phenotype and it will be interesting to test whether PE is externalized in PI3K mutants.

Furthermore, it was previously shown that the ESCRT complex is required for MV release in *tat-5* mutants[1]. As PI3P-containing vesicles are needed to carry the ESCRT complex to the intercellular bridge during abscission[69] and PI3P recruits ESCRT to endosomes[52,58], it would be interesting to check whether the ESCRT complex also needs the class III PI3K to localize to MV bud sites on the plasma membrane. To check this hypothesis, the plasma membrane localization of ESCRT subunits like ESCRT-0, whose membrane localization requires PI3P levels[1,53], should be analyzed in *vps-34* or *bec-1* mutants. It will also be interesting to test whether PI3P is increased at the plasma membrane in *tat-5* mutants, which could be the cause of the increased ESCRT recruitment. These experiments would determine whether PI3P also has a dual role during MV release and is able to promote MV budding.

Despite the important trafficking functions of PI3K, we only detected a mild increase in MV release in *vps-34* and *bec-1* mutants in comparison to a massive increase of MVs released from *tat-5* and *pad-1* knockdown. We used maternal-zygotic mutant *bec-1* embryos, where no new mRNA was transcribed for a generation before we analyzed the embryos. However, mRNA and proteins can persist for days[70]. Furthermore, VPS-34 is the catalytic subunit of the PI3K complex and should be similarly important as its regulatory subunit BEC-1. In contrast, we see less MV release in *vps-34* mutants than in *bec-1* mutants. This may be due to the fact that *vps-34* mutants used in this study are not null mutants because the maternal-zygotic null mutants arrest as larvae[71]. To prevent larval arrest and allow the production of maternal-zygotic embryos, wildtype *vps-34* was expressed from an extrachromosomal array to maintain the strain. These arrays are typically silenced in the germ line and early embryo, but weak expression from the transgene could still occur, which may account for the weaker phenotypes in comparison to *bec-1* mutants. As RNAi depletion of either *bec-1* or *vps-34* failed to show increased MV release, it appears that even a low level of BEC-1 or VPS-34 is sufficient to inhibit MV release.

3.3.4. RME-8 regulates recycling from endosomes and inhibits microvesicle release

We also found that the DnaJ domain-containing protein RME-8 inhibits MV release. RME-8 has been linked to recycling transmembrane proteins to the plasma membrane in addition to retrograde recycling from endosomes to the Trans Golgi Network (TGN)[72]. RME-8 binds to PI3P-containing endosomes, which depends on PI3K[73–75]. Thus RME-8 needs the activity of PI3K to be recruited to the endosomal membrane and is likely to act downstream of BEC-1 and VPS-34 in recycling a transmembrane protein important for inhibiting MV release.

RME-8 acts together with the sorting nexin SNX-1 to define recycling microdomains and restrict cargos from lysosomal degradation[73,76]. This shows that RME-8 has general functions in generating the endosomal domains that decide between cargo recycling and degradation. The recycling of the Notch receptor, Cation-Independent Mannose-6-Phosphate Receptor (CI-MPR), epidermal growth factor receptor (EGFR) and Wntless were disrupted in *rme-8* mutants, showing that RME-8 has important functions in the endosomal trafficking of transmembrane proteins [73,75,77–80]. Therefore, we propose that RME-8 could be involved in recycling TAT-5 to the plasma membrane. Since RME-8 acts together with SNX-1 to separate the recycling microdomain from the degradative microdomains of the sorting endosome[76], SNX-1 could regulate TAT-5 trafficking together with RME-8. However, we did not find an MV inhibitory function of SNX-1 in our screen (also discussed in chapter 4), suggesting that RME-8 must have a different function than SNX-1 in inhibiting MV release. In the following chapter 4, we characterize whether and how RME-8 and SNX-1 regulate TAT-5 localization and PE flipping activity in order to inhibit MV release.

We saw less MV release from *rme-8* RNAi in comparison to *tat-5* or *pad-1* depleted embryos. Since we observed that *rme-8* RNAi causes embryonic lethality, as reported previously[37], we assume that the reduced MV release is not due to an insufficient depletion of RME-8. Due to the general function of RME-8 on recycling domain formation and endosomal tubulation, it is therefore possible that RME-8 regulates the recruitment of unidentified proteins that promote MV release, like lipid floppases and scramblases, in addition to trafficking proteins that inhibit MV release like TAT-5.

We also noticed that ILV-sized EVs were released from *rme-8* depleted cells. Thus, RME-8 could also inhibit exosome release. For example, RME-8 could regulate the localization of transmembrane proteins involved in exosome release, such as SNARE proteins or the V-ATPase required for the fusion of MVBs to the plasma membrane[3]. Thus, it would be interesting to check whether the localization of these exosome release regulators is altered in *rme-8* mutants. Alternatively, RME-8 could be important for limiting ILV formation. When RME-8 is absent, endosomes have larger ESCRT domains[76], which could alter ILV formation and subsequently exosome release. Thus, it will be interesting to test whether RME-8 inhibits exosome release in addition to MV release.

Alternatively, loss of RME-8 could affect the size of MVs. Reduced clathrin recruitment and increased ESCRT-0 accumulation have been shown to decrease the number and size of

ILVs[55]. Loss of RME-8 causes increased accumulation of clathrin on endosomes[73,74,81], as well as an enlarged HGRS-1 (ESCRT-0) subdomain and increased HGRS-1 recruitment to endosomes[76], showing that RME-8 is required for clathrin and ESCRT-0 dynamics. Thus, it is tempting to speculate that RME-8 controls ESCRT-0 and clathrin dynamics on endosomal or plasma membrane bud sites, mediating the proper size of vesicles. Indeed, ILVs were smaller after *rme-8* RNAi than from *bec-1* mutants and *pad-1* RNAi, suggesting that RME-8 is required for the proper size of ILVs. Since ESCRT-0 was required for MV budding[1], we predict that RME-8 could regulate ESCRT-0 and clathrin dynamics on the plasma membrane, which ultimately influences the size of MVs. Taken together, it remains to be determined whether RME-8 affects the size of MVs or inhibits the release of exosomes.

3.3.5. PAD-1 is likely to inhibit microvesicle release through TAT-5

We discovered that the understudied, but conserved Dopey domain-containing protein PAD-1 also inhibits MV budding through an unknown mechanism. Interestingly, the yeast and mammalian orthologs of PAD-1, Dop1 and Dopey2, form a complex with TAT-5 orthologs Neo1 and ATP9A, as well as a large GEF-like protein Mon2[82,83]. This conservation suggests that PAD-1 and MON-2 could directly interact with TAT-5 to inhibit MV release.

Previously, it was reported that the yeast TAT-5 ortholog Neo1 is important for the proper protein levels of the PAD-1 ortholog Dop1, since Neo1 mutants have significantly decreased levels of Dop1[82]. Dop1 mutants also had reduced levels of Neo1, showing a mutual dependency on their protein levels. Thus, it will be interesting to test whether TAT-5 levels are altered in *pad-1* mutants. However, it is unclear whether Dop1 and Neo1 control each other's expression levels or protein stability. Furthermore, it is unclear whether Neo1 and Dop1 can regulate each other's localization or activity beyond regulating their steady state levels. Thus, there are multiple ways that PAD-1 could regulate TAT-5.

One possibility is that PAD-1 could be the β-subunit for TAT-5. β-subunits of the CDC50 family are cofactors required for the activity and ER exit of most P4-ATPases, but not TAT-5 and its orthologs[82,84,85]. CDC50 proteins consist mostly of two transmembrane (TM) domains joined by a large exoplasmic domain[84]. However, it is still under debate whether PAD-1 has a TM domain. The first structure prediction of DopA, the PAD-1 ortholog in *Aspergillus nidulans*, suggested that short hydrophobic residues in the C-term form a putative TM domain[86], but this region was only conserved in *S. cerevisiae* Dop1, not in animals or even in *Candida albicans*. Another study predicted that human DOPEY2 has 9 TM domains and PAD-1 has 13 TM domains by using Tmpred (TM region prediction)[36]. We detected two putative TM domains at the C-terminus of PAD-1 using Phobius (also discussed in 5.3.X)[87], but the majority of the PAD-1 protein is predicted to be cytosolic, including the highly conserved N-terminal DOPEY domain[36,86], which is not present in CDC50 family proteins[84]. Thus, it is unclear whether PAD-1 could act as a ß-subunit to regulate TAT-5 flippase activity or ER exit.

Apart from being a potential TAT-5 activity regulator, PAD-1 is also involved in protein trafficking. For example, the yeast ortholog Dop1 was required for trafficking of the vacuolar hydrolase carboxypeptidase Y (CPY) from the Golgi to the vacuole and mediates the endosome to Golgi recycling of the v-SNARE Snc1[82,88]. Mon2 also regulates the trafficking of CPY in yeast[89,90]. Thus, it is also possible that PAD-1 and MON-2 control TAT-5 localization at endosomes or the plasma membrane. However, both TAT-5 and PAD-1 inhibit MV release, but we did not find MON-2 in our MV inhibitor screen (see also chapter 5.2.X). Similarly, PAD-1 and TAT-5 and their yeast orthologs are essential genes[36,86,91,92], while MON-2 and its yeast ortholog are not essential[93,94]. This suggests that TAT-5 and PAD-1 have more similar functions in inhibiting MV release than MON-2. In chapter 5, we characterize how PAD-1 and MON-2 regulate TAT-5 localization and flippase activity to regulate MV release.

3.3.6. Outlook

In this chapter, we have enhanced the visibility of MV release *in vivo* by re-purposing degron-mediated degradation of abundant plasma membrane reporters to degrade cellular background and reveal MVs. Additionally, we show that degron-tagging cortical proteins can help to identify proteins released inside MVs without the need for super-resolution microscopy or extraction and purification. Since degradation-based techniques are already used in cell extracts and model organisms like drosophila and zebrafish[38,43,95], we believe that this assay can be readily adapted to increase the visibility of EVs in other tissues and animals. Thus, degron-tagging can help to clarify EV functions and release mechanisms from many model systems *in vivo*.

Ultimately, we identified novel inhibitors of MV release, including the class III PI3Kinase complex, RME-8 and PAD-1, shedding new light into the mechanisms of ectocytosis. With these MV inhibitors in hand, we can test whether they regulate each other or the MV inhibitor TAT-5 and build a molecular pathway of MV biogenesis. This will greatly enhance our understanding of the specific mechanisms of EV release by plasma membrane budding (ectocytosis). Since all four proteins are conserved in mammals[36,37,71,96], it is possible that their MV inhibitory function is conserved in mammals. As MVs are released from animals to control development, the immune response and disease, we believe our studies will be of great impact to understand and control the mechanisms of MV release in many fields.

3.4. References

1. Wehman, A. M., Poggioli, C., Schweinsberg, P., Grant, B. D. & Nance, J. The P4-ATPase TAT-5 inhibits the budding of extracellular vesicles in C. elegans embryos. *Curr. Biol.* **21,** 1951–1959 (2011).
2. Naik, J. *et al.* The P4-ATPase ATP9A is a novel determinant of exosome release. *PLoS One* **14,** e0213069 (2019).
3. Beer, K. B. & Wehman, A. M. Mechanisms and functions of extracellular vesicle release in vivo —What we can learn from flies and worms. *Cell Adh. Migr.* **11,** 135–150 (2017).
4. Hyenne, V., Lefebvre, O. & Goetz, J. G. Going live with tumor exosomes and microvesicles. *Cell Adhes. Migr.* **11,** 173–186 (2017).
5. Ramirez, M. I. *et al.* Technical challenges of working with extracellular vesicles. *Nanoscale* **10,** 881–906 (2018).
6. Bobrie, A., Colombo, M., Krumeich, S., Raposo, G. & Théry, C. Diverse subpopulations of vesicles secreted by different intracellular mechanisms are present in exosome preparations obtained by differential ultracentrifugation. *J. Extracell. Vesicles* **1,** 18397 (2012).
7. Hyenne, V. *et al.* Studying the Fate of Tumor Extracellular Vesicles at High Spatiotemporal Resolution Using the Zebrafish Embryo. *Dev. Cell* **48,** 554-572.e7 (2019).
8. Verweij, F. J. *et al.* Live Tracking of Inter-organ Communication by Endogenous Exosomes In Vivo. *Dev. Cell* **48,** 573-589.e4 (2019).
9. Várnai, P. & Balla, T. Visualization and manipulation of phosphoinositide dynamics in live cells using engineered protein domains. *Pflugers Arch. Eur. J. Physiol.* **455,** 69–82 (2007).
10. Viaud, J. *et al.* Phosphoinositides: Important lipids in the coordination of cell dynamics. *Biochimie* **125,** 250–258 (2016).
11. Lemmon, M. A. Pleckstrin homology (PH) domains and phosphoinositides. *Biochem. Soc. Symp.* **74,** 81–93 (2007).
12. Kume, A. *et al.* The pleckstrin homology domain of diacylglycerol kinase η strongly and selectively binds to phosphatidylinositol 4,5-bisphosphate. *J. Biol. Chem.* **291,** 8150–8161 (2016).
13. Di Paolo, G. & De Camilli, P. Phosphoinositides in cell regulation and membrane dynamics. *Nature* **443,** 651–657 (2006).
14. Schermelleh, L. *et al.* Super-resolution microscopy demystified. *Nat. Cell Biol.* **21,** 72–84 (2019).
15. Natsume, T. & Kanemaki, M. T. Conditional Degrons for Controlling Protein Expression at the Protein Level. *Annu. Rev. Genet.* **51,** 83–102 (2017).
16. Foot, N., Henshall, T. & Kumar, S. Ubiquitination and the regulation of membrane proteins. *Physiol. Rev.* **97,** 253–281 (2017).
17. Banaszynski, L. A., Chen, L., Maynard-Smith, L. A., Ooi, A. G. L. & Wandless, T. J. A Rapid, Reversible, and Tunable Method to Regulate Protein Function in Living Cells Using Synthetic Small Molecules. *Cell* **126,** 995–1004 (2006).
18. Bonger, K. M., Chen, L. C., Liu, C. W. & Wandless, T. J. Small-molecule displacement of a cryptic degron causes conditional protein degradation. *Nat. Chem. Biol.* **7,** 531–537 (2011).
19. Nishimura, K., Fukagawa, T., Takisawa, H., Kakimoto, T. & Kanemaki, M. An auxin-based degron system for the rapid depletion of proteins in nonplant cells. *Nat. Methods* **6,** 917–922 (2009).
20. Raina, K. & Crews, C. M. Chemical inducers of targeted protein degradation. *Journal of Biological Chemistry* **285,** 11057–11060 (2010).
21. Renicke, C., Schuster, D., Usherenko, S., Essen, L.-O. & Taxis, C. A LOV2 Domain-Based Optogenetic Tool to Control Protein Degradation and Cellular Function. *Chem. Biol.* **20,** 619–

626 (2013).

22. Reese, K. J., Dunn, M. A., Waddle, J. A. & Seydoux, G. Asymmetric segregation of PIE-1 in C. elegans is mediated by two complementary mechanisms that act through separate PIE-1 protein domains. *Mol. Cell* **6,** 445–455 (2000).
23. Armenti, S. T., Lohmer, L. L., Sherwood, D. R. & Nance, J. Repurposing an endogenous degradation system for rapid and targeted depletion of C. elegans proteins. *Development* **141,** 4640–4647 (2014).
24. DeRenzo, C., Reese, K. J. & Seydoux, G. Exclusion of germ plasm proteins from somatic lineages by cullin-dependent degradation. *Nature* **424,** 685–689 (2003).
25. Beer, K. B. *et al.* Degron-tagged reporters probe membrane topology and enable the specific labelling of membrane-wrapped structures. *Nat. Commun.* **10,** 3490 (2019).
26. Jantsch-Plunger, V. & Glotzer, M. Depletion of syntaxins in the early Caenorhabditis elegans embryo reveals a role for membrane fusion events in cytokinesis. *Curr. Biol.* **9,** 738–745 (1999).
27. Eitan, E., Suire, C., Zhang, S. & Mattson, M. P. Impact of lysosome status on extracellular vesicle content and release. *Ageing Res. Rev.* **32,** 65–74 (2016).
28. Oldenbroek, M. *et al.* Multiple RNA-binding proteins function combinatorially to control the soma-restricted expression pattern of the E3 ligase subunit ZIF-1. *Dev. Biol.* **363,** 388–398 (2012).
29. Olson, S. K., Greenan, G., Desai, A., Müller-Reichert, T. & Oegema, K. Hierarchical assembly of the eggshell and permeability barrier in C. Elegans. *J. Cell Biol.* **198,** 731–748 (2012).
30. Fabritius, A. S., Ellefson, M. L. & McNally, F. J. Nuclear and spindle positioning during oocyte meiosis. *Curr. Opin. Cell Biol.* **23,** 78–84 (2011).
31. Fazeli, G., Stetter, M., Lisack, J. N. & Wehman, A. M. C. elegans Blastomeres Clear the Corpse of the Second Polar Body by LC3-Associated Phagocytosis. *Cell Rep.* **23,** 2070–2082 (2018).
32. Beer, K. B. *et al.* Extracellular vesicle budding is inhibited by redundant regulators of TAT-5 flippase localization and phospholipid asymmetry. *Proc. Natl. Acad. Sci.* **115,** E1127–E1136 (2018).
33. Beckett, K. *et al.* Drosophila S2 cells secrete wingless on exosome-like vesicles but the wingless gradient forms independently of exosomes. *Traffic* **14,** 82–96 (2013).
34. Choi, D. S. *et al.* Proteomic analysis of microvesicles derived from human colorectal cancer cells. *J. Proteome Res.* **6,** 4646–4655 (2007).
35. Ohashi, Y., Tremel, S. & Williams, R. L. VPS34 complexes from a structural perspective. *Journal of Lipid Research* **60,** 229–241 (2019).
36. Guipponi, M. *et al.* C21orf5, a novel human chromosome 21 gene, has a Caenorhabditis elegans ortholog (pad-1) required for embryonic patterning. *Genomics* **68,** 30–40 (2000).
37. Zhang, Y., Grant, B. & Hirsh, D. RME-8, a conserved J-domain protein, is required for endocytosis in Caenorhabditis elegans. *Mol. Biol. Cell* **12,** 2011–2021 (2001).
38. Yamaguchi, N., Colak-Champollion, T. & Knaut, H. zGrad is a nanobody-based degron system that inactivates proteins in zebrafish. *Elife* **8,** (2019).
39. Caussinus, E., Kanca, O. & Affolter, M. Fluorescent fusion protein knockout mediated by anti-GFP nanobody. *Nat. Struct. Mol. Biol.* **19,** 117–121 (2012).
40. Baudisch, B., Pfort, I., Sorge, E. & Conrad, U. Nanobody-directed specific degradation of proteins by the 26s-proteasome in plants. *Front. Plant Sci.* **9,** 130 (2018).
41. Wang, S. *et al.* A toolkit for GFP-mediated tissue-specific protein degradation in C. elegans . *Development* **144,** 2694–2701 (2017).
42. Zhang, L., Ward, J. D., Cheng, Z. & Dernburg, A. F. The auxin-inducible degradation (AID) system enables versatile conditional protein depletion in C. elegans. *Development* **142,** 4374–4384 (2015).
43. Daniel, K. *et al.* Conditional control of fluorescent protein degradation by an auxin-dependent nanobody. *Nat. Commun.* **9,** 3297 (2018).
44. Nance, J. & Frøkjær-Jensen, C. The Caenorhabditis elegans Transgenic Toolbox. *Genetics* **212,** 959–990 (2019).
45. Piper, R. C. & Luzio, J. P. Ubiquitin-dependent sorting of integral membrane proteins for degradation in lysosomes. *Curr. Opin. Cell Biol.* **19,** 459–465 (2007).
46. Kowal, J. *et al.* Proteomic comparison defines novel markers to characterize heterogeneous populations of extracellular vesicle subtypes. *Proc. Natl. Acad. Sci.* **113,** E968–E977 (2016).

47. Van Niel, G., D'Angelo, G. & Raposo, G. Shedding light on the cell biology of extracellular vesicles. *Nat. Rev. Mol. Cell Biol.* **19,** 213–228 (2018).
48. Zhou, X., Sebastian, T. T. & Graham, T. R. Auto-inhibition of Drs2p, a yeast phospholipid flippase, by its carboxyl-terminal tail. *J. Biol. Chem.* **288,** 31807–15 (2013).
49. Natarajan, P. *et al.* Regulation of a Golgi flippase by phosphoinositides and an ArfGEF. *Nat. Cell Biol.* **11,** 1421–1426 (2009).
50. Kalra, H. *et al.* Vesiclepedia: A Compendium for Extracellular Vesicles with Continuous Community Annotation. *PLoS Biol.* **10,** e1001450 (2012).
51. Keerthikumar, S. *et al.* ExoCarta: A Web-Based Compendium of Exosomal Cargo. *J. Mol. Biol.* **428,** 688–692 (2016).
52. Mathieu, M., Martin-Jaular, L., Lavieu, G. & Théry, C. Specificities of secretion and uptake of exosomes and other extracellular vesicles for cell-to-cell communication. *Nat. Cell Biol.* **21,** 9–17 (2019).
53. Raiborg, C., Bache, K. G., Mehlum, A., Stang, E. & Stenmark, H. Hrs recruits clathrin to early endosomes. *EMBO J.* **20,** 5008–21 (2001).
54. Sachse, M., Urbé, S., Oorschot, V., Strous, G. J. & Klumperman, J. Bilayered clathrin coats on endosomal vacuoles are involved in protein sorting toward lysosomes. *Mol. Biol. Cell* **13,** 1313–28 (2002).
55. Wenzel, E. M. *et al.* Concerted ESCRT and clathrin recruitment waves define the timing and morphology of intraluminal vesicle formation. *Nat. Commun.* **9,** (2018).
56. Camus, G. *et al.* The clathrin adaptor complex AP-1 binds HIV-1 and MLV Gag and facilitates their budding. *Mol. Biol. Cell* **18,** 3193–3203 (2007).
57. Bilanges, B., Posor, Y. & Vanhaesebroeck, B. PI3K isoforms in cell signalling and vesicle trafficking. *Nat. Rev. Mol. Cell Biol.* **20,** 515–534 (2019).
58. Backer, J. M. The intricate regulation and complex functions of the Class III phosphoinositide 3-kinase Vps34. *Biochemical Journal* **473,** 2251–2271 (2016).
59. Lu, N., Shen, Q., Mahoney, T. R., Liu, X. & Zhou, Z. Three sorting nexins drive the degradation of apoptotic cells in response to PtdIns(3)P signaling. *Mol. Biol. Cell* **22,** 354–374 (2011).
60. Jia, Z., Ghai, R., Collins, B. M. & Mark, A. E. The recognition of membrane-bound PtdIns3P by PX domains. *Proteins Struct. Funct. Bioinforma.* **82,** 2332–2342 (2014).
61. Xu, Y., Hortsman, H., Seet, L., Wong, S. H. & Hong, W. SNX3 regulates endosomal function through its PX-domain-mediated interaction with Ptdlns(3)P. *Nat. Cell Biol.* **3,** 658–666 (2001).
62. Vergés, M., Sebastián, I. & Mostov, K. E. Phosphoinositide 3-kinase regulates the role of retromer in transcytosis of the polymeric immunoglobulin receptor. *Exp. Cell Res.* **313,** 707–718 (2007).
63. Rincón, E. *et al.* Translocation dynamics of sorting nexin 27 in activated T cells. *J. Cell Sci.* **124,** 776–788 (2011).
64. Cullen, P. J. Endosomal sorting and signalling: An emerging role for sorting nexins. *Nat. Rev. Mol. Cell Biol.* **9,** 574–582 (2008).
65. Dalton, L. E., Bean, B. D. M., Davey, M. & Conibear, E. Quantitative high-content imaging identifies novel regulators of Neo1 trafficking at endosomes. *Mol. Biol. Cell* **28,** 1539–1550 (2017).
66. Wicky, S., Schwarz, H. & Singer-Kruger, B. Molecular Interactions of Yeast Neo1p, an Essential Member of the Drs2 Family of Aminophospholipid Translocases, and Its Role in Membrane Trafficking within the Endomembrane System. *Mol. Cell. Biol.* **24,** 7402–7418 (2004).
67. Van Meer, G., Voelker, D. R. & Feigenson, G. W. Membrane lipids: Where they are and how they behave. *Nat. Rev. Mol. Cell Biol.* **9,** 112–124 (2008).
68. Sharom, F. J. Flipping and flopping-lipids on the move. *IUBMB Life* **63,** 736–746 (2011).
69. Campa, C. C., Martini, M., De Santis, M. C. & Hirsch, E. How PI3K-derived lipids control cell division. *Front. Cell Dev. Biol.* **3,** 61 (2015).
70. Wood, W. B. *et al.* Parental effects and phenotypic characterization of mutations that affect early development in Caenorhabditis elegans. *Dev. Biol.* **74,** 446–469 (1980).
71. Roggo, L. *et al.* Membrane transport in Caenorhabditis elegans: an essential role for VPS34 at the nuclear membrane. *EMBO J.* **21,** 1673–1683 (2002).
72. Gallon, M. & Cullen, P. J. Retromer and sorting nexins in endosomal sorting. *Biochem. Soc. Trans.* **43,** 33–47 (2015).

73. Shi, A. *et al.* Regulation of endosomal clathrin and retromer-mediated endosome to Golgi retrograde transport by the J-domain protein RME-8. *EMBO J.* **28,** 3290–3302 (2009).
74. Xhabija, B., Taylor, G. S., Fujibayashi, A., Sekiguchi, K. & Vacratsis, P. O. Receptor mediated endocytosis 8 is a novel PI(3)P binding protein regulated by myotubularin-related 2. *FEBS Lett.* **585,** 1722–1728 (2011).
75. Ruck, A. *et al.* The Atg6/Vps30/Beclin 1 ortholog BEC-1 mediates endocytic retrograde transport in addition to autophagy in C. elegans. *Autophagy* **7,** 386–400 (2011).
76. Norris, A. *et al.* SNX-1 and RME-8 oppose the assembly of HGRS-1/ESCRT-0 degradative microdomains on endosomes. *Proc. Natl. Acad. Sci.* **114,** E307–E316 (2017).
77. Freeman, C. L., Hesketh, G. & Seaman, M. N. J. RME-8 coordinates the activity of the WASH complex with the function of the retromer SNX dimer to control endosomal tubulation. *J. Cell Sci.* **127,** 2053–2070 (2014).
78. Simonetti, B. & Cullen, P. J. Actin-dependent endosomal receptor recycling. *Curr. Opin. Cell Biol.* **56,** 22–33 (2019).
79. Girard, M. & McPherson, P. S. RME-8 regulates trafficking of the epidermal growth factor receptor. *FEBS Lett.* **582,** 961–966 (2008).
80. Gomez-Lamarca, M. J., Snowdon, L. A., Seib, E., Klein, T. & Bray, S. J. Rme-8 depletion perturbs Notch recycling and predisposes to pathogenic signaling. *J. Cell Biol.* **210,** 303–318 (2015).
81. Popoff, V. *et al.* Analysis of articulation between clathrin and retromer in retrograde sorting on early endosomes. *Traffic* **10,** 1868–1880 (2009).
82. Barbosa, S., Pratte, D., Schwarz, H., Pipkorn, R. & Singer-Krüger, B. Oligomeric Dop1p is part of the endosomal Neo1p-Ysl2p-Arl1p membrane remodeling complex. *Traffic* **11,** 1092–1106 (2010).
83. McGough, I. J. *et al.* SNX3-retromer requires an evolutionary conserved MON2:DOPEY2:ATP9A complex to mediate Wntless sorting and Wnt secretion. *Nat. Commun.* **9,** 3737 (2018).
84. Andersen, J. P. *et al.* P4-ATPases as phospholipid flippases-structure, function, and enigmas. *Front. Physiol.* **7,** 1–23 (2016).
85. Takatsu, H. *et al.* ATP9B, a P4-ATPase (a putative aminophospholipid translocase), localizes to the trans-Golgi network in a CDC50 protein-independent manner. *J. Biol. Chem.* **286,** 38159–38167 (2011).
86. Pascon, R. C. & Miller, B. L. Morphogenesis in Aspergillus nidulans requires Dopey (DopA), a member of a novel family of leucine zipper-like proteins conserved from yeast to humans. *Mol. Microbiol.* **36,** 1250–1264 (2000).
87. Käll, L., Krogh, A. & Sonnhammer, E. L. . A Combined Transmembrane Topology and Signal Peptide Prediction Method. *J. Mol. Biol.* **338,** 1027–1036 (2004).
88. Gillingham, A. K., Whyte, J. R. C., Panic, B. & Munro, S. Mon2, a relative of large Arf exchange factors, recruits Dop1 to the Golgi apparatus. *J. Biol. Chem.* **281,** 2273–2280 (2006).
89. Bonangelino, C. J., Chavez, E. M. & Bonifacino, J. S. Genomic Screen for Vacuolar Protein Sorting Genes in *Saccharomyces cerevisiae*. *Mol. Biol. Cell* **13,** 2486–2501 (2002).
90. Avaro, S., Belgareh-Touzé, N., Sibella-Argüelles, C., Volland, C. & Haguenauer-Tsapis, R. Mutants defective in secretory/vacuolar pathways in the EUROFAN collection of yeast disruptants. *Yeast* **19,** 351–371 (2002).
91. Lyssenko, N. N., Miteva, Y., Gilroy, S., Hanna-Rose, W. & Schlegel, R. A. An unexpectedly high degree of specialization and a widespread involvement in sterol metabolism among the C. elegans putative aminophospholipid translocases. *BMC Dev. Biol.* **8,** 1–17 (2008).
92. Prezant, T. R., Chaltraw, W. E. j. & Fischel-Ghodsian, N. Identification of an overexpressed yeast gene which prevents aminoglycoside toxicity. *Microbiology* **142,** 3407–3414 (1996).
93. Efe, J. A. *et al.* Yeast Mon2p is a highly conserved protein that functions in the cytoplasm-to-vacuole transport pathway and is required for Golgi homeostasis. *J. Cell Sci.* **118,** 4751–4764 (2005).
94. Imae, R. *et al.* Intracellular Phospholipase A 1 and Acyltransferase, Which Are Involved in Caenorhabditis elegans Stem Cell Divisions, Determine the sn -1 Fatty Acyl Chain of Phosphatidylinositol. *Mol. Biol. Cell* **21,** 3114–3124 (2010).
95. Chen, W., Werdann, M. & Zhang, Y. The auxin-inducible degradation system enables

conditional PERIOD protein depletion in the nervous system of Drosophila melanogaster. *FEBS J.* **285,** 4378–4393 (2018).

96. Funderburk, S. F., Wang, Q. J. & Yue, Z. The Beclin 1-VPS34 complex - at the crossroads of autophagy and beyond. *Trends in Cell Biology* **20,** 355–362 (2010).

4. TAT-5 is trafficked by redundant sorting nexin pathways

4.1. Introduction: Endocytic trafficking recycles transmembrane proteins

In the previous chapter, we identified four proteins that inhibit microvesicle (MV) release: two subunits of the PI3Kinase VPS-34 and BEC-1, as well as RME-8 and PAD-1. All four of these proteins are involved in endocytic trafficking[1–4], suggesting that their role in microvesicle release could involve protein trafficking.

Endocytic trafficking is one of several trafficking routes that transmembrane (TM) proteins pass through during their lifetime[5]. TM proteins are first synthesized in the endoplasmic reticulum (ER). They get transported to the Golgi network where they traffic from the cis-Golgi to the trans-Golgi network (TGN), before they are finally trafficked to their target membrane via trafficking vesicles[6]. If targeted to the plasma membrane, TM proteins can also be endocytosed and sorted into endosomes, organelles that organizes the further trafficking of TM proteins[7]. Endosomes form different domains, which are responsible to decide the fate of the TM protein[8]. First, TM proteins can get recycled via the recycling pathway, which means that the proteins are routed back to the plasma membrane[9]. This involves tubulation of the recycling domain of the endosome and recycling vesicle formation[8]. Proteins can also be trafficked back to the Golgi via the retrograde trafficking pathway[5]. This can also lead to recycling to the plasma membrane after passing through the Golgi. Lastly, proteins routed to the degradative pathway are sorted inside intraluminal vesicles (ILVs) of late endosomes, also called multivesicular bodies (MVB), which involves the inward budding of the endosome membrane into the endosome lumen. MVBs then fuse with lysosomes, where the TM proteins on ILVs can be degraded by lysosomal hydrolases[9]. Thus, endosomal trafficking can lead to the recycling or degradation of transmembrane proteins.

Because the newly identified MV inhibitors regulate endosomal trafficking, we wondered whether they could also regulate the endosomal trafficking of the TM protein TAT-5. In this chapter, we examine the role of VPS-34, BEC-1, and RME-8 in TAT-5 trafficking and MV budding. PAD-1 will be discussed in chapter 5.

4.1.1. Class III PI3K determines endosome identity

Trafficking endosomes and membrane organelles can be distinguished from one-another by their phosphatidylinositide (PI) lipid composition[10]. The inositol headgroup can be phosphorylated at three defined positions (3, 4 and 5) to create eight distinct species of PI lipids, which can be recognized by different binding partners[11]. For example, PI phosphorylated at position 3 is called PI3P, which is one of the major determinants for endosome identity and essential for many endosome functions like endosome fusion, signaling and motility[10]. PI3P levels are required for the recruitment of PI3P-binding proteins like FYVE- or PX-domain-containing proteins to endosomes[9]. PI3P levels regulate the function and localization of endosomal proteins like the FYVE domain-containing early endosomal antigen EEA-1[12], which is a tethering molecule required for the fusion of early endosomes[13], and the ESCRT-0 protein HRS required for protein sorting into intraluminal vesicles (ILV), as well as the formation of ILVs[14]. PI3P levels similarly regulate the function and localization of the PX-domain-containing sorting nexins (SNX), which are required for tubular sorting and recycling vesicle formation on endosomes[15,16]. Thus, PI species have important roles recruiting proteins for endosome fusion, endosomal recycling and degradation.

To establish and mature endosomes, a series of PI kinases and phosphatases modify the inositol headgroup on specific PI species. For example, the class III PI3Kinase (PI3K) phosphorylates position 3 of the inositol headgroup on PI on early endosomes and is one of the main sources of cellular PI3P. The class III PI3K is a conserved tetrameric complex in the eukaryote lineage that consists of the core catalytic kinase VPS34, a core regulatory subunit Beclin1 (BEC-1, also called Atg6 in yeast) and the protein kinase-like VPS15 (also known as PIK3R4). These core components form a tetrameric complex with either ATG14 (complex 1 involved in autophagy) or UVRAG (complex 2 involved in endosomal trafficking)[1,17]. PI3K core subunits VPS-34 and BEC-1 are known for their diverse functions on endosomal trafficking, autophagy, phagocytosis and cell division [1,18]. Class III PI3K also controls the maturation of early endosomes to late endosomes by recruitment of effectors that initiate the Rab switch between early endosomal RAB5 and late endosomal RAB7[1]. Thus, the class III PI3K controls intracellular trafficking due to regulation of endosome maturation or fusion[1,17].

As we discovered in chapter 3, VPS-34 and BEC-1 also regulate MV budding, which could include regulating the localization of both inhibitors and activators of MV release, such as the PI3P-binding ESCRT-0 complex. Dalton *et al.* found that the TAT-5 ortholog Neo1 accumulated at endosomes in yeast mutant for the BEC-1 ortholog *vps30*[19], suggesting that the class III PI3K is likely to be required for the endosomal trafficking of TAT-5. Thus, it will be interesting to examine TAT-5 localization in PI3K mutants.

4.1.2. RME-8 is important for endocytosis, recycling and endosomal tubulation

The DnaJ domain-containing protein receptor-mediated endocytosis 8 (RME-8) is a PI3P effector downstream of the class III PI3K (see also 3.3.4.), as it localizes to PI3P-containing endosomes[20–22]. RME-8 was initially identified as an essential gene required for endocytosis in *C. elegans* that is conserved from plants to humans[23]. RME-8 mutants in *Drosophila* also have disrupted endocytosis and altered clathrin localization[24]. RME-8 binds to Hsp70 via its J-domain[24], which is required for both clathrin uncoating and clathrin-coated vesicle formation[25,26], suggesting that Hsp70 and RME-8 are required for clathrin-mediated endocytosis.

RME-8 also orchestrates endosomal recycling. RME-8 recruits the Wiskott-Aldrich Syndrome protein and SCAR homolog (WASH) complex to endosomes, which nucleates actin to control formation and fission of endosomal tubules[3]. RME-8 also binds the sorting nexin SNX-1 and together they restrict recycling microdomains on endosomes to prevent cargo from undergoing lysosomal degradation[20,27]. RME-8 was shown to be required for the retrograde trafficking of Cation-Independent Mannose 6-Phosphate Receptor (CI-MPR), Notch receptor trafficking, reduced lysosomal degradation of epidermal growth factor receptor (EGFR) and Wntless recycling from endosomes to Golgi[3,20,22,28–30]. Taken together, RME-8 has important functions during the formation of endosome domains and tubulation of the endosome membrane.

As discussed in chapter 3, we discovered that RME-8 was required to inhibit MV release, which could be due to its function in endocytosis or in regulating the trafficking of MV release inhibitors. Since previous results showed that TAT-5 is endocytosed and cycles through RME-8-positive vesicles[31], it will be interesting to test whether RME-8 regulates the plasma membrane recycling of TAT-5 to prevent its lysosomal degradation.

4.1.3. Sorting nexins and Retromer are important for recycling and endosomal tubulation

Both PI3K and RME-8 are associated with sorting nexins (SNX)[20], which bind cargos and are required for the tubulation of sorting endosomes to form recycling vesicles[15]. SNX proteins have an evolutionarily-conserved phagocyte oxidase (phox) homology (PX) domain that can bind PI3P[15,16], in addition to membrane-sculpting BAR domains or protein-binding FERM domains (discussed below). Thus, different SNX proteins are thought to interact with different cargos and have different functions.

The SNX-PX protein SNX-3 lacks other domains common to SNX proteins and was already linked to trafficking P4-ATPases. The TAT-5 ortholog Neo1p in yeast was trafficked by Snx3, in conjunction with PI3K activity[19]. Dalton *et al.* also reported that Neo1 accumulated at Snx3-positive vesicles in *vps30* (beclin1) mutants and that Neo1 accumulated in the vacuole in *snx3* mutants. They proposed that Snx3 is required for the endosome to Golgi trafficking of Neo1. They could also show that Snx3 binds Neo1 at an N-terminal FEM motif, which is partially required for Neo1 trafficking, suggesting that Snx3 specifically recognizes Neo1 as cargo. Thus, SNX-3 is a likely candidate to regulate TAT-5 trafficking.

SNX3 binds to two core subunits of the retromer complex, VPS26 and VPS35, and is required for the recruitment of the retromer to PI3P-positive endosomes[32,33]. The retromer complex consists of a conserved trimer of core subunits (VPS26, VPS29, and VPS35), which are required to correctly sort transmembrane cargo proteins on endosomes[34]. This complex was found to interact with trafficking cargo proteins and was therefore called the core cargo-binding complex[35], although SNX3 has also been shown to be important for retromer to bind its cargo[33]. The SNX-PX protein SNX-3 and the retromer are essential for the retrograde trafficking of the Wntless homolog MIG-14 from endosomes to the TGN together with PI3K and RME-8[22,36]. Furthermore, Vps35 mutants in yeast have increased Neo1 accumulation in the vacuole[37], suggesting that the retromer is required for the retrograde recycling of Neo1, similar to Snx3. Thus, SNX-3 could be required for TAT-5 trafficking in combination with the retromer complex.

SNX-BAR proteins have also been shown to regulate trafficking with RME-8 and retromer. SNX-1 and SNX-6 belong to this subgroup of SNXs that have a curved Bin/Amphiphysin/Rvs (BAR) domain in addition to the PX domain[38,39]. These BAR domains are involved in inducing or stabilizing membrane curvature, resulting in endosomal membrane tubulation and recycling vesicle formation[40]. The SNX-BAR SNX-1 acts together with RME-8 to control recycling by the formation of an endosomal subdomain that sorts cargo away from the degradative pathway[27]. The SNX-BAR Vps5 from yeast interacts with the retromer Vps26 at a similar motif to SNX3[33,41], which is also thought to be important for cargo binding. SNX-1 also forms a heterodimer with the SNX-BAR SNX-6[42–44], which together were shown to be required for the endosomal trafficking of CI-MPR and Insulin-like Growth Factor 1 receptor (IGF1R)[45,46]. Thus, SNX-1 and SNX-6 could also be required for the trafficking of TAT-5.

Sorting nexins of the SNX9 family are also involved in endosomal trafficking and contain a BAR domain as well as a Src-homology-3 (SH3) domain. The SH3 domain interacts with class I polyproline sequences, for example in the dynamin GTPase, the actin regulators

WASP and N-WASP, and clathrin[15,47]. SNX9 is required for clathrin-mediated endocytosis and SNX18 was found on endosomal membranes[15,39]. Recently, SNX9 and SNX18 were shown to redundantly traffic a disintegrin and metalloprotease (ADAM9)[48]. Additionally, SNX18 was shown to traffic autophagy-related ATG9A from recycling endosomes to autophagosomes[49], showing that the SNX9 family members are involved in endosomal trafficking. The sole SNX9 family protein in *C. elegans,* LST-4, is most closely related to SNX18 and SNX33 and is required for phagosome maturation and tubulation[43,50]. Thus, it will be interesting to test whether LST-4 is required for the trafficking of TAT-5.

Conserved SNX-FERM proteins like SNX-17 and SNX-27 are also linked to the retromer and involved in endosomal recycling. SNX-FERMs interact with cargo on endosomes through their protein 4.1/ezrin/radixin/moesin (FERM) domain[35,51]. FERM-cargo binding is followed by retromer recruitment and membrane tubulation to traffic cargo to the plasma membrane, thereby retrieving cargo from the degradative pathway[51–53]. A ΦxNxxY motif was reported to be required for cargo binding by the FERM domains of SNX-17 and SNX-27[34]. Intriguingly, TAT-5 contains a VCNQKY motif in its N-terminal domain, which could be recognized by the FERM domains of SNX-17 and SNX-27 (Fig. 17). Thus, it is possible that SNX-17 and SNX-27 could recognize TAT-5 as cargo through their FERM domains.

SNX-27 also traffics cargo through its unique N-terminal PDZ domain, while SNX17 may bind cargo through a unique C-terminal sequence[51], suggesting that these SNX-FERM proteins can traffic different cargos. However, SNX-17 and SNX-27 can have redundant functions, because the recycling of amyloid precursor protein (APP) can be conducted by SNX27 or SNX17[54]. Thus, it is likely that SNX-FERMs have similar and distinct roles in recycling cargo proteins, and it will be important to test whether they regulate TAT-5 trafficking individually or redundantly.

Taken together, given their key roles regulating cargo localization and endosome tubulation, retromer and the various sorting nexins could orchestrate endosomal trafficking of TAT-5. However, none of the sorting nexins or the retromer complex were found to inhibit MV release using degron-mediated degradation of a plasma membrane reporter to screen for MV inhibitors in chapter 3. This could mean that sorting nexins and retromer are not involved in TAT-5 trafficking, or it could indicate that redundant pathways control TAT-5 trafficking and MV release. Either way, studying the role of PI3K, RME-8, sorting nexins, and the retromer complex in TAT-5 trafficking will provide new insights into endosomal recycling as well as the regulation of MV release.

4.2. Results: Endosomal recycling regulators control TAT-5 localization

In this chapter, we show that the recycling of TAT-5 to the plasma membrane depends on the class III PI3K and RME-8 that also inhibit MV release. We also identify multiple trafficking pathways downstream of PI3K and RME-8 that are required for TAT-5 plasma membrane recycling. We test the role of candidate binding sites in TAT-5 to determine how TAT-5 is recognized as cargo. We also find that TAT-5 mislocalization disrupts PE asymmetry, which is normally maintained by TAT-5. Thus, we show that MV budding and TAT-5 flippase activity can be regulated by TAT-5 localization.

4.2.1. TAT-5 antibodies to analyze endogenous TAT-5 localization

To visualize TAT-5 localization, we needed to obtain antibodies that specifically recognize TAT-5. We ordered rabbits immunized against N-terminal (RSL, RRR) and C-terminal TAT-5 peptides (KAL) (see Table 7 in the methods for the full peptide sequence). We also needed to identify a suitable secondary antibody without too much background staining. We tested four secondary antibodies against rabbit antibodies (Table 1). All four secondary antibodies showed staining of the cytoplasm. The Cy3-conjugated antibody from Jackson ImmunoResearch and both secondary antibodies from Molecular Probes additionally stained P-granules or unspecified particles, which appeared similar to cortical granules. The only antibody that exclusively showed cytoplasmic staining was the A488-conjugated antibody from Jackson, which was therefore used to test whether the new rabbit antibodies could bind TAT-5.

2nd Antibody	Source	Catalog number	Lot number	Stained organelle
Cy3 Donkey anti Rabbit	Jackson ImmunoReserach	711-165-152	109623	Cytoplasm P-granules
A488 Donkey anti Rabbit	Jackson ImmunoReserach	711-545-152	109117	Cytoplasm
A488 chicken anti Rabbit	Molecular Probes	A-21441	470144	Cytoplasm Unspecified particles
A568 Donkey anti Rabbit	Molecular Probes	A10042	685254	Cytoplasm Unspecified particles

Table 1: Many secondary antibodies show non-specific binding to *C. elegans* embryos. Fixed embryos were stained with secondary antibodies to test for non-specific binding. All secondary antibodies were incubated overnight at a concentration of 1:200. A488 Donkey anti Rabbit showed only minor cytoplasmic staining, while other antibodies also stained P-granules or unspecified particles, perhaps cortical granules.

The unpurified test serum from peptide-immunized rabbits was screened for TAT-5 binding by immunostaining fixed embryos. Most peptide antibodies bound to cell compartments like the egg shell, nuclear membrane, centrosomes and P-granules (Table 2), which are typical patterns for antibodies derived from nematode contamination in the food of immunized rabbits. Only the TAT-5 C-terminal peptide serum KAL from animal 1 (KAL1) showed plasma membrane staining (Fig. 1A), which was the expected localization of TAT-5 based on previous observations with the functional GFP-tagged TAT-5 transgene[55]. This suggested that the KAL1 antibody was recognizing a protein in the plasma membrane, possibly TAT-5.

Peptide	Serum	Localization				
		Egg shell	**Cell membrane**	**Nuclear membrane**	**Centrosomes**	**P-granules**
RSL1	Test	X	-	X	X	-
	Purified	-	-	-	-	-
RSL2	Test	X	-	-	X	X
	Purified	-	-	-	-	-
RRR1	Test	-	-	X	X	-
	Purified	-	-	-	-	-
RRR2	Test	X	-	X	X	X
	Purified	-	-	-	-	-
KAL1	Test	X	X	X	X	-
	Purified	-	-	-	-	-
KAL2	Test	X	-	-	-	-
	Purified	-	-	-	-	-

Table 2: Localization of TAT-5 peptide antibodies after IHC. The name of the peptide and the localization of the antibodies derived from the unpurified test serum or the affinity-purified serum is indicated. The antibodies were found at different subcellular localizations, although all unpurified test sera besides KAL2 localized to centrosomes. Only KAL1 bound to the plasma membrane, where GFP::TAT-5 predominantly localizes and was suspected to bind to TAT-5. After affinity purification, no specific antibody localization was observed. Observed (X) and not observed (-) localizations are indicated.

To test whether KAL1 specifically recognized TAT-5, we depleted *tat-5* by RNAi. Unfortunately, KAL1 showed strong plasma membrane staining after *tat-5* knockdown (**Error! Reference source not found.**B), similar to the empty vector control (Fig. 1A), demonstrating that the KAL1 serum does not bind TAT-5. This suggests that the KAL1 serum binds another worm protein localized to the plasma membrane.

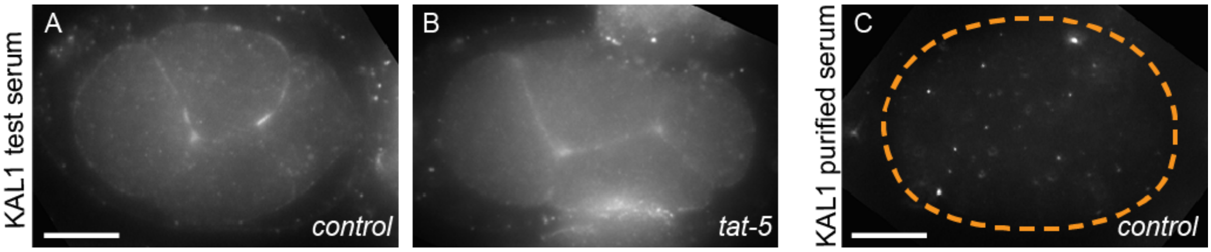

Fig. 1: The KAL1 peptide serum localizes to the plasma membrane, but is not TAT-5-specific. Immunostaining of fixed *C. elegans* embryos with serum from rabbits immunized with the KAL1 peptide. A) In a control 4-cell embryo, unpurified KAL1 test serum stains the plasma membrane. B) After *tat-5* depletion, unpurified KAL1 test serum still stains the plasma membrane of a 4-cell embryo, suggesting that the KAL1 serum does not bind to TAT-5. C) No specific staining was found with the purified KAL1 serum in a 4-cell embryo. Orange line marks the egg shell. Scale bar: 10 µm.

To separate any potential TAT-5 antibodies from other antibodies in the serum, the sera was affinity purified. After receiving the purified serum, we tested all peptide antibodies again using immunostaining. All purified antibodies showed cytoplasmic staining only (see Fig. 1C for KAL1, Table 2), which is the typical background staining of the secondary antibody (Table 1). These data suggest that none of the peptide antibodies recognize endogenous TAT-5 and that the tissue staining seen with the unpurified serums derived from non-specific anti-nematode antibodies.

We also considered whether the peptide antibodies would only work in reducing conditions, because the secondary structure of TAT-5 could hamper antibody binding to the peptides. Therefore, we used the peptide antibodies to western blot GFP::TAT-5 protein[55]. Worm protein extracts were treated with β-mercaptoethanol to reduce disulfide bonds and disrupt secondary structure. A GFP antibody was used as a positive control, which showed one band slightly above 130 kDa (Fig. 2), consistent with the 32 kDa of GFP and the estimated 120 kDa of TAT-5. In contrast, multiple bands at different sizes were detected with the affinity-purified peptide antibodies, confirming that none of the TAT-5 peptide antibodies specifically binds to TAT-5.

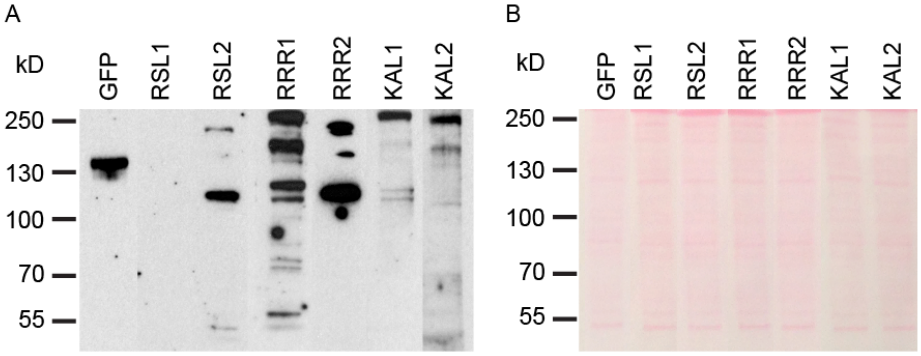

Fig. 2: Western blot with TAT-5 peptide antibodies. A) Western blot of protein extracts from worms expressing GFP::TAT-5 from the *pwIs834* transgene. Blots were stained for GFP and each of the six affinity-purified TAT-5 peptide antibodies. Only the GFP antibody showed a band of the predicted size (~150 kDa). None of the peptide antibodies showed specific GFP::TAT-5 binding. B) Ponceau staining of the same blot showing that equal amounts of protein were loaded and transferred.

4.2.2. TAT-5 plasma membrane localization is altered in PI3K and RME-8 mutants

Because we were unable to visualize endogenous TAT-5 with antibodies, we used a worm strain with GFP-tagged TAT-5 driven under the germ line *pie-1* promotor from the transgene *pwIs834* to observe GFP::TAT-5 localization on the plasma membrane of live embryos[55]. We analyzed GFP::TAT-5 localization in *vps-34(h510)* and *bec-1(ok591)* maternal zygotic mutants and after *rme-8* RNAi to check if these proteins are needed to recycle TAT-5. GFP::TAT-5 localized to prominent structures in the cytoplasm instead of the plasma membrane in *bec-1* or *vps-34* mutants, or after *rme-8* RNAi treatment (Fig. 3A-D). Accordingly, the TAT-5 plasma membrane localization was significantly reduced (Fig. 3E). Thus, the increased EV release might result from TAT-5 loss from the plasma membrane, suggesting that TAT-5 activity on the plasma membrane is needed to inhibit EV release. The overall levels of GFP::TAT-5 were also reduced after *rme-8* knockdown (Fig. 3F), suggesting that mislocalization could alter protein stability, likely causing degradation of GFP::TAT-5 after endocytosis.

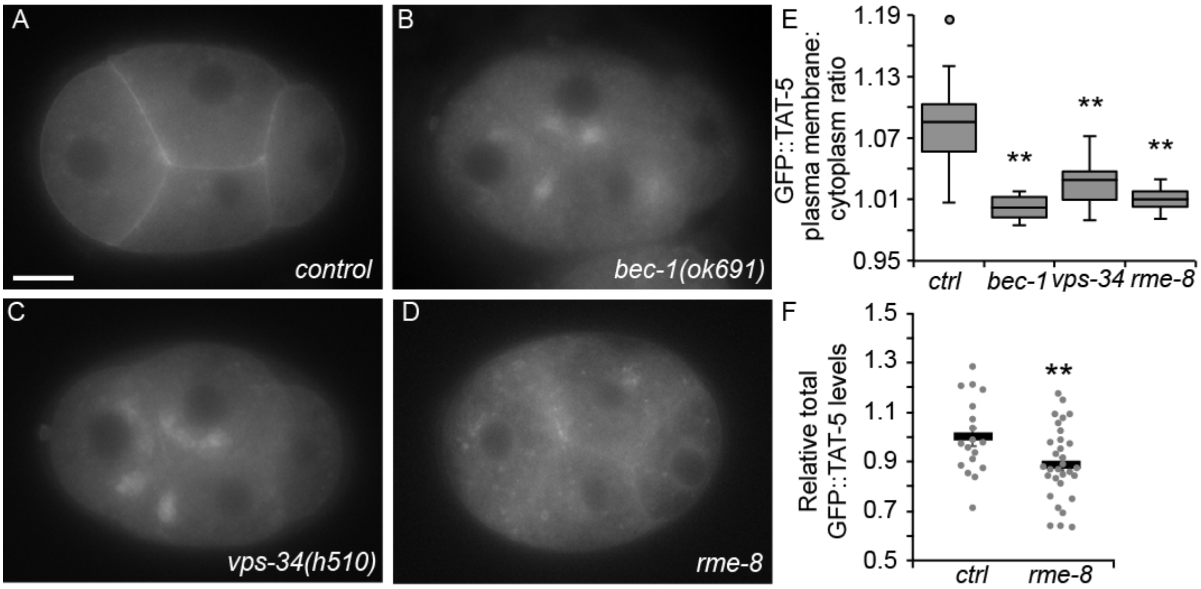

Fig. 3: TAT-5 localization in EV-releasing PI3K and *rme-8* mutants. A-D) GFP::TAT-5(*pwIs834*) localization in 4-cell embryos. A) GFP::TAT-5 localizes to the plasma membrane in a control 4-cell embryo. B-C) GFP::TAT-5 is mislocalized to large cytoplasmic structures in *bec-1* and *vps-34* maternal zygotic mutants. D) GFP::TAT-5 shows a more dispersed localization to cytoplasmic vesicles in *rme-8* RNAi. Scale bar: 10 µm. Numbers of embryos with the indicated phenotype are listed in Table 3. E) Ratio of GFP::TAT-5 fluorescence intensity in the plasma membrane to the intensity of the cytoplasm. Disrupting PI3K subunits and RME-8 had highly significant effects on GFP::TAT-5 plasma membrane localization. More variability is likely seen in *vps-34* mutants due to the presence of a rescuing transgene on an extrachromosomal array (see Methods) (*ctrl*: n=32, *bec-1*: n=12, *vps-34*: n=28, *rme-8*: n=25). One-tailed Student's t-test with Bonferroni correction was used for statistical analysis (*$p<0.05$, **$p<0.001$ compared to control empty vector RNAi). Data was measured with Kenneth Kuhn and Jennifer Rivas-Castillo. F) Total GFP::TAT-5 fluorescence levels in 2- to 4-cell embryos are significantly decreased after *rme-8* RNAi treatment. Student's t-test was used for statistical analysis (*$p<0.05$). Image modified from Beer *et al.,* PNAS 2018[31].

Genotype	RNAi	GFP::TAT-5 not on plasma membrane	
		%	n
+	-	0%	96
	rme-8	39%	89
rme-8(b1023)	-	28%	101
bec-1(ok691)	-	69%	26
vps-34(h510)	-	27%	83

Table 3: Loss of PI3K and RME-8 causes reduced GFP::TAT-5 on the plasma membrane: Number of embryos (n) with GFP::TAT-5 localization defects in control (+) worms expressing GFP::TAT-5 from the *pwIs834* transgene treated with *rme-8* RNAi or in untreated (-) *rme-8* and PI3K mutants. The percentage of embryos showing the indicated phenotype is given.

4.2.3. RME-8 prevents the missorting of TAT-5 into late endosomes

RME-8 limits the degradative microdomains on endosomes to maintain the domain for protein recycling[27]. Accordingly, loss of RME-8 increases degradation of the plasma membrane recycling cargo EGFR[29]. As we saw reduced TAT-5 levels after *rme-8* RNAi (Fig. 3F), we wondered whether TAT-5 is sent to the degradative pathway when RME-8 is lost. Thus, we checked whether TAT-5 was missorted into late endosomes or lysosomes after *rme-8* RNAi. GFP::TAT-5 rarely colocalized with LMP-1 staining in control embryos (Fig. 4A,C) and the Pearson's coefficient showed a negative correlation (Fig. 4D). In contrast, GFP::TAT-5 showed a significant 2- to 3-fold increase in colocalization with LMP-1 in *rme-8* RNAi-treated embryos (Fig. 4B-C). Indeed, the Pearson's coefficient showed a positive correlation in *rme-8* RNAi (Fig. 4D), indicating that more TAT-5 localized to late endosomes or lysosomes when RME-8 was depleted. Thus, RME-8 prevents the localization of TAT-5 to degradative endolysosomes.

To confirm that TAT-5 is mislocalized to late endosomes, we tested whether TAT-5 colocalizes with the Rab2 homolog UNC-108, which is found on the Golgi and is recruited to endosomes after early endosome markers, such as RAB-5 and PI3P, but acts before late endosome markers, such as RAB-7[56,57]. GFP::TAT-5 colocalized with a subset of mCherry-tagged UNC-108 in control embryos, showing a positive Pearson's coefficient (Fig. 4E, G-H). TAT-5 colocalization with UNC-108 increased a significant 2- to 3-fold after *rme-8* knockdown (Fig. 4F-H). These data confirm that GFP::TAT-5 is mislocalized to late endosomes in *rme-8* mutants that cause increased EV release.

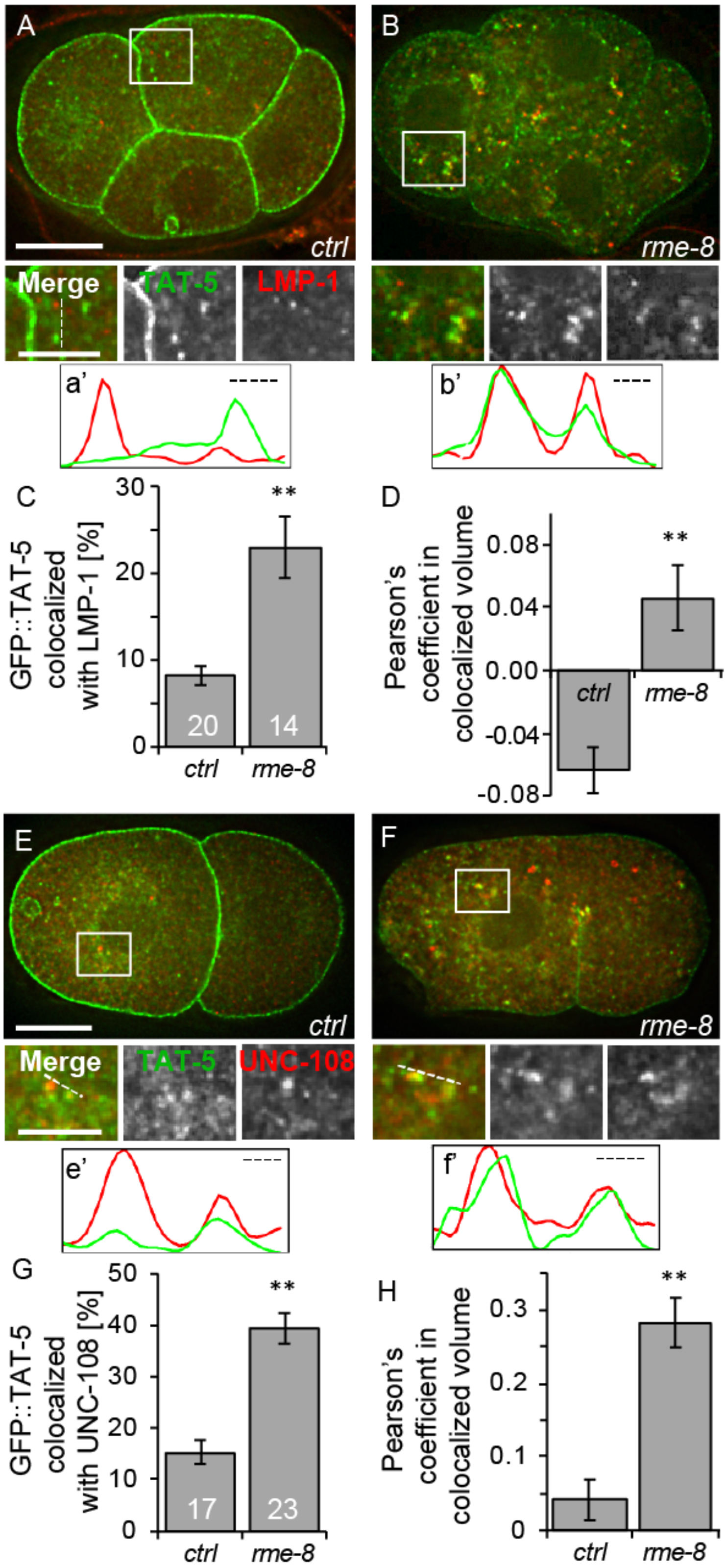
A
ctrl
B
rme-8
Merge
TAT-5
LMP-1
a'
b'
C
GFP::TAT-5 colocalized with LMP-1 [%]
30
20
10
0
**
20
14
ctrl
rme-8
D
Pearson's coefficient in colocalized volume
0.08
0.04
0.00
-0.04
-0.08
**
ctrl
rme-8
E
ctrl
F
rme-8
Merge
TAT-5
UNC-108
e'
f'
G
GFP::TAT-5 colocalized with UNC-108 [%]
50
40
30
20
10
0
**
17
23
ctrl
rme-8
H
Pearson's coefficient in colocalized volume
0.3
0.2
0.1
0
**
ctrl
rme-8

Fig. 4: Loss of RME-8 increases TAT-5 localization to late endosomes or lysosomes. A) GFP::TAT-5 (green) staining localizes primarily to the plasma membrane in control 4-cell embryos. TAT-5 is also found in cytoplasmic vesicles, but they do not often colocalize with LMP-1 staining (red) in late endosomes or lysosomes, as shown in insets. B) Mislocalization of GFP::TAT-5 in *rme-8* RNAi causes increased colocalization with LMP-1. a'-b') Line scans of GFP::TAT-5 and LMP-1 intensity next to the dotted lines. C) The percentage of TAT-5 colocalized with LMP-1 is significantly increased in 2- to 12-cell embryos after *rme-8* RNAi compared to control embryos. Number of embryos scored is indicated for each genotype. D) The Pearson's coefficient of GFP::TAT-5 colocalization with LMP-1 increases significantly from a negative correlation in control embryos to a positive correlation in *rme-8* RNAi. E) Cytoplasmic GFP::TAT-5 vesicles (green) rarely colocalize with mCherry::UNC-108 staining in Golgi and endosomes (red) in 2-cell embryos, as shown in insets. F) TAT-5 colocalization with the Rab2 homolog UNC-108 increases after *rme-8* RNAi. e'-f') Line scans of GFP::TAT-5 and UNC-108 intensity next to the dotted lines. G) The percentage of TAT-5 colocalized with UNC-108 is significantly increased in 2- to 12-cell embryos after *rme-8* RNAi compared to control embryos. Number of embryos scored is indicated for each genotype. H) The Pearson's coefficient of GFP::TAT-5 colocalization with LMP-1 increased significantly in *rme-8* RNAi. Student's t-test with Bonferroni correction was used for statistical analysis (*p<0.05, **p<0.001). Scale bar in A-B & E-F: 10 µm. Inset Scale bar A-B, E-F: 5 µm. Image modified from Beer *et al.* PNAS 2018[31].

4.2.4. TAT-5 PE flipping activity depends on RME-8

As the TAT-5 ortholog Neo1p is able to maintain plasma membrane asymmetry from endosomes[58], we tested whether PE asymmetry is maintained when TAT-5 is not properly localized to the plasma membrane by RME-8. We stained live gonads with the PE-binding lantibiotic duramycin[59] and saw increased duramycin staining in *rme-8* knockdown animals (Fig. 5A), indicating that PE is externalized on the surface of cells and PE asymmetry is lost. Together with our previous result that more TAT-5 localizes to late endosomes and lysosomes in *rme-8* mutants (Fig. 4), we conclude that TAT-5 is not able to maintain PE asymmetry in the plasma membrane when mislocalized to late endosomes or lysosomes.

We next wanted to test whether RME-8 was generally required for trafficking lipid flippases or whether it specifically regulated TAT-5 localization. TAT-1 is a related flippase that maintains the asymmetry of phosphatidylserine (PS) in the *C. elegans* plasma membrane. Therefore, we stained live gonads with Annexin V, a protein with high affinity to PS[60]. As expected[61], loss of TAT-1 caused increased PS externalization (Fig. 5B). In contrast, knocking down RME-8 did not result in an increase in Annexin V staining (Fig. 5B), indicating that PS remains cytofacial and is not externalized in *rme-8* mutants. This suggests that RME-8 is not required to localize the related P4-ATPase TAT-1 that maintains PS asymmetry in the plasma membrane[62]. Thus, RME-8 is not likely to regulate the trafficking of all P4-ATPases, but is specifically required for TAT-5 to localize to the plasma membrane.

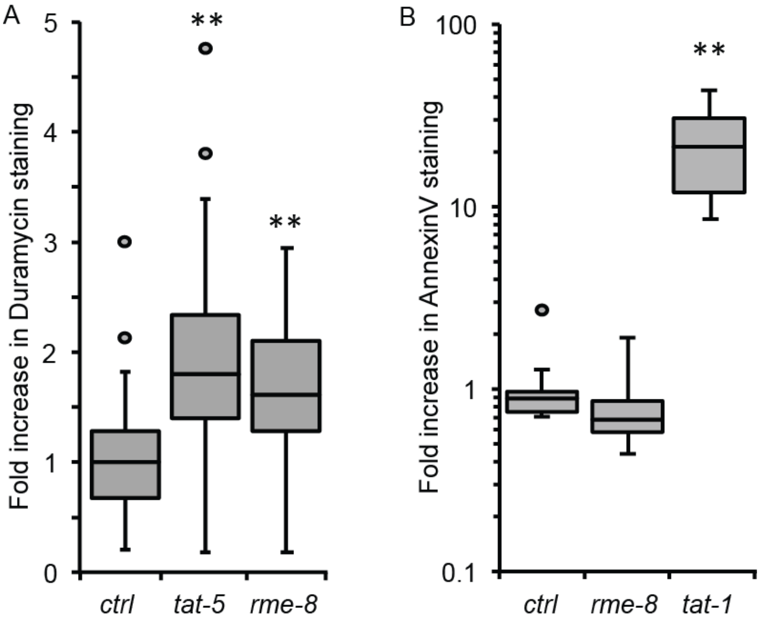

Fig. 5: RME-8 is required to maintain PE asymmetry. A) Duramycin staining is significantly increased on dissected gonads after *rme-8* or *tat-5* RNAi treatment, indicating that RME-8 is required for TAT-5 to maintain PE asymmetry (*ctrl* n=54, *tat-5* n=50, *rme-8* n=15). B) Annexin V staining is not increased on dissected gonads after *rme-8* RNAi treatment ($p>0.05$), indicating that PS is not externalized. Annexin V staining is strongly increased in *tat-1(kr15)* mutants, indicating that RME-8 is not required for TAT-1 PS flippase activity (*ctrl* n=21, *rme-8* n=16, *tat-1* n=12). A one-tailed Student's t-test with Bonferroni correction was used for statistical analysis (asterisks indicate significantly increased values: $*p<0.05$, $**p<0.001$). Graphs are modified from Beer *et al.* PNAS 2018[31].

4.2.5. PI3Kinase, RME-8, and sorting nexins control TAT-5 localization independent of the core retromer

As PI3K and RME-8 regulate multiple recycling pathways and act at early steps of endosome maturation[3,9], we next wanted to determine which specific endosomal recycling pathways are required for TAT-5 localization. Since the retrograde trafficking of Neo1 depends on Snx3 and Retromer in yeast[19,37], we started by examining GFP::TAT-5 localization in mutants for the core retromer subunits VPS-26, VPS-29, and VPS-35, as well as different sorting nexins (SNX) that bind PI3P, including the SNX-PX protein SNX-3, several SNX-BARs and SNX-FERM proteins[2,35,63].

We first checked whether the retromer complex was required for the recycling of TAT-5. GFP::TAT-5 still localized to the plasma membrane in *vps-26* deletion mutants or after *vps-*

26, *vps-29*, or *vps-35* RNAi treatment (Fig. 6A-C, see also Table 4). However, there was a slight, but significant drop in plasma membrane levels measured in *vps-26* mutants, *vps-29* RNAi, and *vps-35* RNAi (Fig. 6J). Thus, the core retromer only mildly controls TAT-5 localization, in contrast to PI3K and *rme-8* knockdown.

As the SNX-BAR heterodimer proteins SNX-1 and SNX-6 interact with RME-8 in addition to the retromer complex[3,64], we tested whether loss of SNX-BARs would disrupt TAT-5 trafficking similar to loss of *rme-8* or retromer subunits. GFP::TAT-5 localization appeared diffuse on the plasma membrane and TAT-5 plasma membrane levels were strongly reduced in *snx-1* or *snx-6* RNAi-treated embryos (Fig. 6D-E, J). This suggests that SNX-1 and SNX-6 are also important to traffic TAT-5 independent of the core retromer.

As the SNX-PX protein SNX-3 carries out endosomal membrane trafficking together with the core retromer complex[51], we expected only mild TAT-5 mislocalization after depleting SNX-3, similar to what we saw after depleting retromer subunits (Fig. 6A-C). In contrast, GFP::TAT-5 appeared significantly more diffuse around the plasma membrane in *snx-3* deletion mutants (Fig. 6F). Indeed, plasma membrane localization decreased similar to PI3K and *rme-8* knockdown (Fig. 6J). This suggests that SNX-3 is required to traffic TAT-5 independent of the core retromer.

We next tested whether this was a common feature of SNX-BAR proteins and tested the SNX9 family member LST-4, which is involved in endocytosis and membrane tubulation[50,65]. In contrast to *snx-1* and *snx-6* RNAi, knocking down *lst-4* did not disrupt GFP::TAT-5 localization (Fig. 6G, Table 4). These data suggest that the SNX-BARs SNX-1 and SNX-6 are specifically required to traffic TAT-5 to the plasma membrane.

The SNX-FERM proteins SNX-17 and SNX-27 are known to be required for endosome to plasma membrane recycling[66], and TAT-5 has a canonical FERM-binding motif. Therefore, we wondered whether SNX-17 and SNX-27 could be candidates to traffic TAT-5. In contrast to *snx-1/-6* and *snx-3* mutants, knocking down *snx-17* or *snx-27* did not disrupt GFP::TAT-5 localization (Fig. 6H, I, Table 4). Therefore, SNX-FERM proteins are not major regulators of TAT-5 trafficking.

In summary, these results indicate that SNX-1/-6 and SNX-3 play a more important role than the core retromer complex and other sorting nexins in TAT-5 localization. Surprisingly, our results further suggest that retromer-associated sorting nexins can traffic cargoes independently of the retromer. Therefore, we hypothesize that TAT-5 is primarily trafficked by one or more retromer-independent pathways that include SNX-3 as well as the SNX-BAR proteins SNX-1 and SNX-6.

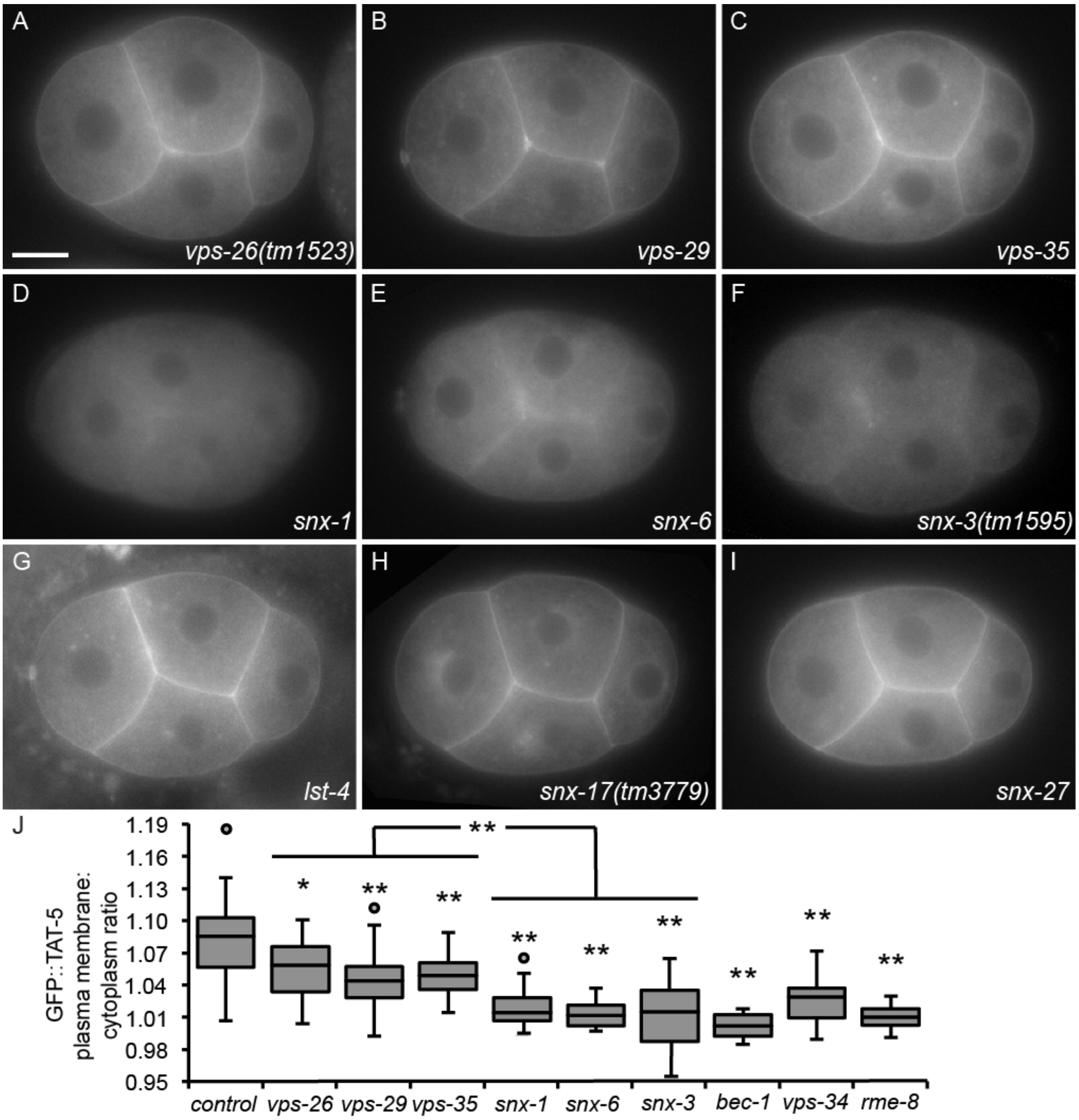
A
vps-26(tm1523)
B
vps-29
C
vps-35
D
snx-1
E
snx-6
F
snx-3(tm1595)
G
lst-4
H
snx-17(tm3779)
I
snx-27
J
GFP::TAT-5 plasma membrane: cytoplasm ratio
1.19
1.16
1.13
1.10
1.07
1.04
1.01
0.98
0.95
**
*
**
**
**
**
**
**
**
**
control
vps-26
vps-29
vps-35
snx-1
snx-6
snx-3
bec-1
vps-34
rme-8

Fig. 6: TAT-5 is recycled by retromer-associated proteins. A-I) 4-cell embryos expressing GFP::TAT-5(*pwIs834*). A-C) GFP::TAT-5 still localizes to the plasma membrane in core retromer *vps-26* deletion mutants and after *vps-29* and *vps-35* RNAi, suggesting that the retromer is not required for TAT-5 trafficking. D-F) In contrast, GFP::TAT-5 plasma membrane localization is weak after *snx-1* and *snx-6* RNAi or in *snx-3* deletion mutants. G-I) GFP::TAT-5 localization is not altered after *lst-4 RNAi*, in *snx-17* deletion mutants or after *snx-27* RNAi. Scale bar: 10 μm. Numbers of embryos with the indicated GFP::TAT-5 localization phenotype are listed in Table 4. J) Ratio of GFP::TAT-5 fluorescence intensity in the plasma membrane to the intensity of the cytoplasm. Knocking down or deleting core retromer proteins resulted in mild, but statistically significant decreases. Disrupting SNX-1/6 and SNX-3 had highly significant effects on GFP::TAT-5 plasma membrane localization, similar to PI3K subunits and RME-8 (*ctrl* n=32, *vps-26* n=32, *vps-29* n=33, *vps-35* n=24, *snx-1* n=29, *snx-6* n=29, *snx-3* n=28, *bec-1* n=12, *vps-34* n=28, *rme-8* n=25). Student's t-test with Bonferroni correction was used

for statistical analysis (*p<0.05, **p<0.001 compared to control empty vector RNAi or comparison between SNXs and retromer). Data was measured with Kenneth Kuhn and Jennifer Rivas-Castillo. All images except G-I are modified from Beer *et al.* PNAS 2018[31].

Genotype	RNAi	GFP::TAT-5 not on plasma membrane	
		%	n
+	-	0%	96
	tat-5	79%	29
	vps-26	0%	41
	vps-29	0%	49
	vps-35	0%	42
	snx-1	31%	36
	snx-3	5%	73
	snx-6	28%	72
	lst-4	0%	72
	snx-17 [i]	0%	26
	snx-27 [i]	0%	21
vps-26(tm1523)	-	0%	52
snx-3(tm1595)	-	26%	53

Table 4: Summary of GFP::TAT-5 localization defects. Control (+) and mutant worms expressing GFP::TAT-5 were treated with RNAi or untreated (-). The percentage of embryos showing the indicated phenotype is given. Embryos (n) from the zygote to 15-cell stage were scored for whether GFP::TAT-5 was visible at the plasma membrane. [i] marks experiments that were only performed ones.

4.2.6. SNX-3 regulates TAT-5 localization independent of binding to retromer

Structural studies have shown how SNX-3 associates with the core-retromer VPS-26 and VPS-35 and recruits the core retromer upon cargo binding, making the SNX-3-retromer interface an important interface for cargo binding[33,36,63,67]. However, as only SNX-3 and not the core-retromer was required for TAT-5 plasma membrane localization, we hypothesized that SNX-3 could regulate TAT-5 localization and EV release independent of binding to the core retromer. A single tyrosine in SNX-3(Y22) is required for VPS-35 binding and cargo trafficking[4]. Accordingly, a SNX-3(Y22A) mutant causes loss of VPS-35 binding and altered Wntless trafficking in *C. elegans*. We expressed GFP::TAT-5 in *snx-3(hu256[Y22A])* mutants and saw that TAT-5 still localized to the plasma membrane (Fig. 7B), in contrast to the significant loss of plasma membrane-localized TAT-5 in *snx-3* deletion mutants (Fig. 6F). This confirms that SNX-3 binding to the core retromer is dispensable for TAT-5 trafficking.

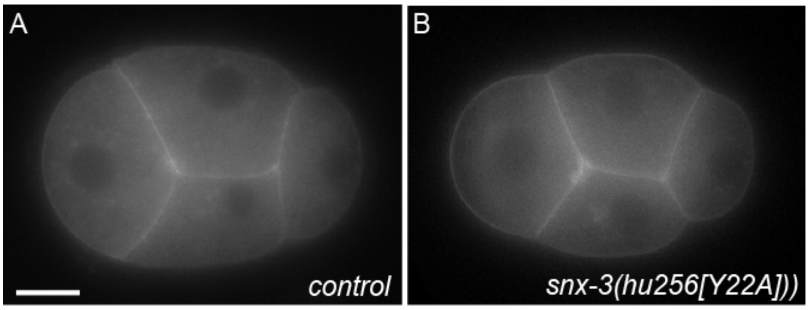

Fig. 7: SNX-3 traffics TAT-5 independent of the retromer complex. A-B) 4-cell embryos expressing GFP::TAT-5(*pwIs834*). GFP::TAT-5 localizes to the plasma membrane in control embryos and in *snx-3(hu256[Y22A])* mutants deficient for VPS-35 binding (n=36), suggesting that SNX-3 regulates TAT-5 localization independent of the retromer complex. Scale bar: 10 µm.

4.2.7. SNX-6 is not required for TAT-5 activity

Given that PE was externalized after *rme-8* RNAi that altered TAT-5 plasma membrane localization (Fig. 5A), we wondered whether PE asymmetry was lost after knocking down sorting nexins that regulate TAT-5 plasma membrane localization (Fig. 6E, J). We stained live gonads with the PE-binding lantibiotic duramycin[59] and saw that PE externalization was not increased after *snx-6* RNAi (Fig. 8). In fact, *snx-6* knockdown animals displayed significantly less PE externalization than control embryos. Thus, TAT-5 is able to maintain PE asymmetry in the plasma membrane when mislocalized in *snx-6* mutants. Thus, although GFP::TAT-5 is largely lost from the plasma membrane in both *rme-8* and *snx-6* mutants, SNX-6-mediated trafficking is not required for TAT-5 activity.

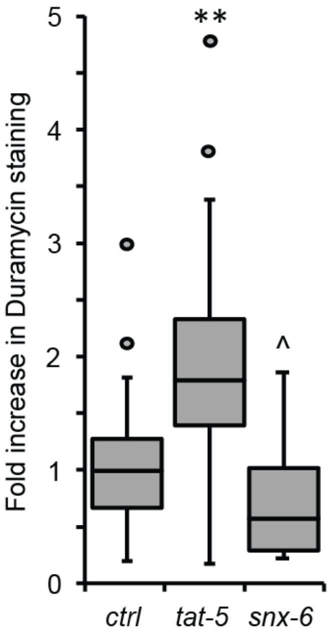

Fig. 8: SNX-6 is not required to maintain PE asymmetry. Duramycin staining is decreased on dissected gonads after *snx-6* RNAi treatment, indicating that SNX-6 is not required for TAT-5 to maintain PE asymmetry (*ctrl* n=54, *tat-5* n=50, *snx-6* n=27). A one-tailed Student's t-test with Bonferroni correction was used for statistical analysis (asterisks indicate significantly increased values: **$p<0.001$, carets indicate significantly decreased values: ^$p<0.05$). Graph is modified from Beer *et al.* PNAS 2018[31].

4.2.8. SNX-1/-6 and SNX-3 redundantly inhibit extracellular vesicle release

Given the significant role of sorting nexins on TAT-5 localization (Fig. 6D-F), but lack of PE externalization in *snx-6* mutants (Fig. 8), we wondered whether sorting nexins also inhibit EV release like class III PI3K and RME-8. Using the PH-degron reporter to label released EVs (see chapter 3), we found that EV release was not increased after individual RNAis targeting *snx-1*, *snx-6*, or *snx-3* (Fig. 9D). We also crossed *snx* mutants to the PH-degron reporter strain and found no increase in EV release in *snx-1* or *snx-3* deletion mutants (Fig. 9A, D), suggesting that TAT-5 was still able to maintain plasma membrane asymmetry despite its reduced levels at the plasma membrane. This is consistent with the lack of externalized PE after *snx-6* RNAi (Fig. 8), suggesting that TAT-5 is still active in *snx* mutants.

As SNX-1 and SNX-6 are thought to act in a different pathway than SNX-3[27], but we found that all three SNX proteins are required for TAT-5 trafficking, we tested whether they act together in the same trafficking pathway, or whether TAT-5 is trafficked by multiple redundant pathways. As the SNX-BAR proteins SNX-1 and SNX-6 form a heterodimer[20], we hypothesized that they would act in the same pathway, while SNX-3 would act in a separate TAT-5 trafficking pathway. We therefore predicted that TAT-5 localization and/or activity would be more disrupted when both the SNX-1/-6 and SNX-3 trafficking pathways are altered.

Given that loss of TAT-5 activity causes sterility and embryonic lethality[68], we checked whether *snx* deletion mutants treated with *snx* RNAi show synthetic phenotypes. No embryonic lethality was observed in single *snx* mutants, but depleting *snx-1* or *snx-6* in *snx-3* deletion mutants caused embryonic lethality and sterility (Table 5), consistent with SNX-3 acting in a different pathway than SNX-1 or SNX-6. However, we did not detect synthetic phenotypes in the reverse experiment, probably because *snx-3* RNAi is only partially effective (discussed further below and in Fig. 10D). We also did not observe synthetic phenotypes when depleting *snx-1* in *snx-6* mutants or vice versa, consistent with SNX-1 and SNX-6 acting together in the same pathway. Taken together, our results suggest a redundant role for trafficking by SNX-3 and trafficking by SNX-1/6 during embryonic development.

Mutant strain	RNAi				
	control	*snx-1*	*snx-3*	*snx-6*	*lst-4*
+	-	-	-	-	-
snx-1 (tm847)	-		-	-	-
snx-3 (tm1595)	Egl	Egl Let Ste Emb		Egl Emb	Egl
snx-6 (tm3790)	-	-	Egl		-
lst-4 (tm2423)	-	-		-	

Table 5: Genetic interactions of double *snx* mutants. Egg-laying-defective (Egl), lethal (Let), sterile (Ste), and embryonic lethal (Emb) phenotypes were screened after knockdown with sorting nexin RNAi in wild type (+) or *snx* mutants (Δ). (-) indicates that none of these phenotypes were detected. Untreated *snx-3* mutants showed an egg-laying defect, while *snx-1/6 snx-3* double mutants showed embryonic lethality, sterility and lethality. All data derive from three independent experiments with each indicated phenotype seen at least once per experiment. Experiments were performed together with Jennifer Rivas-Castillo. Table modified from Beer *et al.* PNAS 2018[31].

To test whether the lethal and sterile phenotypes in *snx* double mutants could be due to increased EV release, we treated *snx* deletion mutants expressing the PH-degron reporter with *snx* RNAi. Increased EV release was observed in *snx-1* mutants treated with *snx-3* RNAi or in *snx-3* mutants treated with *snx-1* or *snx-6* RNAi (Fig. 9B-D). This indicates that the SNX-BARs SNX-1/-6 and the SNX-PX protein SNX-3 control two different TAT-5 trafficking pathways to inhibit EV release. Thus, we think that SNX-1/-6 and SNX-3 act in separate pathways to redundantly traffic TAT-5 to inhibit MV budding.

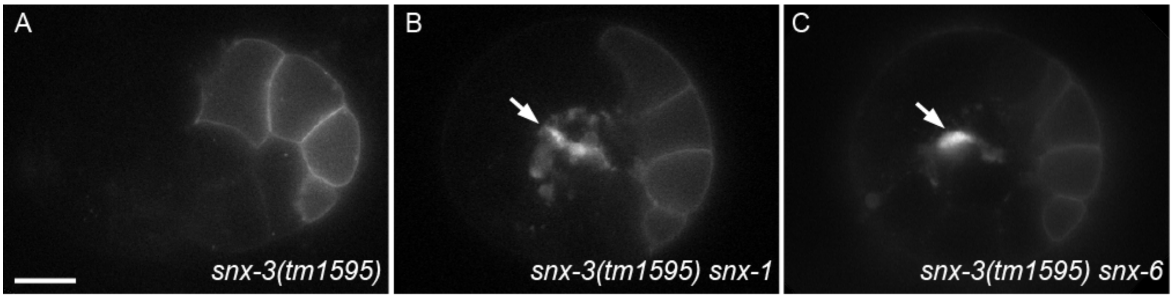

D

Genotype	RNAi	Increased EV release (thick membranes)	
		%	n
+	*snx-1*	0%	60
	snx-6	0%	40
	snx-3	0%	60
snx-1(tm847)	-	0%	24
	snx-3	55%*	20
snx-3(tm1595)	-	1%	69
	snx-1	86%	36
	snx-6	100%	28

Fig. 9: SNX-1/-6 and SNX-3 redundantly inhibit EV release. A-C) 26-cell *snx-3(tm1595)* embryos expressing the mCherry::ZF1::PH$_{PLC1\partial1}$ plasma membrane reporter. A) EV release was not increased in a *snx-3* mutant embryo. B) EVs labeled with mCherry::ZF1::PH$_{PLC1\partial1}$ (arrow) accumulate between cell contacts in a *snx-3* mutant treated with *snx-1* RNAi. C) Increased EV release is also detectable in *snx-3* mutants treated with *snx-6* RNAi. Scale bar: 10 µm. D) Increased EV release was scored by looking for membrane thickenings. Numbers of observed phenotypes from wild type (+) and *snx-1* and *snx-3* mutants that were either untreated (-) or treated with RNAi targeting the indicated genes. *GFP::TAT-5 was used to score EV release in *snx-1(tm847) snx-3* RNAi embryos, which is likely to underestimate EV release as GFP::TAT-5 localization to the plasma membrane was reduced. Images are modified from Beer *et al.* PNAS 2018[31].

4.2.9. SNX-1/-6 and SNX-3 redundantly regulate intracellular TAT-5 trafficking

In order to understand why EV release was only increased when both SNX-1/6 and SNX-3 pathways were targeted, we next analyzed GFP::TAT-5 localization in *snx* double mutants. In addition to the reduced plasma membrane localization seen for the single *snx* mutants, depleting *snx-3* in *snx-1* mutants caused TAT-5 to accumulate in cytosolic compartments (Fig. 10B). Similar cytosolic puncta were also observed after *snx-6* depletion in *snx-3* mutants (Fig. 10C), but were rarely observed in *snx-3* mutants or after single *snx* RNAi (Fig. 10A, Fig. 6D-F). This suggests that TAT-5 is mislocalized to a different intracellular compartment when both SNX-1/6 and SNX-3 are disrupted.

To test whether the plasma membrane levels were lower when both SNX-1/6 and SNX-3 were disrupted, we measured TAT-5 localization as the ratio of GFP::TAT-5 levels in the plasma membrane to GFP::TAT-5 levels in the cytosol. This confirmed that all *snx* double mutants had a significantly reduced TAT-5 plasma membrane ratio compared to control embryos (Fig. 10D). However, the reductions in the TAT-5 plasma membrane ratio were not significantly decreased in double mutants when compared to single mutants ($p>0.05$, one-tailed Student's t-test). Only *snx-3* RNAi had a significantly higher TAT-5 plasma membrane ratio than other mutants, suggesting that *snx-3* RNAi is only partially effective. Taken together, TAT-5 loss from the plasma membrane was not measurably increased by depleting both SNX-1/-6 and SNX-3-dependent trafficking pathways, suggesting that the change in the intracellular accumulation of TAT-5 altered its function.

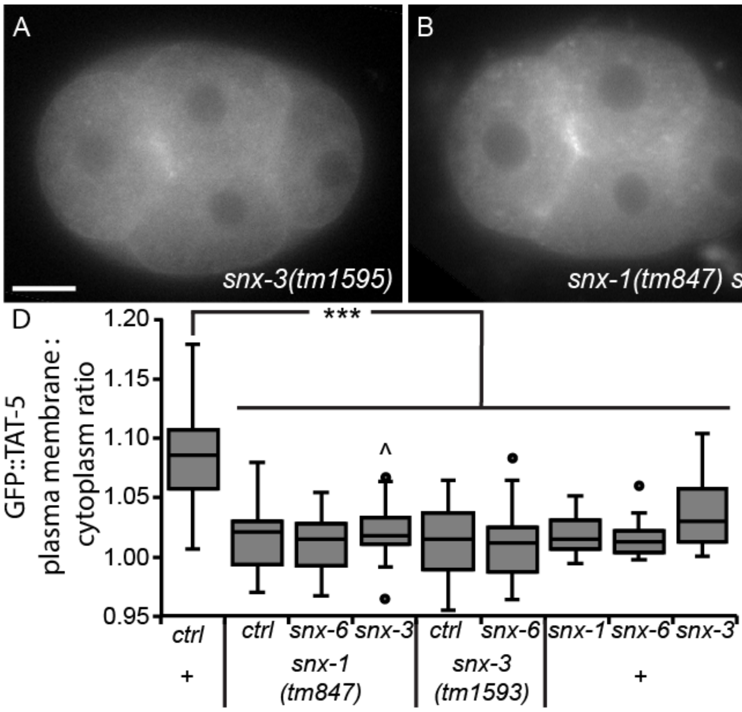

E

Genotype	RNAi	GFP::TAT-5 not on plasma membrane	
		%	n
+	-	0%	96
	snx-1	31%	36
	snx-3	5%	73
	snx-6	28%	72
snx-1(tm847)	-	37%	41
	snx-3	26%	37
snx-3(tm1595)	-	26%	53
	snx-6	36%	53

Fig. 10: TAT-5 trafficking is further altered in *snx-1/-6* and *snx-3* double mutants. A-C) 4-cell embryos of *snx* mutants expressing GFP::TAT-5. A) GFP::TAT-5 plasma membrane localization is dispersed in untreated *snx-3(tm1595)* mutants. B-C) GFP::TAT-5 accumulates in cytoplasmic compartments in *snx-1* deletion mutants after *snx-3* RNAi, as well as in *snx-3* mutants treated with *snx-6* RNAi. Scale bar: 10 µm. D) GFP::TAT-5 ratio between the plasma membrane and the cytosol measured from 2-4-cell embryos. Student's t-test with Bonferroni correction was used for statistical analysis (***$p<0.001$). All *snx* RNAis (*snx-1* n=29, *snx-6* n=30, *snx-3* n=38) and *snx* mutants (*snx-1(tm847) ctrl* n=30, *snx-6* n=33, *snx-3* n=28; *snx-3(tm1595) ctrl* n=28, *snx-6* n=41) had significantly lower GFP::TAT-5 levels on the plasma membrane compared to the vector control (n=32)(***$p<0.001$, compared to empty vector control). TAT-5 mislocalization was not increased in the double mutants compared to individual RNAis ($p>0.05$, one-tailed Student's t-test), although *snx-3* RNAi was

significantly weaker than *snx-3(tm1593)* mutants ($^p<0.05$, one-tailed Student's t-test with Bonferroni correction). E) Numbers and percentage of observed embryos with plasma membrane localization defects are indicated. Wild type (+) or mutant worms expressing GFP::TAT-5 were treated with RNAi or untreated (-). Embryos (n) from the zygote to the 15-cell stage were scored for whether GFP::TAT-5 was visible at the plasma membrane. Images B-D are modified from Beer *et al.* PNAS 2018[31].

4.2.10. Retromer proteins do not redundantly control TAT-5 plasma membrane localization or extracellular release

Given that SNX-1/6 and SNX-3 act redundantly during TAT-5 trafficking and EV release, we decided to revisit the role of the retromer complex in TAT-5 trafficking. The decrease in TAT-5 plasma membrane localization in retromer mutants could be mild because of redundant functions of the core retromer trimer. Therefore, we tested whether they could act redundantly like SNX-1/-6 and SNX-3. Untreated *vps-26* and *vps-35* deletion mutants are egg laying defective (Egl)[69,70], while *vps-35* deletion mutants are also partially sterile (Table 6)[71], giving a first hint that different retromer subunits can have distinct functions. In contrast to the single mutants, we obtained synthetic sterility when we depleted *vps-29* in a *vps-26* or *vps-35* deletion strain. We also observed embryonic lethality when we targeted *vps-35* in a *vps-26* deletion strain, but could only verify synthetic sterility in the opposite experiment. Thus, retromer proteins can act redundantly.

We also tested whether retromer could act redundantly with sorting nexins. Sterility was observed when we depleted *snx-1* in *vps-26* and *vps-35* mutants, while *vps-26* mutants treated with *snx-1* RNAi were also lethal. Lethality was also observed after *snx-3* RNAi in *vps-26* mutants. Depleting the SNX9 ortholog *lst-4* in *vps-26* and *vps-35* mutants (or vice versa) also caused sterility. Thus, retromer proteins can have redundant functions with sorting nexins, which supports our hypothesis that sorting nexins sort cargo dependent and independent of the retromer.

Mutant strain	RNAi							
	control	*vps-26*	*vps-29*	*vps-35*	*snx-1*	*snx-3*	*snx-6*	*lst-4*
+	-	-	-	-	-	-	-	-
vps-26 (tm1523) / +	-		-	Ste	Egl	-	Emb	-
vps-26 (tm1523)	Egl	Egl	Let Egl Ste	Let Egl Ste Emb	Let Egl Ste	Egl Ste Emb		
vps-35 (hu68)	Egl Ste	Egl Ste	Let Egl Ste		Let Egl Ste	Ste	Egl Ste	Egl Ste
snx-1 (tm847)	-	Egl	-	Let Ste				
snx-3 (tm1595)	Egl	Let Egl Ste	Let Egl Ste	Let Egl Ste				
snx-6 (tm3790)	-	-	-	Let Ste				
lst-4 (tm2423)	-	Ste	-	Ste				

Table 6: Genetic interactions of double retromer mutants. Lethal (Let), egg-laying-defective (Egl), sterile (Ste), and embryonic lethal (Emb) phenotypes were detected after knockdown with retromer or sorting nexin RNAis in retromer or sorting nexin deletion mutants (Δ). Synthetic phenotypes were also obtained using a heterozygous *vps-26* deletion strain (Δ/+). Wildtype worms were used as a positive control and are depicted as +. (-) indicates that none of these phenotypes were detected. Untreated *vps-26, vps-35*, and *snx-3* mutants showed an egg-laying defect and untreated *vps-35* mutants were also partially sterile. All data derive from three independent experiments with each indicated phenotype seen at least once per experiment. Experiments were performed together with Jennifer Rivas-Castillo. Table modified from Beer *et al.* PNAS 2018[31].

Given these redundant roles of retromer subunits, we directly tested TAT-5 localization and EV release in retromer double mutants. As presented previously (Fig. 6A, J), *vps-26* mutants have slightly less GFP::TAT-5 on the plasma membrane than control embryos (Fig. 11A, D). In contrast, *vps-26* mutants treated with *vps-29* or *vps-35* RNAi did not show significant changes in plasma membrane localization when compared to control embryos or to *vps-26* single mutants (Fig. 11D-E), demonstrating that the core retromer proteins are not acting redundantly during TAT-5 trafficking. Similarly, RNAi against other retromer subunits in *vps-26* mutants did not increase EV release (Fig. 11E). Therefore, it is unlikely that retromer proteins significantly control TAT-5 localization or are involved in regulating EV release, strengthening the model that SNX-1/-6 and SNX-3 control TAT-5 localization independent of the core retromer.

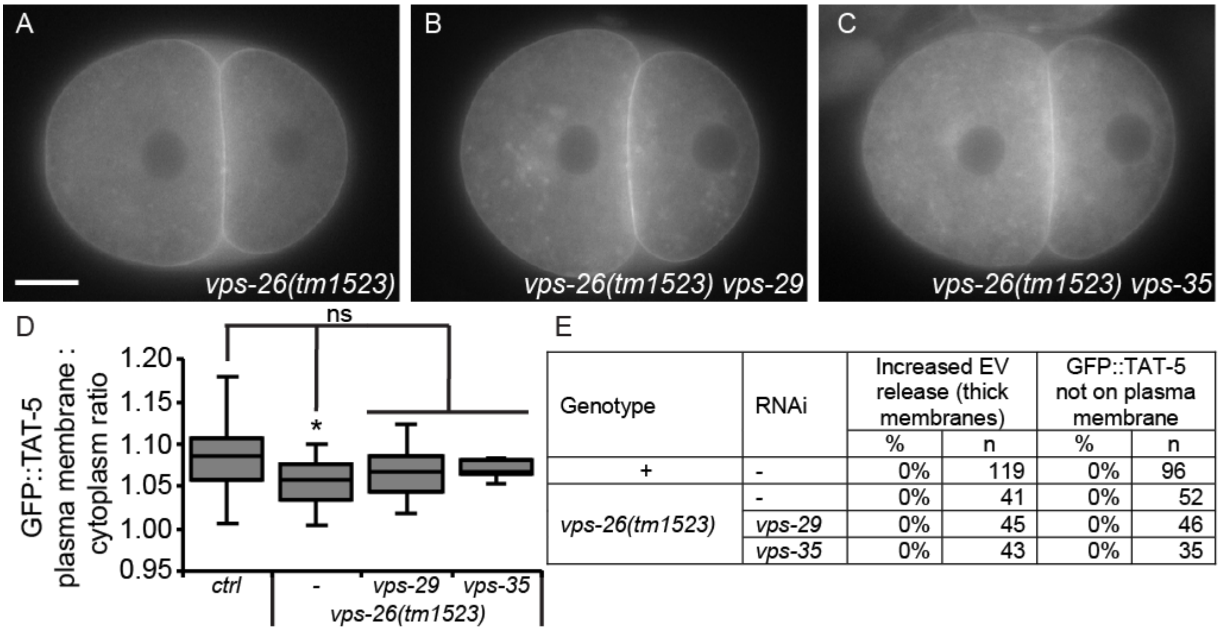

Genotype	RNAi	Increased EV release (thick membranes)		GFP::TAT-5 not on plasma membrane	
		%	n	%	n
+	-	0%	119	0%	96
vps-26(tm1523)	-	0%	41	0%	52
	vps-29	0%	45	0%	46
	vps-35	0%	43	0%	35

Fig. 11: GFP::TAT-5 localizes to the plasma membrane in double retromer mutants. A-C: GFP::TAT-5 localizes to the plasma membrane in *vps-26* mutant 2-cell embryos regardless of *vps-29* or *vps-35* depletion. Scale bar: 10 µm. D) Ratio of GFP::TAT-5 fluorescence intensity between plasma membrane and the cytosol measured from 2-4-cell embryos. Student's t-test with Bonferroni correction was used for statistical analysis (*p<0.05, compared to control empty vector RNAi). No significant difference was observed when comparing *vps-29* (n=13) or *vps-35* (n=8) RNAi-treated *vps-26* mutants to untreated *vps-26* mutants (n=32) or to control GFP::TAT-5 embryos (n=32). E) Summary of EV release and GFP::TAT-5 localization defects in *vps-26* mutants treated with the indicated RNAi. Embryos (n) from the late 4-cell to 102-cell stage were scored for thickened membrane labeling between cells, which is indicative of EV release. Embryos from the zygote to 15-cell stage were scored for whether GFP::TAT-5 was visible at the plasma membrane.

4.2.11. FERM-domain containing sorting nexins are not required for TAT-5 trafficking.

Although GFP::TAT-5 did not need SNX-17 or SNX-27 for its plasma membrane localization (Fig. 6H-I, Fig. 12D), TAT-5 contains a VCNQKY motif in its N-terminal domain (Fig. 17), which could be a ΦxNxxY motif recognized by the FERM domains of SNX-17 and

SNX-27[34]. Therefore, we tested whether SNX-FERM proteins could traffic TAT-5 redundantly. Depleting *snx-27* in the *snx-17* mutant background also did not alter TAT-5 trafficking to the plasma membrane (Fig. 12A, D), suggesting that these SNX-FERM proteins do not redundantly traffic TAT-5 to the plasma membrane. As SNX27 has been shown to act together with SNX3[3], we next took a preliminary look at whether the SNX-FERM proteins traffic TAT-5 redundantly with the SNX-BAR proteins or SNX-3. Depleting *snx-6* in *snx-17* mutants altered TAT-5 recycling to the plasma membrane (Fig. 12B), similar to single *snx-6* RNAi (Fig. 6E). Treating *snx-3* mutants with *snx-27* RNAi also caused reduced GFP::TAT-5 levels at the plasma membrane (Fig. 12C), similar to *snx-3* single mutants (Fig. 6F). So far, we have no evidence suggesting that the SNX-FERM proteins play a role in TAT-5 trafficking.

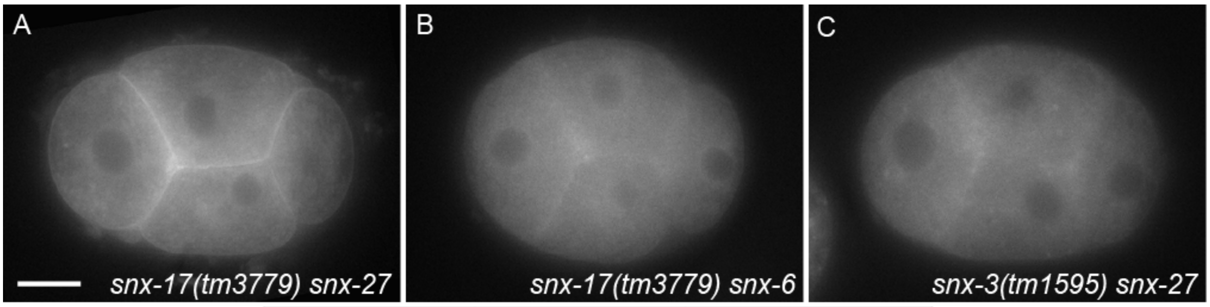

D

Genotype	RNAi	GFP::TAT-5 not on plasma membrane	
		%	n
+	*snx-1*	31%	36
	snx-6	28%	72
	snx-3	5%	73
	snx-17	0%	26
	snx-27	0%	21
	snx-17 + snx-27	0%	12
snx-17(tm3779)	-	0%	8
	snx-1	0%	6
	snx-6	50%	14
	snx-27	0%	19
snx-3(tm1595)	-	26%	53
	snx-6	36%	53
	snx-27	0%	10

Fig. 12: SNX-17 and SNX-27 are unlikely to control redundant TAT-5 trafficking pathways. A-C) GFP::TAT-5 localization in 4-cell embryos. A) GFP::TAT-5 localizes to the plasma membrane in a *snx-17* mutant treated with *snx-27* RNAi. B) Depleting *snx-6* in a *snx-17* mutant background reduces TAT-5 plasma membrane localization, similar to *snx-6* RNAi in a wildtype strain (compare to Fig. 6E). C) Depleting *snx-27* in a *snx-3* mutant background causes decreased TAT-5 plasma membrane localization as in untreated *snx-3* mutants (compare to **Fig. 7**F). Scale bar: 10 µm. D) Numbers and percentage of

observed embryos with plasma membrane localization defects. Wild type (+) or mutant worms expressing GFP::TAT-5 were treated with RNAi or untreated (-).

To check whether SNX-17 and SNX-27 could redundantly regulate EV release, we checked for increased EV budding in *snx-17* and *snx-27* mutants. No EV release was observed in individual *snx-17* mutants or in *snx-17* mutants treated with *snx-27* RNAi (Fig. 13A, D), consistent with the observation of normal TAT-5 localization in SNX-FERM double mutants (Fig. 12A, D). This suggests that SNX-17 and SNX-27 do not regulate EV release singly or redundantly with each other.

We next tested whether either SNX-FERM protein could have a redundant role with the SNX-BARs. We saw thick patches of increased mCh::PH::ZF1-labeling in *snx-17* mutants treated with *snx-1* or *snx-6* RNAi (Fig. 13B, E), consistent with increased EV release. Although similar experiments still need to be carried out with SNX-27, this suggests that at least SNX-17 can control EV release redundantly with SNX-1 and SNX-6.

Finally, we tested whether the SNX-FERMs could have a redundant role with SNX-3. We saw persisting fluorescence of the mCh::PH::ZF1 reporter in *snx-3* mutants treated with either *snx-17* or *snx-27* RNAi (Fig. 13C-D). However, mCh::PH::ZF1 appeared punctate in the cytoplasm of most *snx-17* and some *snx-27* RNAi embryos. There was no increase in PH labeling after *snx-3* knockdown in the *snx-17* mutant (Fig. 13E), with the caveat that the *snx-3* RNAi only causes a partial loss-of-function (Fig. 10D-E, Table 4). Thus, SNX-FERMs could have a redundant role with SNX-3, but the EV release phenotype will need to be confirmed by TEM.

In summary, our preliminary results suggest that SNX-17 could inhibit EV release redundantly with SNX-1/-6 and probably SNX-3. SNX-27 could also control EV release redundantly with at least SNX-3, while redundancy with SNX-1/-6 still needs to be tested. However, it is unclear whether redundant MV release inhibition is through a redundant TAT-5 trafficking pathway or another EV regulator.

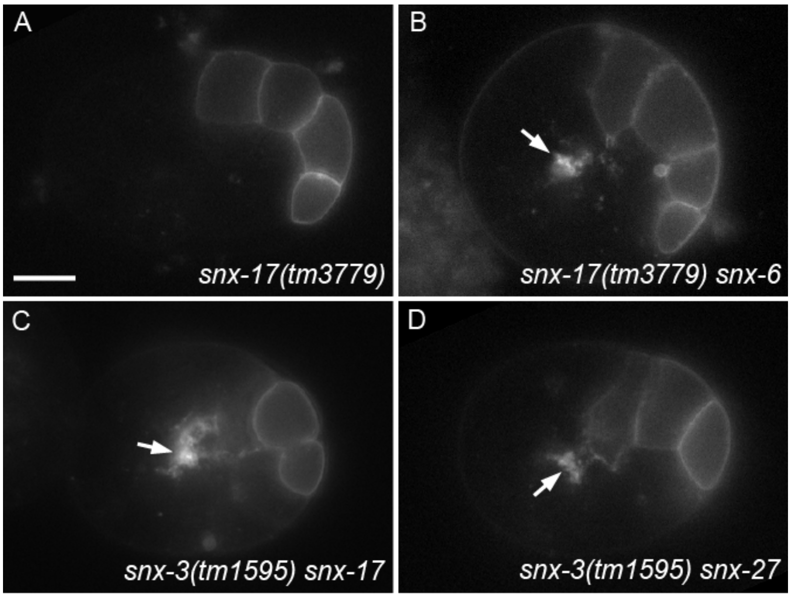

E

Genotype	RNAi	Increased EV release (thick membranes)	
		%	n
+	*snx-1*	0%	60
	snx-6	0%	40
	snx-3	0%	60
	snx-17	0%	26
	snx-27	0%	21
	snx-17 + snx-27	0%	7
snx-17(tm3379)	-	0%	75
	snx-1	19%	52
	snx-6	56%	147
	snx-3	0%	25
	snx-27	0%	22
	vps-35	0%	10
snx-3(tm1595)	-	1%	69
	snx-17	21%	14
	snx-27	37%	19

Fig. 13: SNX-17 and SNX-27 have redundant roles in EV release. A-C) 26-28-cell embryos expressing the mCherry::ZF1::$\mathrm{PH_{PLC1\partial 1}}$ plasma membrane reporter. A) EV release is not increased in a *snx-17* deletion mutant. B) mCherry::ZF1::$\mathrm{PH_{PLC1\partial 1}}$ accumulates between cell contacts (arrow) in over half of *snx-17* mutants treated with *snx-6* RNAi, suggesting there is increased EV release. C-D) mCherry::ZF1::$\mathrm{PH_{PLC1\partial 1}}$ remains fluorescent in *snx-3* deletion mutant embryos treated with *snx-17* (one-fifth) or *snx-27* (one-third) RNAi in a 12-cell embryo, which requires confirmation by TEM to determine whether these are EVs. Scale bar: 10 µm. E) Numbers of thickened membrane phenotypes observed from wild type (+), *snx-17* or *snx-3* deletion mutants that were either untreated (-) or RNAi treated.

4.2.12. Testing SNX-binding motifs in TAT-5

As both the SNX-BAR proteins SNX-1/-6 and the SNX-PX protein SNX-3 control TAT-5 localization, we wondered whether TAT-5 was a direct cargo of these SNXs. Specific consensus sequences in cargo proteins have been defined that are recognized by SNXs and are important for SNX-mediated trafficking. Furthermore, SNX-1/6 and SNX-3 redundantly inhibit EV release, but it remains unclear whether the SNXs recognize TAT-5 through one shared binding site or through different sequences. Therefore, we wanted to identify the SNX-binding sites in TAT-5 to selectively block TAT-5 trafficking and test whether SNX-binding mutants disrupt TAT-5 localization and alter EV release. Potential binding sites for SNX-1/6 and SNX-3 in TAT-5 were identified by sequence homology to reported SNX-binding motifs (Fig. 14A). The functional GFP::TAT-5 plasmid was mutated to change these motifs and re-expressed in the worm germ line to determine its localization (see all generated TAT-5 mutant strains in (Table 7 and Table 8).

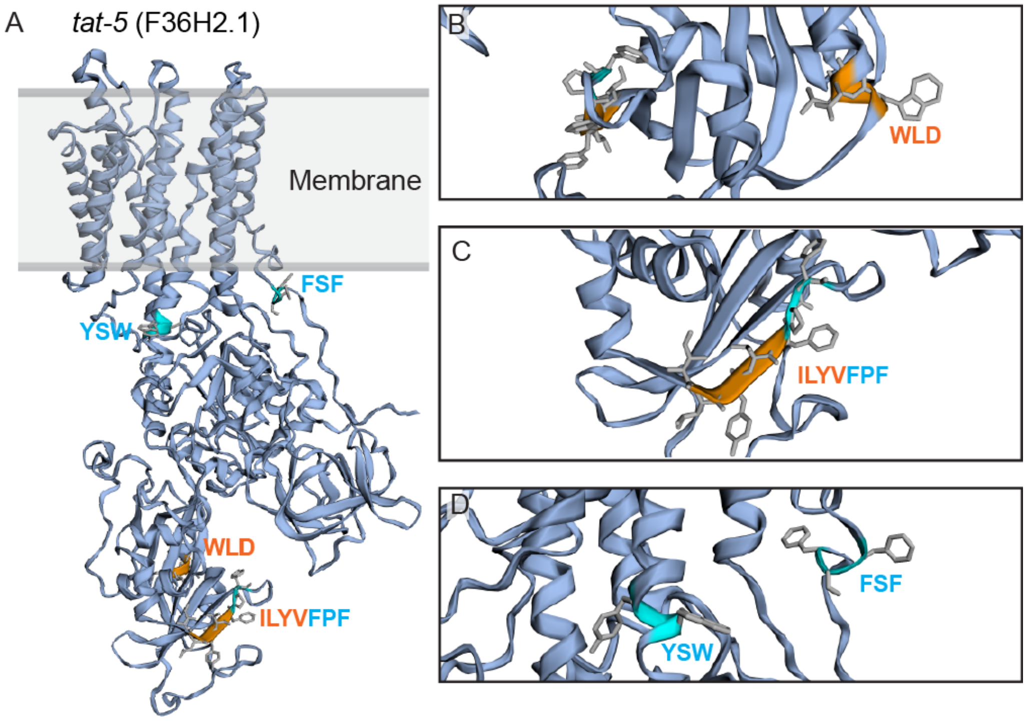

Fig. 14: Potential SNX-binding sites in TAT-5. A) Phyre2 cartoon model of TAT-5A (aa102 to aa1065) based on the structure of a related sodium-potassium P-type ATPase[72]. Potential binding sites for SNX-1/-6 (orange) and SNX-3 (cyan) are displayed. B) The WLD motif (orange) is similar to a SNX5/6-binding WLM motif. C) The hydrophobic ILYVF motif (orange) near the WLD is also similar to a recently discovered SNX5/6 binding site. ILYVF overlaps with an FPF motif (cyan), which is similar to a SNX3-binding motif. D) The FSF motif next to the first transmembrane domain or the YSW motif in the fourth transmembrane domain are also similar to SNX3-binding motifs, as well as the FDF motif (aa68-70), which is in a predicted disordered region that was not modeled.

4.2.12.1. Potential SNX-1/-6 binding sites

We first looked for potential binding sites for SNX-1/6 in TAT-5 based on sequence homology to reported SNX-binding motifs. The hydrophobic WLM motif in the cytosolic tail of CI-MPR serves as a binding site for heterodimers of SNX1/2 and SNX5/6 in mammals[45,46]. TAT-5 contains a similar WLD motif in a large cytosolic domain (Fig. 14A-B), which appears conserved in TAT-5 orthologs (Fig. 15).

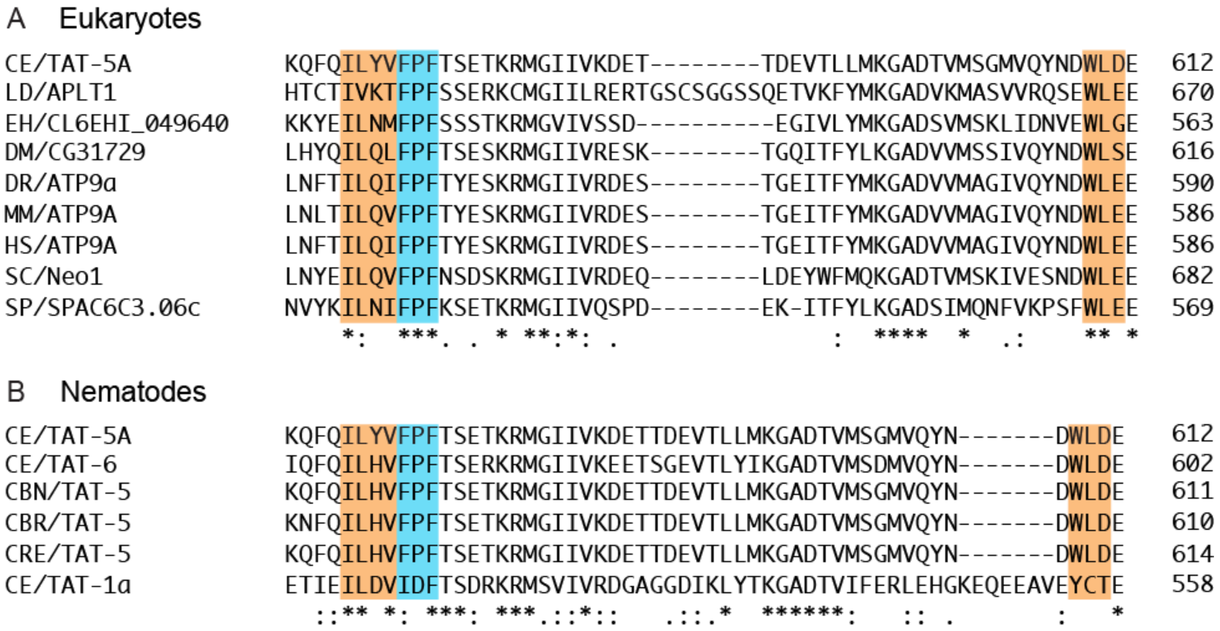

A Eukaryotes

```
CE/TAT-5A           KQFQILYVFPFTSETKRMGIIVKDET--------TDEVTLLMKGADTVMSGMVQYNDWLDE   612
LD/APLT1            HTCTIVKTFPFSSERKCMGIILRERTGSCSGGSSQETVKFYMKGADVKMASVVRQSEWLEE   670
EH/CL6EHI_049640    KKYEILNMFPFSSSTKRMGVIVSSD----------EGIVLYMKGADSVMSKLIDNVEWLGE   563
DM/CG31729          LHYQILQLFPFTSESKRMGIIVRESK--------TGQITFYLKGADVVMSSIVQYNDWLSE   616
DR/ATP9a            LNFTILQIFPFTYESKRMGIIVRDES--------TGEITFYMKGADVVMAGIVQYNDWLEE   590
MM/ATP9A            LNLTILQVFPFTYESKRMGIIVRDES--------TGEITFYMKGADVVMAGIVQYNDWLEE   586
HS/ATP9A            LNFTILQIFPFTYESKRMGIIVRDES--------TGEITFYMKGADVVMAGIVQYNDWLEE   586
SC/Neo1             LNYEILQVFPFNSDSKRMGIIVRDEQ--------LDEYWFMQKGADTVMSKIVESNDWLEE   682
SP/SPAC6C3.06c      NVYKILNIFPFKSETKRMGIIVQSPD--------EK-ITFYLKGADSIMQNFVKPSFWLEE   569
                        *:  ***. . * **:*: .               :  ****  *  .:    ** *
```

B Nematodes

```
CE/TAT-5A           KQFQILYVFPFTSETKRMGIIVKDETTDEVTLLMKGADTVMSGMVQYN-------DWLDE   612
CE/TAT-6            IQFQILHVFPFTSERKRMGIIVKEETSGEVTLYIKGADTVMSDMVQYN-------DWLDE   602
CBN/TAT-5           KQFQILHVFPFTSETKRMGIIVKDETTDEVTLLMKGADTVMSGMVQYN-------DWLDE   611
CBR/TAT-5           KNFQILHVFPFTSETKRMGIIVKDETTDEVTLLMKGADTVMSGMVQYN-------DWLDE   610
CRE/TAT-5           KQFQILHVFPFTSETKRMGIIVKDETTDEVTLLMKGADTVMSGMVQYN-------DWLDE   614
CE/TAT-1a           ETIEILDVIDFTSDRKRMSVIVRDGAGGDIKLYTKGADTVIFERLEHGKEQEEAVEYCTE   558
                      ::** *: ***: ***.::*::   .::.*  ******:   :: .       :   *
```

Fig. 15: The ILYVF, FPF, and WLD motifs are highly conserved in eukaryotic TAT-5 orthologs. A) Clustal Omega multiple sequence alignment of TAT-5 orthologs in eukaryotes. LD *Leishmania donovai*, EH *Entamoeba histolytica*, CE *Caenorhabditis elegans*, DM *Drosophila melanogaster*, DR *Danio rerio*, MM *Mus musculus*, HS *Homo sapiens*, SC *Saccharomyces cerevisiae*, SP *Schizosaccharomyces pombe*. Orange: potential SNX-6 binding motifs ILYVF and WLD, Cyan: potential SNX-3 binding motif FPF. B) Clustal Omega multiple sequence alignment of TAT-5 orthologs in closely related nematodes, plus the C. elegans TAT-5 duplicate TAT-6 and more divergent P4-ATPase TAT-1. CE *Caenorhabditis elegans*, CBN *Caenorhabditis brenneri*, CBR *Caenorhabditis briggsae*, CRE *Caenorhabditis remanei*. Orange: position of the potential SNX-6-binding motifs ILYVF and WLD. Cyan: the potential SNX-3 binding motif FPF.

	Motif	Mutated motif	*tat-5*Δ rescue	Strain	Transgene name
Potential SNX-6 Motifs	**W**LD	**A**LD	░	WEH397	*wurIs142 [GFP::tat-5(W609A)]*
	ILYVF	**D**LYVF	░	WEH476	*wurEx31 [GFP::tat-5(I564D)]*
			░	WEH488	*wurEx32 [GFP::tat-5(I564D)]*
			░	WEH489	*wurEx33 [GFP::tat-5(I564D)]*
	IL**Y**VF	IL**D**VF	-	WEH428	*wurIs154 [GFP::tat-5(Y566D)]*
			-	WEH435	*wurIs156 [GFP::tat-5(Y566D)]*
		IL**Q**VF	░	WEH477	*wurIs167 [GFP::tat-5(Y566Q]*
			░	WEH478	*wurIs174 [GFP::tat-5(Y566Q]*
	ILYV**F**	ILYV**D**	░	WEH419	*wurEx20 [GFP::tat-5(F568D)]*

Table 7: TAT-5 mutants generated for potential SNX-6 binding sites. Strains expressing GFP::TAT-5 mutated at potential SNX-6 binding sites. Mutated amino acids are bold. Lines with genome inserted transgenes are called *wurIs#*, extrachromosomal lines are named *wurEx#*. Some transgenes could rescue sterility (+) in a *tat-5* deletion mutant background, others could not (-). Grey boxes indicate transgenes that where not yet tested to rescue *tat-5(*Δ*)* sterility.

We mutated the bulky, hydrophobic Tryptophan (W) to the non-bulky and weakly hydrophobic Alanine (A) in the functional GFP::TAT-5 plasmid and expressed GFP::TAT-5(W609A) in the germ line and embryos. One integrated strain WEH397 with the ALD mutation was isolated (Table 7). Similar to wild type GFP::TAT-5 (Fig. 3A), GFP::TAT-5(W609A) localized robustly to the plasma membrane (Fig. 16A), suggesting that the WLD motif is not necessary for SNX-1/6-binding.

To confirm whether the WLD motif is necessary for SNX-1/6-binding, we tested whether the localization of GFP::TAT-5(W609A) still changed in *snx* mutants. If the WLD motif is required for SNX-6-dependent TAT-5 trafficking, *snx-6* RNAi should not change the localization of GFP::TAT-5(W609A). In contrast, depleting *snx-3* should cause TAT-5(W609A) mislocalization as mutating this domain should not perturb SNX-3 binding. In both *snx-3* and *snx-6*-depleted GFP::TAT-5(W609A) mutants, TAT-5 was mislocalized similar to *snx-3* or *snx-6* RNAi-treated GFP::TAT-5(WT) (Fig. 16B). This suggests that the WLD motif is not required for SNX-1/6- or SNX-3-mediated trafficking of TAT-5.

Structural studies from Brett Collins' and Peter Cullen's labs have discovered a hydrophobic consensus sequence 15 aa upstream of the WLM motif that appears more directly involved in SNX-1/-6 cargo binding to CI-M6PR[73]. We found that TAT-5 contains a similar hydrophobic region ILYVF 40 aa upstream of the WLD motif (Fig. 14A, C). We predicted that mutating the hydrophobic amino acids Isoleucine (I), Tyrosine (Y) and Phenylalanine (F) to a hydrophilic, polar amino acid like Aspartic acid (D) could block SNX-1/-6 binding.

In contrast to wild type GFP::TAT-5, all three aspartate mutants failed to localize to the plasma membrane and only accumulated at the ER and one spot between cells (Fig. 16C-E). Based on the position of the spot between cells (Fig. 16C-E), the ILYVF mutants may be enriched in remnants of the intercellular bridge between dividing cells[74]. This result was verified in three extrachromosomal I564D lines, in two integrated and six extrachromosomal Y566D lines, and in five extrachromosomal F568D lines (Table 7). GFP::TAT-5(Y566D) was also observed on cytoplasmic vesicles (Fig. 16E). Thus, the ILYVF motif is required for proper TAT-5 localization to the plasma membrane.

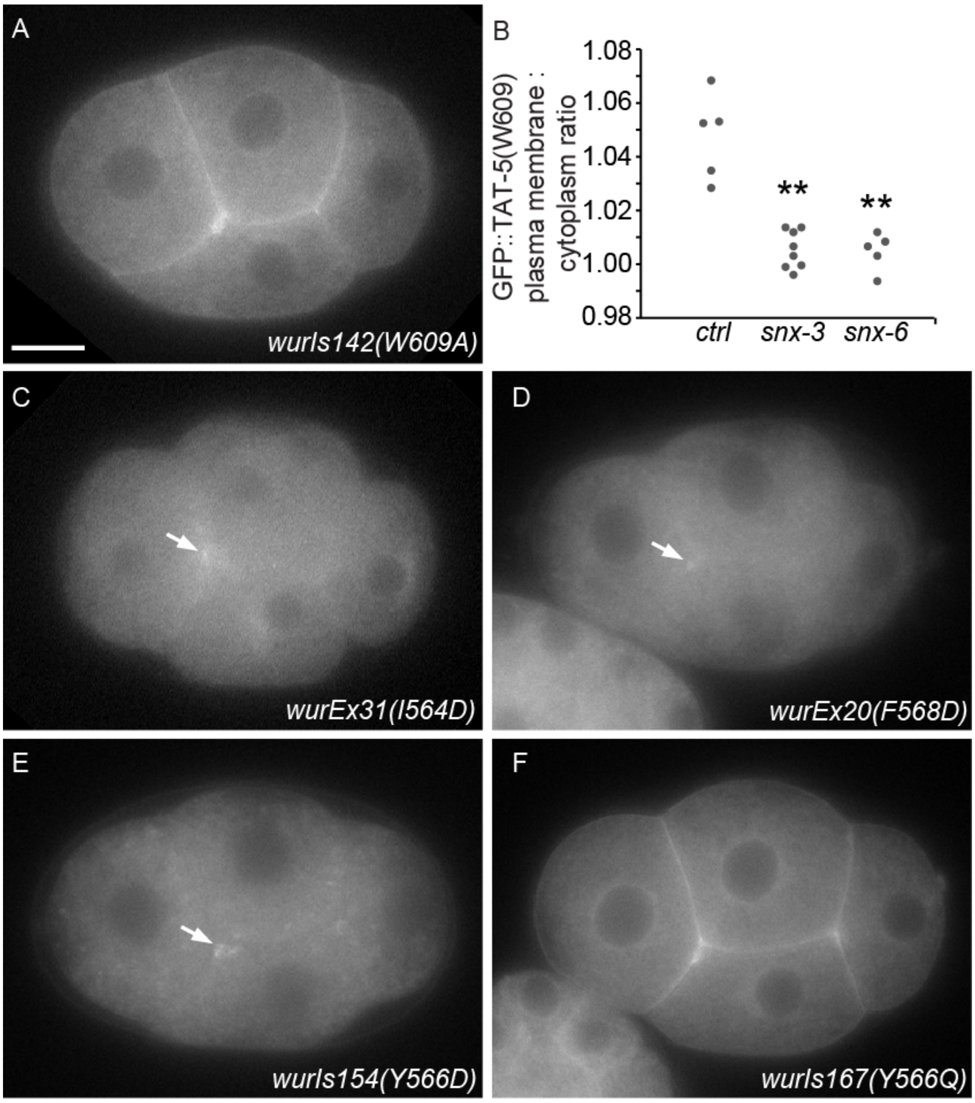
A
wurIs142(W609A)
B
GFP::TAT-5(W609) plasma membrane : cytoplasm ratio
1.08
1.06
1.04
1.02
1.00
0.98
**
**
ctrl
snx-3
snx-6
C
wurEx31(I564D)
D
wurEx20(F568D)
E
wurIs154(Y566D)
F
wurIs167(Y566Q)

Fig. 16: The ILYVF motif is required for TAT-5 plasma membrane localization, not the WLD motif. GFP::TAT-5 mutated for several potential SNX-1/-6 binding sites in 4-cell embryos. A) GFP::TAT-5(W609A) still localizes to the plasma membrane, suggesting that the WLD motif is not essential for SNX-BAR-mediated TAT-5 trafficking. B) Quantification of the GFP::TAT-5(W609) plasma membrane localization ratio from empty vector, *snx-3* and *snx-6* RNAi-treated embryos. Data in A-B was collected with Alida Melse. C-E) GFP::TAT-5 with an I564, F568 or Y566 to D mutation in the ILYVF motif cannot localize to the plasma membrane, although localization to the presumptive midbody remnant (arrow) at the plasma membrane is maintained. F) Mutating Y566 to Q does not disrupt TAT-5 localization to the plasma membrane. Scale Bar: 10 μm.

As TAT-5 can maintain PE asymmetry in the plasma membrane and inhibit EV release when SNX-6 is depleted (Fig. 8, Fig. 9D), we predicted that TAT-5 should remain active when its SNX-6-binding motif is mutated. To check whether the ILYVF mutants are functional, we crossed the GFP::TAT-5(Y566D) transgene that localized to cytoplasmic vesicles into the *tat-5(tm1741)* deletion background. The *tat-5(tm1741)* worms that expressed GFP::TAT-5(Y566D) were sterile (n=3 for *wurIs154*, n=23 for *wurIs156* done by Ann Wehman), similar to the sterility of *tat-5(tm1741)* worms[55]. This suggests that TAT-5(Y566D) is not functional, in contrast to our prediction for a SNX-6 binding motif.

Interestingly, when we compared the sequence of the ILYVF motif to other orthologs of TAT-5 in eukaryotes, we found that the hydrophobic amino acids in this region are highly conserved, except for Y566 (Table 7A-B). In vertebrates, flies and yeast, the hydrophobic and aromatic Y566 is replaced by a hydrophilic, polar Glutamine (Q), or a similarly polar Asparagine (N) in *Entamoeba histolytica* and *Saccharomyces pombe*. As yeast Neo1 and mammalian ATP9A localize to endosomes and the TGN, but not to the plasma membrane[75–77], we asked whether Y566 is required for trafficking to the plasma membrane while Q or N are used to signal that the cargo needs to be trafficked to the TGN. However, mutating the hydrophobic Y566 to a hydrophilic Q did not change the plasma membrane localization of GFP::TAT-5(Y566Q) (Fig. 16F). This suggests that many changes to the amino acid code can be tolerated at this position, suggesting that this amino acid is not as essential as the rest of the ILYVF motif.

Taken together, the WLD motif is not required for TAT-5 plasma membrane localization, while the ILYVF motif is required for both TAT-5 localization and function, although it remains to be determined whether this is due to SNX-6 binding.

4.2.12.2 Potential SNX-3 binding sites

We next looked for potential binding sites for SNX-3 in TAT-5 based on homology to reported SNX3-binding motifs. Human SNX3 recognizes cargo with retromer through an ΩΦΨ sequence, where Ω is an aromatic amino acid, Φ is hydrophobic, and Ψ is aliphatic[33]. These findings are in line with a study in yeast that identified Y/F-x-Φ as a consensus sequence for SNX3 and retromer-based sorting[78]. In yeast, the TAT-5 ortholog Neo1 is recognized by SNX-3 via an FEM motif in the N-terminus[19], but this sequence is not conserved in TAT-5. Four potential SNX-3 binding sites (cyan) were identified by sequence similarities: the FSF motif next to the first transmembrane domain, the YSW motif at the end of the fourth transmembrane helix (Fig. 14D), the FPF motif in a cytosolic domain, which includes the last amino acid of the ILYVF motif (Fig. 14C), and the FDF motif in the N-terminus of TAT-5 isoform A, but not isoform C due to alternative splicing. While FDF is not conserved in other species (Fig. 17), it is found in the N-terminus, like the FEM motif that binds Snx3 in yeast[19]. The sequences of the other three potential SNX-3 bindings sites, FSF, YSW and FPF, are conserved among eukaryotes (Fig. 17), suggesting they could have important conserved functions.

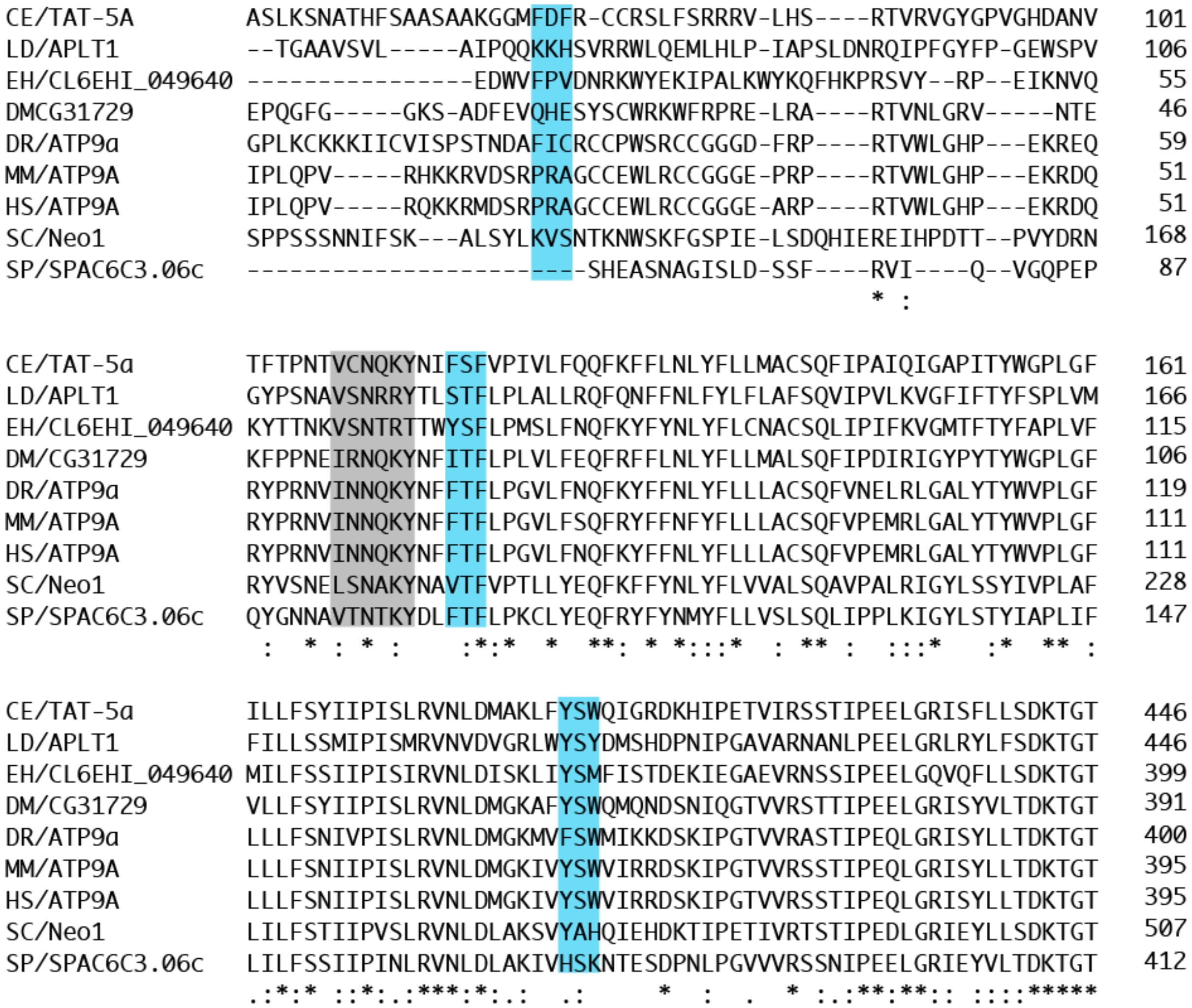

```
CE/TAT-5A        ASLKSNATHFSAASAAKGGMFDFR-CCRSLFSRRRV-LHS----RTVRVGYGPVGHDANV   101
LD/APLT1         --TGAAVSVL-----AIPQQKKHSVRRWLQEMLHLP-IAPSLDNRQIPFGYFP-GEWSPV   106
EH/CL6EHI_049640 ----------------EDWVFPVDNRKWYEKIPALKWYKQFHKPRSVY--RP--EIKNVQ    55
DMCG31729        EPQGFG-----GKS-ADFEVQHESYSCWRKWFRPRE-LRA----RTVNLGRV-----NTE    46
DR/ATP9a         GPLKCKKKIICVISPSTNDAFICRCCPWSRCCGGGD-FRP----RTVWLGHP---EKREQ    59
MM/ATP9A         IPLQPV-----RHKKRVDSRPRAGCCEWLRCCGGGE-PRP----RTVWLGHP---EKRDQ    51
HS/ATP9A         IPLQPV-----RQKKRMDSRPRAGCCEWLRCCGGGE-ARP----RTVWLGHP---EKRDQ    51
SC/Neo1          SPPSSSNNIFSK---ALSYLKVSNTKNWSKFGSPIE-LSDQHIEREIHPDTT--PVYDRN   168
SP/SPAC6C3.06c   ------------------------SHEASNAGISLD-SSF----RVI----Q--VGQPEP    87
                                                             * :

CE/TAT-5a        TFTPNTVCNQKYNIFSFVPIVLFQQFKFFLNLYFLLMACSQFIPAIQIGAPITYWGPLGF   161
LD/APLT1         GYPSNAVSNRRYTLSTFLPLALLRQFQNFFNLFYLFLAFSQVIPVLKVGFIFTYFSPLVM   166
EH/CL6EHI_049640 KYTTNKVSNTRTTWYSFLPMSLFNQFKYFYNLYFLCNACSQLIPIFKVGMTFTYFAPLVF   115
DM/CG31729       KFPPNEIRNQKYNFITFLPLVLFEQFRFFLNLYFLLMALSQFIPDIRIGYPYTYWGPLGF   106
DR/ATP9a         RYPRNVINNQKYNFFTFLPGVLFNQFKYFFNLYFLLLACSQFVNELRLGALYTYWVPLGF   119
MM/ATP9A         RYPRNVINNQKYNFFTFLPGVLFSQFRYFFNFYFLLLACSQFVPEMRLGALYTYWVPLGF   111
HS/ATP9A         RYPRNVINNQKYNFFTFLPGVLFNQFKYFFNLYFLLLACSQFVPEMRLGALYTYWVPLGF   111
SC/Neo1          RYVSNELSNAKYNAVTFVPTLLYEQFKFFYNLYFLVVALSQAVPALRIGYLSSYIVPLAF   228
SP/SPAC6C3.06c   QYGNNAVTNTKYDLFTFLPKCLYEQFRYFYNMYFLLVSLSQLIPPLKIGYLSTYIAPLIF   147
                  :  * : * :    :*:*  *  **: * *:::*  : ** :  :::*   :*  ** :

CE/TAT-5a        ILLFSYIIPISLRVNLDMAKLFYSWQIGRDKHIPETVIRSSTIPEELGRISFLLSDKTGT   446
LD/APLT1         FILLSSMIPISMRVNVDVGRLWYSYDMSHDPNIPGAVARNANLPEELGRLRYLFSDKTGT   446
EH/CL6EHI_049640 MILFSSIIPISIRVNLDISKLIYSMFISTDEKIEGAEVRNSSIPEELGQVQFLLSDKTGT   399
DM/CG31729       VLLFSYIIPISLRVNLDMGKAFYSWQMQNDSNIQGTVVRSTTIPEELGRISYVLTDKTGT   391
DR/ATP9a         LLLFSNIVPISLRVNLDMGKMVFSWMIKKDSKIPGTVVRASTIPEQLGRISYLLTDKTGT   400
MM/ATP9A         LLLFSNIIPISLRVNLDMGKIVYSWVIRRDSKIPGTVVRSSTIPEQLGRISYLLTDKTGT   395
HS/ATP9A         LLLFSNIIPISLRVNLDMGKIVYSWVIRRDSKIPGTVVRSSTIPEQLGRISYLLTDKTGT   395
SC/Neo1          LILFSTIIPVSLRVNLDLAKSVYAHQIEHDKTIPETIVRTSTIPEDLGRIEYLLSDKTGT   507
SP/SPAC6C3.06c   LILFSSIIPINLRVNLDLAKIVHSKNTESDPNLPGVVVRSSNIPEELGRIEYVLTDKTGT   412
                 .:*:* ::*:.:***:*:.:  .:     *  :  .  * :.:**:**:: ::::*****
```

Fig. 17: The FSF, YSW, and VCNQKY motifs are conserved in eukaryotic TAT-5 orthologs. Clustal Omega multiple sequence alignment of an N-terminal region of TAT-5 orthologs in eukaryotes. Motifs matching the SNX-3 consensus Y/F-x-Φ are highlighted in cyan. A motif matching the SNX-FERM consensus ΦxNxxY is labeled in grey. Abbreviations: LD *Leishmania donovai*, EH *Entamoeba histolytica*, CE *Caenorhabditis elegans*, DM *Drosophila melanogaster*, DR *Danio rerio*, MM *Mus musculus*, HS *Homo sapiens*, SC *Saccharomyces cerevisiae*, SP *Schizosaccharomyces pombe*.

	Motif	**Mutated motif**	***tat-5*Δ rescue**	**Strain**	**Transgene name**
Potential SNX-3 Motifs	FDFR	L	-	WEH62	*wurIs45 [GFP::tat-5c cDNA]*
			-	WEH63	*wurIs46 [GFP::tat-5c cDNA]*
	FS**F**	FS**A**	▨	WEH427	*wurEx23 [GFP::tat-5(F118A)]*
			▨	WEH449	*wurIs162 [GFP::tat-5(F118A)]*
			▨	WEH450	*wurIs163 [GFP::tat-5(F118A)]*
			▨	WEH453	*wurIs165 [GFP::tat-5(F118A)]*
	YS**W**	YS**A**	+	WEH401	*wurIs146 [GFP::tat-5(W411A)]*
	FP**F**	FP**A**	▨	WEH421	*wurEx21 [GFP::tat-5(F570A)]*
			-	WEH469	*wurIs168 [GFP::tat-5(F570A)]*
			-	WEH470	*wurIs169 [GFP::tat-5(F570A)]*
			-	WEH471	*wurIs170 [GFP::tat-5(F570A)]*
		FP**D**	▨	WEH473	*wurIs171 [GFP::tat-5(F570D)]*
			▨	WEH474	*wurIs172 [GFP::tat-5(F570D)]*
			▨	WEH475	*wurIs173 [GFP::tat-5(F570D)]*

Table 8: TAT-5 mutants generated for potential SNX-3 binding sites. Strains expressing GFP::TAT-5 mutated at potential SNX-3 binding sites. Mutated amino acids are bold. Lines with genome inserted transgenes are called *wurIs#*, extrachromosomal lines are named *wurEx#*. The TAT-5 isoform C contains Leucine (L) instead of the FDFR sequence, due to alternative splicing. Some transgenes could rescue sterility (+) in a *tat-5* deletion mutant background, others could not (-). Grey boxes indicate transgenes that where not yet tested to rescue *tat-5(*Δ*)* sterility.

The FDF sequence is found at aa68-70 in the N-terminus of TAT-5, lying between alternative splice sites such that it is found in TAT-5 isoform a, but not in TAT-5 isoform c. To test the role of the FDF motif, we cloned TAT-5c from cDNA into the GFP expression vector. Like the wild type genomic GFP::TAT-5 construct, which could express TAT-5a and/or TAT-5c, GFP::TAT-5c localized to the plasma membrane in two integrated strains (Fig. 18A, Table 8). This result is not consistent with TAT-5 mislocalization in *snx-3* mutants (Fig. 6F). Furthermore, GFP::TAT-5c lost plasma membrane localization after *snx-3* RNAi treatment (Fig. 18B), similar to wild type GFP::TAT-5 (Fig. 6F), suggesting that SNX-3 is still required for TAT-5c trafficking.

We next tested whether GFP::TAT-5c was able to rescue the embryonic lethality and sterility phenotypes of *tat-5* deletion mutants[55]. Although embryonic lethality phenotypes were partially rescued in *tat-5* mutants expressing GFP::TAT-5c, the sterility phenotype of *tat-5* mutants was not rescued (experiment conducted by Ann Wehman). As introns can enhance gene expression levels[79], especially in the germ line, intron-less GFP::TAT-5c may not be expressed well enough to rescue the role of TAT-5 in fertility. Thus, further experiments are required to clarify the functionality of TAT-5c and the FDF motif. However, we can conclude that the FDF sequence is not required for TAT-5 trafficking by SNX-3.

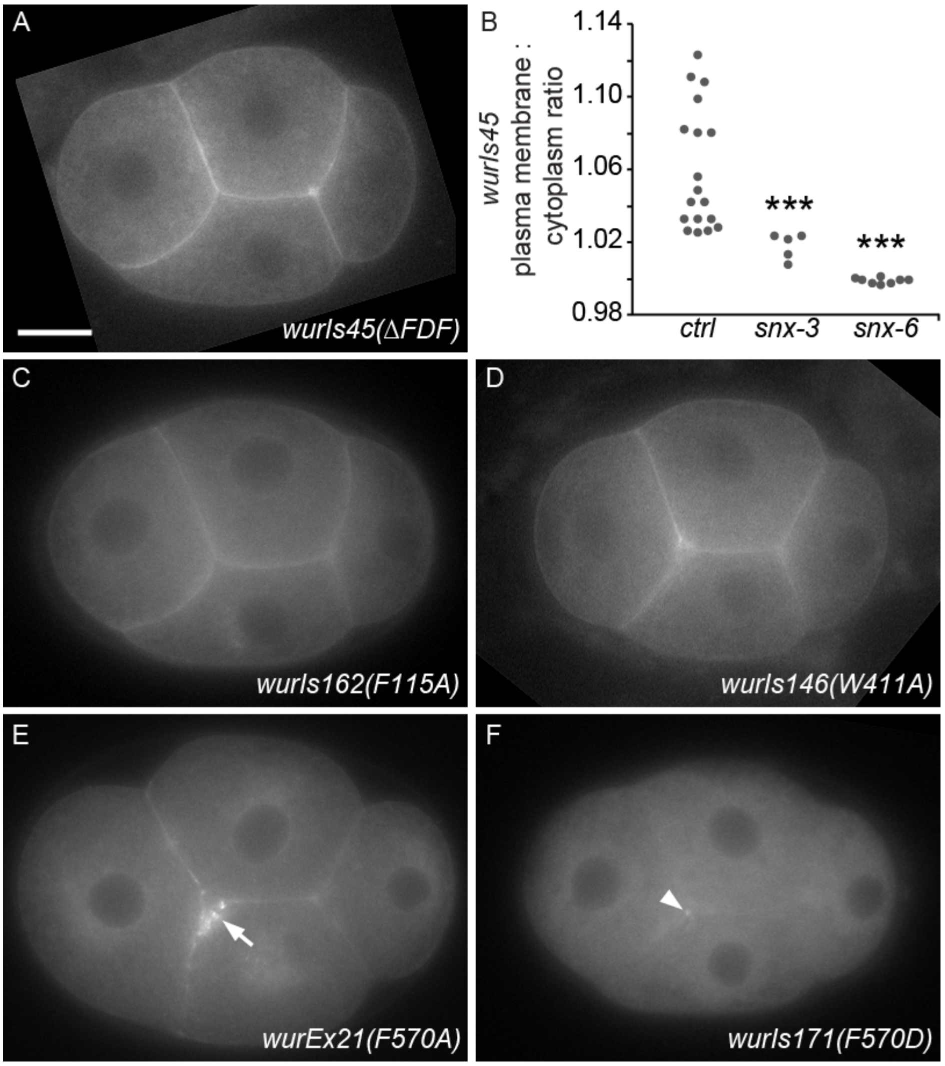
A
wurIs45(ΔFDF)
B
wurIs45
plasma membrane :
cytoplasm ratio
1.14
1.10
1.06
1.02
0.98
***
***
ctrl
snx-3
snx-6
C
wurIs162(F115A)
D
wurIs146(W411A)
E
wurEx21(F570A)
F
wurIs171(F570D)

Fig. 18: Potential SNX-3 binding sites are not required for TAT-5 plasma membrane localization. A) GFP::TAT-5c (*wurIs45)* missing the FDF motif localizes to the plasma membrane like wild type GFP::TAT-5. B) Quantification of the GFP::TAT-5c (*wurIs45*) plasma membrane ratio after empty vector, *snx-3* or *snx-6* RNAi. GFP::TAT-5c (*wurIs45*) plasma membrane levels are reduced after both *snx-1* and *snx-6* RNA. Data in A-B was collected with Alida Melse. C) *wurIs162*, mutant for the FSF motif, D) *wurIs146*, mutant for the YSW motif and E) *wurEx21*, mutant for the FPF motif localize to the plasma membrane. GFP::TAT-5(F570A) additionally localizes to vesicular structures near the three-cell junction (arrow). F) Plasma membrane localization is lost when F570 is mutated to D in *wurIs171*, but localization to the presumptive midbody remnant (arrow) at the plasma membrane is maintained. Scale Bar: 10 µm.

To test the other potential SNX-3 binding sites, we mutated the last hydrophobic amino acid of each motif to Alanine (A). The FSF sequence is found next to the first transmembrane domain of TAT-5, placing it close to the lipid bilayer. We mutated the functional genomic GFP::TAT-5 construct, such that the last F in the FSF motif became A (Fig. 14D). Plasma membrane localization was also not disrupted when we expressed this GFP::TAT-5(F118A) mutant (Fig. 18C), which we verified in three independent insertions and six extrachromosomal lines. This suggests that the F118A mutation is not sufficient to disrupt TAT-5 localization or SNX-3-mediated trafficking.

Similarly, mutating the W to A in the YSW motif in the fourth transmembrane helix of TAT-5 (Fig. 14D) did not change the plasma membrane localization of GFP::TAT-5(W411A) in one integrated line and eight extrachromosomal lines (Fig. 18D, Table 8). Furthermore, embryonic lethality and sterility were rescued when we expressed GFP::TAT-5(W411A) in *tat-5* deletion mutants, suggesting that GFP::TAT-5(W411A) is functional (experiment performed by Ann Wehman). Taken together, the YSW motif also does not appear required for SNX-3-mediated TAT-5 trafficking.

The first F in the FPF motif is part of the previously discussed ILYVF motif, which we found to be required for TAT-5 localization (Fig. 16C-E). Thus, mutating F568 to D may not only disrupt SNX-6 binding, but also SNX-3-dependent trafficking of TAT-5. To test if the last F in the FPF motif is also required for TAT-5 localization, we mutated F570 to A. In contrast to the mutated ILYVF transgenes, plasma membrane localization was not grossly disrupted in GFP::TAT-5(F570A) mutants (Fig. 18E), which was verified in one extrachromosomal and three integrated lines (Table 8). However, we saw punctate GFP::TAT-5(F570A) localization around the tricellular junction (Fig. 18E), which will require further characterization.

As the ILYVF mutants were non-functional (Table 7), we tested whether the FPF mutant was also non-functional. Although GFP::TAT-5(F570A) localized to the plasma membrane, Jona Causemann found that GFP::TAT-5(F570A) was not able to rescue the sterility phenotype of *tat-5* deletion mutants (Table 8)[80]. These data suggest that F570 is important for TAT-5 function, but are not consistent with a role in SNX-3- and/or SNX-6-mediated trafficking.

GFP::TAT-5(F570A) was not lost from the plasma membrane like the aspartate mutants in the neighboring ILYVF motif (Fig. 16D). We speculated that mutating the bulky hydrophobic F to the small, hydrophobic A may not be a big enough difference to block SNX-3 and/or SNX-6 binding. We then checked whether mutating F570 to a hydrophilic D caused TAT-5 mislocalization, similar to mutants in the ILYVF motif. GFP::TAT-5(F570D) did not localize to the plasma membrane (Fig. 18F), as seen in three integrated lines and one extrachromosomal lines (Table 8). It also accumulated at the putative midbody remnant (Fig. 18F). This mislocalization of GFP::TAT-5(F570D) appeared similar to the ILYVF mutants (Fig. 16C-D), demonstrating that F570 can be required for TAT-5 localization. Thus, mutating F570 to A was sufficient to block TAT-5 function, but was not a strong enough change to alter TAT-5 localization.

Taken together, we found no evidence that the FDF, FSF and YSW motifs are required for TAT-5 trafficking by SNX-3. In contrast, the FPF motif is required for TAT-5 localization and function and may define a "hot spot" for TAT-5 trafficking together with the ILYVF motif.

4.3. Discussion: Redundant trafficking pathways control TAT-5 localization and extracellular vesicle release

In this chapter, we defined the trafficking pathways that recycle TAT-5 to the plasma membrane (Fig. 19). We showed that the MV release inhibitors identified in chapter 3, namely the class III PI3K and RME-8, regulate endosomal trafficking of TAT-5. Thus, it is likely that PI3K and RME-8 regulate TAT-5 trafficking to inhibit MV budding. Since PI3K generates PI3P to mediate endosome identity and the recruitment of RME-8 and the SNXs, we propose that VPS-34 and BEC-1 act upstream of the other endosomal trafficking machineries that recycle TAT-5. We found that RME-8 is required to prevent TAT-5 mistrafficking to the degradative pathway and that RME-8 function is required to maintain PE asymmetry, suggesting that TAT-5 cannot maintain the PE asymmetry of the plasma membrane when mislocalized to endolysosomes. Additionally, we found that the redundant SNX-1/-6 and SNX-3 trafficking pathways recycle the majority of TAT-5 to the plasma membrane. Surprisingly, the TAT-5 trafficking function of sorting nexins was independent of the retromer complex, which may be able to traffic a low amount of TAT-5. Thus, multiple trafficking pathways exist from PI3P-positive endosomes to maintain the MV inhibitory function of TAT-5.

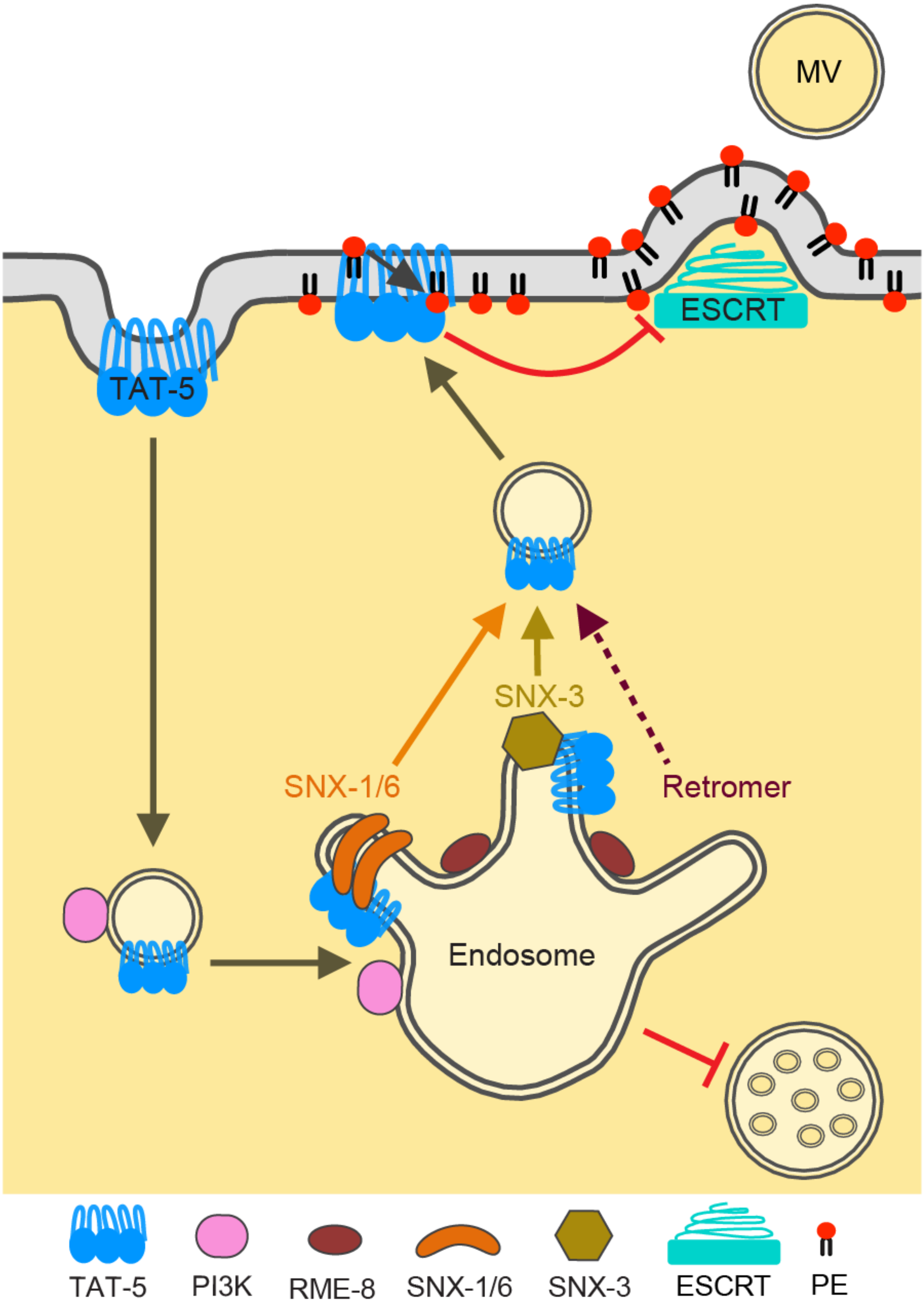
MV
ESCRT
TAT-5
SNX-3
SNX-1/6
Retromer
Endosome
TAT-5
PI3K
RME-8
SNX-1/6
SNX-3
ESCRT
PE

Fig. 19: Model of TAT-5 endosomal trafficking mediated by sorting nexins to inhibit extracellular vesicle release. TAT-5 maintains PE asymmetry in the plasma membrane to inhibit recruitment of the ESCRT machinery, which would release EVs by plasma membrane budding. TAT-5 is endocytosed and needs to be recycled from sorting endosomes. PI3K is required for the identity of endosomes and is thus required for TAT-5 recycling through multiple pathways. RME-8 blocks TAT-5 from being sorted into

endolysosomes (multivesicular body on the bottom right) and therefore mediates TAT-5 recycling away from the degradative pathway. SNX-1/SNX-6- and SNX-3-mediated tubulation and vesicle formation are required to traffic TAT-5 in two independent pathways. The core retromer complex may define a minor pathway involved in recycling TAT-5 to the plasma membrane.

4.3.1. The class III PI3K is required for TAT-5 trafficking

The class III PI3K is needed to create PI3P lipids and we propose that PI3K thereby recruits the sorting and tubulation machineries that are needed to recycle TAT-5 to the plasma membrane. We believe this is likely to occur on endosomes, because our lab did not find a role in EV release for the autophagy-specific subunit of PI3K complex I, Atg14 (chapter 3.3.3.). Thus, it would be interesting to generate mutants for the *C. elegans* UVRAG ortholog, Y34B4A.2, and then examine TAT-5 localization. This experiment would help confirm the endosomal role for PI3K complex II during TAT-5 recycling.

GFP::TAT-5 is mislocalized to large patches in class III PI3K mutants (Fig. 3B-C), but these structures do not appear vesicular and may not be endosomes. In addition to its many functions on endosomes, VPS34 is also required for the formation of COPII vesicles that transport proteins from the ER to the TGN[81]. Therefore, TAT-5 exit from the ER or trafficking through the Golgi could be disrupted in PI3K mutants. Co-staining with ER reporters like the ER-resident signal peptidase SP12 and the TGN-reporter SQV-8would test whether GFP:::TAT-5 is trapped in an enlarged ER or TGN in *vps-34* and *bec-1* mutants[82,83]. To check whether the large patches are enlarged endosomes, endosome reporters that do not require PI3P for their endosomal localization should be used, for example the early endosome reporter RAB-5 GTPase that is required for the localization and activity of VPS-34 on endosomes[84,85]. These experiments would clarify which TAT-5 trafficking step is disrupted in *bec-1* and *vps-34* mutants.

Furthermore, it is unclear whether TAT-5 can maintain PE asymmetry from the large intracellular structures in class III PI3K mutants. If TAT-5 is still partially active from these endosomes, this may explain why *bec-1* and *vps-34* mutants have milder MV release than *tat-5* mutants (chapter 3, Fig. 7E-F). Thus, duramycin staining should be conducted to analyze the PE flipping activity of TAT-5 in class III PI3K mutants. Together, these experiments would define which intracellular structures are capable of maintaining plasma membrane asymmetry.

The production of PI3P on endosomal membranes is required for the localization of many endosomal effector proteins that bind PI3P, for example through PX domains[1,18]. These proteins include the SNXs that contain a PX domain and therefore bind PI3P on endosomes[16]. Furthermore, the N-terminus of RME-8 has PI3P-binding activity that is required for RME-8 localization to endosomes[21]. We propose that the activity of PI3K is required on early endosomes for the recruitment of RME-8 and SNXs (Fig. 19). Thus, VPS-34 and BEC-1 are likely to act upstream of RME-8 and SNXs, which then orchestrate TAT-5 trafficking to the plasma membrane, where it inhibits MV release. Therefore, we hypothesize that BEC-1 and VPS-34 inhibit MV release because PI3P is required for RME-8, SNX-1/-6 and SNX-3 recruitment to endosomes, where they traffic TAT-5.

4.3.2. RME-8 sorts TAT-5 away from the degradative pathway

RME-8 has multiple functions on endosomes, making it unclear which role is important for MV release. RME-8 recruits the WASH complex to endosomes, which nucleates actin to control formation and fission of endosomal recycling tubules[3]. Thus, it is possible that RME-8 is required for endosome tubulation to create recycling vesicles carrying TAT-5 back to the plasma membrane. However, loss of mammalian RME-8 caused increased tubulation of endosomes positive for endosomal trafficking regulators like SNX-1 and retromer[28,86]. Thus, RME-8 could also be important to limit the formation of endosomal recycling tubules.

Another important function of RME-8 is to establish endosomal recycling microdomains to prevent cargo from being degraded. When RME-8 is lost, the degradative microdomains are elongated, resulting in an expansion of the part of the endosome decorated with the ESCRT-complex[27]. WASH-mediated actin polymerization is also thought to promote separation of the recycling microdomain from the degradative microdomain on sorting endosomes[3]. Thus, RME-8 is needed to maintain recycling microdomains on endosomes that oppose the regions of ILV budding, thereby preventing cargo from degradation in late endosomes. Our data is consistent with the role of RME-8 in separating the recycling and degradative domains on endosomes. Loss of RME-8 caused GFP::TAT-5 to colocalize more to LMP-1 positive structures, which could be ILV-containing late endosomes or lysosomes. Since we also observed a general reduction of GFP::TAT-5 levels (Fig. 3F), this suggests that TAT-5 in the degradative microdomain is ultimately degraded. Thus, RME-8 could inhibit MV release by preventing TAT-5 from accumulating at the degradative microdomain on endosomes. Analyzing *rme-8* mutants also provided insights into which intracellular structures TAT-5 can maintain lipid asymmetry. Loss of RME-8 caused increased PE externalization in addition to TAT-5 accumulation in endolysosomes (Fig. 5, Fig. 4). Although the TAT-5 ortholog Neo1 could control plasma membrane PE asymmetry from endosomes, our RME-8 data implies that TAT-5 is not able to maintain PE asymmetry from late endosomes and/or lysosomes. This suggests that endosomal TAT-5 can only maintain plasma membrane asymmetry from early, sorting or recycling endosomes.

Surprisingly, RME-8-dependent trafficking may be specific to the TAT-5 subclass of P4-ATPases, because PS asymmetry was not disrupted when RME-8 was depleted (Fig. 5). The PS flippase TAT-1 also localizes to the plasma membrane and endosomes[61,62], suggesting that it would also need to be recycled. To confirm that RME-8 controls the localization of TAT-5, but not of TAT-1, we need to check whether TAT-1 plasma membrane localization is altered in *rme-8* mutants. If TAT-1 localization is unaltered, then TAT-1 likely uses other pathways to be recycled to the plasma membrane.

Loss of RME-8 increases MV release (chapter 3, Fig. 7C), while multiple SNX pathways must be disrupted to increase MV release (Fig. 9), suggesting that RME-8 might affect multiple trafficking pathways. RME-8 is known to bind SNX1 in mammals and *C. elegans*[20,86], as well as regulate endosomal microdomain formation together with SNX-1 and SNX-6[27], suggesting that RME-8 acts in the SNX-1/-6 pathways. However, RME-8 can also interact with Snx3[87]. Thus, RME-8 may control TAT-5 trafficking by affecting both SNX-1/-6- and SNX-3-dependent TAT-5 trafficking (Fig. 19), possibly by defining the recycling microdomain on endosomes.

4.3.3. SNX-1, SNX-6 and SNX-3 redundantly traffic TAT-5 to the plasma membrane

TAT-5 localization to the plasma membrane depends on the BAR domain-containing sorting nexins SNX-1 and SNX-6, as well as the PX-only sorting nexin SNX-3 (Fig. 6D-F). It was unexpected that we discovered similar effects on TAT-5 localization after disrupting either the SNX-BARs or SNX-3, since the SNX-BAR heterodimer SNX1-SNX6 is thought to traffic distinct cargos from the SNX-PX protein SNX3[63]. By studying TAT-5 trafficking, we were able to show that SNX-3 and the SNX-BAR heterodimer made up of SNX-1 and SNX-6 can traffic the same cargo via two distinct pathways (Fig. 19).

Analyzing PE externalization in *snx-6* mutants also provided insight into where TAT-5 can maintain lipid asymmetry in the plasma membrane. As SNXs are required for cargo recycling from sorting endosomes[15], we predict that TAT-5 accumulates in sorting endosomes in *snx-6* mutants, which requires confirmation with further colocalization studies. As PE was not externalized after *snx-6* RNAi (Fig. 8), TAT-5 is still able to maintain PE asymmetry when mislocalized to certain endosomes. This is similar to studies in yeast showing that the TAT-5 ortholog Neo1p maintains lipid asymmetry in the plasma membrane indirectly by regulating lipid asymmetry in endosomes[58]. Taken together with the *rme-8* results, we predict that TAT-5 can maintain PE asymmetry from sorting endosomes, but not from endolysosomes. Thus, as long as TAT-5 is not mislocalized to the degradative pathway, TAT-5 could inhibit MV release.

As each SNX pathway can traffic multiple cargoes[51], it remains unclear whether MV release is only caused by TAT-5 mislocalization when both the SNX-3 and SNX-1/6 pathways are disrupted. TAT-5 could be mistrafficked to a different compartment in *snx* double mutants than in the individual RNAis, such as endolysosomes. To test this, GFP::TAT-5 should be co-stained with the endolysosome marker LMP-1 in *snx* single and double mutants[9]. It will also be informative to check for externalized PE in sorting nexin double mutants in order to clarify under which conditions TAT-5 can maintain PE asymmetry and inhibit MV release.

On the other hand, other unknown inhibitors of EV release could also be mislocalized in sorting nexin double mutants. To identify new EV inhibitors, one could test whether any of the conserved proteins found in the interactome of both SNX-BARs and SNX3 inhibits MV release in *C. elegans* using our degradation-based assay (chapter 3)[4,45]. This may result in the identification of another MV release inhibitor that could act independent of TAT-5, which increases the toolkit to experimentally control MV release.

4.3.4. SNX-1/-6 and SNX-3 act independent of Retromer to traffic TAT-5

Surprisingly, we found that TAT-5 trafficking involves retromer-associated sorting nexin pathways independent of the core retromer. Even depletion of two retromer subunits did not result in strong TAT-5 mislocalization in *C. elegans.* This is in contrast to yeast, where Neo1p reporters were mislocalized to the vacuole in both Snx3 and core retromer mutants[19,37]. In yeast, retromer is in a complex with SNX-1 and SNX-6 or with SNX-3 and SNX-27[66]. However, recent findings from higher eukaryotes confirm that SNX-1 and SNX-6 heterodimers only transiently associate with retromer in eukaryotes and can traffic cargo independent of retromer[45,46,66]. This suggests that retromer binding to SNXs is not strictly required in higher eukaryotes. However, SNX3 has only been reported to bind cargo in collaboration with the retromer[33,78]. How SNX-3 can recognize and traffic TAT-5 without binding to the retromer remains to be determined (Fig. 7), but it is likely that SNX3 is able to traffic other cargoes independent of the retromer complex.

Although it is clear that the SNXs traffic TAT-5 independent of the retromer, it is unclear whether retromer promotes TAT-5 trafficking independent of SNXs. Retromer proteins do not traffic the major pool of TAT-5, as seen by a consistent GFP::TAT-5 plasma membrane localization in retromer mutants. However, we measured a mild, but significant decrease in the plasma membrane to cytoplasm ratio, suggesting that retromer is required for the trafficking of a small proportion of TAT-5 (Fig. 19). Therefore, it should be tested whether the fluorescence intensity ratio of GFP::TAT-5 on the plasma membrane is slightly reduced in the SNX-3(Y22A) mutant, similar to retromer mutants. This would clarify whether retromer depends on binding to SNX-3 in order to contribute to TAT-5 trafficking.

Retromer can also link sorting nexins and their cargo to the actin-nucleating WASH complex to promote cargo sorting and endosome tubulation[3]. Thus, it is possible that TAT-5 recycling by SNX pathways is slowed in retromer mutants because of reduced WASH complex recruitment to endosomes. To test the dynamics of TAT-5 trafficking, one could synchronize cargo trafficking with approaches like the RUSH (Retention Using Selective Hooks) system[88], and compare the speed of TAT-5 recycling to the plasma membrane in retromer mutants versus wild type. It would also be interesting to test whether disrupting both retromer and SNX-1/-6 or SNX-3 would lead to increased MV release. These experiments would help determine whether retromer supports SNX-mediated trafficking or has its own independent TAT-5 trafficking pathway.

4.3.5. SNX-17 and SNX-27 inhibit microvesicle release when SNX-1/-6 or SNX-3 are absent

We found signs of increased EV release when we depleted both the SNX-FERM SNX-17 or SNX-27 with SNX-1, SNX-6 or SNX-3 (Fig. 13), suggesting that SNX-17 and SNX-27 redundantly inhibit MV release with SNX-1/-6 or SNX-3. However, the plasma membrane reporter appeared punctate in the cytoplasm of most *snx-17* and some *snx-27* RNAi embryos, making it hard to distinguish between cytosolic vesicles and MVs. Therefore, TEM analysis will be necessary to determine whether the reporter is labeling EVs or endocytosed vesicles with delayed lysosomal degradation.

SNX27 helps recycle cargo together with the retromer complex and SNX3[3]. Mammalian SNX27 was also found in the interactome of SNX1 and was reported to traffic cargo like the glucose transporter GLUT1 together with retromer[89], suggesting that SNX-27 could traffic TAT-5 with SNX-1/-6, SNX-3 or retromer. However, depletion of *snx-27* did not cause any obvious change in TAT-5 localization to the plasma membrane (Fig. 12), while *snx-1*, *snx-6* or *snx-3* RNAi did (Fig. 6D-F), suggesting that SNX-27 acts in a separate pathway than SNX-1/-6 and SNX-3. However, it remains to be determined whether there are changes to the intracellular localization of TAT-5, which could shed more light on a role for SNX-27 in SNX-BAR or SNX-3 pathways. To determine whether SNX-27 acts in the same pathway as retromer, we need to test whether we measure a mild reduction of GFP::TAT-5 levels at the plasma membrane in *snx-27* mutants similar to retromer mutants. It could also be informative to examine *snx-27* retromer double mutants to see if they gain any additional phenotypes. These experiments will help to determine how SNX-27 could influence MV budding.

To sum up, our preliminary results on SNX-17 and SNX-27 suggest that they may redundantly inhibit MV release, but their contribution to TAT-5 trafficking still needs to be determined.

4.3.6. The search for SNX binding sites in TAT-5

We identified a number of potential sorting nexin bindings sites based on SNX-retromer consensus sequences, but TAT-5 is trafficked by sorting nexins independent of the retromer. To date, no retromer-independent binding sequences for SNX-3 or SNX-1/6 are known. Thus, elucidating how TAT-5 is recognized by sorting nexins will not only help us to understand TAT-5 trafficking by sorting nexins, but will also give insights into how sorting nexins bind their diverse cargoes.

The hydrophobic WLM-motif in the C-terminus of CI-MPR serves as a binding site for the SNX1/2 and SNX5/6 heterodimer in mammals[45,46], but mutating a similar WLD motif to ALD in a cytosolic domain did not change TAT-5 plasma membrane localization. To verify that the WLD motif is dispensable for SNX-1/-6 binding, we could mutate WLD to AAA, as this was previously used to block binding of the SNX1 and SNX6 heterodimer[45,46]. However, as SNX-BARs assemble close to the plasma membrane[65], while the WLD motif is found in a globular cytoplasmic domain (Fig. 14), it remains unclear whether SNX-6 would bind a cargo sequence this far from the plasma membrane. Thus, we find it unlikely that the WLD motif is a SNX-6 binding site.

We identified potential SNX-3-binding sites based on the Y/F-x-Φ consensus sequence[78], but there are other potential sites based on the ΩΦΨ sequence[33]. The Y/F-x-Φ sequences we examined in TAT-5, namely FDF, FSF and YSW, were not required for TAT-5 trafficking to the plasma membrane, suggesting that they are not necessary for SNX-3 binding. This is in contrast to yeast, where the TAT-5 ortholog Neo1 is recognized by Snx3 via an FEM motif in its N-terminus[19]. Mutating the FEM sequence was sufficient to disrupt the localization of the N-term of Neo1. However, the FEM sequence is not conserved in animals[31], and the FEM motif is not the only Snx3 binding site in Neo1[19]. As SNX-3 may recognize TAT-5 by more than one sequence, mutating more than one potential binding sequence may be necessary to disrupt SNX-3 binding. Additionally, quantifying TAT-5 plasma membrane localization in these mutants could help to determine additive effects of different SNX-3-binding sites.

4.3.7. TAT-5 localization and activity depend on the conserved ILYVFPF motif

The hydrophobic ILYVFPF sequence is required for TAT-5 plasma membrane localization and contains potential binding sequences for SNX-6 and SNX-3. Although it is tempting to speculate that ILYVFPF binds to both SNX-3 and SNX-1/6, it remains to be determined whether the ILYVFPF motif interacts with any SNX. SNX-BAR heterodimers assemble close to the plasma membrane in a typical banana-like shape[65]. Furthermore, retromer-dependent cargo binding by SNX-3 also appears close to the plasma membrane[90], making it unlikely that SNX-BAR or SNX-3 would bind a globular domain located far from the plasma membrane (Fig. 14A). Thus, it is currently unclear why the ILYVFPF sequence is important for TAT-5 localization.

Mutating I564, Y566, F568 or F570 to D caused loss of TAT-5 from the plasma membrane, however, GFP::TAT-5 was visibly brighter at one spot at the tricellular junction. As this localization is similar to the location of the P0 and AB midbodies[74], we hypothesize that the aspartate mutants still localize to the midbody. This suggests that some trafficking to the plasma membrane still occurs, implying that trafficking pathways exist that do not require the ILYVFPF motif for TAT-5 localization.

Surprisingly, mutating F570 to the weakly hydrophobic alanine did not disrupt the plasma membrane localization of TAT-5, although a slight decrease in TAT-5 plasma membrane levels was measurable[80]. This demonstrates that the phenol ring on F570 was not required to localize TAT-5 to the plasma membrane. GFP::TAT-5(F570A) also localized to an unknown vesicular structure at the tricellular junction. Given their location and transient nature, these vesicles could be extracellular, endocytic or exocytic vesicles. In the future, we need to identify these vesicles by co-labeling with organelle reporters, which may give further insight into TAT-5 trafficking or function.

Recently, the first structures of lipid flippases have been solved, including yeast Drs2 and mammalian ATP8A[91,92]. These structures show that the ILYVFPF motif is buried in a globular region and does not face the cytoplasm in these PS flippases, in contrast to the prediction of the Phyre model based on a more distantly related P-type ATPase (Fig. 14). Introducing aspartates inside a hydrophobic, globular region could disrupt proper protein folding. Thus, the dispersed appearance of GFP::TAT-5 in I564D, Y566D, F568D and F570D mutants could be due to degradation of the protein as a result of the unfolded protein response. As unfolded proteins in the ER are ubiquitinated and degraded by the proteasome[93], it would be interesting to test whether proteasomal inhibition increases the levels of the ILYVFPF mutant proteins.

Intriguingly, the last F of the ILYVFPF sequence, which is F570 in TAT-5, is also conserved in the PS flippases Drs2 (LLNICEF) and ATP8 (ILNVLEF). This F localizes at an interface of the N (nucleotide binding) and P (phosphorylation) domains and interacts with the adenine ring of ATP when the flippase is in the E1 state[91,92]. In the E1 state, the flippase binds ATP and transfers a phosphate to the conserved Aspartate in the DKTGT motif to transition the flippase into the E1P state, which initiates the lipid translocation cycle[94]. Blocking the interaction of the flippase and ATP would maintain the flippase in the E1 state and thereby disrupt lipid translocation. This suggests that F570 could be required for TAT-5 flippase activity. Indeed, although GFP::TAT-5(F570A) localizes to the plasma membrane, it does not rescue the sterility phenotype of *tat-5* mutants[80], suggesting that TAT-5(F570A) is not functional. However, we believe TAT-5(F570A) could represent a partial loss-of-function allele, as the E1P/E2P states are thought to be important for trafficking out of the ER[95]. Mutating the key Aspartate in the DKTGT motif in TAT-5(D439E) creates a flippase that cannot be phosphorylated, is stuck in the E1 state, and remains in the ER[55]. Consistently, phosphorylation of the key Aspartate is essential for the ER exit of mammalian ATP9A and ATP9B[95]. That GFP::TAT-5(F570A) is still able to localize to the plasma membrane suggests that TAT-5(F570A) can still be phosphorylated to enter the catalytic cycle. This needs to be confirmed using biochemical assays to test whether the F570A mutant weakens ATP binding and thereby impairs the E1 to E1P transition. Thus, our studies looking for SNX-binding sites may have discovered key residues important for the flippase activity of TAT-5, providing more insight into this conserved family of essential proteins. Furthermore, having a partial loss-of-function allele could be useful for genetic techniques such as suppressor/enhancer screens, which will allow us to identify novel TAT-5 interactors and MV release regulators.

In summary, determining the interactors and regulators of TAT-5 function will help to understand the conserved mechanisms of MV budding. With the set of proteins in hand that control MV release, it will ultimately be possible to determine the physiological roles of MVs during health and disease.

4.4. References

1. Bilanges, B., Posor, Y. & Vanhaesebroeck, B. PI3K isoforms in cell signalling and vesicle trafficking. *Nat. Rev. Mol. Cell Biol.* **20**, 515–534 (2019).
2. Gallon, M. & Cullen, P. J. Retromer and sorting nexins in endosomal sorting. *Biochem. Soc. Trans.* **43**, 33–47 (2015).
3. Simonetti, B. & Cullen, P. J. Actin-dependent endosomal receptor recycling. *Curr. Opin. Cell Biol.* **56**, 22–33 (2019).
4. McGough, I. J. *et al.* SNX3-retromer requires an evolutionary conserved MON2:DOPEY2:ATP9A complex to mediate Wntless sorting and Wnt secretion. *Nat. Commun.* **9**, 3737 (2018).
5. Sato, K., Norris, A., Sato, M. & Grant, B. D. C. elegans as a model for membrane traffic. *WormBook* 1–47 (2014).
6. Bonifacino, J. S. & Glick, B. S. The Mechanisms of Vesicle Budding and Fusion. *Cell* **116**, 153–166 (2004).
7. Grant, B. D. & Donaldson, J. G. Pathways and mechanisms of endocytic recycling. *Nat. Rev. Mol. Cell Biol.* **10**, 597–608 (2009).
8. Gruenberg, J. The endocytic pathway: A mosaic of domains. *Nature Reviews Molecular Cell Biology* **2**, 721–730 (2001).
9. Naslavsky, N. & Caplan, S. The enigmatic endosome – sorting the ins and outs of endocytic trafficking. *J. Cell Sci.* **131**, jcs216499 (2018).
10. Di Paolo, G. & De Camilli, P. Phosphoinositides in cell regulation and membrane dynamics. *Nature* **443**, 651–657 (2006).
11. Odorizzi, G., Babst, M. & Emr, S. D. Phosphoinositide signaling and the regulation of membrane trafficking in yeast. *Trends Biochem. Sci.* **25**, 229–235 (2000).
12. Gaullier, J.-M., Rønning, E., Gillooly, D. J. & Stenmark, H. Interaction of the EEA1 FYVE Finger with Phosphatidylinositol 3-Phosphate and Early Endosomes. *J. Biol. Chem.* **275**, 24595–24600 (2000).
13. Simonsen, A. *et al.* EEA1 links PI(3)K function to Rab5 regulation of endosome fusion. *Nature* **394**, 494–498 (1998).
14. Hurley, J. H. ESCRTs are everywhere. *EMBO J.* **34**, 2398–2407 (2015).
15. Cullen, P. J. Endosomal sorting and signalling: An emerging role for sorting nexins. *Nat. Rev. Mol. Cell Biol.* **9**, 574–582 (2008).
16. Seet, L. F. & Hong, W. The Phox (PX) domain proteins and membrane traffic. *Biochimica et Biophysica Acta - Molecular and Cell Biology of Lipids* **1761**, 878–896 (2006).
17. Backer, J. M. The intricate regulation and complex functions of the Class III phosphoinositide 3-kinase Vps34. *Biochemical Journal* **473**, 2251–2271 (2016).
18. Viaud, J. *et al.* Phosphoinositides: Important lipids in the coordination of cell dynamics. *Biochimie* **125**, 250–258 (2016).
19. Dalton, L. E., Bean, B. D. M., Davey, M. & Conibear, E. Quantitative high-content imaging identifies novel regulators of Neo1 trafficking at endosomes. *Mol. Biol. Cell* **28**, 1539–1550 (2017).
20. Shi, A. *et al.* Regulation of endosomal clathrin and retromer-mediated endosome to Golgi retrograde transport by the J-domain protein RME-8. *EMBO J.* **28**, 3290–3302 (2009).
21. Xhabija, B., Taylor, G. S., Fujibayashi, A., Sekiguchi, K. & Vacratsis, P. O. Receptor mediated endocytosis 8 is a novel PI(3)P binding protein regulated by myotubularin-related 2. *FEBS Lett.* **585**, 1722–1728 (2011).
22. Ruck, A. *et al.* The Atg6/Vps30/Beclin 1 ortholog BEC-1 mediates endocytic retrograde transport in addition to autophagy in C. elegans. *Autophagy* **7**, 386–400 (2011).
23. Zhang, Y., Grant, B. & Hirsh, D. RME-8, a conserved J-domain protein, is required for endocytosis in Caenorhabditis elegans. *Mol. Biol. Cell* **12**, 2011–2021 (2001).
24. Chang, H. C., Hull, M. & Mellman, I. The J-domain protein Rme-8 interacts with Hsc70 to control clathrin-dependent endocytosis in Drosophila. *J. Cell Biol.* **164**, 1055–1064 (2004).
25. Hannan, L. A., Newmyer, S. L. & Schmid, S. L. ATP- and cytosol-dependent release of adaptor proteins from clathrin-coated vesicles: A dual role for Hsc70. *Mol. Biol. Cell* **9**, 2217–29 (1998).

26. Jiang, R., Gao, B., Prasad, K., Greene, L. E. & Eisenberg, E. Hsc70 chaperones clathrin and primes it to interact with vesicle membranes. *J. Biol. Chem.* **275**, 8439–47 (2000).
27. Norris, A. *et al.* SNX-1 and RME-8 oppose the assembly of HGRS-1/ESCRT-0 degradative microdomains on endosomes. *Proc. Natl. Acad. Sci.* **114**, E307–E316 (2017).
28. Freeman, C. L., Hesketh, G. & Seaman, M. N. J. RME-8 coordinates the activity of the WASH complex with the function of the retromer SNX dimer to control endosomal tubulation. *J. Cell Sci.* **127**, 2053–2070 (2014).
29. Girard, M. & McPherson, P. S. RME-8 regulates trafficking of the epidermal growth factor receptor. *FEBS Lett.* **582**, 961–966 (2008).
30. Gomez-Lamarca, M. J., Snowdon, L. A., Seib, E., Klein, T. & Bray, S. J. Rme-8 depletion perturbs Notch recycling and predisposes to pathogenic signaling. *J. Cell Biol.* **210**, 303–318 (2015).
31. Beer, K. B. *et al.* Extracellular vesicle budding is inhibited by redundant regulators of TAT-5 flippase localization and phospholipid asymmetry. *Proc. Natl. Acad. Sci.* **115**, E1127–E1136 (2018).
32. Harrison, M. S. *et al.* A mechanism for retromer endosomal coat complex assembly with cargo. *Proc. Natl. Acad. Sci. U. S. A.* **111**, 267–72 (2014).
33. Lucas, M. *et al.* Structural Mechanism for Cargo Recognition by the Retromer Complex. *Cell* **167**, 1623-1635.e14 (2016).
34. Burd, C. & Cullen, P. J. Retromer: A Master Conductor of Endosome Sorting. *Cold Spring Harb. Perspect. Biol.* **6**, a016774 (2014).
35. Liu, J.-J. Retromer-Mediated Protein Sorting and Vesicular Trafficking. *J. Genet. Genomics* **43**, 165–177 (2016).
36. Harterink, M. *et al.* A SNX3-dependent retromer pathway mediates retrograde transport of the Wnt sorting receptor Wntless and is required for Wnt secretion. *Nat. Cell Biol.* **13**, 914–923 (2011).
37. Wu, Y., Takar, M., Cuentas-Condori, A. A. & Graham, T. R. Neo1 and phosphatidylethanolamine contribute to vacuole membrane fusion in Saccharomyces cerevisiae. *Cell. Logist.* **6**, e1228791 (2016).
38. Cullen, P. J. & Korswagen, H. C. Sorting nexins provide diversity for retromer-dependent trafficking events. *Nat. Cell Biol.* **14**, 29–37 (2011).
39. Carlton, J. G. & Cullen, P. J. Sorting nexins. *Curr. Biol.* **15**, R819–R820 (2005).
40. van Weering, J. R. T., Verkade, P. & Cullen, P. J. SNX-BAR proteins in phosphoinositide-mediated, tubular-based endosomal sorting. *Seminars in Cell and Developmental Biology* **21**, 371–380 (2010).
41. Kovtun, O. *et al.* Structure of the membrane-assembled retromer coat determined by cryo-electron tomography. *Nature* **561**, 561–564 (2018).
42. Yong, X. *et al.* Expression and purification of the SNX1/SNX6 complex. *Protein Expr. Purif.* **151**, 93–98 (2018).
43. Lu, N., Shen, Q., Mahoney, T. R., Liu, X. & Zhou, Z. Three sorting nexins drive the degradation of apoptotic cells in response to PtdIns(3)P signaling. *Mol. Biol. Cell* **22**, 354–374 (2011).
44. Wassmer, T. *et al.* A loss-of-function screen reveals SNX5 and SNX6 as potential components of the mammalian retromer. *J. Cell Sci.* **120**, 45–54 (2007).
45. Kvainickas, A. *et al.* Cargo-selective SNX-BAR proteins mediate retromer trimer independent retrograde transport. *J. Cell Biol.* **216**, 3677–3693 (2017).
46. Simonetti, B., Danson, C. M., Heesom, K. J. & Cullen, P. J. Sequence-dependent cargo recognition by SNX-BARs mediates retromer-independent transport of CI-MPR. *J. Cell Biol.* **216**, 3695–3712 (2017).
47. Lundmark, R. & Carlsson, S. R. SNX9 - A prelude to vesicle release. *Journal of Cell Science* **122**, 5–11 (2009).
48. Mygind, K. J. *et al.* Sorting nexin 9 (SNX9) regulates levels of the transmembrane ADAM9 at the cell surface. *J. Biol. Chem.* **293**, 8077–8088 (2018).
49. Søreng, K. *et al.* SNX 18 regulates ATG 9A trafficking from recycling endosomes by recruiting Dynamin-2. *EMBO Rep.* **19**, e44837 (2018).
50. Almendinger, J. *et al.* A conserved role for SNX9-family members in the regulation of phagosome maturation during engulfment of apoptotic cells. *PLoS One* **6**, 1–11 (2011).

51. Wang, J. *et al.* Endosomal receptor trafficking: Retromer and beyond. *Traffic* **19**, 578–590 (2018).
52. Steinberg, F., Heesom, K. J., Bass, M. D. & Cullen, P. J. SNX17 protects integrins from degradation by sorting between lysosomal and recycling pathways. *J. Cell Biol.* **197**, 219–230 (2012).
53. Yin, W. *et al.* SNX17 regulates Notch pathway and pancreas development through the retromer-dependent recycling of Jag1. *Cell Regen.* **1**, 1:4 (2012).
54. Zhang, H. *et al.* The retromer complex and sorting nexins in neurodegenerative diseases. *Frontiers in Aging Neuroscience* **10**, 79 (2018).
55. Wehman, A. M., Poggioli, C., Schweinsberg, P., Grant, B. D. & Nance, J. The P4-ATPase TAT-5 inhibits the budding of extracellular vesicles in C. elegans embryos. *Curr. Biol.* **21**, 1951–1959 (2011).
56. Lu, Q. *et al.* C. elegans Rab GTPase 2 is required for the degradation of apoptotic cells. *Development* **135**, 1069–1080 (2008).
57. Cattin-Ortolá, J., Topalidou, I., Dosey, A., Merz, A. J. & Ailion, M. The dense-core vesicle maturation protein CCCP-1 binds RAB-2 and membranes through its C-terminal domain. *Traffic* **18**, 720–732 (2017).
58. Takar, M., Wu, Y. & Graham, T. R. The essential Neo1 protein from budding yeast plays a role in establishing aminophospholipid asymmetry of the plasma membrane. *J. Biol. Chem.* **291**, 15727–15739 (2016).
59. Stafford, J. H. & Thorpe, P. E. Increased exposure of phosphatidylethanolamine on the surface of tumor vascular endothelium. *Neoplasia* **13**, 299–308 (2011).
60. van Engeland, M., Nieland, L. J., Ramaekers, F. C., Schutte, B. & Reutelingsperger, C. P. Annexin V-affinity assay: a review on an apoptosis detection system based on phosphatidylserine exposure. *Cytometry* **31**, 1–9 (1998).
61. Darland-Ransom, M. *et al.* Role of C. elegans TAT-1 Protein in Maintaining Plasma Membrane Phosphatidylserine Asymmetry. *Science (80-.).* **320**, 528–531 (2008).
62. Ruaud, A. F. *et al.* The C. elegans P4-ATPase TAT-1 regulates lysosome biogenesis and endocytosis. *Traffic* **10**, 88–100 (2009).
63. Lucas, M. & Hierro, A. Retromer. *Curr. Biol.* **27**, R687–R689 (2017).
64. Chamberland, J. P. & Ritter, B. Retromer revisited: Evolving roles for retromer in endosomal sorting. *J. Cell Biol.* **216**, 3433–3436 (2017).
65. Wang, Q., Kaan, H. Y. K., Hooda, R. N., Goh, S. L. & Sondermann, H. Structure and Plasticity of Endophilin and Sorting Nexin 9. *Structure* **16**, 1574–1587 (2008).
66. Chen, K. E., Healy, M. D. & Collins, B. M. Towards a molecular understanding of endosomal trafficking by Retromer and Retriever. *Traffic* **20**, 465–478 (2019).
67. Zhang, P., Wu, Y., Belenkaya, T. Y. & Lin, X. SNX3 controls Wingless/Wnt secretion through regulating retromer-dependent recycling of Wntless. *Cell Res.* **21**, 1677–1690 (2011).
68. Lyssenko, N. N., Miteva, Y., Gilroy, S., Hanna-Rose, W. & Schlegel, R. A. An unexpectedly high degree of specialization and a widespread involvement in sterol metabolism among the C. elegans putative aminophospholipid translocases. *BMC Dev. Biol.* **8**, 1–17 (2008).
69. Shafaq-Zadah, M. *et al.* Persistent cell migration and adhesion rely on retrograde transport of β1 integrin. *Nat. Cell Biol.* **18**, 54–64 (2016).
70. Coudreuse, D. Y. M., Roël, G., Betist, M. C., Destrée, O. & Korswagen, H. C. Wnt gradient formation requires retromer function in Wnt-producing cells. *Science* **312**, 921–4 (2006).
71. Kamath, R. S. & Ahringer, J. Genome-wide RNAi screening in Caenorhabditis elegans. *Methods* **30**, 313–321 (2003).
72. Kelley, L. A., Mezulis, S., Yates, C. M., Wass, M. N. & Sternberg, M. J. E. The Phyre2 web portal for protein modeling, prediction and analysis. *Nat. Protoc.* **10**, 845–858 (2015).
73. Simonetti, B. *et al.* Molecular identification of a BAR domain-containing coat complex for endosomal recycling of transmembrane proteins. *Nat. Cell Biol.* **21**, 1219–1233 (2019).
74. Fazeli, G., Trinkwalder, M., Irmisch, L. & Wehman, A. M. C. elegans midbodies are released, phagocytosed and undergo LC3-dependent degradation independent of macroautophagy. *J. Cell Sci.* **129**, 3721–3731 (2016).
75. Wicky, S., Schwarz, H. & Singer-Kruger, B. Molecular Interactions of Yeast Neo1p, an Essential Member of the Drs2 Family of Aminophospholipid Translocases, and Its Role in Membrane

Trafficking within the Endomembrane System. *Mol. Cell. Biol.* **24**, 7402–7418 (2004).

76. Tanaka, Y. *et al.* The phospholipid flippase ATP9A is required for the recycling pathway from the endosomes to the plasma membrane. *Mol. Biol. Cell* **27**, 3883–3893 (2016).
77. Takatsu, H. *et al.* ATP9B, a P4-ATPase (a putative aminophospholipid translocase), localizes to the trans-Golgi network in a CDC50 protein-independent manner. *J. Biol. Chem.* **286**, 38159–38167 (2011).
78. Bean, B. D. M., Davey, M. & Conibear, E. Cargo selectivity of yeast sorting nexins. *Traffic* **18**, 110–122 (2017).
79. Shaul, O. How introns enhance gene expression. *Int. J. Biochem. Cell Biol.* **91**, 145–155 (2017).
80. Causemann, J. Identifying Motifs Involved in the Trafficking of the Essential Lipid Flippase TAT-5 in Caenorhabditis elegans Embryos. *Bachelor Thesis, Univ. Würzbg.* (2019).
81. Ge, L., Zhang, M. & Schekman, R. Phosphatidylinositol 3-kinase and COPII generate LC3 lipidation vesicles from the ER-Golgi intermediate compartment. *Elife* **3**, (2014).
82. Poteryaev, D., Squirrell, J. M., Campbell, J. M., White, J. G. & Spang, A. Involvement of the actin cytoskeleton and homotypic membrane fusion in ER dynamics in Caenorhabditis elegans. *Mol. Biol. Cell* **16**, 2139–2153 (2005).
83. Hadwiger, G., Dour, S., Arur, S., Fox, P. & Nonet, M. L. A monoclonal antibody Toolkit for C. elegans. *PLoS One* **5**, (2010).
84. Murray, J. T., Panaretou, C., Stenmark, H., Miaczynska, M. & Backer, J. M. Role of Rab5 in the Recruitment of hVps34/p150 to the Early Endosome. *Traffic* **3**, 416–427 (2002).
85. Law, F. & Rocheleau, C. E. Vps34 and the Armus/TBC-2 Rab GAPs: Putting the brakes on the endosomal Rab5 and Rab7 GTPases. *Cell. Logist.* **7**, e1403530 (2017).
86. Popoff, V. *et al.* Analysis of articulation between clathrin and retromer in retrograde sorting on early endosomes. *Traffic* **10**, 1868–1880 (2009).
87. Vardarajan, B. N. *et al.* Identification of Alzheimer disease-associated variants in genes that regulate retromer function. *Neurobiol. Aging* **33**, 2231.e15-2231.e30 (2012).
88. Boncompain, G. *et al.* Synchronization of secretory protein traffic in populations of cells. *Nat. Methods* **9**, 493–498 (2012).
89. Steinberg, F. *et al.* A global analysis of SNX27–retromer assembly and cargo specificity reveals a function in glucose and metal ion transport. *Nat. Cell Biol.* **15**, 461–471 (2013).
90. Johannes, L. & Wunder, C. Retromer Sets a Trap for Endosomal Cargo Sorting. *Cell* **167**, 1452–1454 (2016).
91. Timcenko, M. *et al.* Structure and autoregulation of a P4-ATPase lipid flippase. *Nature* **571**, 366–370 (2019).
92. Hiraizumi, M., Yamashita, K., Nishizawa, T. & Nureki, O. Cryo-EM structures capture the transport cycle of the P4-ATPase flippase. *Science.* **365**, 1149–1155 (2019).
93. Guerra, D. D. & Callis, J. Ubiquitin on the move: the ubiquitin modification system plays diverse roles in the regulation of endoplasmic reticulum- and plasma membrane-localized proteins. *Plant Physiol.* **160**, 56–64 (2012).
94. Andersen, J. P. *et al.* P4-ATPases as phospholipid flippases-structure, function, and enigmas. *Front. Physiol.* **7**, 1–23 (2016).
95. Tone, T., Nakayama, K., Takatsu, H. & Shin, H. ATPase reaction cycle of P4-ATPases affects their transport from the endoplasmic reticulum. *FEBS Lett.* 1873-3468.13629 (2019).

5. PAD-1 and MON-2 control TAT-5 localization and activity

5.1. Introduction: TAT-5 orthologs form a complex with PAD-1 and MON-2 orthologs

In yeast and mammals, TAT-5 orthologs form a complex with orthologs of the conserved Dopey-domain protein PAD-1 and the GEF-like protein Mon2[1–3]. In chapter 3, we discovered that PAD-1 inhibits MV release, similar to TAT-5, leading us to hypothesize that PAD-1 could be a regulator of TAT-5. Therefore, we characterize PAD-1 localization and function in this chapter in order to determine how TAT-5 localization and flippase activity are regulated. Furthermore, we speculated that MON-2 could also regulate TAT-5 and/or PAD-1, and we characterize MON-2 localization and function in this chapter as well in order to better understand the role of this complex in endocytic trafficking and microvesicle (MV) budding.

5.1.1. The Dopey domain-containing protein PAD-1

PAD-1 is a large scaffolding protein that belongs to the Dopey leucine zipper-like family. PAD-1 orthologs DopA, Dop1 and DOPEY1/2 are named after their N-terminal Dopey domain[4,5], while PAD-1 is named for its loss of function phenotype, PAtterning Defective. Loss of PAD-1 causes morphogenesis defects, which ultimately lead to embryonic lethality[5]. A temperature sensitive DopA mutant in *Aspergillus nidulans* has similarly important functions during morphogenesis[4]. Like the TAT-5 ortholog Neo1, Dop1 is also an essential gene in yeast, where it is required for normal ER morphology[6]. These findings demonstrate that TAT-5 orthologs and PAD-1 orthologs share essential roles in many species, suggesting that they have common functional roles.

In contrast to the multipass transmembrane protein TAT-5, PAD-1 and orthologs are thought to be cytosolic proteins with conserved N- and C-terminal domains[1,4,5,7]. Although highly conserved, the function of the N-terminal Dopey domain is unknown. The C-terminal part of PAD-1 and orthologs consists of a flexible region and a series of leucine zippers that cannot be modelled into a 3D structure[5,8]. Leucine zippers are known to be involved in protein-protein interaction[9], suggesting that PAD-1 has a scaffolding function, interacting with multiple proteins. In yeast, Dop1 forms dimers in addition to binding to Neo1 and Mon2[2]. Dop1 and Mon2 also bind to the Arf-like small GTPase Arl1[2,10]. Thus, PAD-1 is likely to interact with TAT-5, MON-2, and ARL-1 in *C. elegans*.

If PAD-1 interacts with TAT-5, we would expect PAD-1 to be expressed ubiquitously, since TAT-5 expression is ubiquitous in worms[11]. Indeed, a GFP-tagged 5’ regulatory element of PAD-1 is expressed ubiquitously in adult worms[12]. Thus, the expression patterns of PAD-1 and TAT-5 overlap, consistent with a conserved interaction. PAD-1 orthologs in yeast and mammals reside in endosomes and Golgi[6,13], similar to TAT-5 orthologs in other species. As GFP::TAT-5 is predominantly found on the plasma membrane in *C. elegans*[14], it will be interesting to test whether PAD-1 localizes to the plasma membrane or to endosomes and Golgi. Plasma membrane localization would support the hypothesis that PAD-1 interacts with TAT-5.

The PAD-1 ortholog Dop1 has been shown to have roles in vacuolar and retrograde trafficking. Vacuolar trafficking transports proteins to the vacuole, while retrograde trafficking transports proteins from endosomes back to the Golgi, from which proteins can also be recycled back to the plasma membrane[15,16]. For example, Dop1 is required for the trafficking of a vacuolar hydrolase carboxypeptidase Y (CPY) from Golgi to vacuoles[2], as well as the endosome to Golgi recycling of the v-SNARE Snc1[6]. PAD-1 has also been linked to retrograde trafficking in *C. elegans*. β-catenin cortical localization is controlled by an intracellular phospholipase A_1 (PLA_1), which is required for asymmetric division. In *ipla-1* mutants, the seam cell division plane is disrupted due to altered β-catenin localization[17]. Knock down of *pad-1* suppressed the seam cell phenotype of *ipla-1* mutants, similar to knock down of other retrograde trafficking regulators, including retromer (*vps-26, vps-29, vps-35*) and sorting nexins *snx-1* and *snx-3*[17,18]. This suggests that PAD-1 has functions in endocytic trafficking similar to retromer and sorting nexins. Thus, PAD-1 could be a major regulator of TAT-5 trafficking like SNX-1 and SNX-3 or it could be a minor regulator of TAT-5 trafficking like retromer (discussed in chapter 4). However, it is unclear whether PAD-1 acts in these endocytic trafficking pathways, or forms an independent pathway alongside retromer and sorting nexins.

PAD-1 orthologs are also important to maintain proper organelle size and shape. Both Dop1 and Neo1 mutants have fragmented vacuoles and accumulate tubular structures[6,19,20], suggesting that vacuole fusion is disrupted. In contrast, knock down of Dop1 in *Tetrahymena thermophila* caused enlarged vacuoles[21]. A rat strain with a truncated DOPEY1 has abnormal, enlarged vacuoles in several neural tissues and was therefore named the Vacuole Formation (VF) rat [22]. In *C. elegans*, *tat-5* mutants also have enlarged endolysosomes[14], suggesting that PAD-1 and TAT-5 could have a conserved function regulating the size of endolysosomes together.

The two mammalian PAD-1 orthologs, DOPEY1 and DOPEY2, have important functions in the nervous system. DOPEY1 is highly expressed in rat neurons and oligodendrocytes in the spinal cord, and a premature stop codon in DOPEY1 in the VF rat results in abnormal, enlarged vacuoles in some, but not all neural tissues[22]. This suggests that the function of DOPEY1 may be restricted to specific cells, although it is unknown whether DOPEY2 can compensate for DOPEY1 function in some cells. The VF mutants also have decreased myelination[23], which is proposed to be caused by defective trafficking of myelin components for myelinogenesis[13], based on analogy to the trafficking function of Dop1 in yeast. The VF rat strain has a nonsense mutation at the C-term of DOPEY1 that would truncate the last 142 aa of the 2456 aa sequence, but results in greatly reduced expression of DOPEY1[13], probably due to nonsense-mediated mRNA decay[24]. However, it is unclear whether this premature stop codon completely disrupts DOPEY1 function.

In addition to loss-of-function phenotypes, Dopey family proteins have also been associated with overexpression phenotypes. In humans, DOPEY2 is found on chromosome 21 and its expression was increased in Down syndrome patients with chromosome 21 trisomy[25]. DOPEY2 is expressed early in the developing nervous system in mice embryos[26], but mice overexpressing DOPEY2 have mild cognition defects[7,25]. Thus, it is proposed that overexpression of DOPEY2 may contribute to some of the mental retardation phenotypes of Down syndrome patients. Dopey proteins are also expressed in non-nervous tissues, including DOPEY2 in the heart, liver and intestine[7], suggesting that they may have non-neuronal roles in mammals. In any case, these loss-of-function and overexpression studies demonstrate that PAD-1 orthologs have important functions in the brain.

Thus, Dopey domain-containing proteins have essential roles in many organisms, emphasizing the importance of determining the function of this conserved protein.

5.1.2. The GEF-like protein MON-2

MON-2 is a large, non-essential scaffolding protein that belongs to the BIG family of Arf guanine-nucleotide exchange factors (GEFs), but is not thought to function as a GEF. Mon2 contains the regulatory DCB (dimerization and Cyp5 binding) and HUS (homology upstream of Sec7) domains common in the BIG-family of Arf GEFs[1,6], but lacks the catalytic Sec7 domain[6], which is required for guanine-nucleotide exchange activity[27]. Although Mon2 interacts with the Arf-like GTPase Arl1, it has no GEF activity towards Arl1[6,28,29], leading to the suggestion that it is a GEF-like protein. Mon2 also possesses three additional conserved domains of unknown function[1], which are proposed to be involved in protein binding. Thus, MON-2 is thought to function as a scaffold for bringing proteins together.

Mon2 was originally named Ysl2 in yeast, which stands for *ypt51* synthetic lethal, and was identified in a screen for proteins that have synthetic effects with the endosomal Rab

GTPase *ypt51/vps21* mutants, which display impaired membrane trafficking[30,31]. Later, Mon2 was named after its Monensin sensitivity phenotype, a drug that affects intracellular transport[32]. Like PAD-1 orthologs, MON-2 orthologs in yeast, flies and mammals reside in endosomes and Golgi[1,6,29], where they are involved in many protein trafficking steps. For example, Mon2 was found to be required for the trafficking of the hydrolases CPY and aminopeptidase I (Ape1) from Golgi to the yeast vacuole[1,28,33,34], similar to Dop1. In addition, the localization of the transmembrane protein Mrh1 shifted from the plasma membrane to internal structures in a yeast Mon2 mutant, suggesting that Mon2 is required for the recycling of membrane proteins. Thus, it will be important to test whether MON-2 is required for TAT-5 trafficking.

Mon2 could also regulate organelle size, as vacuoles appear fragmented in a yeast Mon2 mutant [28,33], similar to Dop1 and Neo1 vacuoles[6,19]. Since *tat-5* mutants also display enlarged endolysosomes, it will be interesting to test whether MON-2 also controls endolysosome size in *C. elegans*. This result would support the hypothesis that MON-2 and TAT-5 function together in a complex.

Several studies showed that MON-2 orthologs are required for the retrograde trafficking of proteins. The endosome to Golgi recycling of the v-SNARE Snc1 is disrupted after loss of Mon2, similar to Dop1[1,6]. In *C. elegans,* a *mon-2(xh22)* nonsense mutant was identified in a screen for *ipla-1* suppressors; *mon-2* mutants suppressed the seam cell division defects caused by *ipla-1* mutants, similar to *pad-1,* retromer and sorting nexins[17]. The *mon-2(xh22)* mutant bears a premature stop codon in the middle of the protein at W^{787} that would result in loss of the C-terminus[17], which is essential for yeast Mon2 function[1,17]. Knock down of *mon*-2 also altered the localization of MIG-14/Wntless[35], which is recycled via the retrograde pathway by the activities of retromer and sorting nexins[36–38]. This suggests that MON-2 has retrograde trafficking functions like retromer and sorting nexins. However, it remains unclear whether MON-2 would act in conjunction with retromer and sorting nexins or whether it acts independent in a separate trafficking pathway.

Mon2 is thought to be involved in regulating vesicle formation during endocytic trafficking by interacting with the actin cytoskeleton and coat proteins. In *Drosophila*, Mon2 interacts with the actin nucleators Cappuccino (Capu) and Spire (Spir) and is required for the formation of F-actin projections, suggesting that Mon2 is required for actin dynamics. Actin dynamics are important to cluster cargo on endosomal membranes and to induce endosomal membrane tubulation, tubule fission and transport of trafficking vesicles[39]. Furthermore, in yeast and human cell culture, Mon2 was required for the recruitment of the clathrin adaptors Gga1 and Gga2, which localize to endosomal tubules and the TGN[40]. However, it is not clear whether MON-2 is required for recycling endosome tubulation or whether it controls endocytic trafficking through different mechanisms.

Interestingly, human Mon2 was previously reported to be required for HIV budding[41]. HIV can bud from the plasma membrane by recruiting the ESCRT complex via interaction of the viral Gag protein with Tsg101 (ESCRT-I)[42]. As ESCRT-dependent budding is also used to release MVs from *tat-5* mutants[14], this raises the possibility that MON-2 could be required for MV budding. However, Gag-induced HIV release was decreased in Mon2 mutants due to reduced plasma membrane recruitment of Gag[41], which could suggest that Mon2 promotes the intracellular trafficking of Gag rather than MV release. Thus, it needs to be tested whether MON-2 could have the same or opposite function on MV release than TAT-5 and PAD-1.

As MON-2 proteins have trafficking functions in different organisms, it is likely that its functions are conserved in worms and other organisms. Identifying how MON-2 regulates TAT-5 localization or activity will provide further insight into the mechanisms of endocytic trafficking. Furthermore, it may reveal new insights into the release of MVs.

5.2. Results: PAD-1 and MON-2 have separable roles in regulating TAT-5

Here, we demonstrate that PAD-1 and MON-2 localize to the plasma membrane, where they could interact with TAT-5. We find that they do not normally traffic TAT-5. Instead, PAD-1 and MON-2 only impact TAT-5 recycling in the absence of the major TAT-5 trafficking pathways discussed in chapter 4, namely SNX-1/-6 and SNX-3. We also discovered that PAD-1 is required to maintain PE asymmetry, while MON-2 is not, suggesting that PAD-1 specifically activates TAT-5 flippase activity.

5.2.1. PAD-1 inhibits microvesicle release, but MON-2 and ARL-1 do not

As PAD-1 is required to inhibit microvesicle release (chapter 3, Fig.7), we tested whether MV release was altered in *mon-2* mutants. We did not find increased EV release after *mon-2* RNAi in our screen looking for EV inhibitors using ZF1-degron tagged PH plasma membrane reporters in chapter 3, but wanted to confirm this was not due to partial knockdown. After crossing the untagged PH plasma membrane reporter into the *mon-2* mutant background, we found that *mon-2* nonsense mutants do not show bright membrane patches indicative of increased MV release (Fig. 15A, Table 1), even when additionally treated with *mon-2* RNAi (Table 1). This demonstrates that MON-2 is not required to inhibit MV release. Consistently, *mon2/mon-2* mutants are viable in yeast and worms[6,17], in contrast to lethal *dop1/pad-1* and *neo1/tat-5* mutants[5,6,11,43], showing that MON-2 has distinct roles from PAD-1 and TAT-5.

As human Mon2 is required for HIV budding from the plasma membrane[41], we also considered whether MON-2 could act in opposition to TAT-5 and PAD-1 and be an inducer of MV budding. However, *pad-1* RNAi still caused MV release in *mon-2* mutants (Table 1), showing that MON-2 is not required for MV release. Together, these data suggest that MON-2 does not directly promote or inhibit MV release. However, this could also indicate that PAD-1 acts downstream of MON-2. Thus, it would be necessary to test whether MON-2 can promote MV release using a PAD-1-independent assay to completely rule out a role for MON-2 in regulating MV release.

The Arl1 GTPase has also been shown to be part of the Neo1p/Dop1p/Mon2p complex in yeast[2,10]. In one initial experiment, we depleted ARL-1 in *C. elegans* embryos expressing the GFP::ZF1::PH reporter, but saw no membrane thickenings indicative of increased EV release after *arl-1* RNAi (Table 1). Thus, ARL-1 is also unlikely to regulate MV release.

Genotype	**RNAi**	**Increased MV release (thick membranes)**	
		%	**n**
+	-	0%	119
	tat-5	90%	31
	pad-1	89%	55
	mon-2	0%	72
	arl-1 [i]	0%	20
pad-1(wur02)	-	100%	11
mon-2(xh22)	-	0%	105
	mon-2	0%	270
	pad-1	76%	78

Table 1: MON-2 and ARL-1 do not inhibit MV release. Control (+) and mutant worms expressing fluorescent PH reporters were treated with RNAi or untreated (-). The percentage of embryos showing the indicated phenotype is given. Embryos (n) from the late 4-cell to 102-cell stage were scored for thickened membrane labeling between cells, which is indicative of MV release. [i] indicates experiments that were only performed once.

5.2.2. Loss of PAD-1 causes sterility

In addition to embryonic lethality, *tat-5* deletion mutants are sterile[14], while *mon-2* nonsense mutants are fertile[17]. As MV release in *pad-1* and *tat-5* RNAi-treated embryos disrupts morphogenesis, we wondered whether MV release in gonads could cause sterility. Therefore, we first tested whether *pad-1* mutants are sterile. We generated two *pad-1* deletion alleles removing 99.5% of the *pad-1* coding sequence by using CRISPR/Cas9 to create double-strand breaks near the start and stop codons of *pad-1* (Fig. 1A-B). For *pad-1(wur02)*, a 23.6 kb deletion and 21 bp insertion was achieved. Thus, only 4 aa of the N-term, 7 aa of new sequence, and 9 aa of the C-term are predicted to remain of the 2417 aa PAD-1 protein. The *pad-1(wur03)* allele has a 23.3 kb deletion verified by sequencing, including 238 bp of the last intron and the complete last exon of *pad-1* remaining. The shorter deletion in *wur03* is probably due to partial repair[44]. The *wur03* deletion keeps the first 5 aa of the N-term, but translation of the intronic sequence would be predicted to terminate after 30 aa. Thus, even if a truncated protein were expressed in either allele, it would be unlikely to bear any PAD-1 functions. Therefore, we predict that both *wur02* and *wur03* would be null alleles. Both the *pad-1(wur02)* and *pad-1(wur03)* mutant worms were largely sterile (Table 2), with rare fertile *pad-1* deletion worms laying round eggs that were embryonic lethal, similar to *tat-5* deletion mutants[14].

As these large deletions could possibly alter neighboring genes, we also generated more subtle mutations in *pad-1*. Using CRISPR/Cas9 to target sequence near the start codon, we created several indels in the first exon prior to the conserved Dopey domain (Fig. 1C). Seven out of eight strains with in-frame indels were viable (Table 2), suggesting that changes to the protein sequence can be tolerated at the extreme N-terminus of PAD-1. All five out-of-frame indels caused premature stop codons and resulted in sterility similar to the two large *pad-1* deletion mutants (Table 2). The sterile in-frame insertion in *wur07* changed the fifth amino acid from a serine to a stop codon, creating a nonsense mutant. Thus, *pad-1* nonsense and deletion mutants are sterile, which suggests a function for PAD-1 in gonads.

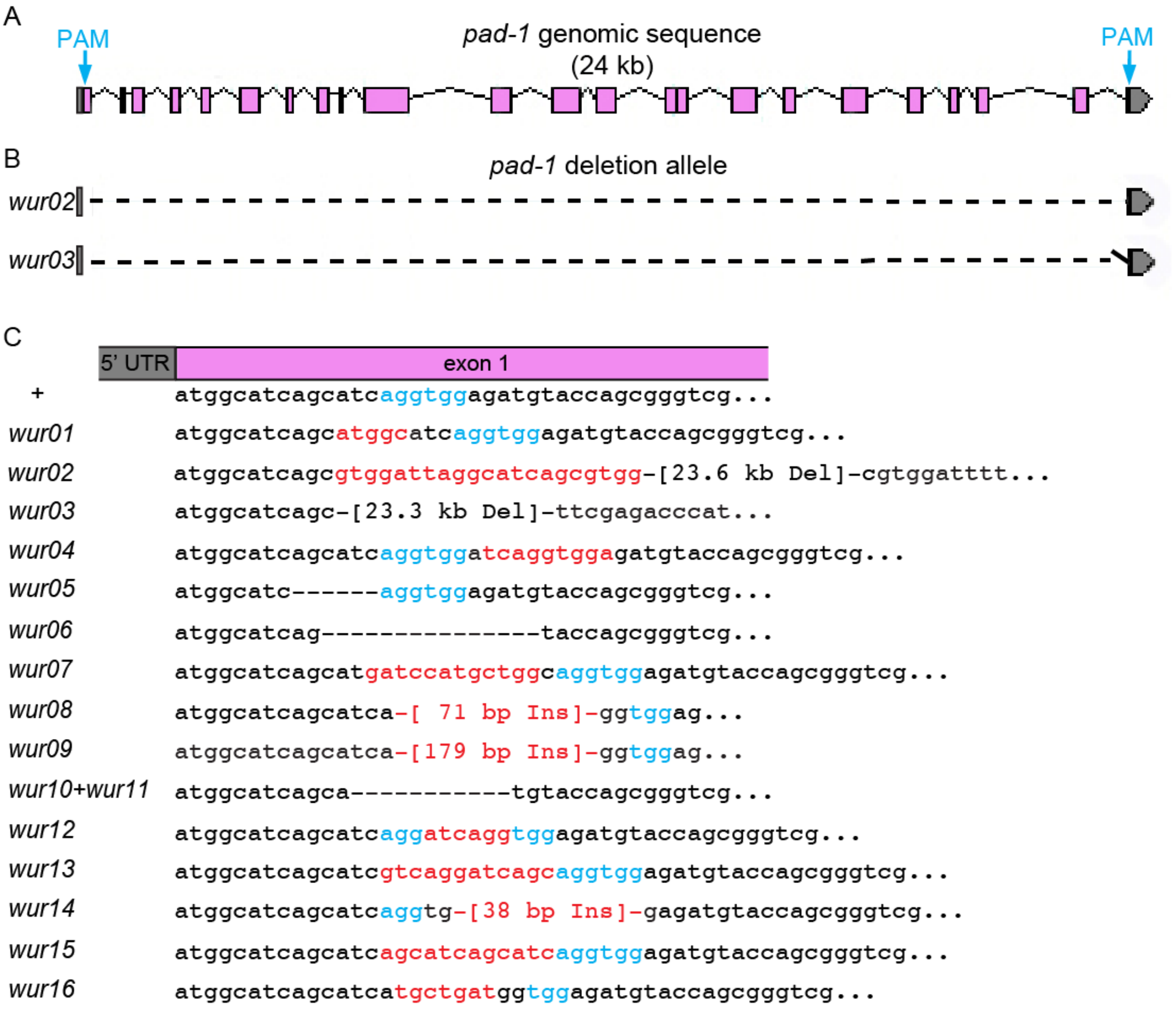
A
PAM
pad-1 genomic sequence
(24 kb)
PAM
B
pad-1 deletion allele
wur02
wur03
C
5' UTR
exon 1
+ atggcatcagcatcaggtggagatgtaccagcgggtcg...
wur01 atggcatcagcatggcatcaggtggagatgtaccagcgggtcg...
wur02 atggcatcagcgtggattaggcatcagcgtgg-[23.6 kb Del]-cgtggatttt...
wur03 atggcatcagc-[23.3 kb Del]-ttcgagacccat...
wur04 atggcatcagcatcaggtggatcaggtggagatgtaccagcgggtcg...
wur05 atggcatc------aggtggagatgtaccagcgggtcg...
wur06 atggcatcag---------------taccagcgggtcg...
wur07 atggcatcagcatgatccatgctggcaggtggagatgtaccagcgggtcg...
wur08 atggcatcagcatca-[71 bp Ins]-ggtggag...
wur09 atggcatcagcatca-[179 bp Ins]-ggtggag...
wur10+wur11 atggcatcagca-----------tgtaccagcgggtcg...
wur12 atggcatcagcatcaggatcaggtggagatgtaccagcgggtcg...
wur13 atggcatcagcatcgtcaggatcagcaggtggagatgtaccagcgggtcg...
wur14 atggcatcagcatcaggtg-[38 bp Ins]-gagatgtaccagcgggtcg...
wur15 atggcatcagcatcagcatcagcatcaggtggagatgtaccagcgggtcg...
wur16 atggcatcagcatcatgctgatggtggagatgtaccagcgggtcg...

Fig. 1: Sequences of *pad-1* indel mutants: A) Genomic sequence of *pad-1* according to WormBase[45]. Pink: exons, Cyan: PAM sites recognized by the Cas9 enzyme using start and stop guide RNAs, grey: untranslated regions, lines represent introns. B) We achieved a 23.6 kb deletion of *pad-1* in *wur02* and a 23.3 kb deletion in *wur03* (dotted lines) using CRISPR/Cas9. C) Genomic sequence of the first exon of *pad-1* from wild type N2 worms (+), *pad-1* deletion mutants and all N-terminal *pad-1* mutant alleles. *wur01-03* were generated by injecting sgRNAs for both start and stop PAM sites. *wur04-wur16* were only injected with sgRNA targeting the double PAM near the start site (cyan). Inserted base pairs are marked in red, numbers of inserted base pairs are given for long insertions.

Allele	Mutation	Amino acid code	Phenotype
+	-	MASASGGDVPA…	WT
wur01	6 bp ins	MASA**MA**SGGDVPA…	WT
wur02	23.6 kb del 21 bp ins	MASA**WIRHQRG**VDFSEHLQF*	Ste
wur03	23.3 kb del	MASAS*RPIRVIPCAFRKKIKEKVFFVEKLVKKPEN**	Ste
wur04	9 bp ins	MASA**SGG**SGGDVPA…	WT
wur05	6 bp del	MAS--GGDVPA…	WT
wur06	15 bp del	MAS-----VPA…	WT
wur07	12 bp ins	MASA***SMLA**GGDVPA… (* at AA 5)	Ste
wur08	71 bp ins of mKate2	MASAS**[24AA of mKate2]KVK***VEMY*… (* at AA 54)	Ste
wur09	179 bp ins of mKate2	MASAS**[59AA of mKate2]R***VEMY*… (* at AA 90)	Ste
wur10/11	11 bp del	MASA**CTSGSRKR***… (* at AA 13)	Ste
wur12	6 bp ins	MASASG**SG**GDVPA…	WT
wur13	12 bp ins	MASAS**SGSA**GGDVPA…	WT
wur14	38 bp ins	MASASG**VRCHQVSGVRHQV***EMY*… (* at AA 43)	Ste
wur15	12 bp ins	MASAS**ASAS**GGDVPA…	WT
wur16	7 bp ins	MASAS**C*W***WRC*... (* at AA 7)	Ste

Table 2: Resulting PAD-1 alleles created using CRISPR/Cas9. The resulting amino acid sequence from *pad-1* mutations in the first exon are listed. The length of insertions (ins) and deletions (del) are indicated in base pairs (bp) or kilobases (kb). Single letter amino acid code of wild type (+) and each mutant (*wur#*) is given. Changed and inserted amino acids are written in bold. (–) stands for one deleted amino acid. * indicates premature stop codons. Italicized letters represent out of frame *pad-1* sequences that are not part of the inserted sequence. Adult wild type worms and mutants with in-frame base pair mutations were viable and fertile (WT). Mutant worms with out-of-frame mutations and premature stop codons had no progeny (Ste).

We next observed how gonad morphology was disrupted in sterile *tat-5* and *pad-1* mutants. In *C. elegans* hermaphrodites, the gonad forms an ovotestis which produces both oocytes and sperm[46]. The wild type gonad is U-shaped, beginning at the distal tip cell (DTC) and extending as a syncytium for almost half the length of the worm (Fig. 2A). After the gonad turns in adult worms, oocytes increase in size and cellularize to become completely surrounded by individual cell membranes in the proximal gonad. We discovered that both *tat-5* and *pad-1* deletion mutants have malformed and shortened gonads (Fig. 2B-C). The distal and proximal gonad, as well as the gonadal turn, are present, suggesting that gonad formation is not generally blocked. Most prominently, we noticed that oocytes were rarely observed in the proximal gonad of *pad-1* and *tat-5* mutants, suggesting that defects in oogenesis were responsible for sterility.

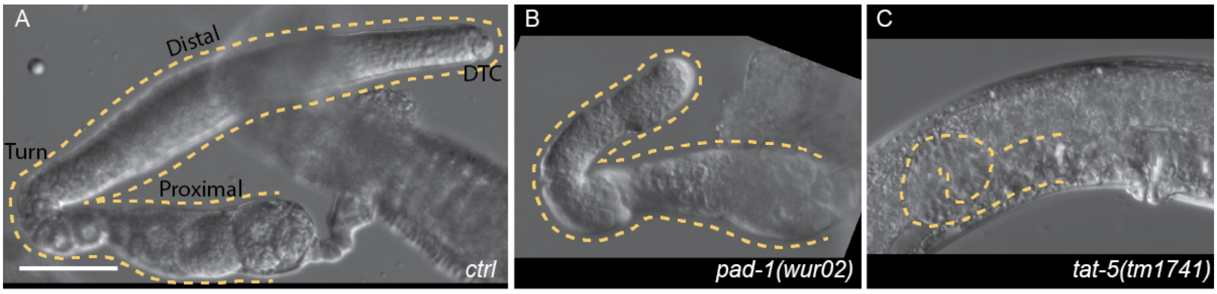

Fig. 2: Altered gonad morphology in MV-releasing *tat-5* and *pad-1* mutants. A) The dissected germline of wild type worms consists of a distal part starting with the Distal Tip Cell (DTC), the gonad turn and the proximal part of the gonad that contains a line of growing oocytes (n=54). B) The dissected germline of *pad-1* mutants contains a shortened distal and proximal part. No oocytes can be recognized (n=13). C) Similar to *pad-1* mutants, *tat-5* mutant gonads are short and no oocytes can be recognized in an adult worm (n=8). Scale Bar: 50 µm.

Given the lack of oocytes, we wondered whether *pad-1* mutants would also have a defect in spermatogenesis. Using electron microscopy on whole worm sections from *pad-1* deletion mutants, we could identify primary spermatocytes by the presence of the sperm-specific membranous organelles (MO) consisting of a fibrous body (FB) surrounded by a phagophore-like membrane [47]. The membranous organelles appeared normal in *pad-1* mutant micrographs (Fig. 3B), although the extracellular milieu appeared full of organelles, which could be EVs or could be caused by cells losing plasma membrane integrity. Thus, PAD-1 appears not to be required for early steps of spermatogenesis.

As plasma membrane remodeling plays a crucial role in both oogenesis and spermatogenesis [48], we wondered whether the small gonad phenotype correlates with increased

MV release in the germline. Using electron microscopy, we discovered EV accumulation between distal germ cells (Fig. 3A,A’), suggesting increased EV release from immature germ cells in the gonad. This suggests that TAT-5 and PAD-1 may also be required for gonad morphology by inhibiting membrane budding.

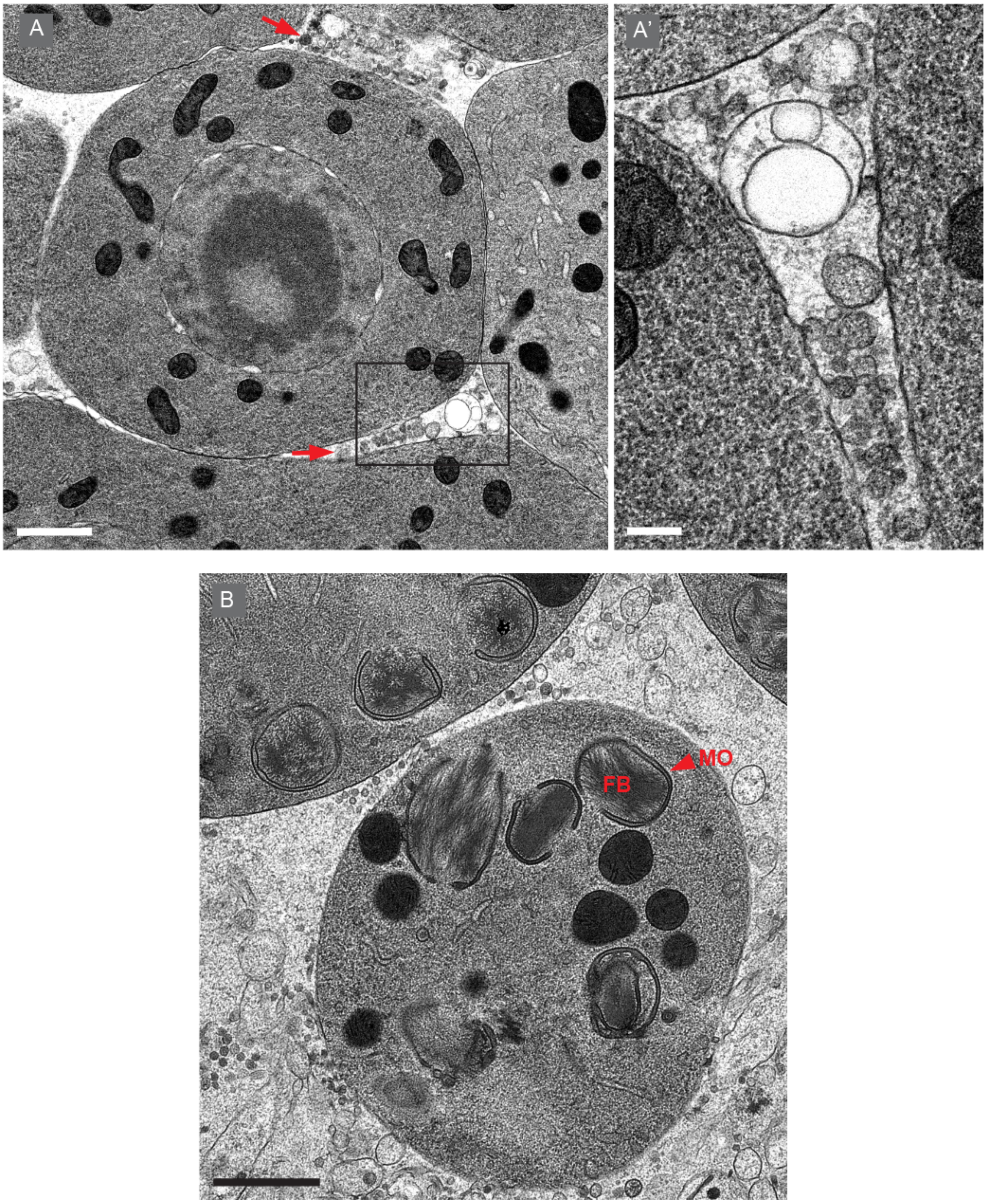

Fig. 3: Loss of PAD-1 causes increased EV release from gonads: A) Electron micrograph of the distal germ line from a *pad-1* mutant. Numerous EVs (arrow) accumulate between germ cells. Scale Bar: 1 μm. A') Magnification of boxed region with EVs in A, 90° rotated. Scale bar: 200 nm. B) Spermatocyte in a *pad-1* mutant with Membranous Organelles (MO), identifiable as Fibrous Bodies (FB) surrounded by phagophore-like membranes. The spermatocytes are surrounded by numerous vesicular structures, which could be EVs or organelles from cells that lost membrane integrity. Scale bar: 1 μm.

5.2.3. Generating peptide antibodies to analyze endogenous PAD-1 localization

To understand the function of PAD-1 in *C. elegans*, we first wanted to see in which cellular compartments PAD-1 localizes. In yeast and mammals, PAD-1 and TAT-5 orthologs localize to the same subcellular compartments, the TGN and the endosomal network[2,3,10,49]. However, TAT-5 predominantly localizes to the plasma membrane in *C. elegans* embryos[14,50]. To check whether PAD-1 could interact with TAT-5, we developed tools to test whether PAD-1 also localizes to the plasma membrane.

To visualize endogenous PAD-1 localization in *C. elegans*, we designed and ordered two peptides in the N-terminus (starting with GRE or AKF) and three peptides in the C-terminus (LAE, DKT, RDA) for immunization in two rabbits each by Davids Biotechnology. Full sequences of the peptides are available in Methods (chapter 2 Table 7). The test serum was screened using immunostaining of fixed embryos. We found various staining patterns in addition to the cytoplasmic background staining of the secondary antibody (Table 3, Chapter 4 Table 2). In particular, three antibodies targeting the C-terminus localized to the plasma membrane (LAE2, DKT2, RDA2) (Table 3), giving us hope that they could recognize PAD-1.

After affinity purification, immunostaining was performed again to check for plasma membrane localization. The LAE2 and RDA2 antibodies lost the previous cell membrane staining (Table 3), while DKT2 maintained plasma membrane staining and also localized to cytosolic vesicles (Fig. 4A), appearing similar to GFP::TAT-5 (Chapter 4 Fig. 3A). Surprisingly, the purified AKF1 antibodies also started weakly staining the plasma membrane (Fig. 4C), which was not observed with the test serum (Table 3). In contrast, AKF2 continued to stain the nuclear membrane (Fig. 4E), which was also sometimes observed with AKF1 (Table 3). Thus, in contrast to TAT-5 peptide antibodies, which lost all protein binding after purification (chapter 4 Fig. 1C), the PAD-1 antibodies retained specific membrane staining after affinity purification.

To test whether the affinity-purified DKT2, AKF1 or AKF2 membrane staining was specific to PAD-1, we depleted PAD-1 using RNAi treatment. Neither the plasma membrane staining nor the nuclear membrane staining were lost after *pad-1* RNAi (Fig. 4B, D, F). Consistent with loss of *pad-1* causing increased MV release, we observed increased membrane labeling with the DKT2 antibody (Fig. 4B). We also confirmed successful *pad-1* depletion by scoring for embryo lethality. Thus, it is unlikely that these peptide antibodies recognize PAD-1, suggesting efficient binding to other proteins than PAD-1.

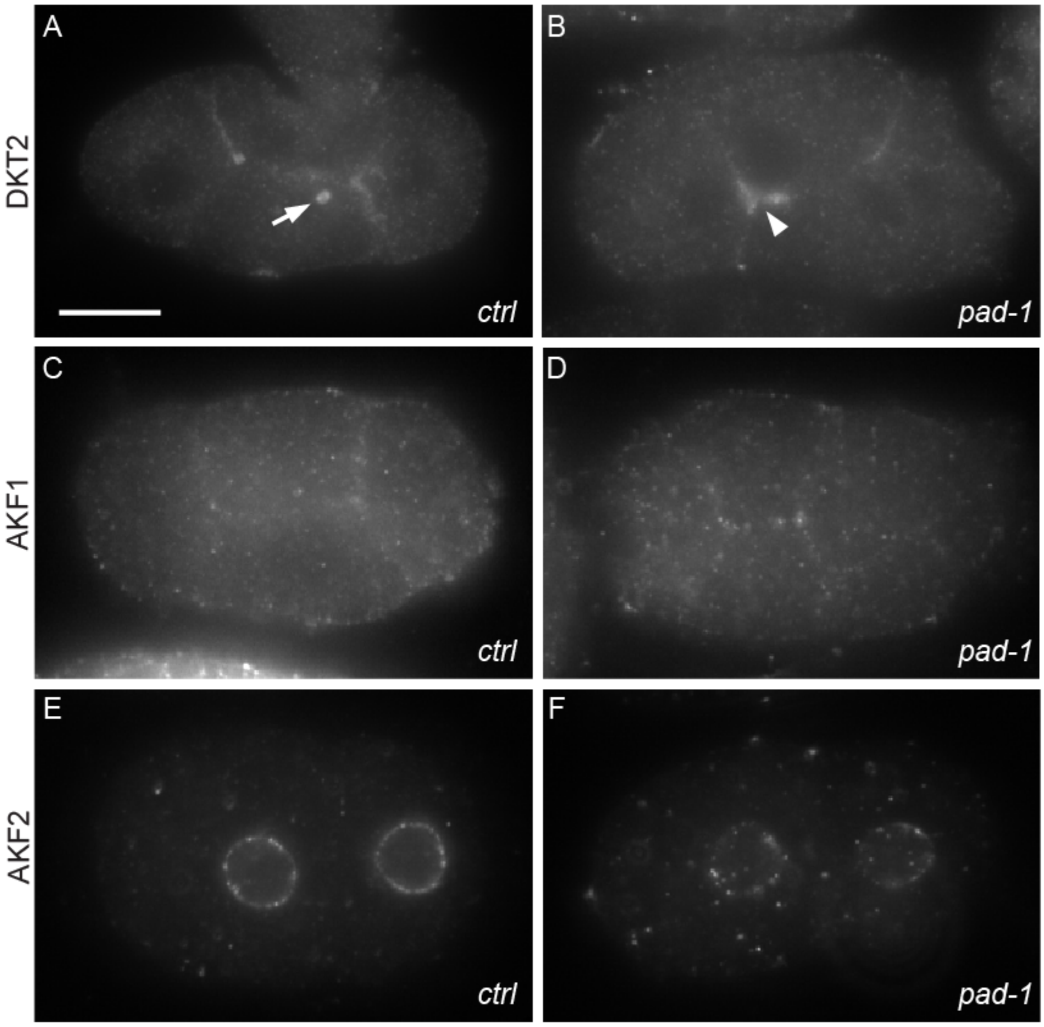

Fig. 4: Purified PAD-1 peptide antibodies do not specifically stain PAD-1. Immunostaining of fixed C. elegans embryos with PAD-1 peptide antibodies derived from affinity-purified serum. A) In a control 4-cell embryo, the DKT2 antibody stains the plasma membrane and intracellular vesicles (arrow). B) After *pad-1* depletion, the DKT2 antibody still stains the plasma membrane of a 4-cell embryo, suggesting that the DKT2 antibody does not specifically recognize PAD-1. Arrowhead points to thickened membranes indicative of increased MV release as a result of successful *pad-1* depletion. C) In a control 4-cell embryo, the AKF1 antibody stains puncta along the plasma membrane. D) The plasma

membrane staining of AKF1 is maintained in a 6-cell embryo after *pad-1* depletion, suggesting that AKF1 does not specifically recognize PAD-1. E) The AKF2 antibody stains the nuclear membrane in a 2-cell control embryo. F) After *pad-1* RNAi, the AKF2 antibody still stains the nuclear membrane, suggesting that the AKF2 antibody does not specifically recognize PAD-1. Scale bar: 10 µm.

Peptide	**Serum**	**Localization**				
		Egg shell	**Plasma membrane**	**Nuclear membrane**	**Centrosomes**	**P-granules**
GRE1	Test	X	-	-	X	-
	Purified	X	-	-	-	-
GRE2	Test	X	-	-	X	-
	Purified	X	-	-	-	-
AKF1	Test	X	-	X	X	-
	Purified	X	X	X	-	-
AKF2	Test	X	-	X	X	-
	Purified	-	-	X	-	-
LAE1	Test	X	-	X	X	X
	Purified	-	-	-	-	-
LAE2	Test	X	X	X	X	-
	Purified	X	-	-	-	-
DKT1	Test	X	-	X	X	-
	Purified	-	-	-	X	-
DKT2	Test	X	X	-	X	-
	Purified	-	X	-	-	-
RDA1	Test	X	-	-	X	-
	Purified	X	-	-	-	-
RDA2	Test	X	X	X	X	-
	Purified	X	-	-	-	-

Table 3: PAD-1 peptide antibody localization in embryos after IHC. The name of the peptide and the localization of the antibodies derived from the unpurified test serum or the affinity-purified serum are indicated. All antibodies bound to centrosomes in the test serum, as well as other locations. After affinity purification, almost all staining was gone, except for the cell membrane staining of DKT2 and AKF1 antibodies, the centrosome staining of DKT1 antibody and the nuclear membrane localization of AKF2 antibody. Indicated are observed (X) and not observed (-) localizations.

We wondered whether these PAD-1 peptide antibodies would work better in reducing-conditions, because secondary structure could hamper antibody binding to the peptides. Therefore, we performed a western blot using worm protein extracts. To do so, we first needed a positive control to compare to the band sizes of the peptide antibodies. Therefore, we inserted EGFP into the N-terminus of PAD-1 using CRISPR/Cas9. In this worm strain, the ATG of *pad-1* was replaced by the sequence of GFP, allowing us to determine whether the tagged protein was still functional. In contrast to sterile *pad-1* deletion and nonsense mutants (Fig. 1, Table 2), GFP::PAD-1 worms are viable and fertile, showing that GFP insertion at the N-term did not disrupt the essential functions of PAD-1. Therefore, we could use an anti-GFP antibody in combination with GFP::PAD-1 worm extracts to test the peptide antibodies.

To disrupt disulfide bonds that could lead to secondary structure, extracts from GFP::PAD-1 worms were boiled and treated with β-mercaptoethanol. The GFP antibody showed one band above the 250 kD protein ladder, consistent with 32 kD of GFP bound to the estimated 267 kD band of PAD-1 (Fig. 5A-B). In contrast, multiple bands at different sizes were detected with the affinity-purified peptide antibodies, suggesting that none of the peptide antibodies specifically bind to PAD-1. However, RDA1 and RDA2 showed a slightly higher band (Fig. 5A-B), while GRE2 showed a slightly lower band than GFP::PAD-1 (Fig. 5B). Therefore, we tested whether these antibodies could bind PAD-1 by depleting *pad-1* using RNAi. The embryonic lethality phenotype was again used to verify successful *pad-1* depletion. Although GFP::PAD-1 levels were strongly reduced based on anti-GFP staining (Fig. 5D), none of the bands of the PAD-1 peptide antibodies were decreased (Fig. 5C). In fact, only the bands from control worms had slightly less RDA1 antibody staining. After repeating the RDA1 western blot, there was no difference between *pad-1* RNAi and control (Fig. 5D). Thus, none of the peptide antibodies recognized GFP::PAD-1 and they cannot be used to stain endogenous PAD-1 protein.

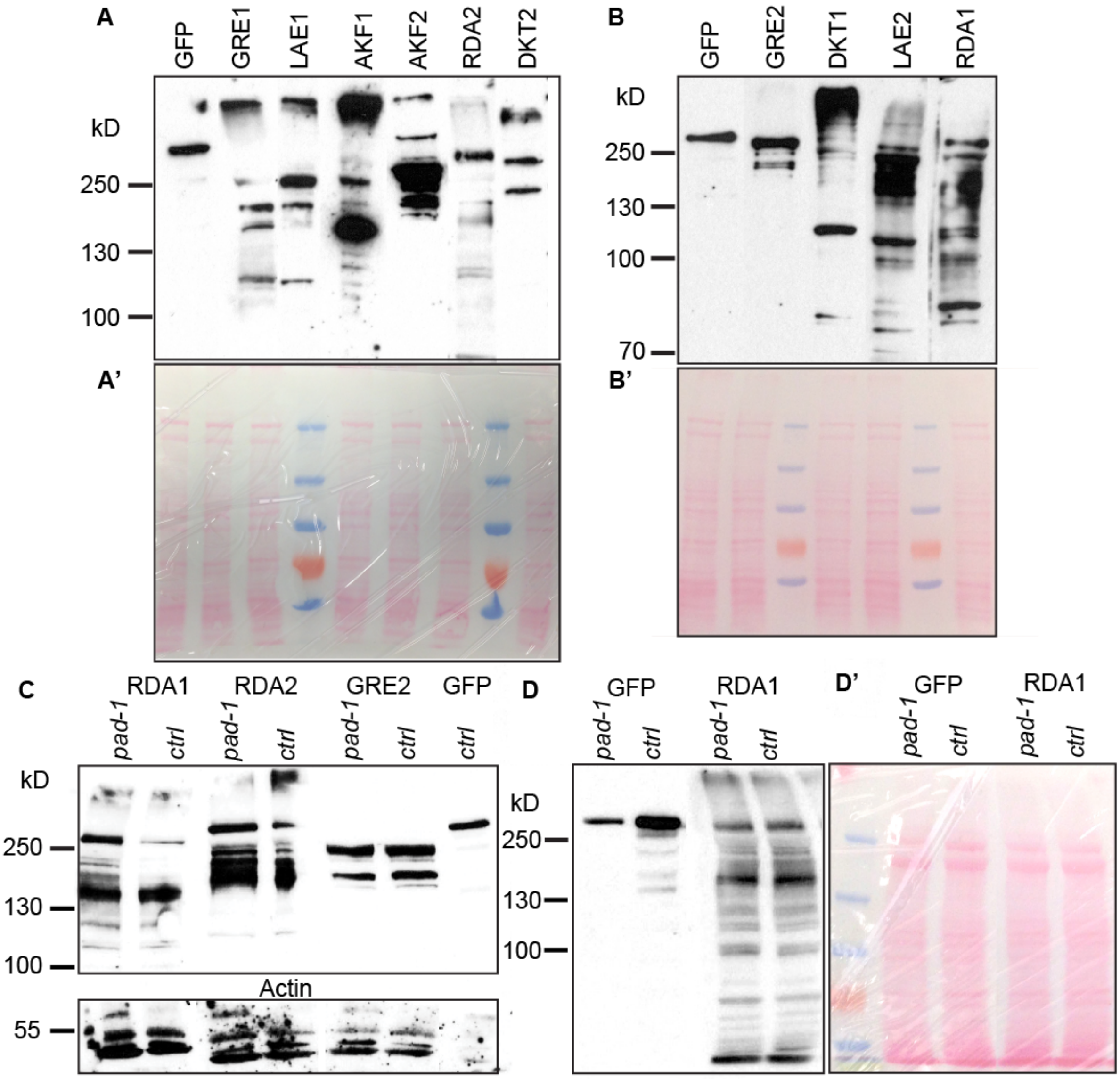
A
GFP
GRE1
LAE1
AKF1
AKF2
RDA2
DKT2
kD
250
130
100
A'
B
GFP
GRE2
DKT1
LAE2
RDA1
kD
250
130
100
70
B'
C
RDA1
RDA2
GRE2
GFP
pad-1
ctrl
pad-1
ctrl
pad-1
ctrl
ctrl
kD
250
130
100
Actin
55
D
GFP
RDA1
pad-1
ctrl
pad-1
ctrl
kD
250
130
100
D'
GFP
RDA1
pad-1
ctrl
pad-1
ctrl

Fig. 5: Purified PAD-1 peptide antibodies do not recognize PAD-1. A) Western blot from protein extracts of GFP::PAD-1 worms stained for GFP and six affinity-purified PAD-1 peptide antibodies. Only RDA2 showed a band near the size of GFP::PAD-1. A') Ponceau staining of the blot used for antibody staining in A. B) Western blot from protein extracts of GFP::PAD-1 worms stained for GFP and five additional PAD-1 peptide antibodies. RDA1 and GRE2 show a band at a similar height as GFP::PAD-1. B') Ponceau staining of the blot used for antibody staining in B. C) Extracts from GFP::PAD-1 worms treated with either control (*ctrl*) or *pad-1* RNAi and stained with PAD-1 peptide antibodies. None of the bands from the peptide antibodies were reduced after *pad-1* RNAi, suggesting no specific recognition of PAD-1. Below is the blot from the same samples strained with actin antibody. D) Western blot with GFP::PAD-1 worm extracts after *pad-1* or control RNAi. GFP::PAD-1 levels are reduced after *pad-1* RNAi, as detected with the GFP antibody. Repeating RDA1 staining showed identical staining in both *pad-1* and control RNAi, indicating no specificity for PAD-1. D') Ponceau staining of the blot used for antibody staining in D.

5.2.4. PAD-1 and MON-2 localize to domains of the plasma membrane

As there are no PAD-1 antibodies available, we used the GFP-tagged PAD-1 reporter strain to check whether PAD-1 localizes to the plasma membrane like TAT-5. We first observed GFP::PAD-1 localization in adult worms. GFP::PAD-1 expression *in vivo* was only dimly visible in the excretory system, which is required for osmotic regulation and waste secretion[51,52], similar to the renal system in vertebrates. Thus, PAD-1 could have important functions in the excretory system.

To better visualize the localization of GFP::PAD-1, we stained adult worms with an antibody for GFP. GFP::PAD-1 was brightly stained along the plasma membrane in the H-shaped excretory canal cell (EC), which spans the whole length of the worm, and in the fused pair of excretory gland cells (EG) (Fig. 6A, C). Similar to Dopey1 and Dopey2 expression in mammalian nerve cells[13,25], GFP::PAD-1 was also found on the nerve ring, a large collection of nerve cells surrounding the pharynx (Fig. 6B), as well as on vesicular structures in the intestine (Fig. 6C) and in the gonad (Fig. 6D). Thus, PAD-1 is expressed in many tissues, suggesting that PAD-1 has a general function in cells.

We next examined the subcellular localization of PAD-1. In oocytes, GFP::PAD-1 localized to cortical granules(Fig. 6D), which secrete the egg shell after fertilization[53]. Additionally, we found GFP::PAD-1 on the plasma membrane (Fig. 6D) of oocytes. Interestingly, GFP::TAT-5 expressed from a germ line promotor also localized to cortical granules and oocyte plasma membranes (Fig. 6E), showing that PAD-1 and TAT-5 localize to the same structures in oocytes. These data are consistent with PAD-1 and TAT-5 interacting in *C. elegans*.

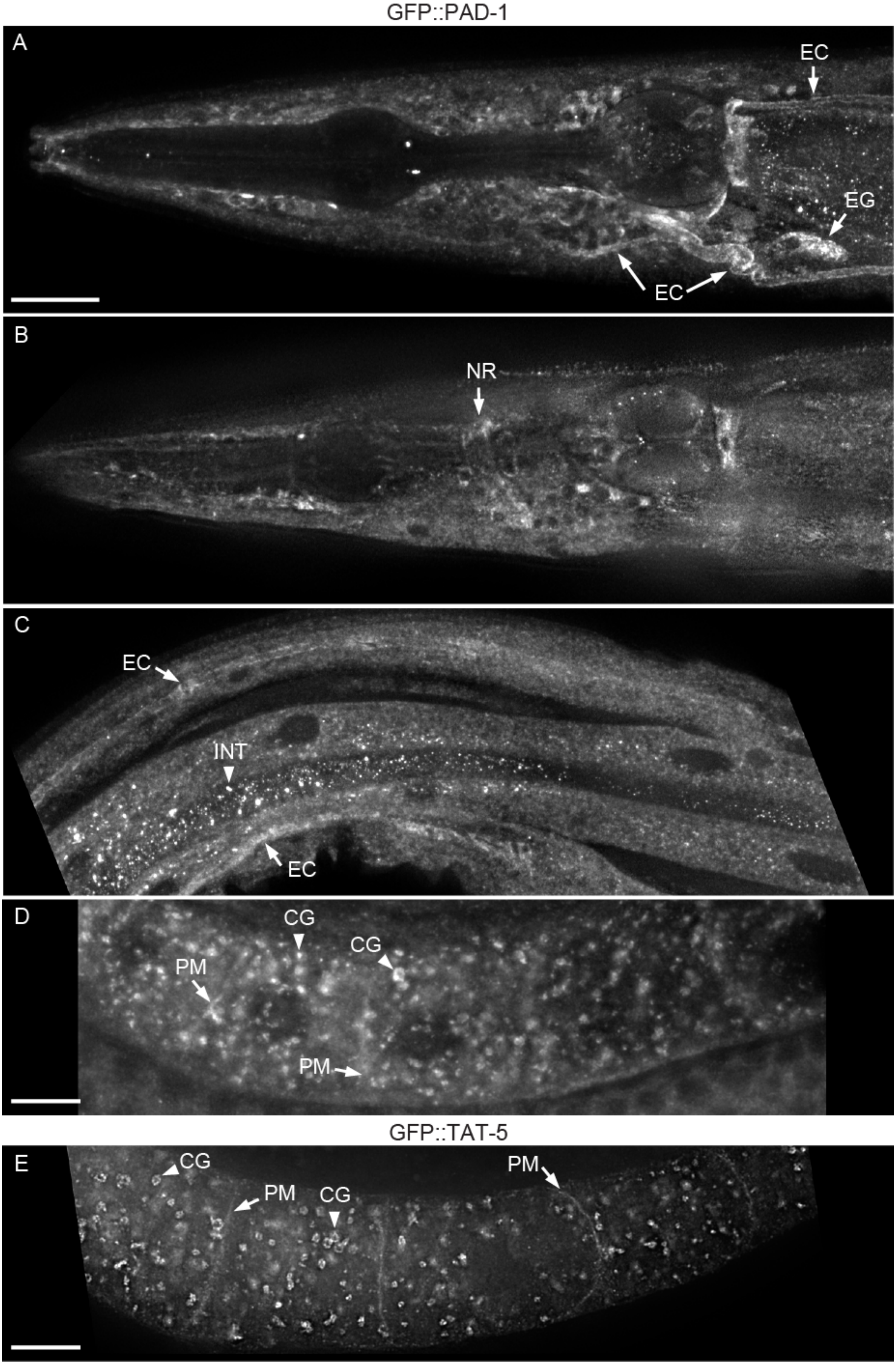
GFP::PAD-1
A
EC
EG
EC
B
NR
C
EC
INT
EC
D
CG
CG
PM
PM
GFP::TAT-5
E
CG
PM
CG
PM

Fig. 6: GFP::PAD-1 localizes to various tissues in adult *C. elegans* worms: A-E) Adult *C. elegans* worm with GFP knocked into the *pad-1* locus was stained for GFP. A) GFP::PAD-1 is expressed in the excretory gland (EG) and the H-shaped excretory canal cell (EC). B) GFP::PAD-1 is found on cells of the nerve ring (NR). C) GFP::PAD-1 is expressed in the intestine (INT). Scale bar A-C: 20 µm. D) GFP::PAD-1 localizes to cortical granules (CG) (arrowhead) in oocytes in the proximal part of the gonad. GFP::PAD-1 also accumulates on the plasma membrane (PM) of oocytes (PM, arrow). E) GFP::TAT-5 expressed from integrated array *pwIs834* is also found on cortical granules and the plasma membrane of oocytes. Scale bar in D-E: 10 µm. Anterior is to the left.

We next analyzed PAD-1 localization in early embryos and compared it to MON-2 localization, as MON-2 is also predicted to form a complex with TAT-5 and PAD-1[2,3]. As no MON-2 antibodies were available, we expressed a fosmid clone of *mon-2* where GFP and Flag tags were inserted at the C-terminus[54]. Due to the low expression levels of GFP::PAD-1 and MON-2::GFP::3xFlag in live embryos (Fig. 12A), we stained fixed embryos with anti-GFP antibodies to visualize their subcellular localization. GFP::PAD-1 and MON-2::GFP::3xFlag mostly localized to cytoplasmic puncta, but were also found at the plasma membrane (Fig. 7A, D). Thus, TAT-5 localization appears distinct, but overlapping with the soluble proteins PAD-1 and MON-2.

Given that MON-2 and PAD-1 associate with membranes without a transmembrane domain[1,2], a signal is required to recruit them to membranes. As TAT-5 is an integral membrane protein, we wondered whether TAT-5 can recruit PAD-1 and MON-2 to the plasma membrane. Therefore, we tested whether depletion of TAT-5 disrupts PAD-1 or MON-2 localization to the cell cortex in *C. elegans*. In 1- or 2-cell stage embryos, there was no loss of MON-2::GFP::3xFlag or GFP::PAD-1 from the plasma membrane after *tat-5* knockdown (Fig. 7B,E). Thus, TAT-5 is not required to recruit MON-2 or PAD-1 to the plasma membrane.

Yeast and mammalian MON2 recruit PAD-1 orthologs to the TGN[6,10,55]. Therefore, we tested whether MON-2 and PAD-1 are required for each other's localization to the plasma membrane. GFP::PAD-1 localized to the plasma membrane after *mon-2* RNAi (Fig. 7C), and MON-2::GFP::3xFlag localized to the plasma membrane after *pad-1* RNAi (Fig. 7F). Thus, in contrast to yeast and mammalian MON-2, *C. elegans* MON-2 does not appear to be required for PAD-1 localization, although the intracellular localization needs to be examined.

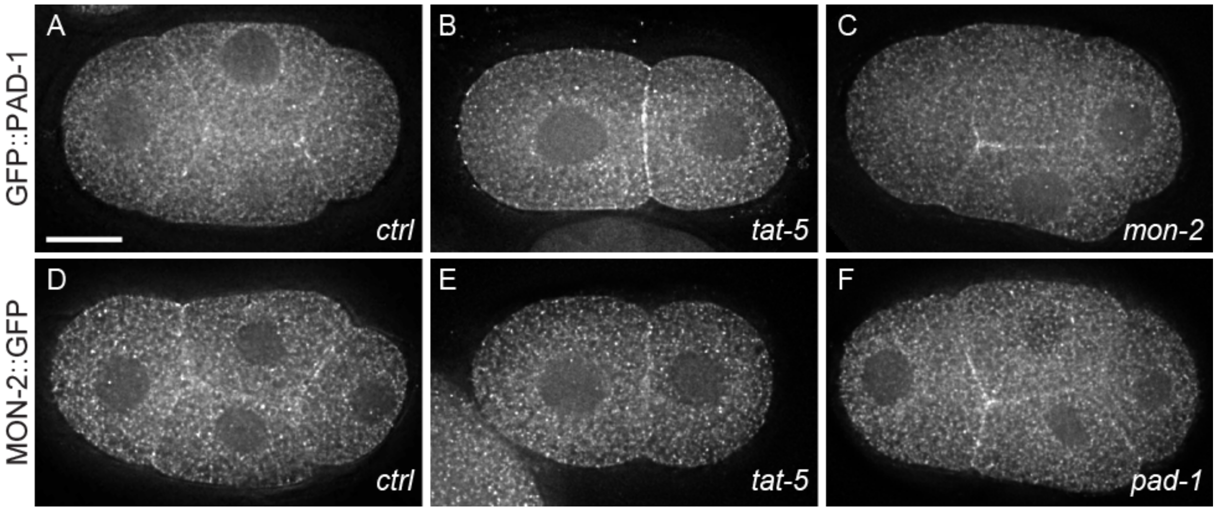

Fig. 7: PAD-1 and MON-2 localize to the cell cortex and cytoplasm. A) GFP::PAD-1 staining is found on cytoplasmic puncta as well as at the plasma membrane in a 4-cell embryo. B) GFP::PAD-1 localization is not significantly altered after *tat-5* RNAi treatment in a 2-cell embryo. C) GFP::PAD-1 still localizes to the plasma membrane after *mon-2* RNAi treatment in a 4-cell embryo. D) MON-2::GFP::3xFlag staining also localizes to cytoplasmic puncta as well as at the plasma membrane in a 4-cell embryo. E) MON-2::GFP::3xFlag localization is not significantly altered after *tat-5* RNAi treatment in a 2-cell embryo. F) MON-2::GFP::3xFlag still localizes to the plasma membrane after *pad-1* RNAi treatment in a 4-cell embryo. Scale bar: 10 μm. All images from Beer *et al.*, PNAS 2018[50].

To confirm that the GFP tags do not disrupt PAD-1 and MON-2 function, we checked whether endolysosomes were enlarged. Loss of Mon2 causes increased late endosome size in yeast, similar to the enlarged multivesicular bodies after loss of Neo1 or enlarged LMP-1-positive endolysosomes in *tat-5*[1,14,19]. To check whether the MON-2::GFP::3xFlag transgene is functional, we first crossed the fluorescent reporter into a *mon-2* nonsense mutant background[17], and then stained the resulting strain and the GFP::PAD-1 knock-in for the late endosome and lysosome marker LMP-1. In wild type embryos, small endolysosomes are dispersed throughout the cytoplasm (Fig. 8A). In contrast, LMP-1 positive organelles are enlarged and localize more to the cell cortex in *pad-1* RNAi-treated, *mon-2* RNAi-treated and *mon-2(xh22)* mutant embryos (Fig. 8B, D-E). LMP-1-positive endolysosomes appear similar in size to wild type embryos in GFP::PAD-1 worms (Fig. 8C) or when we expressed MON-2::GFP::3xFlag in *mon-2* mutants (Fig. 8F), demonstrating functional rescue. These data confirm that GFP-tagged PAD-1 maintains endosomal functions and suggest that the MON-2::GFP::3xFlag transgene is functional.

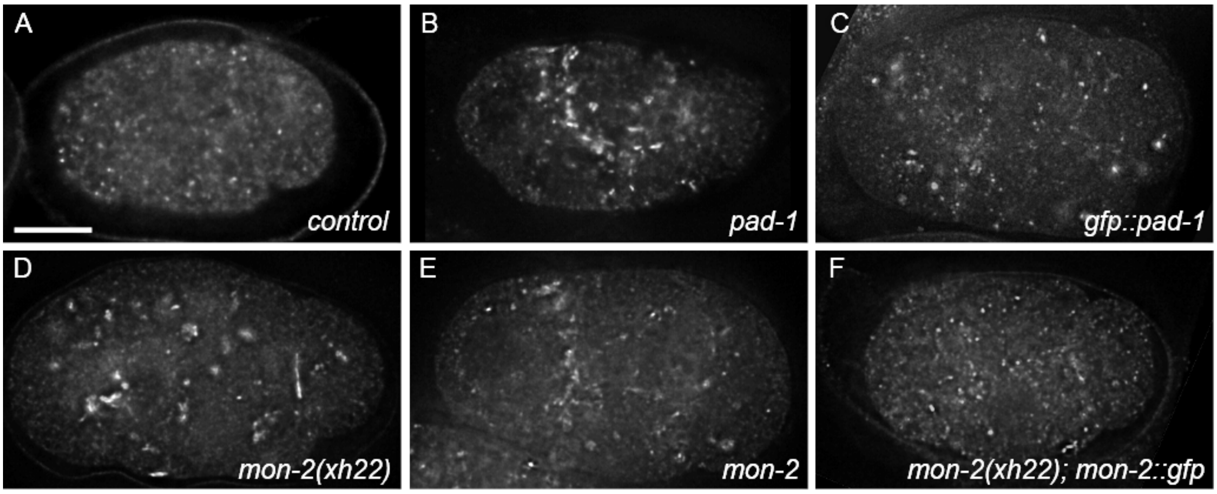

Fig. 8: GFP-tagged PAD-1 and MON-2 prevent enlargement of LMP-1-positive organelles: A-F) LMP-1 antibody staining of embryos. A) Antibody staining shows small LMP-1-positive late endosomes or lysosomes in 4-cell control embryos. B) LMP-1-positive vesicles are enlarged in *pad-1* knockdown embryos. C) LMP-1 positive vesicles are not enlarged in worms expressing GFP::PAD-1. D-E) LMP-1-positive vesicles are enlarged in *mon-2(xh22)* nonsense mutants and after *mon-2* knockdown. F) The enlarged LMP-1-positive vesicles are rescued when MON-2::GFP::3xFlag is introduced into *mon-2(xh22)* mutants, showing that the MON-2::GFP::3xFlag reporter is functional. Scale bar: 10 µm. All images besides C) are from Beer *et al.,* PNAS 2018[50].

5.2.5. PAD-1 and MON-2 appear enriched in the midbody remnant

We noticed that GFP::PAD-1 and MON-2::GFP are enriched at one distinct spot at the plasma membrane between cells, which based on its location could be the midbody remnant[56]. The midbody remnant forms at the end of cytokinesis, after abscission of the two daughter cells at the intercellular bridge. Abscission requires the ESCRT complex to thin and cut the intercellular bridge[57], leaving ESCRT-III filaments trapped inside the midbody remnant. Therefore, we wondered whether PAD-1 and MON-2 would colocalize with the ESCRT-III subunit VPS-32 at the midbody remnant. In untreated control embryos, VPS-32 is visible at a single spot between daughter cells, representing the midbody remnant (Fig. 9A-B). GFP::PAD-1 and MON-2::GFP::3xFlag colocalize with the single VPS-32 spot at the intercellular bridge, indicating that PAD-1 and MON-2 may also be trapped inside the midbody remnant (Fig. 9B-C). This localization suggests that PAD-1 and MON-2 could have a role during abscission.

As the ESCRT-complex is also required to bud MVs away from the cytoplasm[14], we speculated that ESCRT localization on the plasma membrane would not overlap with the MV budding inhibitor PAD-1. Given that we found no role for MON-2 in promoting or inhibiting MV budding, testing whether MON-2 colocalizes with bud sites would also be informative.

Interactions of ESCRT-III with MV budding membranes are transient, because of the ATPase VPS-4, which catalyzes the release of ESCRT-III filaments[58,59]. Therefore, to be able to observe ESCRT recruitment to the plasma membrane, we performed *vps-4* RNAi, which traps VPS-32 at bud sites[60]. In 2-cell *vps-4* RNAi-treated embryos, we saw accumulation of GFP::PAD-1, MON-2::GFP::3xFlag and VPS-32 at several patches along the cell-cell contact (Fig. 9C-D). In the magnified insets, we noticed that PAD-1 and MON-2 localization appears complementary to VPS-32, with only occasional overlap (yellow arrow in the insets of Fig. 9C-D). However, due to the limited resolution, it is hard to predict whether the apparently colocalizing proteins are only close neighbors. Thus, both MON-2 and PAD-1 appear to have complementary localization to the MV budding mediator ESCRT-III, which suggests that PAD-1 and MON-2 are rarely found at sites of outward plasma membrane budding (ectocytic sites).

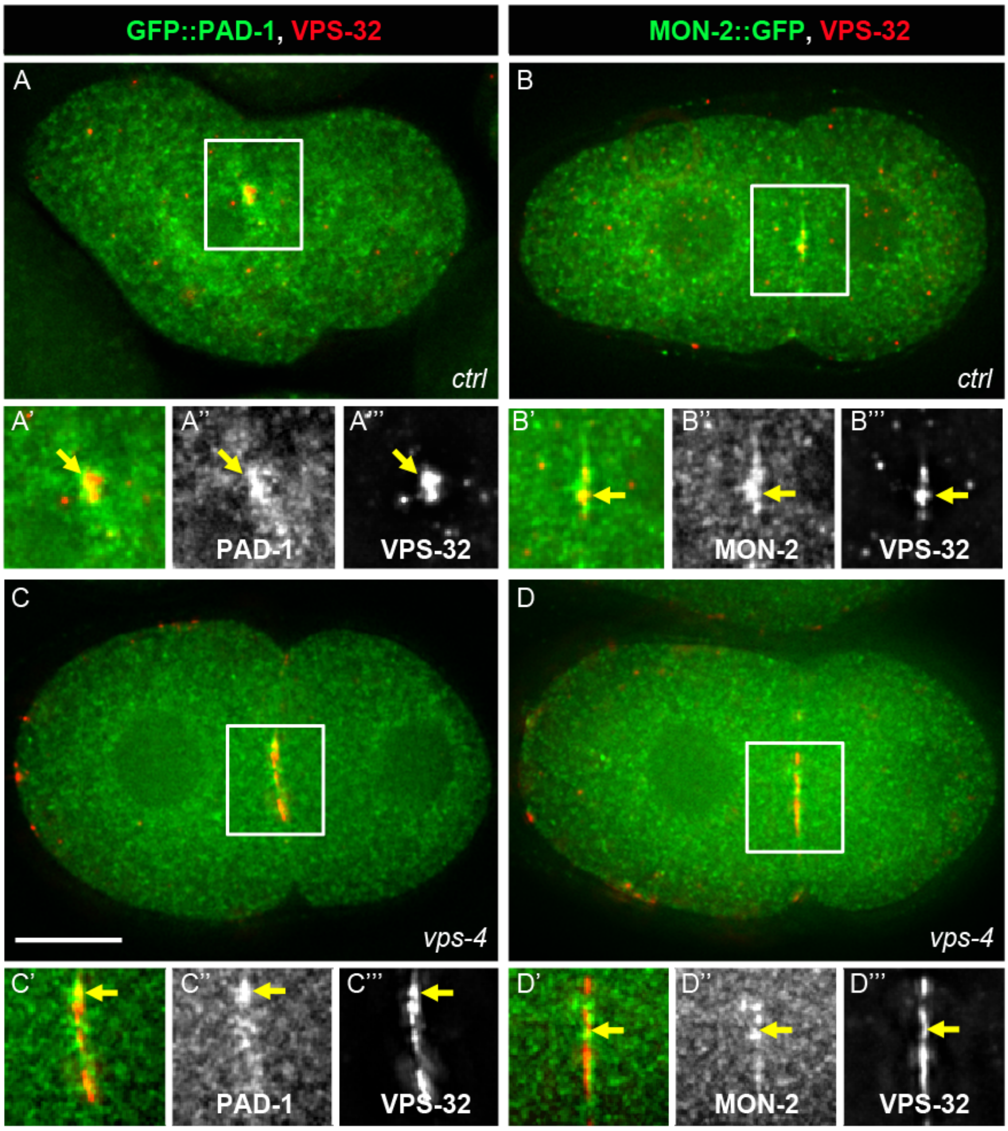
GFP::PAD-1, VPS-32
MON-2::GFP, VPS-32
A
B
ctrl
ctrl
A'
A''
A'''
PAD-1
VPS-32
B'
B''
B'''
MON-2
VPS-32
C
D
vps-4
vps-4
C'
C''
C'''
PAD-1
VPS-32
D'
D''
D'''
MON-2
VPS-32

Fig. 9: PAD-1 and MON-2 localize to the midbody remnant. A) GFP::PAD-1 and VPS-32 accumulate at the same spot between daughter cells (arrow), suggesting that PAD-1 is inside the midbody remnant (n=2). Boxed region is magnified in A'-A'''. B) Similar colocalization (arrow) on the midbody remnant was observed with MON-2::GFP::3xFlag and VPS-32 in a 2-cell embryo(n=9). Boxed region is magnified in B'-B'''. C) 2-cell GFP::PAD-1 embryo treated with *vps-4* RNAi and stained for VPS-32 and GFP. Boxed region is magnified in C'-C'''. PAD-1 and VPS-32 accumulate at complementary positions at the cell-cell contact, only rarely colocalizing (arrow). D) Similar observations were made after treating a 2-cell MON-2::GFP::3xFlag embryo with *vps-4* RNAi. Boxed region is magnified in D'-D'''. Scale Bar: 10 µm.

5.2.6. PAD-1 and MON-2 do not regulate TAT-5 localization

PAD-1 orthologs regulate protein trafficking[3,13,55,61] and loss of Dop1 causes reduced Neo1 levels in yeast[2]. Thus, we asked whether PAD-1 could regulate MV release by maintaining proper TAT-5 levels or by localizing TAT-5 to the plasma membrane to maintain PE asymmetry. We treated GFP::TAT-5 worms with *pad-1* RNAi and saw that GFP::TAT-5 still localized to the plasma membrane (Fig. 10A). In fact, loss of PAD-1 caused increased GFP::TAT-5 labeling at the cell surface (Fig. 10A-B, Fig. 11A), similar to the increased plasma membrane labeling of membrane reporters in MV-releasing mutants. Therefore, we speculated that TAT-5 at the plasma membrane is released in MVs in *pad-1* mutants. Additionally, the overall GFP::TAT-5 levels were not decreased after *pad-1* knockdown (Fig. 10E). Instead, we observed a slight, but significant increase in GFP::TAT-5 levels, which may be due to TAT-5 release in MVs (Fig. 10A, E). To confirm that this phenotype was not due to incomplete *pad-1* depletion, we expressed GFP::TAT-5 in a *pad-1(wur02)* deletion mutant. Rare embryos collected from this strain showed GFP::TAT-5 localized to the plasma membrane (Fig. 10B), suggesting that PAD-1 is not required for TAT-5 plasma membrane localization or post-translational levels. This demonstrates that PAD-1 inhibits MV release through a different function than regulating TAT-5 localization to the plasma membrane.

MON-2 orthologs are also required for protein trafficking and Mon2 is required for proper Neo1 levels in yeast[1,2,6,29,55,62], therefore we tested whether TAT-5 plasma membrane localization depends on MON-2. GFP::TAT-5 localized robustly to the plasma membrane after *mon-2* RNAi (Fig. 10C), as well as in *mon-2* mutant embryos (Fig. 17A, Table 8). Additionally, the overall GFP::TAT-5 levels were not decreased after *mon-2* knockdown (Fig. 10E), demonstrating that MON-2 is not required for TAT-5 to localize to the plasma membrane or for protein stability.

We next examined whether MON-2 and PAD-1 could redundantly regulate TAT-5 localization. GFP::TAT-5 still localized to the plasma membrane after *pad-1* was knocked down in a *mon-2* mutant background (Fig. 10D, Table 8). In summary, these data demonstrate that MON-2 and PAD-1 are not required to maintain TAT-5 levels or to regulate TAT-5 localization to the plasma membrane.

We also checked whether the Arf-like small GTPase ARL-1, which interacts with Mon2, Dop1 and Neo1 in yeast, affects TAT-5 localization[2,28]. We observed no change in TAT-5 localization after *arl-1* RNAi or after *arl-1* RNAi in a *mon-2* mutant background (Table 8), demonstrating that ARL-1 is also not required for TAT-5 to localize to the plasma membrane.

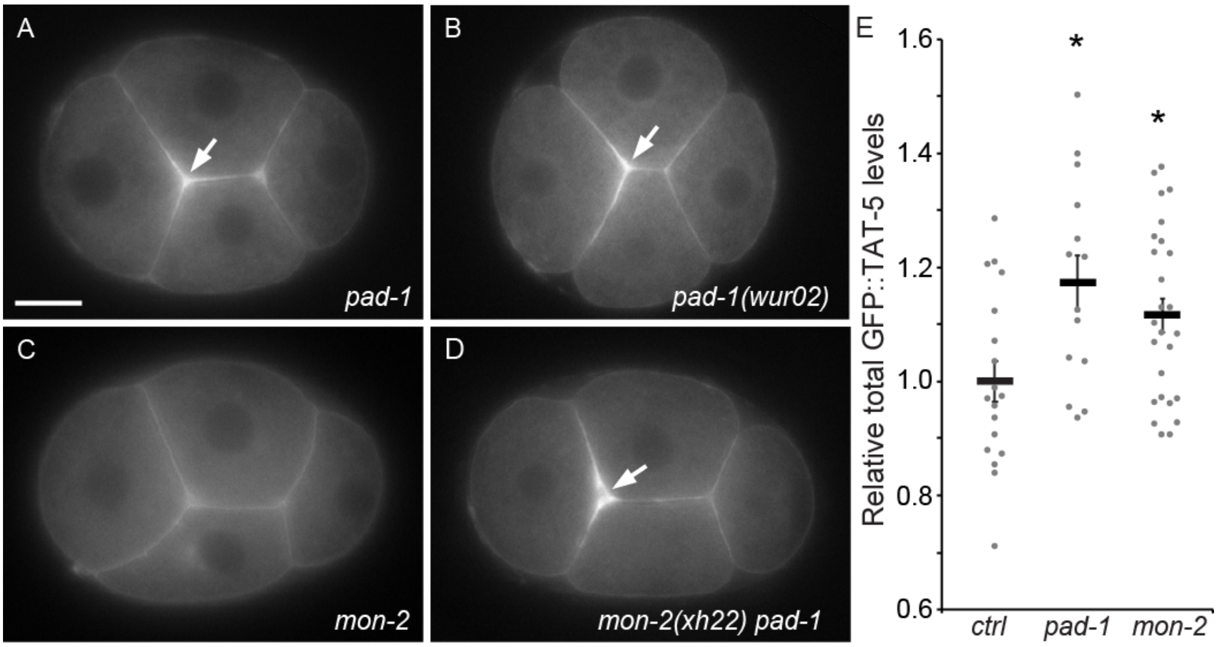

Fig. 10: TAT-5 localization is not altered in PAD-1 and MON-2 mutants. A-D) GFP::TAT-5 localization in 4-cell embryos. A) GFP::TAT-5 localization is not altered after *pad-1* RNAi. Additionally, GFP::TAT-5 appears in thick patches on the plasma membrane (arrow), suggesting that TAT-5 is released in MVs. B) GFP::TAT-5 still localizes to the plasma membrane and is released in MVs (arrow) in a *pad-1(wur02)* maternal-zygotic deletion mutant embryo. C) *mon-2* RNAi does not change the plasma membrane localization of GFP::TAT-5. D) GFP::TAT-5 is in the plasma membrane and released on MVs (arrow) in a *mon-2(xh22)* mutant treated with pad-1 RNAi, indicating that MON-2 and PAD-1 do not redundantly regulate TAT-5 localization. Scale bar: 10 μm. E) Relative total GFP::TAT-5 fluorescence measured from 2- to 8-cell control (n=18) and RNAi-treated embryos. TAT-5 levels are significantly increased after *pad-1* (n=14) or *mon-2* RNAi (n=26) (*p<0.01). Bars represent mean ± S.E.M. One-tailed Student's t-test with Bonferroni correction was used for statistical analysis (*p<0.01). All images modified from Beer *et al*., PNAS 2018[50].

5.2.7. TAT-5, PAD-1 and MON-2 are trafficked into microvesicles

As MON-2 and PAD-1 localize to the cell cortex independent of TAT-5 (Fig. 7B, E), but appear to localize in complementary domains to MV bud sites (Fig. 9C-D), we wondered whether PAD-1 and MON-2 would be released in MVs like GFP::TAT-5 (Fig. 11A). In stained *tat-5* RNAi-treated embryos, we noticed increased GFP::PAD-1 and MON-2::GFP::3xFlag localization at the cell surface (Fig. 11B-C, Table 4), suggesting that MON-2 and PAD-1 can also be released in MVs. These results confirm that TAT-5 is not needed for MON-2 or PAD-1 to localize to the plasma membrane, but may indicate a role for TAT-5 in preventing MON-2 and PAD-1 from localizing to MV bud sites.

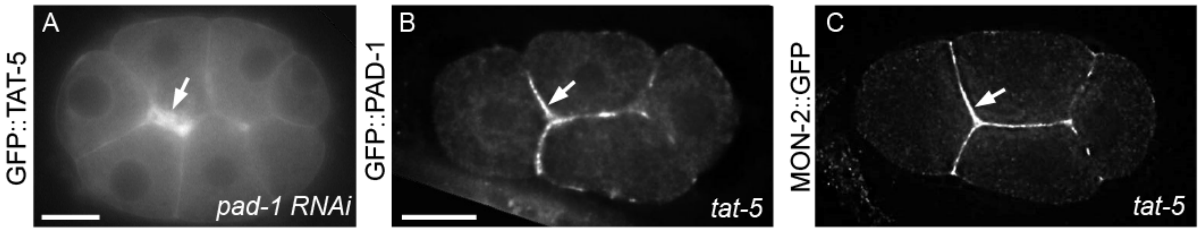

Fig. 11: TAT-5, PAD-1, and MON-2 are released in MVs. A) GFP::TAT-5 accumulates between cells (arrow) after *pad-1* RNAi in an 8-cell embryo, showing that TAT-5 is released in MVs. B-C) Staining for GFP::PAD-1 and MON-2::GFP::3xFlag is increased at the cell surface (arrow) after *tat-5* RNAi treatment in 4-cell embryos, suggesting that cortical PAD-1 and cortical MON-2 are released outside cells in MVs. Scale bars: 10 µm. Images from Beer *et al.*, PNAS 2018[50].

Reporter	RNAi	Released in MVs	
		%	n
GFP::TAT-5	*pad-1*	89%	27
GFP::PAD-1	*tat-5*	89%	47
MON-2::GFP::3xFlag	*tat-5*	88%	49
	pad-1	2%	65

Table 4: Predicted TAT-5 interactors localize to microvesicles. The percentage [%] of embryos with thick patches of the indicated reporter at cell contacts after induction of MV release by *pad-1* or *tat-5* RNAi. The total number [n] of embryos observed is indicated.

We next tested whether PAD-1 is required for MON-2 release in MVs. The normally dim cytosolic fluorescence of MON-2::GFP in live embryos accumulates in MVs after *tat-5* RNAi treatment (Fig. 12A-B, Table 5). In contrast, MON-2 did not accumulate in MVs after *pad-1* knockdown (Fig. 12C, Table 5), despite *pad-1* RNAi having no effect on MON-2 localization to the plasma membrane (Fig. 7F). Therefore, TAT-5, MON-2 and PAD-1 are not required for each other's localization to the plasma membrane, but PAD-1 is needed for MON-2 sorting into MVs.

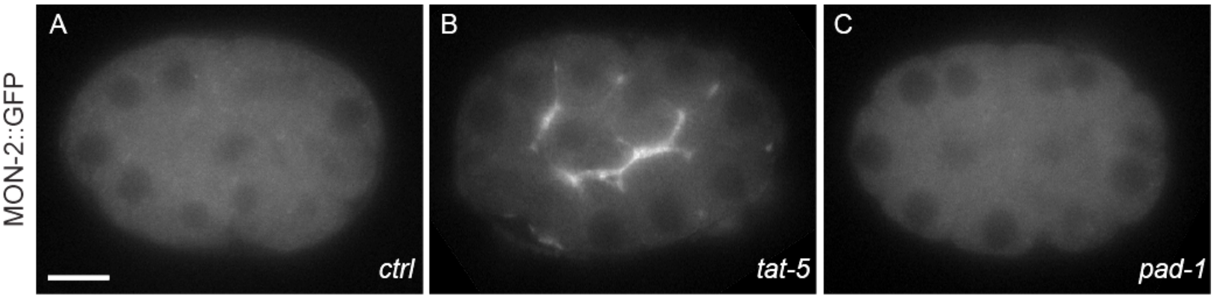

Fig. 12: MON-2 release in MVs depends on PAD-1. A) In live 26-cell embryos, MON-2::GFP::3xFlag puncta are barely visible above cellular autofluorescence. B) MON-2::GFP::3xFlag is increased at the cell surface after *tat-5* RNAi treatment, showing that cortical MON-2 is released outside cells in MVs. C) MON-2::GFP::3xFlag is not increased at the cell surface after *pad-1* RNAi treatment, suggesting that PAD-1 is required for MON-2 localization in MVs. Scale bar: 10 µm. Image from Beer *et al.*, PNAS 2018[50].

5.2.8. A subset of cortical proteins are released in microvesicles

Extracellular vesicles can have many cargo molecules, differing between organisms and tissues[63]. As MVs bud from the plasma membrane, we checked which proteins localized to the cell surface or cell cortex would become MV cargos in *C. elegans*. As PAD-1, but not TAT-5 is needed to release MON-2 inside MVs, we also asked whether the release of potential MV cargo depended on TAT-5 and/or PAD-1 by examining the localization of proteins after performing *tat-5* or *pad-1* RNAi.

Actin is an abundant cytoskeletal protein known to be a MV cargo in other species [63]. Thus, we first examined actin-binding reporters seen at the cortex, including the ezrin-radixin-moesin ortholog ERM-1, which links membrane proteins to F-actin[64], as well as the actin-binding domain of *Drosophila* Moesin[65]. ERM-1 and GFP::Moesin accumulated between cells after *pad-1* or *tat-5* RNAi (Table 5), indicating that actin-binding proteins are released in MVs. This suggests that actin is also likely to be released in *C. elegans* MVs.

The non-muscle myosin motor protein NMY-2 is part of the actomyosin cytoskeleton, labels the cytokinetic ring, and is released inside midbody remnants[56,66]. NMY-2::GFP localizes to the cell cortex and brightly labels midbody remnants in control embryos (Fig. 13A). After *tat-5* RNAi, NMY-2::GFP was still released in midbody remnants and we noticed a slight increase in overall NMY-2::GFP cortical levels (Fig. 13B). However, we saw no large accumulations of NMY-2::GFP between cells indicative of localization in MVs (compare to Fig. 13E-F), suggesting that NMY-2 is not released in MVs (Table 5). After *pad-1* RNAi, NMY-2::GFP still localized inside midbody remnants and did not accumulate between cells (Fig. 13C, Table 5). Thus, NMY-2 appears not to be a significant cargo of MVs, indicating that not all actin-binding proteins are released in *C. elegans* MVs.

FP Reporter or Antibody	**RNAi**	**Released in MVs**	
		%	**n**
GFP::Moesin	*tat-5*[i]	100%	20
	pad-1[i]	71%	14
ERM-1 Ab	*pad-1*[i]	95%	19
NMY-2::GFP	*tat-5*	0%	61
	pad-1	0%	45
DYN-1::GFP or DYN-1 Ab	*tat-5*[i]	100%	21
	pad-1	72%	60
RME-1 Ab	*tat-5*[i]	100%	8
	pad-1[i]	100%	19
CAV-1 Ab	*tat-5*[i]	0%	18
	pad-1[i]	4%	28
CHC-1::mCh::ZF1	*tat- 5*	0%	55
	pad-1	0%	42
GFP::SNX-1	*ctrl*	0%	34
	tat-5	0%	29
	pad-1	0%	17

Table 5: Localization of proteins to MVs. Increased release in MVs was scored when thick patches of the reporter accumulated at cell contacts. The percentage [%] of embryos with thick patches of the reporter and the total number [n] of all observed embryos is indicated. [i] indicates experiments that were only performed once. RME-1 data from *tat-5* RNAi was quantified from images taken by Ann Wehman.

The GTPase dynamin is also present at the cell cortex[67,68], where it bundles actin and is required for vesicle scission during endocytosis[69]. We used GFP-tagged DYN-1 or antibody staining against endogenous DYN-1 to visualize its localization after *tat-5* or *pad-1* RNAi (Fig. 13D). In both cases, DYN-1 and DYN-1::GFP accumulated between cells (Fig. 13E-F, Table 5), suggesting that it is released from the cell cortex in MVs. Thus, DYN-1 is a MV cargo and neither TAT-5 nor PAD-1 are required for DYN-1 release in MVs.

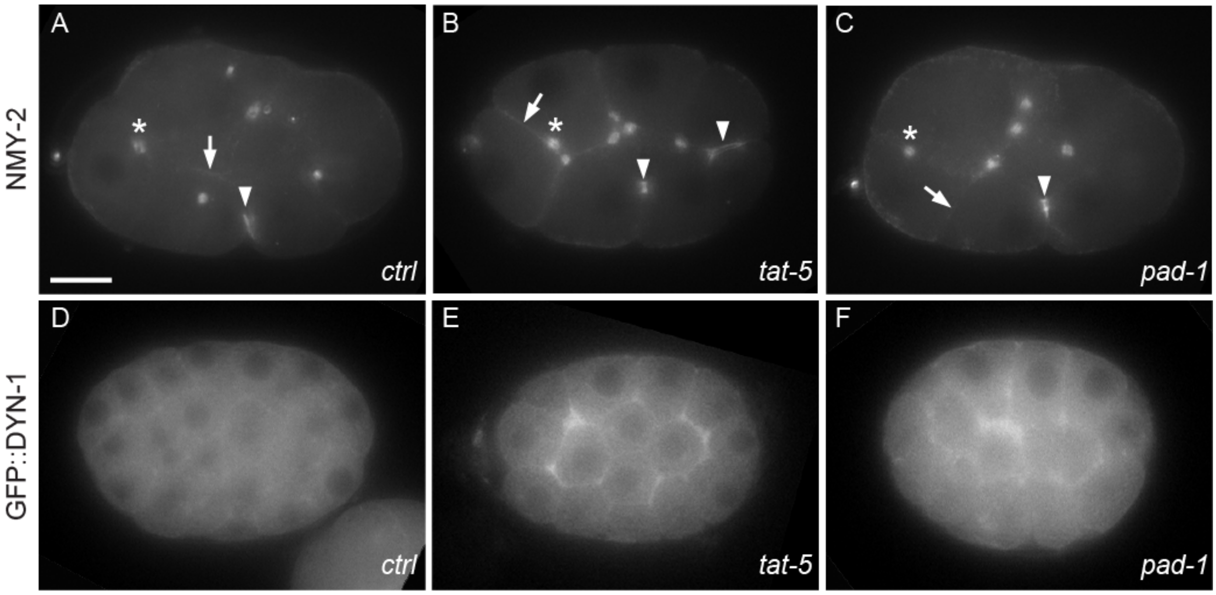

Fig. 13: DYN-1 is released in MVs, but NMY-2 is only released in midbody remnants. A) NMY-2::mCh localizes weakly to the cell cortex (arrow), is found in midbody rings (arrowhead), and is released inside midbody remnants (asterisk on ABx midbody) in a 7-cell embryo. B) NMY-2::GFP is recruited to midbody rings, released inside midbody remnants and accumulates at the cell surface, but does not show the thickened patches typical of MV release after *tat-5* RNAi in an 8-cell embryo. C) In a *pad-1* RNAi treated 7-cell embryo, NMY-2::GFP is found on cytokinetic rings and released inside midbody remnants, but localizes weakly to the cell cortex. D) GFP::DYN-1 localizes weakly to the cell cortex in control embryos. E-F) DYN-1 is increased at the cell surface after *tat-5* and *pad-1* RNAi, suggesting that DYN-1 is released in MVs.

We had previously observed that clathrin accumulates on the plasma membrane after *tat-5* RNAi, but is not released in MVs (see chapter 3 Fig 6), despite its release in EVs in other systems[70,71]. Therefore, we checked whether clathrin heavy chain CHC-1 was released in MVs in *pad-1* mutants. The degron-tagged CHC-1::mCh::ZF1 reporter was not protected from proteasomal degradation in *pad-1* RNAi embryos (Table 5), suggesting that clathrin was not released in MVs. Thus, clathrin appears to either not be an MV cargo in *C. elegans* embryos or to depend on both PAD-1 and TAT-5 for its sorting into MVs. However, CHC-1::mCh::ZF1 was increased at the plasma membrane after *pad-1* RNAi (data not shown), similar to *tat-5* RNAi embryos (chapter 3 Fig 6), demonstrating that more clathrin localizes to the plasma membrane in both mutants. Thus, PAD-1 and TAT-5 have similar roles limiting clathrin accumulation at the plasma membrane.

We next asked whether other cortical proteins involved in membrane trafficking are released in MVs, including the recycling endosome reporter RME-1[72], the caveolae marker caveolin CAV-1[68], and the sorting nexin SNX-1. RME-1 accumulated between cells after *tat-5* or *pad-1* RNAi (Table 5), indicating that it was released in MVs. In contrast, CAV-1 was still found on the cell cortex, but did not accumulate between cells after *tat-5* or *pad-1* RNAi (Table 5), indicating it was not released in MVs. GFP::SNX-1 localizes to peripheral endosomes near the cell cortex (Fig. 14A) and did not accumulate between cells in *tat-5* or *pad-1* RNAi-treated embryos (Fig. 14B-C), suggesting that SNX-1 was not released in MVs. Additionally, GFP::SNX-1 still localized to cortical endosomes after *tat-5*, *pad-1* or *mon-2* RNAi (Fig. 14B-D), suggesting that TAT-5, PAD-1 and MON-2 are not required for SNX-1 localization. In summary, only a subset of cortical trafficking proteins are released in MVs. Furthermore, while PAD-1 is required for MON-2 release in MVs, it seems not to be a general MV cargo sorting protein, as several cargos are found in MVs in both *tat-5* and *pad-1* mutants.

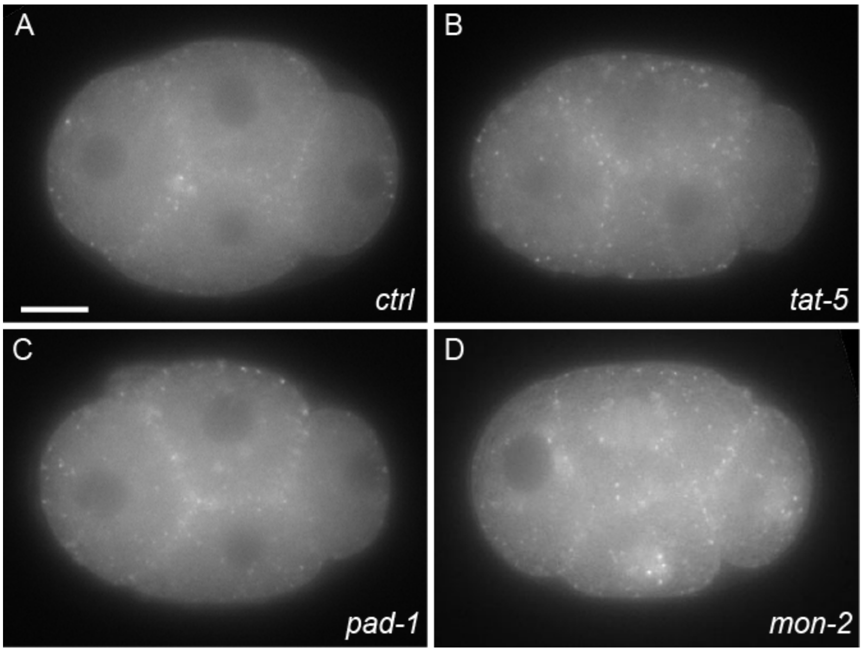

Fig. 14: SNX-1 localization does not depend on TAT-5, PAD-1 or MON-2: A-D) 4-cell embryos expressing GFP::SNX-1. Scale bar: 10 μm. A) GFP::SNX-1 is found near the cell cortex in a 4-cell control embryo. B-D) GFP::SNX-1 localization to cortical endosomes is not disrupted after *tat-5, pad-*

1 or *mon-2* RNAi and there is no sign of thickened membranes, indicating that SNX-1 is not released in MVs.

5.2.9. MON-2 and PAD-1 regulate endosomal trafficking

MON-2 and PAD-1 orthologs in yeast and mammals have been implicated in retrograde trafficking between endosomes and Golgi [29,73]. MON2 was found in the interactome of SNX3 in mammals and regulated Wntless secretion together with SNX3[3]. Given the redundant retrograde trafficking pathways of sorting nexins (chapter 4), we wondered whether MON-2 or PAD-1 could traffic TAT-5 redundantly with other retrograde regulators. Therefore, we first asked whether MON-2 can interact genetically with the core retromer subunits (VPS-26, VPS-29, and VPS-35) or sorting nexins (SNX-1, SNX-3, SNX-6, LST-4). We performed retromer or *snx* RNAi in the *mon-2* mutant background and obtained synthetic developmental phenotypes, including sterility and embryonic lethality with both core retromers and *snx-1*, *snx-6* and *snx-3*, but not with *lst-4* (Table 6). In addition, *vps-26* and *snx-3* mutants showed phenotypes like lethality and embryonic lethality when they were treated with *mon-2* RNAi. This implies that MON-2 can act redundantly with retromer and the sorting nexins SNX-1, SNX-6 and SNX-3 in some essential processes.

Mutant strain	RNAi								
	control	*mon-2*	*vps-26*	*vps-29*	*vps-35*	*snx-1*	*snx-3*	*snx-6*	*lst-4*
+	-		-	-	-	-	-	-	-
mon-2 (xh22)	-	-	Egl Ste	Egl Ste	Egl Ste Let	Egl Emb	Emb	Ste Emb	-
vps-26 (tm1523)	Egl	Egl Let Ste							
snx-3 (tm1595)	Egl	Egl Emb							

Table 6: Genetic interactions of *mon-2* mutants. Lethal (Let), egg-laying-defective (Egl), sterile (Ste), and embryonic lethal (Emb) phenotypes were detected after knockdown with retromer or sorting nexin RNAis in a *mon-2* nonsense allele (-) or after *mon-2* knockdown in retromer or sorting nexin deletion mutants (Δ). Wildtype worms were used as a control and are depicted as +. (-) indicates that none of these phenotypes were detected. Untreated *vps-26* and *snx-3* mutants showed an egg-laying defect. All data derive from three independent experiments with each indicated phenotype seen at least once per experiment. Experiments were performed together with Jennifer Rivas-Castillo.

As increased EV release is associated with embryonic lethality and sterility (see chapter 3, Fig. 9)[14], we checked whether the synthetic phenotypes in *mon-2* mutants after retromer or sorting nexin depletion were caused by increased EV release. PH::mCh labeling was increased between cells when we knocked down the SNX-BAR proteins SNX-1 or SNX-6 or the SNX-PX protein SNX-3 in *mon-2* mutants (Fig. 15B-D,Table 7), consistent with increased EV release that could explain the synthetic lethality and sterility phenotypes. No sign of increased EV release was seen when we depleted MON-2 together with any of the core retromer proteins (Table 7), leaving the enhanced lethality of *mon-2* retromer double mutants unexplained. We also found no increase in EV release when we depleted the SNX-FERM proteins SNX-17 or SNX-27 in a *mon-2* mutant background (Table 7). Together, these data reveal that MON-2 is likely to regulate the trafficking of multiple cargos, some of which are also trafficked by SNX-1/-6 and SNX-3 to inhibit EV release.

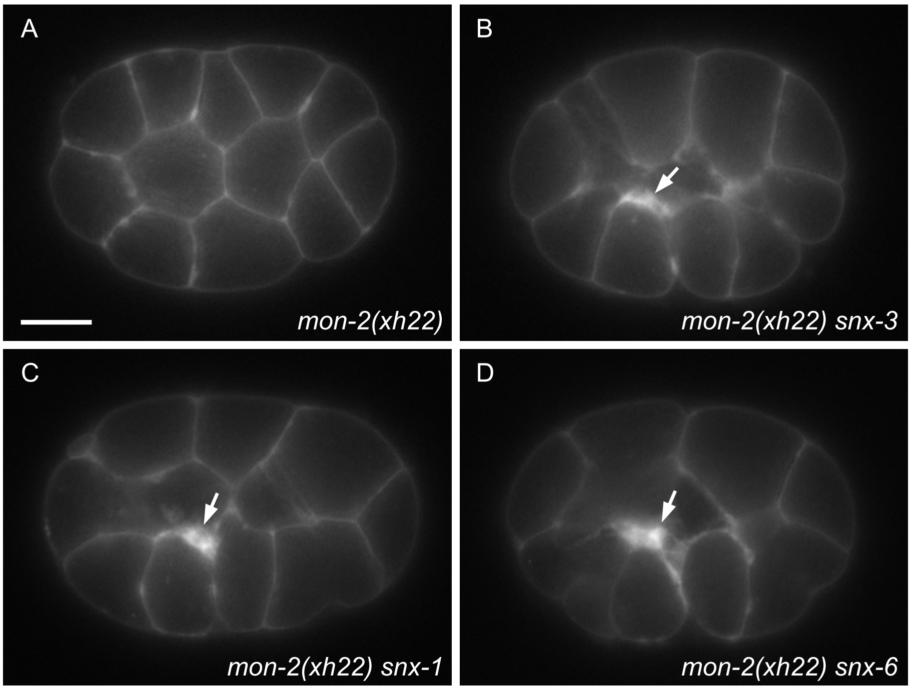

Fig. 15: MON-2 redundantly regulates EV release with SNX-1/6 and SNX-3. A) The plasma membrane marker PH$_{PLC1\partial1}$::mCh appears normal in a 15-cell *mon-2(xh22)* mutant embryo. B-D) Thickened patches of PH$_{PLC1\partial1}$::mCh (arrow) are observed between cells in *mon-2(xh22)* mutants treated with *snx-3, snx-1* or *snx-6* RNAi, indicating increased EV release, thus demonstrating that SNX-1/-6, SNX-3 and MON-2 redundantly inhibit EV release. Scale bar: 10 µm. All images except panel C are from Beer *et al.*, PNAS 2018[50].

Genotype	RNAi	Increased EV release (thick membranes)	
		%	n
+	-	0%	119
	mon-2	0%	72
	pad-1	89%	55
	vps-26	0%	73
	vps-29	0%	40
	vps-35	0%	40
	snx-1	0%	60
	snx-6	0%	40
	snx-3	0%	60
snx-3(tm1595)	-	1%	69
	mon-2	86%	31
	pad-1	100%	28
snx-17(tm3379)	-	0%	75
	mon-2	0%	46
	pad-1[i]*	100%	7
mon-2(xh22)	-	0%	105
	mon-2	0%	270
	pad-1	76%	78
	vps-26	0%	102
	vps-29	0%	97
	vps-35	0%	79
	snx-1	77%	87
	snx-6	96%	95
	snx-3	51%	84
	snx-17[i]	0%	24
	snx-27	0%	42

Table 7: Summary of EV release in *mon-2* mutants: Control (+) and mutant worms expressing fluorescent PH-reporters were treated with RNAi or untreated (-). Embryos (n) from the late 4-cell to 102-cell stage were scored for thickened membrane labeling between cells, which is indicative of EV release and presented as a percentage. As a positive control for EV release, *pad-1* RNAi was also performed. [i] indicates experiments that were only performed once. *GFP::TAT-5 was used to score EV release in *snx-17(tm3379) pad-1* RNAi embryos.

As SNX-1/6 and SNX-3 both traffic TAT-5, we tested whether the increased EV release was due to changes in TAT-5 trafficking in *mon-2 snx* double mutants. Although GFP::TAT-5 was still weakly visible on the plasma membrane of most *mon-2* mutants treated with *snx-6* RNAi (Table 8), GFP::TAT-5 also localized to prominent 0.5 - 2 µm cytoplasmic vesicles (Fig. 16B). Similar vesicles were observed when *snx-1* or *snx-3* were depleted in *mon-2* mutants. These large GFP::TAT-5 vesicles were not seen when sorting nexins were knocked down in a wild type background (chapter 4 Fig 6D-F), but were seen after *pad-1* knockdown in a *snx-1* mutant background (Fig. 16C), suggesting that MON-2 and PAD-1 are required to prevent TAT-5 from trafficking to these large vesicles.

To check whether TAT-5 localization to the plasma membrane was further decreased in *mon-2* mutants treated with sorting nexin RNAis, we measured GFP::TAT-5 fluorescence intensity in double mutants and compared it to individual *mon-2* or sorting nexin RNAis. No decrease in TAT-5 plasma membrane localization was observed in *mon-2* mutants, or in *mon-2* mutants treated with *pad-1* RNAi (Fig. 16A, D), supporting our previous result that MON-2 does not regulate TAT-5 localization redundantly with PAD-1 (Fig. 10D). However, GFP::TAT-5 plasma membrane levels were significantly decreased in *mon-2* mutants treated with RNAis against the SNX-BARs SNX-1/-6 or SNX-3 in comparison to untreated *mon-2* mutants (Fig. 17B, D). Similarly, *snx-1* mutants treated with *pad-1* RNAi also had decreased GFP::TAT-5 levels in comparison to *pad-1* RNAi or *mon-2* mutants treated with *pad-1* RNAi (Fig. 16C, D). However, in comparison to individual *snx-1, snx-6* and *snx-3* RNAi, *mon-2* mutants treated with sorting nexin RNAi had no further decrease in TAT-5 plasma membrane localization (Fig. 16D). Similarly, quantifying the number of embryos with no visible GFP::TAT-5 at the plasma membrane showed similar percentages between *snx* single mutants and *mon-2 snx* double mutants (Table 8). This suggests that SNX-1/-6 and SNX-3 control the major trafficking pathway of TAT-5 to the plasma membrane, while MON-2 and PAD-1 could regulate another step of endolysosomal trafficking, which only impacts TAT-5 trafficking when sorting nexins are absent.

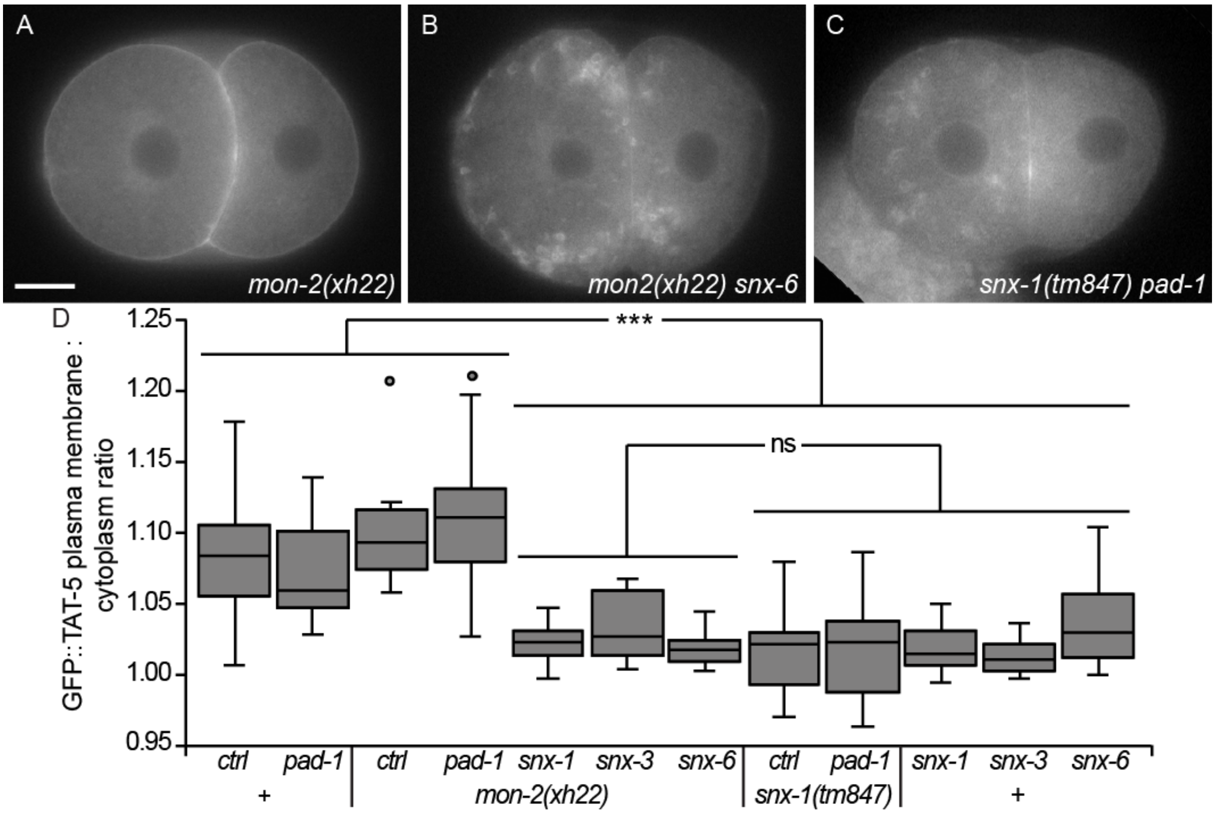

Fig. 16: GFP::TAT-5 localizes to large intracellular vesicles in *mon-2 snx* or *pad-1 snx* double mutants. A) GFP::TAT-5 localizes to the plasma membrane in a 2-cell *mon-2(xh22)* mutant embryo. B) GFP::TAT-5 localizes to prominent cytosolic vesicles after *snx-6* RNAi treatment in *mon-2(xh22)* mutants. Similar phenotypes were also seen after *snx-1* or *snx-3* RNAi treatment in *mon-2(xh22)* mutants, suggesting that MON-2 acts redundantly with sorting nexins to control TAT-5 localization. C) GFP::TAT-5 localizes to large cytosolic vesicles after *pad-1* RNAi in *snx-1(tm847)* mutants, demonstrating that PAD-1 also acts redundantly with sorting nexins during TAT-5 trafficking. Scale bar: 10 µm. D) The ratio of GFP::TAT-5 fluorescence between the plasma membrane and the cytoplasm was quantified from control(+) (n=32), *mon-2(xh22)* and *snx-1(tm847)* mutants treated with the indicated RNAis. *mon-2(xh22)* (n=20) missense mutants or *pad-1* RNAi (*ctrl pad-1* RNAi: n=22, *mon-2(xh22) pad-1* RNAi: n=27) only show significantly decreased TAT-5 plasma membrane levels when sorting nexins are depleted (*mon-2(xh22) snx-1*: n=28, *mon-2(xh22) snx-3*: n=14, *mon-2(xh22) snx-6*: n=21), but the decrease is not significantly different from *snx* mutants (*snx-1(tm847)*: n=30, *snx-1(tm847) pad-1*: n=29) or *snx* RNAi alone (*snx-1*: n=29, *snx-3*: n=32, *snx-6*: n=29) ($p>0.05$). One-tailed Student's t-test with Bonferroni correction was used for statistical analysis (***$p<0.001$). Images A-C and D modified from Beer *et al.*, PNAS 2018[50].

Genotype	**RNAi**	**GFP::TAT-5 not on plasma membrane**	
		%	**n**
+	-	0%	96
	pad-1	0%	60
	mon-2	0%	47
	arl-1[i]	0%	10
	snx-1	31%	36
	snx-3	5%	73
	snx-6	28%	72
pad-1(wur02)	-[i]	0%	3
snx-1(tm847)	-	37%	41
	pad-1	13%	40
	snx-3	26%	37
snx-17(tm3779)	-	0%	8
	pad-1[i]	0%	8
	mon-2[i]	0%	20
mon-2(xh22)	-	0%	28
	mon-2	0%	33
	pad-1	0%	44
	arl-1[i]	0%	8
	vps-26	0%	44
	vps-29	0%	39
	vps-35	0%	34
	snx-1	16%	45
	snx-3	25%	28
	snx-6	37%	30

Table 8: Summary of GFP::TAT-5 localization defects. Control (+) and mutant worms expressing GFP::TAT-5 were treated with RNAi or untreated (-). Embryos (n) from the zygote to 15-cell stage were scored for whether GFP::TAT-5 was visible at the plasma membrane, which is presented as a percentage. [i] marks experiments that were only performed one.

As SNX-3 associates with the core-retromer and recruits VPS-35 upon cargo binding[74], we wondered whether we could expose a redundant role for SNX-3 binding to VPS-35 in *mon-2* mutants. A single tyrosine in SNX-3(Y22) is required for VPS-35 binding and cargo trafficking[3]. Accordingly, a SNX-3(Y22A) mutant causes loss of VPS-35 binding and altered trafficking of SNX-3-retromer cargos. We expressed GFP::TAT-5 in *snx-3(hu256[Y22A])* mutants and saw that TAT-5 still localized to the plasma membrane, even after *mon-2* depletion (Fig. 17A-B). This confirms that the redundant TAT-5 trafficking activity of SNX-3 is retromer-independent.

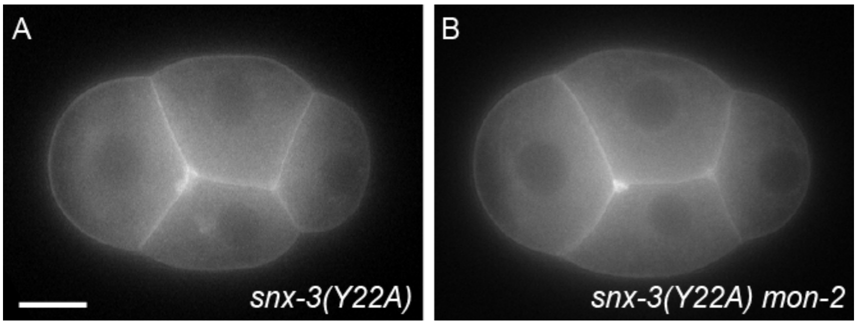

Fig. 17: Trafficking of TAT-5 by SNX-3 and MON-2 is independent of the core retromer. A) GFP::TAT-5 localizes to the plasma membrane in *snx-3(hu256[Y22A])* mutants deficient for VPS-35 binding (n=36). B) GFP::TAT-5 localization is not changed when *snx-3(hu256[Y22A])* mutants are additionally treated with *mon-2* RNAi (n=29). Scale bar: 10 µm.

5.2.10. MON-2, PAD-1, and TAT-5 regulate multivesicular endosome size

The large vesicles in *mon-2 snx-1/-3/-6* and *pad-1 snx-1* double mutants appeared similar to the enlarged LMP-1-positive endolysosomes we had previously observed in *pad-1*, *mon-2* and *tat-5* mutants (Fig. 8)[14]. As LMP-1 localizes to both late endosomes and lysosomes[75], we wondered whether PAD-1, MON-2 and TAT-5 regulate the size of these organelles. We measured the diameter of multivesicular endosomes and electron-dense lysosomes from electron micrographs and found that multivesicular endosomes were significantly larger in *pad-1* and *tat-5* RNAi-treated embryos in comparison to wild type embryos (Fig. 18G-I, 320±140 nm in control, 470±290 nm in *pad-1*, 410±170 nm in *tat-5*). In contrast, electron-dense lysosomes had a similar diameter (Fig. 18J, control: 490±150 nm, *pad-1*: 500±200 nm, *tat-5:* 470±120 nm). Intriguingly, despite the increased size of multivesicular endosomes, the number of intraluminal vesicles per multivesicular endosome was not significantly changed (control: 8±9, *pad-1*: 8±10, *tat-5*: 10±7), suggesting that PAD-1 and TAT-5 are not required for the formation of intraluminal vesicles. Given that intraluminal vesicles have the same budding topology as microvesicles and that there is no increase in intraluminal vesicle number, PAD-1 and TAT-5 are likely to have different functions at the plasma membrane and on endosomal membranes. Therefore, we predict that MON-2, PAD-1, and TAT-5 regulate an intracellular trafficking pathway that impacts late endosome size.

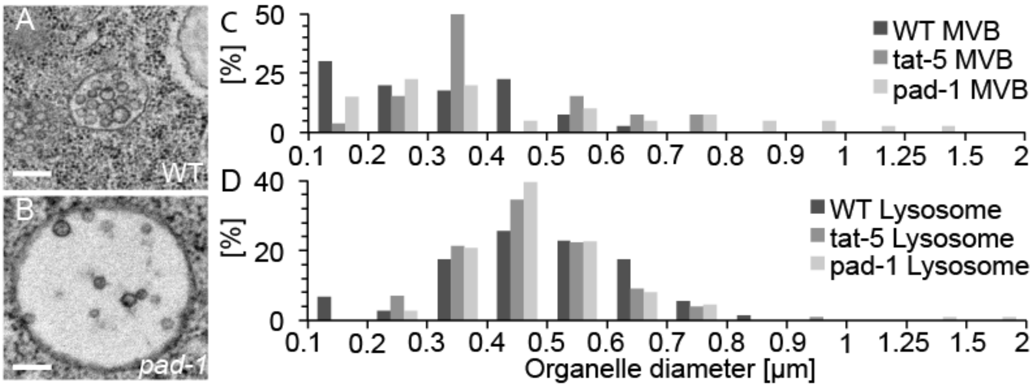

Fig. 18: Late endosomes are enlarged in *tat-5* and *pad-1* mutants. A-C) Multivesicular bodies (MVB) are significantly enlarged after *pad-1* or *tat-5* knockdown, as shown by electron micrographs and a histogram of MVB diameter (n=40 MVBs from 5 N2 and *pad-1* RNAi-treated embryos, $p<0.01$, n=26 MVBs from *tat-5* RNAi-treated embryos, $p<0.05$). D) Electron-dense lysosomes are not significantly enlarged after *pad-1* or *tat-5* knockdown, as shown by a histogram of lysosome diameter (n>70 lysosomes from 5 N2, *pad-1* RNAi, and *tat-5* RNAi embryos, $p>0.05$). One tailed Student's t-test with Bonferroni correction was used for statistical analysis. Image from Beer *et al*., PNAS 2018[50].

5.2.11. MON-2 and SNX prevent the missorting of TAT-5 into late endosomes

Given the mislocalization of TAT-5 to enlarged vesicles (Fig. 16) and the observation of enlarged LMP-1-positive multivesicular endosomes (Fig. 18), we wondered whether TAT-5 was mislocalized to the enlarged multivesicular endosomes in *mon-2* sorting nexin double mutants. Therefore, we characterized the enlarged GFP::TAT-5 vesicles in *mon-2* mutants treated with *snx-6* RNAi with a panel of endosomal markers. We first tested whether TAT-5 was mislocalized to early endosomes using a tandem PI3P-binding domain of EEA-1 (2xFYVE)[76]. GFP::TAT-5 showed minor colocalization with mCherry-tagged 2xFYVE in control embryos (Fig. 19A, C), which was not increased in *mon-2* mutants treated with *snx-6* RNAi (Fig. 19B-C), confirming that TAT-5 is not mislocalized to early endosomes. Furthermore, the large TAT-5 vesicles in *mon-2 snx-6* mutants were not often PI3P-positive (Fig. 19B, Fig. 20G), suggesting that these are not early endosomes.

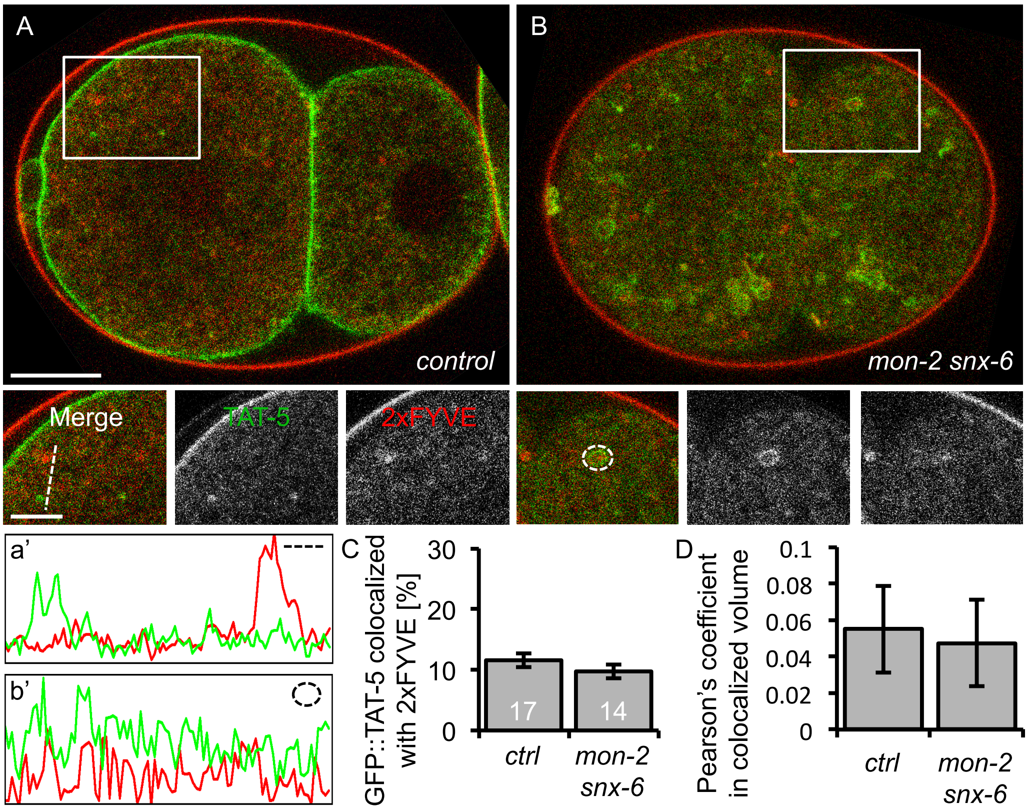
A
B
control
mon-2 snx-6
Merge
TAT-5
2xFYVE
a'
b'
C
GFP::TAT-5 colocalized with 2xFYVE [%]
30
20
10
0
17
14
ctrl
mon-2 snx-6
D
Pearson's coefficient in colocalized volume
0.1
0.08
0.06
0.04
0.02
0
ctrl
mon-2 snx-6

Fig. 19: GFP::TAT-5 does not accumulate in early endosomes in *mon-2 snx-6* mutants. A) Confocal images of GFP::TAT-5 localizing primarily to the plasma membrane in a live 2-cell control embryo. GFP::TAT-5 is also found on cytoplasmic vesicles, but they do not often colocalize with mCherry::2xFYVE, as shown in the insets. B) Mislocalization of TAT-5 to large vesicles in *mon-2* mutants treated with *snx-6* RNAi does not increase colocalization with 2xFYVE. A'-B') Line scans of GFP::TAT-5 and 2xFYVE intensity next to the dotted lines or circle in insets. C) The percentage of TAT-5 colocalized with 2xFYVE is not increased in 2- to 12-cell *mon-2* mutant embryos after *snx-6* RNAi compared to control embryos. Number of embryos scored is indicated for each genotype. D) The Pearson's coefficient of GFP::TAT-5 colocalization with 2xFYVE does not change in *mon-2(xh22)* mutants treated with *snx-6* RNAi. Image from Beer *et al.*, PNAS 2018[50].

We next asked whether TAT-5 localized to late endosomes or lysosomes using the LMP-1 antibody in *mon-2* mutants treated with *snx-6* RNAi. GFP::TAT-5 rarely colocalized with LMP-1 staining in control embryos (Fig. 20B) and the Pearson's coefficient showed a negative correlation (Fig. 20C). In contrast, GFP::TAT-5 showed a significant 2- to 3-fold increase in colocalization with LMP-1 in *mon-2* mutants treated with *snx-6* RNAi (Fig. 20A-B). Indeed, the Pearson's coefficient showed a positive correlation (Fig. 20C), indicating that more TAT-5 localized to late endosomes or lysosomes. The large GFP::TAT-5-containing vesicles found in *mon-2* mutants treated with *snx* RNAi frequently have LMP-1-positive subdomains (Fig. 20a’,G), which in combination with the TEM analysis of late endosomes and lysosomes (Fig. 18G-J) suggests that TAT-5 is mislocalized to late endosomes in *mon-2* mutants treated with *snx-6* RNAi.

To confirm that TAT-5 is mislocalized to late endosomes, we tested whether TAT-5 colocalizes with the Rab2 homolog UNC-108, which is found on the Golgi and is recruited to endosomes after early endosome markers, such as RAB-5 and PI3P, but acts before late endosome markers, such as RAB-7[77,78]. GFP::TAT-5 colocalized with a subset of mCherry-tagged UNC-108 in control embryos, showing a positive Pearson’s coefficient (Fig. 20E-F). TAT-5 colocalization with UNC-108 increased in *mon-2* mutants treated with *snx-6* RNAi (Fig. 20D-E), although the Pearson's coefficient was not significantly increased (Fig. 20E). In contrast to LMP-1, the large TAT-5 vesicles were not often positive for UNC-108 (Fig. 20d’, G), suggesting that the enlarged endosomes have already progressed past the Rab2-positive stage. Together, these data demonstrate that TAT-5 is mislocalized to degradative compartments in trafficking mutants that cause increased MV release.

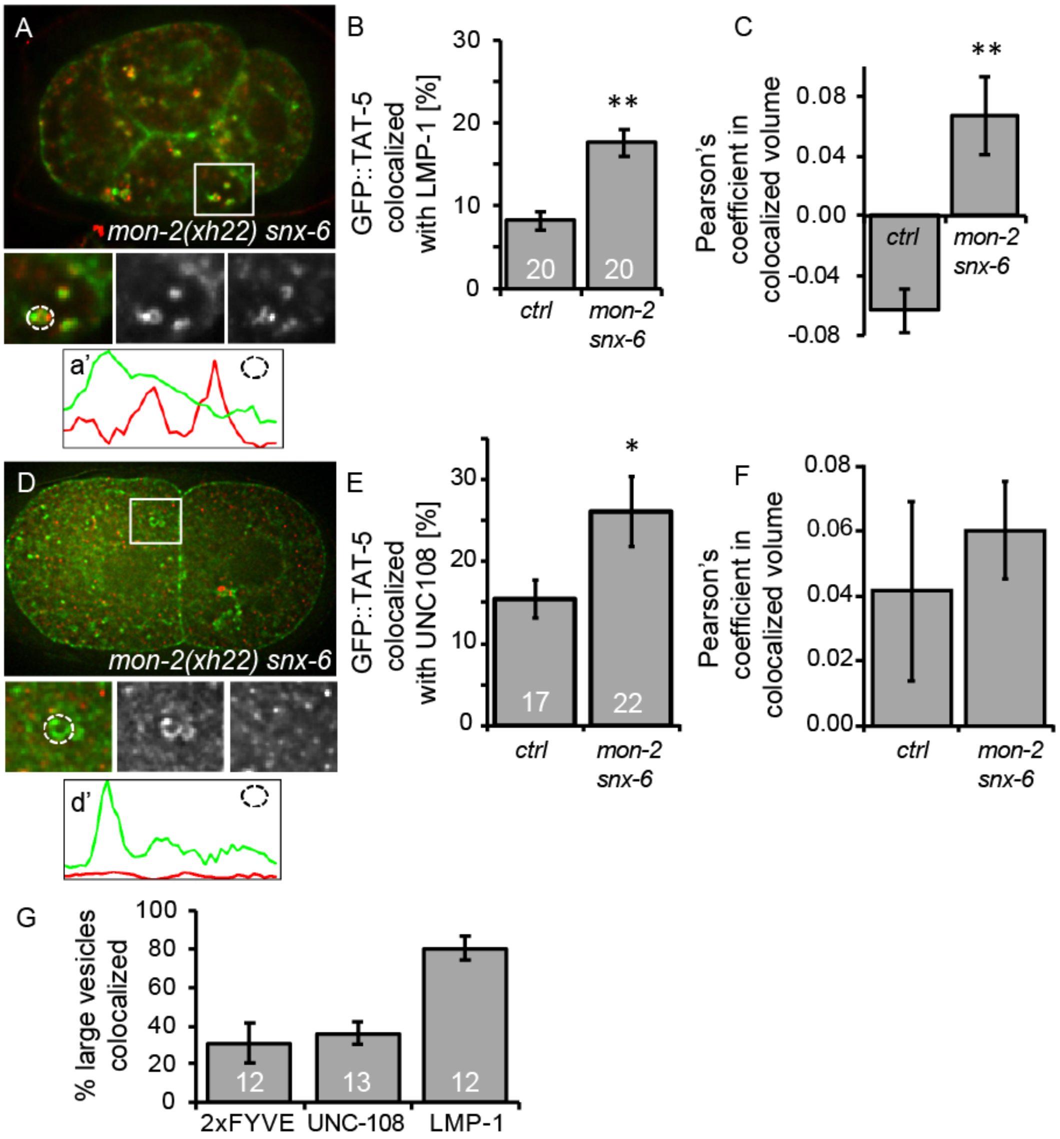

Fig. 20: TAT-5 localization to late endosomes increases in EV-releasing mutants. A) Large GFP::TAT-5-positive (green) cytoplasmic vesicles colocalize with LMP-1 in a *mon-2(xh22)* mutant embryo treated with *snx-6* RNAi. a') Line scan of GFP::TAT-5 and LMP-1 intensity next to the dotted lines or circle in insets. B) The percentage of TAT-5 colocalized with LMP-1 is significantly increased in 2- to 12-cell embryos in *mon-2(xh22)* mutants treated with *snx-6* RNAi compared to control embryos. Number of embryos scored is indicated for each genotype. C) The Pearson's coefficient of GFP::TAT-5 colocalization with LMP-1 increases significantly from a negative correlation in control embryos to a positive correlation. D) TAT-5 colocalization with UNC-108 increased slightly in *mon-2* mutants treated with *snx-6* RNAi. d') Line scan of GFP::TAT-5 and UNC-108 intensity next to the dotted lines or circle in insets. E) The percentage of TAT-5 colocalized with UNC-108 is significantly increased in 2- to 12-cell embryos in *mon-2(xh22)* mutants treated with *snx-6* RNAi compared to control embryos. Number of embryos scored is indicated for each genotype. F) The Pearson's coefficient of GFP::TAT-5 is not increased in *mon-2(xh22)* mutants treated with *snx-6* RNAi. G) Enlarged GFP::TAT-5 vesicles

colocalize significantly more often with LMP-1 (n=54 vesicles) than the PI3P reporter 2xFYVE (n=85) or UNC-108 (n=89). Percentages are expressed in relation to the total number of large vesicles. Number of embryos scored is indicated for each genotype. One-tailed Student's t-test with Bonferroni correction was used for statistical analysis (*p<0.05, **p<0.001). All images modified from Beer *et al.*, PNAS 2018[50].

To confirm that the size of TAT-5-positive late endosomes is controlled by MON-2 and PAD-1, we checked whether *snx-6* RNAi also causes enlarged LMP-1-positive structures. In contrast to *mon-2* or *pad-1* mutants (Fig. 8B,D,E), LMP-1-positive vesicles are not enlarged after *snx-6* knockdown in a wild type background (Fig. 21B), suggesting that the enlarged vesicles in double mutants are due to loss of MON-2 or PAD-1. This shows that MON-2, PAD-1, and TAT-5 act in a trafficking pathway that controls late endosome size independent of the SNX-1/6 pathway.

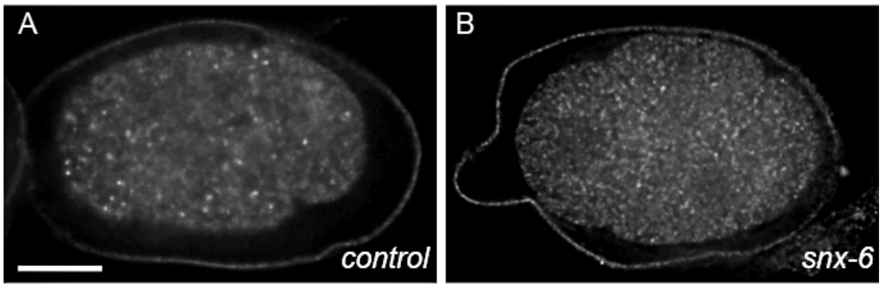

Fig. 21: SNX-6 is not required for late endosome size. A) Antibody staining shows small LMP-1-positive late endosomes or lysosomes in a 4-cell control embryo. B) LMP-1-positive vesicles are not enlarged in a 4-cell embryo after *snx-6* knockdown. Scale bar: 10 µm. Panel A from Beer *et al.*, PNAS 2018[50].

5.2.12. TAT-5 cannot maintain PE asymmetry on the plasma membrane when mislocalized to enlarged late endosomes

Although the TAT-5 ortholog Neo1p maintains plasma membrane asymmetry from some endosomes[79], we found that TAT-5 cannot maintain PE asymmetry from LMP-1-positive endolysosomes in *rme-8* mutants (Chapter 4 Fig 5A). Therefore, we tested whether PE is externalized when TAT-5 is mislocalized to enlarged LMP-1-positive late endosomes in *mon-2* mutants treated with *snx-6* RNAi. Knocking down *snx-6* in a *mon-2* mutant background significantly increased duramycin staining in comparison to untreated *mon-2* mutants (Fig. 22), demonstrating that PE is externalized when TAT-5 is mislocalized to late endosomes and EVs are released. We also observed that PE externalization was significantly decreased from control animals in untreated *mon-2* mutants, similar to *snx-6* RNAi, suggesting that MON-2 does influence PE asymmetry independent of SNX-6. However, it is worth noting that *mon-2* mutants treated with *snx-6* RNAi did not have significantly more PE externalization in comparison to wild type control embryos, suggesting that relative PE levels may be more relevant than absolute levels. Taken together, we propose that MON-2 and sorting nexins prevent TAT-5 trafficking to the degradative pathway, where TAT-5 would no longer be able to maintain plasma membrane PE asymmetry.

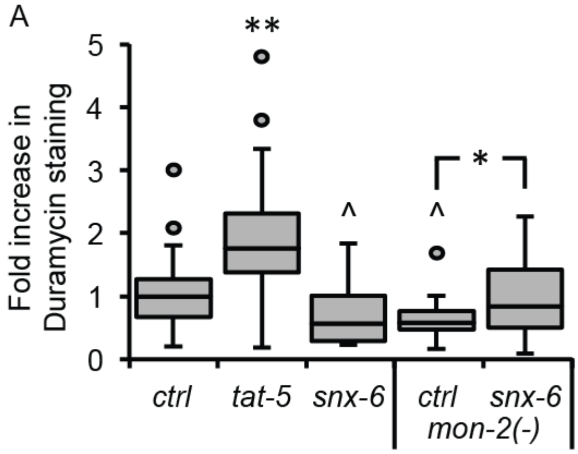

Fig. 22: MON-2 is required together with SNX-6 for TAT-5 flippase activity: A) PE-specific duramycin staining is significantly decreased after *snx-6* RNAi (n=27) and in untreated *mon-2(xh22)* mutants (n=20) (*ctrl*: n=54, *tat-5*: n=50). Duramycin staining is increased on dissected gonads after *snx-6* RNAi treatment in *mon-2(xh22)* nonsense mutants (n=34), in comparison to untreated *mon-2(xh22)* mutants, suggesting that TAT-5 is not able to maintain PE asymmetry from enlarged late endosomes. One-tailed Student's t-test with Bonferroni correction was used for statistical analysis (asterisks indicate significantly increased values: $^{**}p<0.001$, carets indicate significantly decreased values: $^{\wedge}p<0.05$). Image modified from Beer *et al.*, PNAS 2018[50].

5.2.13. PAD-1 is specifically necessary to maintain PE asymmetry

TAT-5 was released in MVs in *pad-1* mutants (Fig. 10A-B), similar to an ATPase-dead *tat-5* mutant[14]. Therefore, we tested whether PAD-1 is required for TAT-5 flippase activity to maintain PE asymmetry. In *pad-1* RNAi-treated worms, duramycin staining was increased on the surface of cells (Fig. 23A), indicating that PE is externalized and suggesting that PAD-1 is required for TAT-5 flippase activity. Moreover, duramycin staining was significantly increased after *pad-1* RNAi in comparison to *tat-5* RNAi (p<0.001), implying that PAD-1 could also regulate PE asymmetry through another protein in addition to TAT-5.

To determine whether PAD-1 is a specific cofactor for TAT-5, we tested whether PAD-1 was needed for the flippase activity of another P4-ATPase, TAT-1, which maintains PS on the plasma membrane[80]. Annexin V staining was not increased when PAD-1 was depleted, indicating that PS is not externalized (Fig. 23B). This shows that PAD-1 does not regulate the activity of the PS flippase TAT-1, suggesting that PAD-1 specifically controls TAT-5 flippase activity to maintain PE asymmetry in the plasma membrane.

Given that *mon-2* mutants had an opposite effect on PE externalization than *pad-1* mutants (Fig. 23A), we also tested whether MON-2 would influence the flipping activity of TAT-1 to maintain PS asymmetry. We saw neither a decrease nor an increase in Annexin V staining in *mon-2* mutants (Fig. 23B), suggesting that the lipid phosphatidylserine (PS) was not externalized more or less than in wild type. This suggests that MON-2 does not control PS asymmetry and specifically influences PE asymmetry, although opposite to PAD-1 and TAT-5.

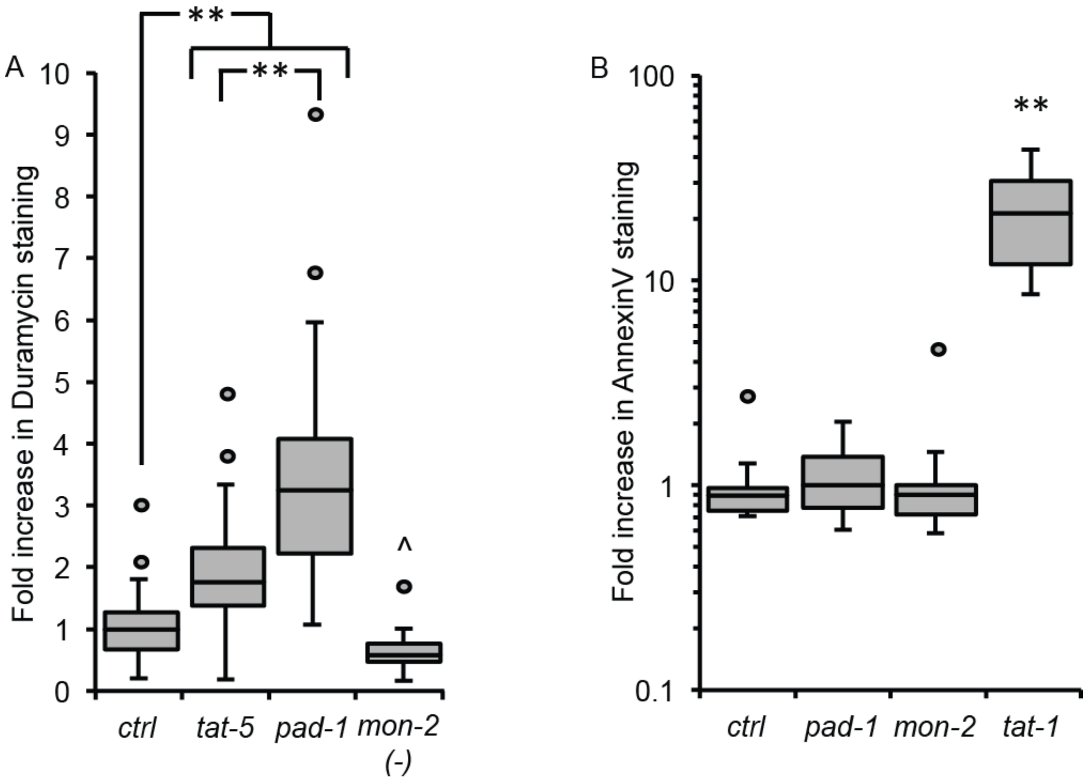

Fig. 23: PAD-1 is required to maintain PE asymmetry. A) PE-specific duramycin staining is significantly increased on dissected gonads after *pad-1* (n=36) or *tat-5* RNAi treatment (n=50), indicating that PAD-1 is required for TAT-5 to maintain PE asymmetry. The increase after *pad-1* RNAi is also significantly more than *tat-5* knockdown, suggesting that PAD-1 may influence PE asymmetry

through more than TAT-5 activity. Duramycin staining is significantly decreased in untreated *mon-2(xh22)* mutants (n=20). B) PS-specific Annexin V staining is not increased on dissected gonads after *pad-1* (n=33) or *mon-2* RNAi treatment (n=16) ($p>0.05$), indicating that PS is not externalized. Annexin V staining is strongly increased in *tat-1(kr15)* mutants (n=12), together indicating that PAD-1 and MON-2 are not required for TAT-1 PS flippase activity. One-tailed Student's t-test with Bonferroni correction was used for statistical analysis (asterisks indicate significantly increased values: **$p<0.001$, carets indicate significantly decreased values: ^$p<0.05$). Images modified from Beer *et al.*, PNAS 2018[50].

5.2.14. PAD-1 inhibits microvesicle release through the same pathway as TAT-5

As PAD-1 is required for TAT-5 PE flipping activity, we predicted that PAD-1 would regulate the same MV release pathway as TAT-5. The conserved Endosomal Sorting Complex Required for Transport (ESCRT)-complex proteins MVB-12 (ESCRT-I) and VPS-32 (ESCRT-III) are known to be recruited to the plasma membrane to bud MVs in *tat-5* mutants[14]. Therefore, we asked whether MVB-12 is recruited to the plasma membrane in *pad-1* mutants. In wild type cells, ESCRT proteins only transiently interact with bud sites[81]. To increase the visibility of ESCRT recruitment to the plasma membrane, we inhibited the final step of ESCRT-mediated scission by knocking down VPS-4. After *vps-4* RNAi treatment, a few GFP::MVB-12 puncta localized to the plasma membrane in control embryos, as reported previously[14,81]. After we treated worms with both *pad-1* and *vps-4* RNAi, we saw increased GFP::MVB-12 localization to the plasma membrane (Fig. 24B), similar to *tat-5 vps-4* RNAi[14]. Thus, PAD-1 regulates TAT-5 PE flipping activity to inhibit MV release by ESCRT-mediated ectocytosis.

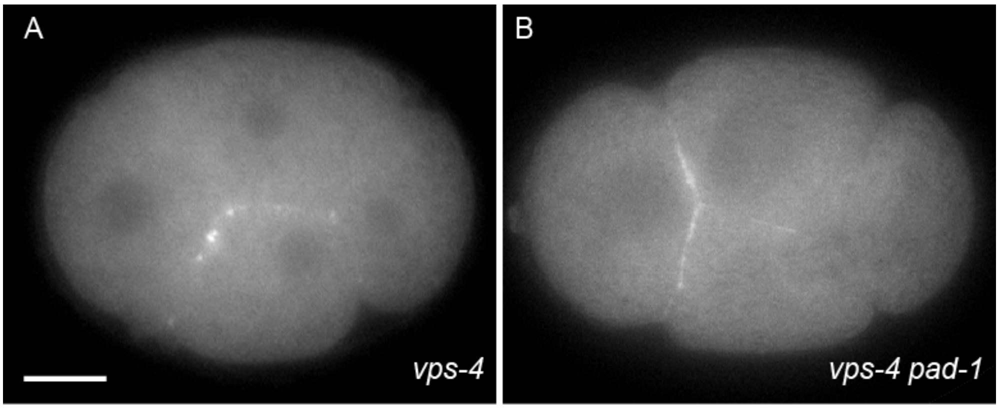

Fig. 24: PAD-1 inhibits ESCRT recruitment to the plasma membrane: A) The ESCRT-I reporter GFP::MVB-12 localizes to a few presumptive MV bud sites at the plasma membrane in a 4-cell embryo treated with *vps-4* RNAi in order to visualize the transient plasma membrane interactions of MVB-12.

B) Increased GFP::MVB-12 accumulates along the plasma membrane in an embryo depleted of both *pad-1* and *vps-4* (n=12), similar to *tat-5* and *vps-4* double depletion. Scale bar: 10 µm.

5.3. Discussion

In this chapter, we showed that PAD-1 and MON-2 have separable roles in protein trafficking and MV release. PAD-1 and MON-2 together regulate endosomal trafficking redundantly with the SNX-1/SNX-6 and SNX-3 trafficking pathways (Fig. 25A). They thereby prevent TAT-5 routing to the degradative pathway, allowing TAT-5 flippase activity to maintain PE asymmetry in the plasma membrane. Additionally, PAD-1 and MON-2 localize to the plasma membrane, where they could interact with TAT-5, but PAD-1 is required to maintain PE asymmetry and inhibit ESCRT-mediated microvesicle (MV) budding independent of MON-2 (Fig. 25B). Thus, our study reveals novel insights into the endosomal trafficking function of PAD-1 and MON-2 and proposes a new role for the understudied protein PAD-1 in regulating TAT-5 PE flipping activity, as well as providing further support for the hypothesis that PE asymmetry regulates ectocytosis.

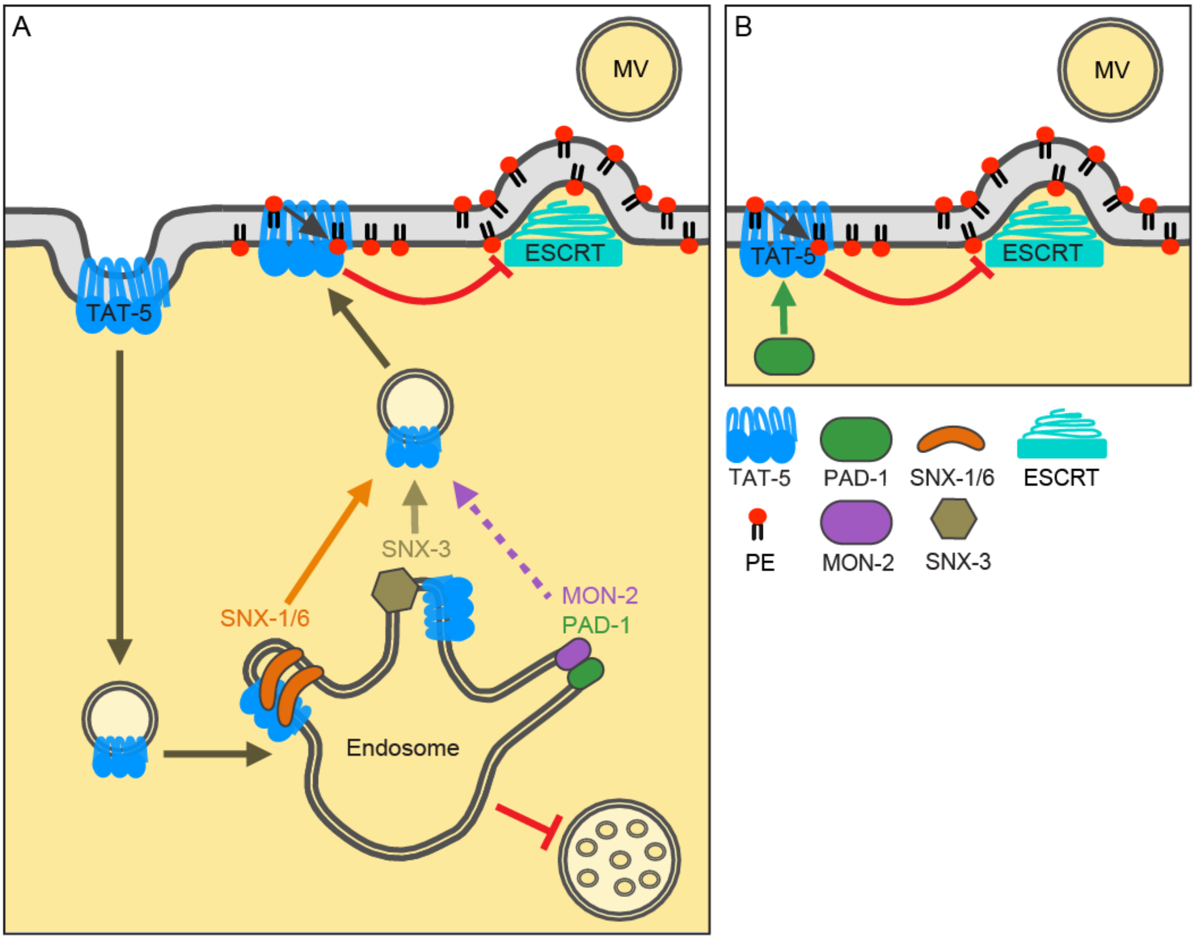

Fig. 25: Model of PAD-1 and MON-2 function. A) MON-2 and PAD-1 regulate an unknown step of endosomal trafficking, here drawn as a third recycling pathway preventing membrane cargos from being delivered to multivesicular endosomes for degradation. When both SNX-mediated recycling and MON-2/PAD-1-mediated trafficking are lost, TAT-5 is mislocalized to late endosomes where it can no longer maintain plasma membrane asymmetry. B) PAD-1 also localizes to the plasma membrane and is required for TAT-5 flippase activity, which inhibits the externalization of PE and ESCRT-mediated MV release.

5.3.1. The ubiquitous localization of PAD-1 suggests important functions in many cells

Although our study primarily focused on the role of PAD-1 in embryos, we found that endogenously tagged PAD-1 localized to many cells throughout development. In adults, we observed PAD-1 in numerous tissues including the excretory cell, intestine, germ line, and neurons. Several of these cell types have also been shown to release EVs outside *C. elegans* worms, including the excretory system and ciliated neurons[82,83]. We observed EV release in the distal germ line in *pad-1* mutants, suggesting that PAD-1 has a conserved role in embryos and germ cells. However, whether PAD-1 contributes to EV secretion from excretory cells, intestinal cells, or neurons remains open. As EV release occurs in all types of cells, we predict that PAD-1 will have a conserved role inhibiting MV release in many tissues. Furthermore, establishing an adult tissue in which to investigate the mechanisms of MV release could provide complementary advantages to our studies in the relatively inaccessible embryo.

PAD-1 was mostly found on cytosolic vesicles in adults and embryos, including cortical granules in oocytes. Cortical granules are secretory vesicles, whose fusion is regulated by fertilization to modify the extracellular space and prevent polyspermy[84]. The localization of PAD-1 and TAT-5 to these granules could mean that they have functions in the production or release of cortical granules. However, cortical granule dynamics do not appear to be disrupted after *tat-5* RNAi[14], suggesting that TAT-5 is not involved in their production, secretion, or compensatory endocytosis. However, whether PAD-1 is required needs to be determined, for example by examining CAV-1 dynamics. Alternatively, PAD-1 and TAT-5 could be put on cortical granules for their delivery to the plasma membrane at fertilization. Loss of lipid asymmetry is associated with cell-cell fusion[85,86], making it tempting to speculate that PAD-1 and TAT-5 levels are kept low at the oocyte plasma membrane to allow sperm-oocyte fusion. However, we observed plasma membrane-localized PAD-1 and TAT-5 prior to cortical granule secretion, suggesting that cortical granules are not the only source of TAT-5 and PAD-1 at the plasma membrane. Thus, the functions of PAD-1 and TAT-5 in cortical granules remain open.

Most of the cytosolic vesicles to which PAD-1 and MON-2 localize are not yet identified. Since PAD-1 and MON-2 orthologs were found on Golgi and endosomes in yeast and mammals[1,3,6,13], these are likely structures for PAD-1 and MON-2 to localize to. To analyze the intracellular localization of PAD-1 and MON-2, we plan a set of co-localization experiments to known reporters of the endolysosomal system, such as early endosome reporters RAB-5, EEA-1, UNC-108/Rab2, late endosome and lysosome reporter LMP-1 and the Golgi reporter α Mannosidase II (AMAN-2). Identifying the types of endosomes on which PAD-1 and MON-2 localize could provide new insights into their trafficking function.

PAD-1 and MON-2 also localize to subdomains of the plasma membrane in embryos and oocytes, although this localization was not reported for their orthologs in yeast and mammalian cells. However, TAT-5 orthologs were also not seen to localize to the plasma membrane [20,87], but surface biotinylation and fractionation experiments could prove that ATP9A is at least transiently on the plasma membrane[88,89]. Thus, it is possible that MON-2 and PAD-1 orthologs also localize to the plasma membrane transiently to interact with TAT-5 orthologs in other species.

Of note, although GFP::PAD-1 worms are viable and have normally-sized late endosomes, recent unpublished data from Dr. Gholamreza Fazeli shows that GFP::PAD-1 worms have defects in midbody remnant phagocytosis. Thus, although GFP::PAD-1 rescues the essential functions of PAD-1, this knock-in strain has defects that do not disrupt worm development. This suggests that the placement of GFP directly at the N-terminus of PAD-1 disrupts a subset of protein interactions. For example, the N-terminus of Dopey1 was recently shown to bind Kinesin1[55], and it will be interesting to test whether Kinesin1 binding is disrupted in the GFP::PAD-1 strain. Although these findings show the need to develop a fully functional fluorescently-tagged PAD-1 reporter or specific PAD-1 antibodies for further studies, they also define the GFP::PAD-1 allele as a partial loss-of-function allele, whose characterization will provide further insights into the distinct functions and functional interactions of the large scaffolding protein PAD-1.

5.3.2. Potential conserved neural functions of PAD-1 and TAT-5 orthologs

The high levels of PAD-1 in neurons is provocative, because expression of its orthologs DOPEY1 and DOPEY2 is also highly enriched in nerve cells from rats or mice[7,13]. Neurons from many animals release EVs[90], suggesting that a function for PAD-1 in EV release could be conserved in neurons. Furthermore, since the TAT-5 ortholog ATP9A was found to inhibit EV release from mammalian cells[89], it is likely that the MV inhibitory function of PAD-1 is also conserved in mammalian orthologs.

As oligodendrocytes release EVs to inhibit myelination and oligodendrocyte differentiation[91], it will be interesting to test whether the VF rat shows increased MV release. VF rats have a nonsense mutation in DOPEY1 and reduced myelination[13,22], which could be an effect of increased release of EVs. Reexamination of electron micrographs from VF rat brain tissue[13] could answer whether EV release is increased in DOPEY1 mutant brains. Furthermore, EVs can be extracted from spinal fluid and quantified[92], which would demonstrate whether DOPEY1 also inhibits MV release. *C. elegans* neurons are not myelinated[93,94], but given the tremor and enlarged vacuole phenotypes of VF rats[13,22], it would be interesting to test the sterile *pad-1* mutant strains for behavioral phenotypes. Thus, using *C. elegans* as a model system could help to better understand the role of EVs in the mammalian nervous system.

It will also be interesting to test whether DOPEY2-overexpressing mice have reduced MV release. In humans, DOPEY2 expression was increased in Down syndrome patients with chromosome 21 trisomy[25], but EV release from Down syndrome brain tissue was elevated[95]. Mice overexpressing DOPEY2 have mild cognition defects[7,25], suggesting that DOPEY2 may contribute to some of the mental retardation phenotypes of Down syndrome patients, but the levels of EV release have not yet been examined. Interestingly, EV release is thought to reduce the enlarged endosomal pathologies of Down syndrome fibroblasts *in vitro*[95], suggesting that reduced EV release could worsen some pathologies of Down syndrome patients. Thus, studying the function of PAD-1 and its orthologs in brain development could tell us more about the role and release mechanisms of MVs in neural cells. In the long run, they could also offer new understanding and treatment opportunities for people with Down syndrome.

5.3.3. TAT-5, PAD-1, and MON-2 are likely to form a complex in *C. elegans*

We believe that PAD-1 and MON-2 are likely to form a complex with TAT-5, given their similar localization, functions, and data from other orthologs. GFP::PAD-1 and MON-2::GFP were found on the plasma membrane of embryos, similar to GFP::TAT-5[14]. In HeLa cells, MON2, DOPEY2 and ATP9A were found on the same cellular vesicles using fluorescence microscopy and all three proteins were able to co-immunoprecipitate one another[3]. Biochemical studies from yeast showed that Dop1 and Mon2 physically interact and co-purify Neo1[2], showing that the three proteins can form a complex. As we saw joint functions of MON-2 and PAD-1 in TAT-5 trafficking, we propose that the three proteins may also form a complex in *C. elegans*.

Interestingly, GFP::PAD-1 and MON-2::GFP localize to subdomains of the plasma membrane, while GFP::TAT-5 appears more uniform on the plasma membrane[14]. The GFP::TAT-5 construct is expressed from a *pie-1* promotor which drives strong expression from multi-copy insertions in the adult germ line[96,97]. Thus, *gfp::tat-5* expression is likely to be higher than wild type *tat-5* mRNA. To clarify whether TAT-5 localizes more broadly on the plasma membrane than MON-2 and PAD-1, it will be necessary to determine TAT-5 subcellular localization using a knock-in allele or a specific antibody.

Besides forming a heterotrimeric complex, more diverse interactions of MON-2, PAD-1, and TAT-5 proteins are also possible. As mammalian ATP9A could not co-immunoprecipitate MON2 without DOPEY1[3], and yeast Mon2 is not required for Dop1 to co-purify Neo1[2], it is also possible that TAT-5 and PAD-1 can form a complex without MON-2. In yeast, approximately 50% of Dop1 colocalized with Mon2, suggesting that Dop1 is not always in a complex with Mon2[1]. Since we observed MON-2-independent functions of PAD-1 on inhibiting MV release and TAT-5 PE flipping activity, we postulate that a subpopulation of PAD-1 forms a complex with TAT-5 independent of MON-2. To determine how often and where PAD-1 and TAT-5 colocalize without MON-2, quantitative multi-color high-resolution imaging of endogenously tagged proteins is required.

Recently, Mahajan *et al.* reported that MON2 is required for DOPEY1 dimerization, which is one redundant signal necessary for DOPEY1 association to Golgi membranes[55]. Similarly, Mon2 was required to recruit Dop1 to the Golgi in yeast[6,10]. This suggests that the interaction of PAD-1 and MON-2 could promote PAD-1 dimerization and be important for PAD-1 recruitment to specific membranes. These data also raise the possibility that MON2 and DOPEY1 form a complex and carry out functions without ATP9A.

The small GTPase Arl1 is also linked to the Neo1/Dop1/Mon2 complex in yeast and mammals[2]. Mon2 and Dop1 interact with Arl1, and Arl1 was required for the interaction of Dop1 to Neo1[2,10,28]. However, *arl-1* knockdown did not show increased MV release, unlike *pad-1* or *tat-5* knockdown. In yeast, Arl1 is required for Neo1 localization to the Golgi[10]. However, we did not find an effect of ARL-1 on GFP::TAT-5 plasma membrane localization. Nevertheless, ARL-1 could be like MON-2 in that its trafficking role is only revealed when sorting nexins are disrupted. Thus, it will be interesting to analyze TAT-5 localization in *arl-1 snx* double mutants to check whether ARL-1 has a similar trafficking function as PAD-1 and MON-2. Checking for enlarged LMP-1-positive endolysosomes in *arl-1* mutants would also provide evidence that ARL-1 acts similar to MON-2. These experiments could demonstrate whether ARL-1 is part of the MON-2/PAD-1 trafficking pathway.

5.3.4. PAD-1 likely maintains PE asymmetry and microvesicle release through TAT-5

We showed that the essential proteins TAT-5 and PAD-1 control MV release and maintain PE asymmetry, unlike the non-essential protein MON-2. Thus, we propose that the PE flipping activity of TAT-5 is the essential biochemical function of the complex. As PAD-1 has no ATP-binding cassette (ABC) or P4-ATPase domains associated with lipid transport (Fig. 26)[4,98], it is unlikely that PAD-1 can promote PE translocation autonomously. Since PAD-1 localizes to the same structures as TAT-5, we propose that PAD-1 is required for the PE flipping activity of TAT-5. To test this possibility, it is necessary to know how PAD-1 interacts with TAT-5 (potential regions are discussed in 5.3.5.). These binding sites should then be mutated. If PAD-1 interaction with TAT-5 was required for TAT-5 PE flipping activity, we would expect increased PE externalization from such a PAD-1 mutant.

PAD-1 is also likely to interact with proteins beyond TAT-5 to regulate lipid asymmetry and inhibit EV release. The duramycin staining for PE after *pad-1* RNAi was significantly higher than after *tat-5* RNAi, suggesting that PAD-1 may be required for the activity of another PE flippase. TAT-5 is 89% similar with TAT-6, which was thought to have developed by a recent TAT-5 gene duplication[11]. For example, only *C. brenneri* has both a TAT-5 and a TAT-6 ortholog, while other closely related Caenorhabditis species *C. briggsae, C. remanei* or *C. japonica* only have TAT-5 (Wormbase[45], accessed Oct 2019). Thus, PAD-1 could also regulate TAT-6 activity. However, it first needs to be proven that TAT-6 is expressed in the gonads of adult worms, where we measured PE externalization. TAT-6 expression is low, peaking at early larval stages and in dauer larvae (WormBase[45], accessed Sept 2019), when the germ line is only a few cells, suggesting it is likely to act in a subset of somatic cells. However, it would be interesting to test whether TAT-6 is upregulated in *tat-5* mutants as a form of genetic compensation[99]. Thus, *pad-1* mutants may have more PE externalized because they may be equivalent to *tat-5; tat-6* double mutants.

PAD-1 could also interact with the PS flippase TAT-1. Drs2, the yeast ortholog of TAT-1, has been shown to mostly flip PS, but can also flip PE *in vitro*. TAT-1 is unlikely to flip large amounts of PE, since PE externalization was not increased in *tat-1* mutants[14]. However, it is possible that TAT-1 can flip PE and might counteract PE externalization in *tat-5* mutants. Therefore, as TAT-1 and TAT-5 are 51% similar in sequence, TAT-1 could be regulated by PAD-1. However, we did not observe an increase in PS externalization after *pad-1* knock down, making it unlikely that PAD-1 normally activates TAT-1. Thus, PAD-1 could only be expected to activate TAT-1 in the absence of TAT-5.

PAD-1 could also interact with other P4-ATPases, including TAT-2, TAT-3, and TAT-4. The substrate of TAT-2 is unclear, but TAT-2 is homologous to the mammalian PS flippase ATP8B[11], which can flip PS, PC and PE to a lesser extent[100,101]. TAT-3 and TAT-4 are the orthologs of mammalian ATP10[11], which was reported to translocate PC[102]. However, since no one has tested whether PAD-1 or even TAT-5 regulate PC translocation, it remains possible that PAD-1 is required for TAT-3 and TAT-4 activity. Thus, PAD-1 could activate other P4-ATPases that can flip PE and TAT-5 could flip other lipids in addition to PE.

On the other hand, PAD-1 may inhibit an unidentified PE scramblase that causes PE externalization. So far, it is unclear which protein would be the scramblase opposing the PE internalization activity of TAT-5. Any1 (also called Cfs1p) is a PQ-loop membrane protein in yeast, which is thought to be either the opposing scramblase of Neo1 or a Neo1 activity inhibitor[103–105]. Any1 was also shown to physically interact with Dop1[106], and loss of Any1 suppresses the growth defects of Neo1, Mon2 and Dop1 mutants[103,105]. Based on sequence homology, there is one putative homolog of Any1 in worms, T19A6.1. Thus, it should be tested whether T19A6.1 depletion can inhibit PE externalization and MV budding in *tat-5* or *pad-1* mutants. Thus, as lipid externalization is normally caused by both inhibition of the flippase and activation of the scramblase[107,108], we propose that PAD-1 could inhibit MV release by both activating the PE flippase and inhibiting the counteracting scramblase.

5.3.5. MON-2 could disrupt PE asymmetry to induce microvesicle release

Finding the proteins that oppose TAT-5 flippase activity and promote MV release will be key to understand the mechanisms that regulate ectocytosis. Human Mon2 is required for HIV budding[41], which bud from the plasma membrane using the ESCRT complex like MVs [109]. Thus, MON-2 would be expected to be an activator of ectocytosis, possibly by promoting PE externalization. The decrease in PE externalization after *mon-2* depletion could suggest that MON-2 is required to inactivate TAT-5 or that MON-2 may enhance the activity of an opposing scramblase. Nevertheless, we show that loss of *mon-2* could not disrupt EV release after *pad-1* RNAi (Table 1), suggesting that either redundant budding activators exist or that MON-2 is not an activator of MV release. On the other hand, MON-2 could regulate TAT-5 through PAD-1. For example, MON-2 could induce PE externalization by disrupting PAD-1's ability to activate the flippase activity of TAT-5. This could be accomplished by redirecting PAD-1 to another membrane compartment, consistent with MON2's role in regulating Dopey1 Golgi recruitment[6,55]. Thus, the role of MON-2 on disrupting PE asymmetry and regulating MV release is still unclear, but we predict that it would be through regulating PAD-1 and its interaction with TAT-5.

5.3.6. Molecular interactions of PAD-1

If PAD-1 maintains PE asymmetry by activating TAT-5 flippase activity, then it needs to have specific interactions with TAT-5. PAD-1 appears mostly unstructured, consisting of several Armadillo-type folds, which form protein-binding platforms[110], and conserved N- and C-terminal domains of unknown function. Based on the Armadillo folds, PAD-1 is likely to be a scaffold involved in protein-protein binding. A large internal fragment of Dop1 can bind Neo1 in yeast[2], suggesting that the TAT-5 binding site is not in the conserved N- or C-term of PAD-1, but in an internal region between aa 551-1759 (Fig. 26). Interestingly, a similar region of Dopey1 also binds Mon2 in mammalian cells[55], corresponding to aa 804-1130 in PAD-1. Thus, it will be important to narrow down this region to see whether MON-2 and TAT-5 bind PAD-1 at neighboring or overlapping sites, which could bring further insight into their cooperative or antagonistic roles.

The proper localization and flippase activity of the non-essential P4-ATPases is regulated by CDC50 family proteins, which are transmembrane proteins with a large extracellular domain that forms a tight complex with the P4-ATPase[111,112]. However, CDC50 proteins are not required for the localization or activity of the essential P4-ATPases, i.e. TAT-5 and its orthologs in yeast and mammals[50,100,113]. Furthermore, PAD-1 does not share any sequence homology with CDC50 proteins, suggesting that PAD-1 would regulate TAT-5 PE flipping activity through a different mechanism.

Although the name-giving Dopey domain at the N-terminus of PAD-1 orthologs Dop1 and Dopey1/2 is not within the predicted TAT-5 interaction region (Fig. 26)[2,4], its high conservation suggests a conserved function, which may still impact TAT-5 activity. Recent studies showed that the extreme N-terminus is required for Dopey1 to interact with the kinesin1 subunit KLC[55], corresponding to aa 1-153 in PAD-1 (Fig. 26). From our CRISPR/Cas9 results, we can conclude that at least the first 8 aa are not likely to be required for TAT-5 activity, as in-frame indels did not alter viability or fertility. The KLC-binding region contains a conserved EWAD sequence found at aa 38-41 of PAD-1 (Fig. 26), which is required for KLC binding to Dopey1[55]. Mutating this motif in PAD-1 would provide insight into whether KLC-binding is required for PAD-1's inhibition of PE externalization, MV budding, and lysosome enlargement, as well as PAD-1's role in phagocytosis.

Modeling PAD-1 in a structure prediction program (Phyre2) suggested that most of the protein is unstructured, but aa 84-256 of the Dopey domain appear similar to a microtubule-binding Tog domain (Fig. 26). Although this remains to be confirmed experimentally, it suggests that the conserved Dopey domain may consist of multiple protein-binding regions that coordinate PAD-1 interactors, such as the microtubule motor protein kinesin and tubulin. Therefore, it will be interesting to test whether the Dopey domain of PAD-1 is required for TAT-5 activity and/or PAD-1 localization by deleting the Dopey domain or creating Dopey-only *pad-1* mutant. Alternatively, the Dopey domain may only be important for the endosomal roles of PAD-1, for example by using microtubule motors to promote endosome tubulation. In summary, there are many open questions when it comes to the molecular mechanism by which PAD-1 could activate TAT-5.

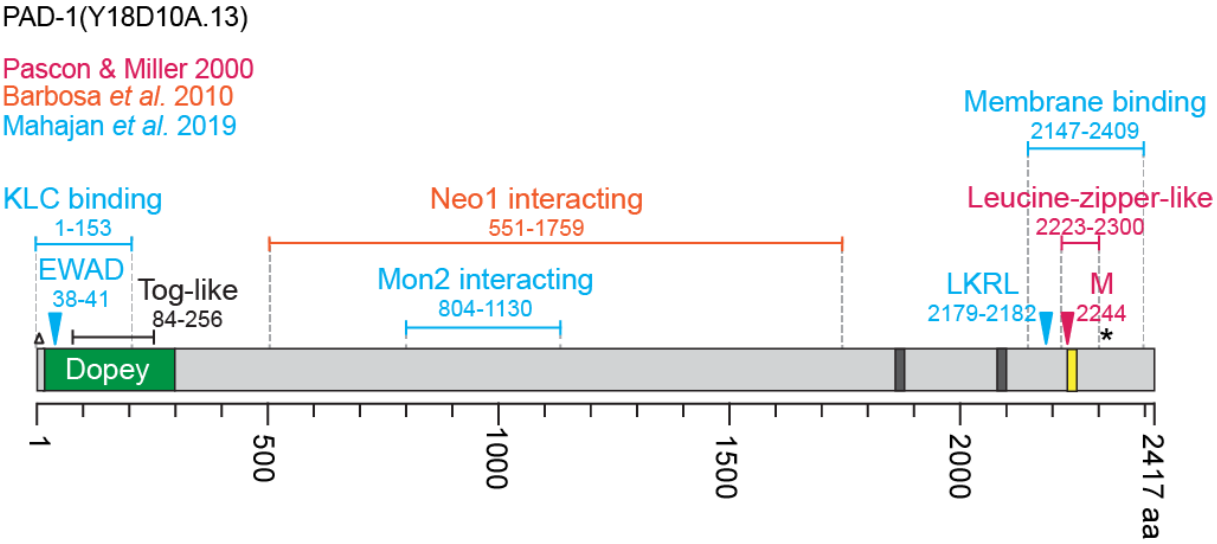
PAD-1(Y18D10A.13)
Pascon & Miller 2000
Barbosa et al. 2010
Mahajan et al. 2019
Membrane binding
2147-2409
KLC binding
1-153
Neo1 interacting
551-1759
Leucine-zipper-like
2223-2300
EWAD
38-41
Tog-like
84-256
Mon2 interacting
804-1130
LKRL
2179-2182
M
2244
*
Dopey
1
500
1000
1500
2000
2417 aa

Fig. 26 : Model of PAD-1 protein domains: PAD-1 contains a highly conserved Dopey domain labelled in green at the N-term(16-301 aa), based on InterPro[8]. The Dopey domain also includes a region that looks like a Tog domain (84-256 aa), based on Phyre2 models of PAD-1[114]. The first 15 aa do not belong to the conserved Dopey domain and in-frame mutations at aa 4-8 (small triangle) are viable and fertile, suggesting that this region is not required for essential PAD-1 functions. The internal and C-terminal segment appear largely unstructured (light grey). Phobius predicts two putative transmembrane domains (dark grey, 1870-1891 aa and 2087-2104 aa) and a coiled-coil structure (yellow, 2245-2265 aa)[115]. The function of ortholog sequences are labeled as the corresponding fragments in PAD-1 (red DopA: Pascon and Miller 2000, orange Dop1: Barbosa *et al.* 2010, blue Dopey1: Mahajan *et al.* 2019). Amino acid numbers of the corresponding PAD-1 sequence were determined using the Needleman-Wunsch algorithm in Needle (EMBOSS). The conserved EWAD sequence is required for KLC binding. The conserved LKRL motif is required for binding PI4P-containing membranes. The temperature-sensitive DopA mutant from *A. nidulans* (I1695R) hits a conserved region of eight putative leucine-zippers. The corresponding M^{2244} is indicated. The VF rat mutant has a stop codon in the predicted membrane-binding region. The corresponding position of PAD-1 at aa 2305 is indicated (*).

5.3.7. Potential mechanisms of PAD-1 localization to membranes

PAD-1 localizes to the plasma membrane and intracellular vesicles, but its mechanisms of membrane association are unclear. It is debated whether PAD-1 and its orthologs have a transmembrane (TM) domain. The first report about the structure of DopA, the PAD-1 ortholog in *Aspergillus nidulans*, suggested that short hydrophobic residues in the C-term form a putative TM domain[4]. They showed that this region was conserved in *Saccharomyces* yeast Dop1, but not in *Candida* yeast or animal orthologs. It was also reported that human DOPEY2 has 9 TM domains and PAD-1 has 13 TM domains using Tmpred[5]. However, when we searched for TM domains in PAD-1, Phobius only proposed two putative transmembrane domains (Fig. 26)[115]. In contrast, Efe *et al.* reported that yeast Dop1 was found in the P100 high-speed pellet after subcellular fractionation, suggesting that Dop1 has no putative TM domain, but peripherally associates with membranes[1]. In addition, Dopey1 could be extracted in low detergent conditions, consistent with no TM domains[55]. We efficiently extracted GFP::PAD-1 after boiling, a method that caused aggregation of TAT-5 and other transmembrane proteins. Thus, the experimental evidence suggests that PAD-1 is a peripheral membrane protein, not a transmembrane protein.

PAD-1 could associate with membranes by binding lipids. Human Dopey1 can bind liposomes through its C-term[55], and Mahajan *et al.* discovered a conserved LKRL motif that mediates binding to PI4P-containing membranes (Fig. 26). Since PI4P is found on both the Golgi and the plasma membrane[116], it is possible that this motif is required for PAD-1 plasma membrane localization. Thus, it is important to test the localization and function of a LKRL mutant to determine whether this motif regulates PAD-1 localization or its ability to activate TAT-5.

As lipid-protein interactions tend to be weak, many membrane interactions require multiple lipid-binding domains or dimerization[117]. Dopey1 dimerization enhances localization to membranes, which was increased by Mon2 binding[55]. Dimerization of yeast Dop1 was also detected and depended on the C-terminus[2], which contains a conserved leucine-zipper-like coiled coil structure proposed to be required for dimerization (Fig. 26)[4]. In yeast, Mon-2 and Arl1 were required for the intracellular localization of Dop1[6], probably because Arl1 can stabilize the interaction of Dop1 and Mon2[10]. Similarly, Mon2 was required for the Golgi localization of Dopey1 in human cells, but not of Dopey2[55]. We found that MON-2 was not required for PAD-1 plasma membrane localization, but have not tested whether it plays a role in its recruitment to other organelles. Thus, we predict that PAD-1 dimerization could be induced by MON-2 and ARL-1 to enhance its membrane association.

Interestingly, Pascon *et al.* studied a temperature sensitive DopA mutant in *Aspergillus nidulans* with a mutation in one amino acid of the conserved leucine-zippers. This Isoleucine (I^{1695}) is conserved in yeast and shifted to Methionine (M) in animals (M^{2244}, Fig. 26). As this motif is in the region required for Golgi localization and dimerization, it would be interesting to see if mutating M^{2244} affects the plasma membrane localization of PAD-1 and determine whether it alters the essential or non-essential roles of PAD-1.

The VF rat strain contains a nonsense mutation at the C-term that would remove the last 142 aa of the 2456 aa sequence of DOPEY1[13]. The mutated amino acid in rats is R^{2330}, which corresponds to H^{2305} in PAD-1. This would create a stop codon after the leucine zipper-like region, which is within the region identified as required for membrane binding in human DOPEY1 (Fig. 26)[4,55]. However, the expression and protein levels of DOPEY1 are strongly reduced in the VF rat[13], suggesting that the premature stop codon can affect DOPEY1 expression and/or protein stability, likely by nonsense-mediated decay[24]. Thus, it would be interesting to test whether a similar mutant in *C. elegans* has effects on PAD-1 localization and/or expression levels to get a better understanding about how the C-terminus regulates membrane localization and function.

It is worth noting that the C-terminus of PAD-1 is unlikely to be the only region important for membrane association. An internal fragment of Dop1 also localized to the TGN and endosomes (labeled "Neo1 interacting" in Fig. 26)[2], suggesting that the C-terminal coiled coil and PI4P-binding motif are not the only regions important for membrane association. Although we did not see any change to PAD-1 plasma membrane recruitment in *tat-5* or *mon-2* mutants, it remains possible that binding TAT-5 or MON-2 is one of several redundant localization mechanisms. Thus, there are likely to be multiple regions required for the membrane localization of PAD-1.

5.3.8. PAD-1 and MON-2 as endosomal trafficking regulators

We have shown that PAD-1 and MON-2 control an endosomal trafficking pathway, consistent with their proposed function in the retrograde trafficking pathway from sorting endosomes to the TGN (introduced in 5.1.)[1,6,17]. We know that TAT-5 is not normally a cargo of MON-2 and PAD-1 trafficking, as MON-2 and PAD-1 are not required for TAT-5 plasma membrane localization. However, MON-2 and PAD-1 can rescue TAT-5 from being sorted into the degradative pathway in sorting nexin mutants, as TAT-5 accumulated in late endosomes in *mon-2 snx* or *pad-1 snx* double mutants. Thus, we propose that the early steps of intracellular trafficking like endocytosis and recycling endosome formation are not disrupted in PAD-1 and MON-2 mutants. This suggests that MON-2 and PAD-1 are likely to act on sorting endosomes.

Our primary model is that PAD-1 and MON-2 provide a redundant endosomal recycling pathway alongside SNX-1/SNX-6 and SNX-3 (Fig. 25A). In this case, the MON-2/PAD-1 recycling pathway could have specific cargos (potential cargos are discussed in 5.3.10.), it could be a bulk recycling pathway with no cargo specificity, or it could promote recycling by all pathways. Determining the molecular functions of MON-2 and PAD-1 will be key to understanding their cellular role.

MON-2 and PAD-1 were recently proposed to be part of the SNX-3 retrograde pathway. It was shown that *C. elegans* and human MON-2/Mon2 and PAD-1/Dopey2 interact with SNX3 and control the retrograde trafficking of Wntless[3]. Loss of MON-2 and PAD-1 caused disruptions in Q-cell migration, a model used to study Wntless secretion in *C. elegans.* However, defects were only seen in a sensitized background where retromer trafficking is disrupted. These data are equally consistent with MON-2 and PAD-1 providing a redundant endosomal recycling pathway alongside the retromer. We find that PAD-1 and MON-2 are unlikely to be part of the SNX-3 trafficking pathway, as MON-2 redundantly regulates MV budding with SNX-3. MON-2 also redundantly regulates MV budding with SNX-1/6, suggesting that MON-2 and PAD-1 are also not part of the SNX-1/6 pathway. Thus, we propose that PAD-1 and MON-2 regulate a trafficking pathway independent of SNX-1/-6, SNX-3, and retromer.

For example, MON-2 and PAD-1 could act in the SNX-FERM trafficking pathway. Our preliminary results showed that SNX-17 and SNX-27 can redundantly inhibit MV release with SNX-1/-6 and SNX-3, but not redundantly with MON-2. Thus, it is possible that MON-2 and PAD-1 act in the SNX-17 and SNX-27-mediated trafficking pathways, but this preliminary hypothesis requires further investigation.

Alternatively, PAD-1 and MON-2 may regulate bulk recycling or general steps of all endosomal trafficking pathways. Consistent with this idea, late endosomes are enlarged after loss of PAD-1 and MON-2, suggesting that there is a significant increase in flux to degradative pathways, which could be due to a large decrease in recycling. To test this idea, it will be necessary to perform flux assays by extracellular labeling of receptors or by synchronizing cargo with approaches like the RUSH (Retention Using Selective Hooks) system[118]. Thus, MON-2 and PAD-1 may have specific or general roles in trafficking.

There are a number of molecular observations that could suggest that MON-2 and PAD-1 could promote general recycling or support multiple trafficking pathways. For example, Mon2 regulates F-actin projections in Drosophila by serving as a scaffold for actin regulators[62]. Actin is required at endosomal membranes for endosome biogenesis, tubulation and protein sorting[39]. Actin is rapidly turned over within 20 sec on endosomal membranes showing that actin is dynamically assembled[119]. When actin dynamics are disrupted, it causes enlarged dysfunctional endosomes [39]. To test whether altered endosomal actin dynamics cause the enlarged late endosomes in *mon-2* mutants, we should observe the localization of actin regulators and actin-binding proteins like Moesin and the F-actin to membrane protein linker ERM-1 on *mon-2* mutant endosomes. In the future, it would also be interesting to analyze the localization of components of the conserved Wiskott-Aldrich Syndrome protein and SCAR Homolog (WASH) complex, which is the major activator of Arp2/3-dependent actin polymerization on endosomes. WASH and Arp2/3 were shown to be required to reduce the size of endosomes by inducing the tubulation and fission of endosomes[120,121]. Thus, MON-2 may be required for actin dynamics to promote the formation of recycling vesicles.

Furthermore, a recent study in mammalian cells showed that Dopey1 and Mon2 act as a link between membranes and the minus-end-directed motor protein kinesin 1, which is required for the centrifugal movement of organelles along microtubules [55]. Microtubules are also thought to help to extend endosomal tubules to create recycling vesicles [122–124]. Thus, PAD-1 and MON-2 may induce endosome tubulation by docking endosome membranes to both actin and microtubules.

In addition to acting as a scaffold, PAD-1 and MON-2 may also be able to promote membrane deformation to tubulate membranes. Multimers commonly have a role in membrane deformation, like BAR domain-containing proteins or clathrin[125]. Dop1 and Mon2 form dimers in yeast and P4-ATPases also form oligomers, including Neo1[1,2,55]. Thus, oligomerization of the large MON-2 and PAD-1 proteins could help to tubulate membranes during endosomal trafficking. Tubulation may also be enhanced by further oligomerization with TAT-5 and/or by recruitment and concentration of proteins required for membrane tubulation like actin and microtubule regulators. In summary, MON-2 and PAD-1 could contribute to many trafficking pathways.

5.3.9. PAD-1, MON-2 and TAT-5 in regulating late endosome size

The enlarged late endosomes in *tat-5, pad-1*, and *mon-2* mutants could be caused by decreased endosomal tubulation, as discussed in the previous section, but it could also be caused by increased endosome-endosome fusion, decreased intraluminal vesicle (ILV) budding, or changes to endolysosomal enzymes. Given the topological similarity of ILV budding to MV budding, as well as the similar molecular players, including ESCRT-dependence[126,127], we may have expected changes in ILV budding. However, *pad-1* and *tat-5* mutants did not show increased or decreased ILV formation, and there was also no change in ILV size (this study and [14]). Thus, TAT-5 and PAD-1 are unlikely to regulate ILV budding.

In yeast, Mon2, Dop1 and Neo1 mutants have fragmented vacuoles[6,19,33], which could be caused by defects in fusion. Greatly simplified, the yeast vacuole is like a large lysosome that grows to 10-20% of the yeast size due to SNARE-dependent fusion with pre-vacuoles or late endosomes[128]. Since Neo1, Mon2 and Dop1 traffic SNARE proteins[6,129](see also 5.1 and 5.3.9), which are required for membrane fusion, it was proposed that fragmented vacuoles appear because of disrupted membrane fusion. Intriguingly, PE in the cytosolic leaflet of the vacuole membrane is also required for SNARE-mediated vacuole fusion[130], suggesting that Neo1 PE flipping activity could promote vacuole fusion. To test whether the late endosomes are more fragmented in *pad-1*, *mon-2* and *tat-5* mutants, the numbers of late endosomes or LMP-1 puncta should be counted and compared to wild type samples.

However, we observed enlarged late endosomes in *pad-1*, *mon-2* and *tat-5* mutants (Fig. 8,Fig. 18), which would be more consistent with an increase in endosome fusion. To test this possibility, SNARE proteins should be depleted in the mutant background to block fusion. If endosome fusion is increased in *pad-1*, *mon-2* and *tat-5* mutants, additional loss of SNARE proteins should restore the size of late endosomes. Alternatively, live imaging of LMP-1::GFP could be performed to observe and quantify fusion events. These experiments would test whether there are changes to endosome fusion.

In addition to affecting the membrane of late endosomes, MON-2, PAD-1 and TAT-5 could be required for the trafficking and/or function of vacuolar proteins. Neo1 mutants have hyperacidified vacuoles[19,131], thus, it was proposed that Neo1 is required for the function of a protein that controls vacuolar pH. These could be the Vacuolar ATPase that mediates acidification of lysosomes or molecules that control the activity of the V-ATPase[132]. The pH of the enlarged endolysosomes in *mon-2*, *pad-1*, and *tat-5* mutants has not been determined, but it could also be interesting to see whether more V-ATPase localizes to mutant endolysosomes. Yeast Mon2, Dop1 and Neo1 are required for the trafficking of CPY and the hydrolase Ape1 to the vacuole [1,19,33,49]. Therefore, we speculate that MON-2, PAD-1 and TAT-5 could also regulate the recruitment of hydrolases to lysosomes and therefore disrupt macromolecule digestion. Loss of the amino acid transporting function of SLC-36.1 causes enlarged, vacuole-like lysosomes in *C. elegans* embryos or adults [133], showing that amino acid transport out of the lysosomes is required for lysosome shrinkage. Thus, it would be interesting to analyze whether SLC-36.1 and other amino acid transporters localize to the enlarged late endosomes in *tat-5, pad-1* and *mon-2* mutants. These experiments would help determine the cause of the enlarged late endosomes and shed light on the trafficking cargos of MON-2, PAD-1, and TAT-5.

5.3.10. Potential cargoes of MON-2/PAD-1/TAT-5-dependent endosomal trafficking

It is unknown which cargo besides TAT-5 is trafficked by PAD-1 and MON-2. It is also unclear whether TAT-5 acts in the same trafficking pathway as PAD-1 and MON-2. However, studies using yeast and human cells showed that MON-2, PAD-1 or TAT-5 orthologs are capable of trafficking several cargoes that could be conserved in *C. elegans* (Table 9).

SNARE proteins are the most likely to be primary cargos of MON-2, PAD-1, and TAT-5. The conserved v-SNARE VAMP/Synaptobrevin Snc1 and the t-SNARE syntaxin Sso1 cycle between the plasma membrane, endosomes and Golgi in yeast[134]. In Dop1 and Mon2 mutants, Snc1 was absent from the plasma membrane and accumulated inside the cell[6], suggesting that Mon2 and Dop1 are required for v-SNARE localization. A similar mislocalization was observed with a modified Sso1, which contains an additional NPF endocytosis signal. A Neo1 missense mutant depleted for Cdc50, the noncatalytic subunit of the PS flippase Drs2, also shows accumulation of Snc1 and the t-SNARE Tlg1 in enlarged intracellular structures[129]. However, it was not reported whether Neo1 can control Snc1 and Tlg1 trafficking independent of Cdc50, which would be expected from the studies on Dop1 and Mon2[6]. Thus, Mon2, Dop1, and Neo1 appear to play a major role in SNARE trafficking.

It was also shown that ATP9A and ATP8B are required for the secretion of insulin from pancreatic cells[88]. Although they are many steps involved in insulin secretion, this could mean that ATP9 proteins are required for the fusion of insulin secretory granules with the plasma membrane or for the transport of proteins required for insulin secretion. Given the links between Neo1 and SNARE proteins that mediate membrane fusion[129], we predict that SNARE proteins will be the relevant ATP9A/B cargos involved in insulin secretion.

Interestingly, Dop1, Neo1 and Mon2 all physically interact with the t-SNARE Tlg2 based on yeast two-hybrid studies[106]. This could suggest that Tlg2 is a cargo of Mon2/Dop1/Neo1 trafficking. Alternatively, Tlg2 could be an important part of the Mon2-Dop1-Neo1 complex and play a role in this trafficking pathway. Thus, it will be interesting to investigate whether the *C. elegans* ortholog SYX-16 is required for TAT-5 trafficking or whether TAT-5, MON-2, and PAD-1 are required for SYX-16 trafficking. In the screen for EV inhibitors Birgit Karmann found no increased EV release after *syx-16* RNAi (n=40), thus we would expect a redundant trafficking function similar to MON-2. These studies would identify an important cargo or cofactor of MON-2/PAD-1/TAT-5-dependent endosomal trafficking.

In *C. elegans* adults, another cargo of MON-2, PAD-1, and TAT-5 has recently been identified. Loss of MON-2 and PAD-1 causes decreased levels of the Wntless ortholog MIG-14 and a resulting reduction in Wnt secretion and Wnt-dependent posterior migration of the QL neuroblast descendants[3]. However, MIG-14 was only mistrafficked to the degradative pathway when PAD-1, MON-2 or TAT-5 were depleted in a *vps-29* mutant background. Consistently, our lab did not observe any changes to MIG-14 levels in embryos after *tat-5* knockdown in a wild type background (data from Ann Wehman), suggesting that MIG-14 is not a major cargo. Together these data suggest that MON-2, PAD-1, and TAT-5 act redundantly with retromer-dependent pathways to control the trafficking of MIG-14. Thus, RNAi depletions need to be conducted in a retromer-sensitized background in order to observe whether MIG-14 is a cargo trafficked by MON-2, PAD-1 and TAT-5 in embryos.

Alternatively, MON-2, PAD-1, and TAT-5 could only regulate a subset of MIG-14 localization. MON-2 was shown to be required for the localization of MIG-14 to lateral domains of the plasma membrane in adult intestinal cells, but not its other localization in these cells[35], suggesting that MON-2 is only required for certain trafficking pathways. Thus, it would be interesting to test whether PAD-1 and TAT-5 are required for the localization of MIG-14 to lateral domains in polarized intestinal cells, which would demonstrate that MIG-14 is a primary cargo of MON-2/PAD-1/TAT-5 trafficking.

Taken together, the most likely cargo of PAD-1, MON-2 or TAT-5 in *C. elegans* are SNARE proteins, although MIG-14 could be a secondary cargo when its primary trafficking pathways are disrupted. Other candidate cargos are listed in Table 9, whose localization should be tested in *pad-1, mon-2* and *tat-5* mutants to identify the trafficking potentials of this pathway. More potential cargoes could also be identified by analyzing the surfaceome of *pad-1, mon-2* and *tat-5* mutants. Elucidating which proteins are trafficked by MON-2, PAD-1, and TAT-5 will help to understand the physiological relevance of this trafficking pathway and may identify additional proteins involved in MV release.

Cargo	Protein Type	Organism	Transporter	*C. elegans* ortholog	Reference
Mrh1	Hsp30p-like TM protein	Yeast	Mon2	-	[135]
Snc1	v-SNARE	Yeast	Neo1[i] Mon2 Dop1	SNB-1 SNB-2	[6] [129]
Sso1	t-SNARE	Yeast	Mon2 Dop1	SYX-4 UNC-64 SYX-3 SYX-2	[6]
Tlg1	t-SNARE	Yeast	Neo1[i]	-	[129]
Wls	Wntless	Human cells	ATP9A MON2	MIG-14	[3]
MIG-14		*C. elegans*	TAT-5[i] PAD-1[i] MON2[i]		
Tfn	Transferrin	Human cells	ATP9A	-	[87]
GLUT1	Glucose transporter	Human cells	ATP9A	FGT-1	[87]
Insulin secretion	Insulin	Human cells	ATP9A	ILPs (Insulin-Like Proteins)	[88]

Table 9: Cargoes of MON-2, PAD-1 and TAT-5 orthologs. List of proteins whose trafficking was dependent on MON-2, PAD-1 or TAT-5 orthologs. The organism where trafficking was found and which orthologs were involved in trafficking are indicated. The references where cargo trafficking was observed is given. The potential orthologs in *C. elegans* are noted or marked with "-", when no ortholog is reported in *C. elegans*. [i]) indicates trafficking observed in sensitized backgrounds. MIG-14 trafficking of TAT-5, MON-2 and PAD-1 was examined in a *vps-29(tm1320)* mutant. Neo1-mediated trafficking of Snc1 and Tlg1 was examined in a Cdc50 mutant background.

5.3.11. PAD-1 as scaffold for MON-2 release in microvesicles

We found that PAD-1 is required for the release of MON-2 in MVs, but TAT-5 is not. This further demonstrates that TAT-5 is not required for MON-2 localization. As other cortical proteins were still released in MVs after *pad-1* RNAi, we do not think that PAD-1 is a general scaffold for sorting cortical proteins into MVs. Rather, we predict that MON-2 is brought to MV budding sites by binding PAD-1. Notably, PAD-1 is not required for MON-2 localization to the plasma membrane. PAD-1 orthologs in mammals are not required for the Golgi localization of mammalian MON2[55], suggesting that MON-2 and orthologs can localize to membranes independent of PAD-1. Together, these data suggest that PAD-1 may regulate to which microdomains MON-2 localizes on the plasma membrane. On the other hand, PAD-1 may function as a scaffold for an unknown regulator that traffics MON-2 into MVs. As MON2 is also released in EVs from human cancer cells(Vesiclepedia[136], accessed in September 2019), understanding how MON-2 is packaged into MVs may help to understand the conserved mechanisms of how cargos are sorted into MVs.

Another potential regulator of MON-2 release in MVs may be the small GTPase ARL-1. Arl1 stabilizes Mon2p-Dop1p binding in yeast and thereby promotes Dop1p membrane association[1,6,10]. Thus, it will be interesting to test whether ARL-1 is required for MON-2 binding to PAD-1. Furthermore, it will be interesting to check if ARL-1 is released in MVs in *tat-5* or *pad-1* mutants and whether this release further depends on MON-2. ARL1 is released in EVs from several cancer cell types(Vesiclepedia[136], accessed in September 2019), suggesting that ARL1 and MON2 localize to sites of MV release on the plasma membrane or sites of ILV budding on endosomes. ARL-1 depletion in an increased MV release background can clarify the requirement of ARL-1 for MON-2 release in MVs. This may show the regulatory networks required for the release of MON-2 in MVs.

5.3.12. PAD-1 and TAT-5 may regulate PE externalization and microvesicle release during abscission

One major question unanswered by our study is under which physiological conditions PAD-1 and TAT-5 reestablish PE asymmetry and regulate MV release. Provocatively, PE asymmetry is lost during cytokinesis and needs to be re-established for abscission[137]. MV release is also seen at the intercellular bridge in both *C. elegans* embryos and mammalian cells[138,139], which could help to sculpt membranes to thin the bridge during abscission. Intriguingly, *tat-5* mutant embryos occasionally have multinuclear cells due to retraction of the cleavage furrow[14], which suggests that restricting MV budding to the intercellular bridge promotes successful abscission. Thus, we propose that TAT-5 and PAD-1 need to be inactivated at the intercellular bridge in order to enable membrane sculpting by release of MVs. However, we observed that PAD-1 and MON-2 accumulate in midbody remnants, suggesting that the complex is present in the bridge during abscission. Thus, determining how PAD-1 and TAT-5 activity are regulated in the bridge is an important question that will help determine the conserved role of PE externalization and MV release from the intercellular bridge during abscission.

When we inhibited ESCRT disassembly, we found that PAD-1 and MON-2 are enriched on the plasma membrane neighboring the intercellular bridge in opposing domains with the ESCRT complex, which promote both MV release and abscission [127]. This suggests that the location of MV release and the location of PE internalization are separable domains of the membrane. To restrict MV budding to the intercellular bridge, PAD-1 may induce TAT-5 PE flipping activity next to the intercellular bridge. Thus, the precise subcellular localization needs examination using super-resolution techniques to define the role of PAD-1 during abscission. It will also be important to analyze abscission in *pad-1* mutants to confirm that PAD-1 is activating TAT-5 during this process. Analyzing the location and function of PAD-1 during abscission will provide further insights into the physiological role of this pathway.

Taken together, we propose that thinning membrane bridges may be a crucial physiological function of MV budding regulated by PE asymmetry. However, MV release also needs to be restricted, as excessive MV budding can disrupt cytokinesis and cell adhesion[14]. These observations show the need to tightly regulate PE flipping activity during development and homeostasis, emphasizing the importance of understanding the regulation of the PE flippase TAT-5 and its activator PAD-1.

5.4. References

1. Efe, J. A. *et al.* Yeast Mon2p is a highly conserved protein that functions in the cytoplasm-to-vacuole transport pathway and is required for Golgi homeostasis. *J. Cell Sci.* **118**, 4751–4764 (2005).
2. Barbosa, S., Pratte, D., Schwarz, H., Pipkorn, R. & Singer-Krüger, B. Oligomeric Dop1p is part of the endosomal Neo1p-Ysl2p-Arl1p membrane remodeling complex. *Traffic* **11**, 1092–1106 (2010).
3. McGough, I. J. *et al.* SNX3-retromer requires an evolutionary conserved MON2:DOPEY2:ATP9A complex to mediate Wntless sorting and Wnt secretion. *Nat. Commun.* **9**, 3737 (2018).
4. Pascon, R. C. & Miller, B. L. Morphogenesis in Aspergillus nidulans requires Dopey (DopA), a member of a novel family of leucine zipper-like proteins conserved from yeast to humans. *Mol. Microbiol.* **36**, 1250–1264 (2000).

5. Guipponi, M. *et al.* C21orf5, a novel human chromosome 21 gene, has a Caenorhabditis elegans ortholog (pad-1) required for embryonic patterning. *Genomics* **68**, 30–40 (2000).
6. Gillingham, A. K., Whyte, J. R. C., Panic, B. & Munro, S. Mon2, a relative of large Arf exchange factors, recruits Dop1 to the Golgi apparatus. *J. Biol. Chem.* **281**, 2273–2280 (2006).
7. Rachidi, M., Lopes, C., Costantine, M. & Delabar, J. M. C21orf5, a new member of Dopey family involved in morphogenesis, could participate in neurological alterations and mental retardation in Down syndrome. *DNA Res.* **12**, 203–210 (2005).
8. Mitchell, A. L. *et al.* InterPro in 2019: improving coverage, classification and access to protein sequence annotations. *Nucleic Acids Res.* **47**, D351–D360 (2019).
9. Landschulz, W. H., Johnson, P. F. & McKnight, S. L. The leucine zipper: A hypothetical structure common to a new class of DNA binding proteins. *Science* **240**, 1759–1764 (1988).
10. Dalton, L. E., Bean, B. D. M., Davey, M. & Conibear, E. Quantitative high-content imaging identifies novel regulators of Neo1 trafficking at endosomes. *Mol. Biol. Cell* **28**, 1539–1550 (2017).
11. Lyssenko, N. N., Miteva, Y., Gilroy, S., Hanna-Rose, W. & Schlegel, R. A. An unexpectedly high degree of specialization and a widespread involvement in sterol metabolism among the C. elegans putative aminophospholipid translocases. *BMC Dev. Biol.* **8**, 1–17 (2008).
12. Hunt-Newbury, R. *et al.* High-Throughput In Vivo Analysis of Gene Expression in Caenorhabditis elegans. *PLoS Biol.* **5**, e237 (2007).
13. Tanaka, M. *et al.* The VF rat with abnormal myelinogenesis has a mutation in Dopey1. *Glia* **62**, 1530–1542 (2014).
14. Wehman, A. M., Poggioli, C., Schweinsberg, P., Grant, B. D. & Nance, J. The P4-ATPase TAT-5 inhibits the budding of extracellular vesicles in C. elegans embryos. *Curr. Biol.* **21**, 1951–1959 (2011).
15. Sato, K., Norris, A., Sato, M. & Grant, B. D. C. elegans as a model for membrane traffic. *WormBook* 1–47 (2014).
16. Feyder, S., De Craene, J. O., Bär, S., Bertazzi, D. L. & Friant, S. Membrane trafficking in the yeast Saccharomyces cerevisiae model. *International Journal of Molecular Sciences* **16**, 1509–1525 (2015).
17. Kanamori, T. *et al.* β-Catenin asymmetry is regulated by PLA1and retrograde traffic in C. elegans stem cell divisions. *EMBO J.* **27**, 1647–1657 (2008).
18. Gallon, M. & Cullen, P. J. Retromer and sorting nexins in endosomal sorting. *Biochem. Soc. Trans.* **43**, 33–47 (2015).
19. Hua, Z. & Graham, T. R. Requirement for Neo1p in Retrograde Transport from the Golgi Complex to the Endoplasmic Reticulum. *Mol. Biol. Cell* **14**, 4971–4983 (2003).
20. Wicky, S., Schwarz, H. & Singer-Kruger, B. Molecular Interactions of Yeast Neo1p, an Essential Member of the Drs2 Family of Aminophospholipid Translocases, and Its Role in Membrane Trafficking within the Endomembrane System. *Mol. Cell. Biol.* **24**, 7402–7418 (2004).
21. Cheng, C. Y. *et al.* The piggyBac transposon-derived genes TPB1 and TPB6 mediate essential transposon-like excision during the developmental rearrangement of key genes in Tetrahymena thermophila. *Genes Dev.* **30**, 2724–2736 (2016).
22. Nakane, Y. *et al.* A novel mutation vf causing abnormal vacuoles in the central nervous system maps on rat chromosome 8. *Exp. Anim.* **51**, 149–55 (2002).
23. Tanaka, M. *et al.* Abnormal myelinogenesis in the central nervous system of the VF mutant rat with recoverable tremor. *Brain Res.* **1488**, 104–112 (2012).
24. Kervestin, S. & Jacobson, A. NMD: a multifaceted response to premature translational termination. *Nat. Rev. Mol. Cell Biol.* **13**, 700–712 (2012).
25. Rachidi, M., Delezoide, A. L., Delabar, J. M. & Lopes, C. A quantitative assessment of gene expression (QAGE) reveals differential overexpression of DOPEY2, a candidate gene for mental retardation, in Down syndrome brain regions. *Int. J. Dev. Neurosci.* **27**, 393–398 (2009).
26. Lopes, C., Chettouh, Z., Delabar, J. M. & Rachidi, M. The differentially expressed C21orf5 gene in the medial temporal-lobe system could play a role in mental retardation in Down syndrome and transgenic mice. *Biochem. Biophys. Res. Commun.* **305**, 915–924 (2003).
27. Chardin, P. *et al.* A human exchange factor for ARF contains Sec7- and pleckstrin-homology domains. *Nature* **384**, 481–484 (1996).
28. Jochum, A., Jackson, D., Schwarz, H., Pipkorn, R. & Singer-Krüger, B. Yeast Ysl2p,

homologous to Sec7 domain guanine nucleotide exchange factors, functions in endocytosis and maintenance of vacuole integrity and interacts with the Arf-Like small GTPase Arl1p. *Mol. Cell. Biol.* **22**, 4914–28 (2002).
29. Mahajan, D. *et al.* Mammalian Mon2/Ysl2 regulates endosome-to-Golgi trafficking but possesses no guanine nucleotide exchange activity toward Arl1 GTPase. *Sci. Rep.* **3**, (2013).
30. Singer-Krüger, B. & Ferro-Novick, S. Use of a synthetic lethal screen to identify yeast mutants impaired in endocytosis, vacuolar protein sorting and the organization of the cytoskeleton. *Eur. J. Cell Biol.* **74**, 365–375 (1997).
31. Grosshans, B. L., Ortiz, D. & Novick, P. Rabs and their effectors: Achieving specificity in membrane traffic. *Proc. Natl. Acad. Sci.* **103**, 11821–11827 (2006).
32. Murén, E., Oyen, M., Barmark, G. & Ronne, H. Identification of yeast deletion strains that are hypersensitive to brefeldin A or monensin, two drugs that affect intracellular transport. *Yeast* **18**, 163–72 (2001).
33. Bonangelino, C. J., Chavez, E. M. & Bonifacino, J. S. Genomic Screen for Vacuolar Protein Sorting Genes in *Saccharomyces cerevisiae*. *Mol. Biol. Cell* **13**, 2486–2501 (2002).
34. Avaro, S., Belgareh-Touzé, N., Sibella-Argüelles, C., Volland, C. & Haguenauer-Tsapis, R. Mutants defective in secretory/vacuolar pathways in the EUROFAN collection of yeast disruptants. *Yeast* **19**, 351–371 (2002).
35. Zhu, M. *et al.* Serum- and Glucocorticoid-Inducible Kinase-1 (SGK-1) Plays a Role in Membrane Trafficking in Caenorhabditis elegans. *PLoS One* **10**, e0130778 (2015).
36. Shi, A. *et al.* Regulation of endosomal clathrin and retromer-mediated endosome to Golgi retrograde transport by the J-domain protein RME-8. *EMBO J.* **28**, 3290–3302 (2009).
37. Yang, P. T. *et al.* Wnt Signaling Requires Retromer-Dependent Recycling of MIG-14/Wntless in Wnt-Producing Cells. *Dev. Cell* **14**, 140–147 (2008).
38. Hardin, J. & King, R. S. The long and the short of Wnt signaling in C. elegans. *Curr. Opin. Genet. Dev.* **18**, 362–7 (2008).
39. Simonetti, B. & Cullen, P. J. Actin-dependent endosomal receptor recycling. *Curr. Opin. Cell Biol.* **56**, 22–33 (2019).
40. Singer-Krüger, B. *et al.* Yeast and human Ysl2p/hMon2 interact with Gga adaptors and mediate their subcellular distribution. *EMBO J.* **27**, 1423–1435 (2008).
41. Tomita, Y. *et al.* The cellular factors Vps18 and Mon2 are required for efficient production of infectious HIV-1 particles. *J. Virol.* **85**, 5618–27 (2011).
42. Bieniasz, P. D. The cell biology of HIV-1 virion genesis. *Cell Host Microbe* **5**, 550–8 (2009).
43. Prezant, T. R., Chaltraw, W. E. j. & Fischel-Ghodsian, N. Identification of an overexpressed yeast gene which prevents aminoglycoside toxicity. *Microbiology* **142**, 3407–3414 (1996).
44. Xu, S. The application of CRISPR-Cas9 genome editing in Caenorhabditis elegans. *J. Genet. Genomics* **42**, 413–21 (2015).
45. Lee, R. Y. N. *et al.* WormBase 2017: molting into a new stage. *Nucleic Acids Res.* **46**, D869–D874 (2018).
46. Albert Hubbard, E. J. & Greenstein, D. The Caenorhabditis elegans gonad: A test tube for cell and developmental biology. *Developmental Dynamics* **218**, 2–22 (2000).
47. Ward, S. & Klass, M. The location of the major protein in Caenorhabditis elegans sperm and spermatocytes. *Dev. Biol.* **92**, 203–208 (1982).
48. Hanna, M., Wang, L. & Audhya, A. Worming Our Way In and Out of the *Caenorhabditis elegans* Germline and Developing Embryo. *Traffic* **14**, 471–478 (2013).
49. Zhao, S. B. *et al.* Yeast Dop1 is required for glycosyltransferase retrieval from the trans-Golgi network. *Biochim. Biophys. Acta - Gen. Subj.* **1863**, 1147–1157 (2019).
50. Beer, K. B. *et al.* Extracellular vesicle budding is inhibited by redundant regulators of TAT-5 flippase localization and phospholipid asymmetry. *Proc. Natl. Acad. Sci.* **115**, E1127–E1136 (2018).
51. Nelson, F. K. & Riddle, D. L. Functional study of theCaenorhabditis elegans secretory-excretory system using laser microsurgery. *J. Exp. Zool.* **231**, 45–56 (1984).
52. Buechner, M. Tubes and the single C. elegans excretory cell. *Trends Cell Biol.* **12**, 479–484 (2002).
53. Stein, K. K. The C. elegans eggshell. *WormBook* 1–35 (2015). doi:10.1895/wormbook.1.179.1
54. Sarov, M. *et al.* A genome-scale resource for in vivo tag-based protein function exploration in

C. elegans. *Cell* **150**, 855–866 (2012).

55. Mahajan, D., Tie, H. C., Chen, B. & Lu, L. Dopey1-Mon2 complex binds to dual-lipids and recruits kinesin-1 for membrane trafficking. *Nat. Commun.* **10**, 3218 (2019).
56. Fazeli, G., Trinkwalder, M., Irmisch, L. & Wehman, A. M. C. elegans midbodies are released, phagocytosed and undergo LC3-dependent degradation independent of macroautophagy. *J. Cell Sci.* **129**, 3721–3731 (2016).
57. Morita, E. *et al.* Human ESCRT and ALIX proteins interact with proteins of the midbody and function in cytokinesis. *EMBO J.* **26**, 4215–4227 (2007).
58. Babst, M., Wendland, B., Estepa, E. J. & Emr, S. D. The Vps4p AAA ATPase regulates membrane association of a Vps protein complex required for normal endosome function. *EMBO J.* **17**, 2982–2993 (1998).
59. Adell, M. A. Y. *et al.* Recruitment dynamics of ESCRT-III and Vps4 to endosomes and implications for reverse membrane budding. *Elife* **6**, (2017).
60. Michelet, X. *et al.* The ESCRT-III protein CeVPS-32 is enriched in domains distinct from CeVPS-27 and CeVPS-23 at the endosomal membrane of epithelial cells. *Biol. Cell* **101**, 599–615 (2009).
61. Zhou, F. *et al.* Rab5-dependent autophagosome closure by ESCRT. *J. Cell Biol.* **218**, 1908–1927 (2019).
62. Tanaka, T., Kato, Y., Matsuda, K., Hanyu-Nakamura, K. & Nakamura, A. Drosophila Mon2 couples Oskar-induced endocytosis with actin remodeling for cortical anchorage of the germ plasm. *Development* **138**, 2523–2532 (2011).
63. Van Niel, G., D'Angelo, G. & Raposo, G. Shedding light on the cell biology of extracellular vesicles. *Nat. Rev. Mol. Cell Biol.* **19**, 213–228 (2018).
64. van Furden, D., Johnson, K., Segbert, C. & Bossinger, O. The C. elegans ezrin-radixin-moesin protein ERM-1 is necessary for apical junction remodelling and tubulogenesis in the intestine. *Dev. Biol.* **272**, 262–276 (2004).
65. Edwards, K. A., Demsky, M., Montague, R. A., Weymouth, N. & Kiehart, D. P. GFP-Moesin Illuminates Actin Cytoskeleton Dynamics in Living Tissue and Demonstrates Cell Shape Changes during Morphogenesis inDrosophila. *Dev. Biol.* **191**, 103–117 (1997).
66. Shelton, C. A., Carter, J. C., Ellis, G. C. & Bowerman, B. The nonmuscle myosin regulatory light chain gene mlc-4 is required for cytokinesis, anterior-posterior polarity, and body morphology during Caenorhabditis elegans embryogenesis. *J. Cell Biol.* **146**, 439–51 (1999).
67. Fazeli, G., Stetter, M., Lisack, J. N. & Wehman, A. M. C. elegans Blastomeres Clear the Corpse of the Second Polar Body by LC3-Associated Phagocytosis. *Cell Rep.* **23**, 2070–2082 (2018).
68. Hadwiger, G., Dour, S., Arur, S., Fox, P. & Nonet, M. L. A monoclonal antibody Toolkit for C. elegans. *PLoS One* **5**, (2010).
69. Marie-Anaïs, F., Mazzolini, J., Herit, F. & Niedergang, F. Dynamin-Actin Cross Talk Contributes to Phagosome Formation and Closure. *Traffic* **17**, 487–499 (2016).
70. Beckett, K. *et al.* Drosophila S2 cells secrete wingless on exosome-like vesicles but the wingless gradient forms independently of exosomes. *Traffic* **14**, 82–96 (2013).
71. Choi, D. S. *et al.* Proteomic analysis of microvesicles derived from human colorectal cancer cells. *J. Proteome Res.* **6**, 4646–4655 (2007).
72. Grant, B. *et al.* Evidence that RME-1, a conserved C. elegans EH-domain protein, functions in endocytic recycling. *Nat. Cell Biol.* **3**, 573–579 (2001).
73. Liu, K., Surendhran, K., Nothwehr, S. F. & Graham, T. R. P4-ATPase requirement for AP-1/clathrin function in protein transport from the trans-Golgi network and early endosomes. *Mol. Biol. Cell* **19**, 3526–35 (2008).
74. Chen, K. E., Healy, M. D. & Collins, B. M. Towards a molecular understanding of endosomal trafficking by Retromer and Retriever. *Traffic* **20**, 465–478 (2019).
75. Treusch, S. *et al.* Caenorhabditis elegans functional orthologue of human protein h-mucolipin-1 is required for lysosome biogenesis. *Proc. Natl. Acad. Sci. U. S. A.* **101**, 4483–4488 (2004).
76. Andrews, R. & Ahringer, J. Asymmetry of Early Endosome Distribution in C. elegans Embryos. *PLoS One* **2**, e493 (2007).
77. Lu, Q. *et al.* C. elegans Rab GTPase 2 is required for the degradation of apoptotic cells. *Development* **135**, 1069–1080 (2008).
78. Cattin-Ortolá, J., Topalidou, I., Dosey, A., Merz, A. J. & Ailion, M. The dense-core vesicle

maturation protein CCCP-1 binds RAB-2 and membranes through its C-terminal domain. *Traffic* **18**, 720–732 (2017).

79. Takar, M., Wu, Y. & Graham, T. R. The essential Neo1 protein from budding yeast plays a role in establishing aminophospholipid asymmetry of the plasma membrane. *J. Biol. Chem.* **291**, 15727–15739 (2016).
80. Züllig, S. *et al.* Aminophospholipid Translocase TAT-1 Promotes Phosphatidylserine Exposure during C. elegans Apoptosis. *Curr. Biol.* **17**, 994–999 (2007).
81. Audhya, A., McLeod, I. X., Yates, J. R. & Oegema, K. MVB-12, a fourth subunit of metazoan ESCRT-I, functions in receptor downregulation. *PLoS One* **2**, e956 (2007).
82. Wang, J. *et al.* C. elegans ciliated sensory neurons release extracellular vesicles that function in animal communication. *Curr. Biol.* **24**, 519–525 (2014).
83. Russell, J. C. *et al.* Isolation and characterization of extracellular vesicles from Caenorhabditis elegans for multi-omic analysis. *bioRxiv* 476226 (2018). doi:10.1101/476226
84. Liu, M. The biology and dynamics of mammalian cortical granules. *Reprod. Biol. Endocrinol.* **9**, 149 (2011).
85. Lucy, J. A. Loss of phospholipid asymmetry in cell fusion. in *Biochemical Society Transactions* **21**, 280–283 (Portland Press, 1993).
86. Fadeel, B. & Xue, D. The ins and outs of phospholipid asymmetry in the plasma membrane: roles in health and disease. *Crit. Rev. Biochem. Mol. Biol.* **44**, 264–277 (2009).
87. Tanaka, Y. *et al.* The phospholipid flippase ATP9A is required for the recycling pathway from the endosomes to the plasma membrane. *Mol. Biol. Cell* **27**, 3883–3893 (2016).
88. Ansari, I. U. H. *et al.* Characterization of P4 ATPase phospholipid translocases (flippases) in human and rat pancreatic beta cells: Their gene silencing inhibits insulin secretion. *J. Biol. Chem.* **290**, 23110–23123 (2015).
89. Naik, J. *et al.* The P4-ATPase ATP9A is a novel determinant of exosome release. *PLoS One* **14**, e0213069 (2019).
90. Budnik, V., Ruiz-Cañada, C. & Wendler, F. Extracellular vesicles round off communication in the nervous system. *Nat. Rev. Neurosci.* **17**, 160–172 (2016).
91. Bakhti, M., Winter, C. & Simons, M. Inhibition of myelin membrane sheath formation by oligodendrocyte-derived exosome-like vesicles. *J. Biol. Chem.* **286**, 787–96 (2011).
92. Street, J. M. *et al.* Identification and proteomic profiling of exosomes in human cerebrospinal fluid. *J. Transl. Med.* **10**, 5 (2012).
93. White, J. G., Southgate, E., Thomson, J. N. & Brenner, S. The Structure of the Nervous System of the Nematode Caenorhabditis elegans. *Philos. Trans. R. Soc. B Biol. Sci.* **314**, 1–340 (1986).
94. Oikonomou, G. & Shaham, S. The glia of Caenorhabditis elegans. *Glia* **59**, 1253–63 (2011).
95. Gauthier, S. A. *et al.* Enhanced exosome secretion in Down syndrome brain - a protective mechanism to alleviate neuronal endosomal abnormalities. *Acta Neuropathol. Commun.* **5**, 65 (2017).
96. Berezikov, E. Homologous gene targeting in Caenorhabditis elegans by biolistic transformation. *Nucleic Acids Res.* **32**, e40 (2004).
97. Praitis, V., Casey, E., Collar, D. & Austin, J. Creation of low-copy integrated transgenic lines in Caenorhabditis elegans. *Genetics* **157**, 1217–1226 (2001).
98. Jensen, M. S. *et al.* Phospholipid flipping involves a central cavity in P4 ATPases. *Sci. Rep.* **7**, 1–13 (2017).
99. El-Brolosy, M. A. *et al.* Genetic compensation triggered by mutant mRNA degradation. *Nature* **568**, 193–197 (2019).
100. Lopez-Marques, R. L., Theorin, L., Palmgren, M. G. & Pomorski, T. G. P4-ATPases: Lipid flippases in cell membranes. *Pflugers Arch. Eur. J. Physiol.* **466**, 1227–1240 (2014).
101. Shin, H.-W. & Takatsu, H. Substrates of P4-ATPases: beyond aminophospholipids (phosphatidylserine and phosphatidylethanolamine). *FASEB J.* **33**, 3087–3096 (2018).
102. Naito, T. *et al.* Phospholipid flippase ATP10A translocates phosphatidylcholine and is involved in plasma membrane dynamics. *J. Biol. Chem.* **290**, 15004–15017 (2015).
103. Takar, M., Huang, Y. & Graham, T. R. The PQ-loop protein Any1 segregates Drs2 and Neo1 functions required for viability and plasma membrane phospholipid asymmetry. *J. Lipid Res.* **60**, 1032–1042 (2019).
104. Yamamoto, T., Fujimura-Kamada, K., Shioji, E., Suzuki, R. & Tanaka, K. Cfs1p, a novel

membrane protein in the PQ-loop family, is involved in phospholipid flippase functions in yeast. *G3 Genes, Genomes, Genet.* **7**, 179–192 (2017).

105. Van Leeuwen, J. *et al.* Exploring genetic suppression interactions on a global scale. *Science* **354**, (2016).
106. Tarassov, K. *et al.* An in Vivo Map of the Yeast Protein Interactome. *Science* **320**, 1465–1470 (2008).
107. van Meer, G. Dynamic transbilayer lipid asymmetry. *Cold Spring Harb. Perspect. Biol.* **3**, 1–11 (2011).
108. Daleke, D. L. Regulation of transbilayer plasma membrane phospholipid asymmetry. *Journal of Lipid Research* **44**, 233–242 (2003).
109. Nolte-'t Hoen, E., Cremer, T., Gallo, R. C. & Margolis, L. B. Extracellular vesicles and viruses: Are they close relatives? *Proc. Natl. Acad. Sci.* **113**, 9155–9161 (2016).
110. Tewari, R., Bailes, E., Bunting, K. A. & Coates, J. C. Armadillo-repeat protein functions: Questions for little creatures. *Trends in Cell Biology* **20**, 470–481 (2010).
111. Timcenko, M. *et al.* Structure and autoregulation of a P4-ATPase lipid flippase. *Nature* **571**, 366–370 (2019).
112. Hiraizumi, M., Yamashita, K., Nishizawa, T. & Nureki, O. Cryo-EM structures capture the transport cycle of the P4-ATPase flippase. *Science* **365**, 1149–1155 (2019).
113. Takatsu, H. *et al.* ATP9B, a P4-ATPase (a putative aminophospholipid translocase), localizes to the trans-Golgi network in a CDC50 protein-independent manner. *J. Biol. Chem.* **286**, 38159–38167 (2011).
114. Kelley, L. A., Mezulis, S., Yates, C. M., Wass, M. N. & Sternberg, M. J. E. The Phyre2 web portal for protein modeling, prediction and analysis. *Nat. Protoc.* **10**, 845–858 (2015).
115. Käll, L., Krogh, A. & Sonnhammer, E. L. . A Combined Transmembrane Topology and Signal Peptide Prediction Method. *J. Mol. Biol.* **338**, 1027–1036 (2004).
116. Viaud, J. *et al.* Phosphoinositides: Important lipids in the coordination of cell dynamics. *Biochimie* **125**, 250–258 (2016).
117. Lemmon, M. A. Membrane recognition by phospholipid-binding domains. *Nature Reviews Molecular Cell Biology* **9**, 99–111 (2008).
118. Boncompain, G. *et al.* Synchronization of secretory protein traffic in populations of cells. *Nat. Methods* **9**, 493–498 (2012).
119. Puthenveedu, M. A. *et al.* Sequence-dependent sorting of recycling proteins by actin-stabilized endosomal microdomains. *Cell* **143**, 761–773 (2010).
120. Duleh, S. N. & Welch, M. D. WASH and the Arp2/3 complex regulate endosome shape and trafficking. *Cytoskeleton* **67**, NA-NA (2010).
121. Derivery, E. *et al.* The Arp2/3 Activator WASH Controls the Fission of Endosomes through a Large Multiprotein Complex. *Dev. Cell* **17**, 712–723 (2009).
122. Freeman, C. L., Hesketh, G. & Seaman, M. N. J. RME-8 coordinates the activity of the WASH complex with the function of the retromer SNX dimer to control endosomal tubulation. *J. Cell Sci.* **127**, 2053–2070 (2014).
123. Delevoye, C. *et al.* Recycling endosome tubule morphogenesis from sorting endosomes requires the kinesin motor KIF13A. *Cell Rep.* **6**, 445–454 (2014).
124. Gomez, T. S. & Billadeau, D. D. A FAM21-Containing WASH Complex Regulates Retromer-Dependent Sorting. *Dev. Cell* **17**, 699–711 (2009).
125. McMahon, H. T. & Gallop, J. L. Membrane curvature and mechanisms of dynamic cell membrane remodelling. *Nature* **438**, 590–596 (2005).
126. Campsteijn, C., Vietri, M. & Stenmark, H. Novel ESCRT functions in cell biology: Spiraling out of control? *Current Opinion in Cell Biology* **41**, 1–8 (2016).
127. Hurley, J. H. ESCRTs are everywhere. *EMBO J.* **34**, 2398–2407 (2015).
128. Armstrong, J. Yeast vacuoles: more than a model lysosome. *Trends Cell Biol.* **20**, 580–585 (2010).
129. Takeda, M., Yamagami, K. & Tanaka, K. Role of phosphatidylserine in phospholipid flippase-mediated vesicle transport in Saccharomyces cerevisiae. *Eukaryot. Cell* **13**, 363–375 (2014).
130. Wu, Y., Takar, M., Cuentas-Condori, A. A. & Graham, T. R. Neo1 and phosphatidylethanolamine contribute to vacuole membrane fusion in Saccharomyces cerevisiae. *Cell. Logist.* **6**, e1228791 (2016).

131. Brett, C. L. *et al*. Genome-wide analysis reveals the vacuolar pH-stat of Saccharomyces cerevisiae. *PLoS One* **6**, e17619 (2011).
132. Kane, P. M. The Where, When, and How of Organelle Acidification by the Yeast Vacuolar H+-ATPase. *Microbiol. Mol. Biol. Rev.* **70**, 177–191 (2006).
133. Gan, Q. *et al*. The amino acid transporter SLC-36.1 cooperates with PtdIns3P 5-kinase to control phagocytic lysosome reformation. *J. Cell Biol.* jcb.201901074 (2019). doi:10.1083/jcb.201901074
134. Gurunathan, S., Chapman-Shimshoni, D., Trajkovic, S. & Gerst, J. E. Yeast Exocytic v-SNAREs Confer Endocytosis. *Mol. Biol. Cell* **11**, 3629–3643 (2000).
135. Bircham, P. W. *et al*. Secretory pathway genes assessed by high-throughput microscopy and synthetic genetic array analysis. *Mol. Biosyst.* **7**, 2589 (2011).
136. Kalra, H. *et al*. Vesiclepedia: A Compendium for Extracellular Vesicles with Continuous Community Annotation. *PLoS Biol.* **10**, e1001450 (2012).
137. Emoto, K., Inadome, H., Kanaho, Y., Narumiya, S. & Umeda, M. Local change in phospholipid composition at the cleavage furrow is essential for completion of cytokinesis. *J. Biol. Chem.* **280**, 37901–37907 (2005).
138. Elia, N., Sougrat, R., Spurlin, T. A., Hurley, J. H. & Lippincott-Schwartz, J. Dynamics of endosomal sorting complex required for transport (ESCRT) machinery during cytokinesis and its role in abscission. *Proc. Natl. Acad. Sci. U. S. A.* **108**, 4846–4851 (2011).
139. König, J., Frankel, E. B., Audhya, A. & Müller-Reichert, T. Membrane remodeling during embryonic abscission in *Caenorhabditis elegans*. *J. Cell Biol.* **216**, 1277–1286 (2017).

6. Concluding discussion

6.1. Summary of major findings

In this thesis, we developed a degradation-based technique to specifically label microvesicles (MV), which enabled us to identify conserved TAT-5 regulators that inhibit MV release. We identified four MV release inhibitors associated with retrograde recycling: the class III PI3Kinase VPS-34, the Beclin1 homolog BEC-1, the DnaJ protein RME-8, and the uncharacterized Dopey homolog PAD-1. We showed that VPS-34, BEC-1, RME-8, as well as redundant sorting nexin SNX-1/-6 and SNX-3-dependent trafficking pathways are required for the plasma membrane recycling of TAT-5, in addition to several minor pathways. We also discovered that PAD-1 and the GEF-like protein MON-2 do not traffic TAT-5, unless sorting nexin-mediated recycling is disrupted. We found that mistrafficking TAT-5 to endolysosomes disrupts TAT-5 PE flipping activity, suggesting that TAT-5 needs to be sorted away from the degradative pathway to maintain PE asymmetry and inhibit MV release. In addition, we demonstrated that PAD-1 is specifically required for the lipid flipping activity of TAT-5.

Taken together, we accomplished two major things. First: We have identified regulatory mechanisms that control the activity of the conserved and essential flippases TAT-5. We uncovered redundant intracellular trafficking pathways of TAT-5, which shows how the localization of this conserved P4-ATPase can be controlled without β-subunits. Furthermore, we were able to reveal regulators of TAT-5 flippase activity, which increases the understanding of how cells can adjust TAT-5 PE flipping activity to release the right amount of MVs at the right time. Our studies also confirm the previous hypothesis that loss of PE asymmetry is involved in membrane budding to release MVs. Second: The ectocytosis inhibitors identified here provide the first toolkit to experimentally control MV formation, which will be helpful to understand the mechanisms that regulate disease-mediated EV release, membrane sculpting and viral budding. Ultimately, this will help to test the *in vivo* roles of MVs to understand their contribution to EV-related functions and pathologies.

6.2. Multiple trafficking pathways regulate TAT-5 localization

Our results illustrate that a multitude of trafficking pathways are required for TAT-5 localization. Two redundant trafficking pathways that depend on SNX-1/-6 and SNX-3-mediated trafficking are required for the majority of TAT-5 localization (discussed in chapter 4.3.). We also found a role for retromer in trafficking a minor, but measurable amount of TAT-5 (discussed in chapter 4.3.). A fourth trafficking pathway depends on MON-2 and PAD-1, which could function as a back-up trafficking pathway (discussed in chapter 5.3.). Further research is required to determine whether SNX-17 and SNX-27 also contribute to TAT-5 trafficking, which could define either a fifth and sixth pathway or act together with the MON-2/PAD-1 trafficking pathway (discussed in chapter 4.3. and 5.3.). Thus, two major and at least two minor trafficking pathways redundantly localize TAT-5, suggesting that multiple redundant pathways contribute to the proper localization of TAT-5.

Why so many redundant pathways exist to traffic one protein remains enigmatic. As TAT-5 is an essential protein, one possibility is that TAT-5 trafficking by multiple pathways evolved to ensure proper TAT-5 trafficking. Multiple trafficking routes have been described for other cargos, too. For example, SNX-3 regulates Wntless trafficking[1–3], but retromer *vps-29* mutants only partially altered Wntless trafficking, suggesting that redundant Wntless trafficking mechanisms exist[2]. Depleting *snx-1* in a *vps-29* retromer mutant caused altered Wntless trafficking similar to *snx-3* RNAi, showing that SNX-1 and retromer do form redundant Wntless trafficking pathways. Very recently, it was also reported that two different CI-MPR subpopulations are trafficked by SNX3 or SNX1-dependent trafficking routes[4]. Thus, trafficking by multiple SNX pathways can be a feature of several transmembrane cargoes.

On the other hand, the GFP::TAT-5 transgene used for our studies is a multi-copy insertion and is expressed from a promotor from another gene. The *pie-1* promotor drives strong expression from multi-copy insertions in the adult germ line[5,6], while *tat-5* is ubiquitously expressed at a lower level. Thus, the expression levels of GFP::TAT-5 are likely to be higher in comparison to endogenous TAT-5, which could lead GFP::TAT-5 to accumulate differently than endogenous TAT-5. As we were unable to find a TAT-5 antibody using peptide antigens, it would be necessary to generate new TAT-5 antibodies to study the endogenous localization of TAT-5. Using purified domains as antigens, such as the N-terminal cytoplasmic domain of TAT-5, could work better in generating a specific antibody. Another possibility is to generate a TAT-5 fluorescent line with endogenous expression levels. This could be achieved for example by using CRISPR/Cas9 to knock in a fluorescent protein between the endogenous *tat-5* promotor and the *tat-5* sequence. Another possibility is to use MosSci to insert a single copy of fluorescent protein-tagged *tat-5* into a defined locus in the genome[7]. Development of a way to visualize TAT-5 under endogenous expression levels will be necessary to confirm whether endogenous TAT-5 is trafficked by as many pathways.

6.3. TAT-5 PE flipping activity and endosomal trafficking

Domains of the conical-shaped lipid PE are thought to induce negative membrane curvature[8], where microdomains of externalized PE on the plasma membrane would lead to outward budding (ectocytosis) and internalized PE would lead to inward budding (endocytosis). As PE is an abundant lipid that is found on all organelle membranes[9], PE-mediated curvature formation could regulate budding on many membranes in addition to the plasma membrane. Therefore, we predict that TAT-5 could regulate ectocytosis, endocytosis, and endosomal budding.

The correlation of increased MV release and PE externalization observed across several *C. elegans* mutants in our studies supports the hypothesis that PE localization regulates plasma membrane budding. To directly test whether PE externalization can induce ectocytosis, we need to induce PE externalization independent of TAT-5 or its regulators. The lantibiotics cinnamycin and duramycin induce PE transbilayer lipid movements and trap PE on the external leaflet of the plasma membrane[10–13], which has been shown to promote membrane tubulation in *in vitro* assays[11]. Tubulation of the plasma membrane could result in MV release. Thus, it would be interesting to test whether cells incubated with cinnamycin or duramycin would release more MVs. These experiments would demonstrate whether PE externalization induces MV release, providing new insight into the biology of PE. Furthermore, they could define a treatment to induce MV release, which could be useful for biomarker studies.

Apart from inhibiting MV budding, TAT-5 and its orthologs are also required for endosomal trafficking[3,14,15], which may indicate that PE asymmetry is also regulated on endosomes. McGough *et al.* 2018 reported that TAT-5 is required for SNX-3-dependent Wntless trafficking redundantly with VPS-29 and hypothesized that the flipping activity of TAT-5 mediates endosomal tubulation in the SNX-3 trafficking pathway. Dalton *et al.* 2017 showed that Neo1 is required to prevent vacuolar accumulation of the Snx3 cargo A-ALP, which is a fusion protein of the cytoplasmic domain of DPAP A and the luminal domains of alkaline phosphatase that localizes to the TGN in yeast[16]. This suggests that TAT-5 PE flipping activity is required on sorting endosomes to mediate retrograde cargo trafficking.

Insight into how lipid flipping could regulate SNX-dependent endosomal trafficking comes from studies in Hye-Won Shin's lab. They showed that the flipping activity of the mammalian phosphatidylcholine (PC) flippase ATP10A initiates membrane curvature and recruits BAR domains that generate membrane tubulation by oligomerization[17]. While the N-BAR domains of SNX-BARs can induce membrane curvature autonomously using their N-terminal alpha-helix that stabilizes or induces membrane bending[17,18], N-BAR domains lacking the N-terminal alpha-helix, as well as F-BAR domains, cannot induce tubulation autonomously and require the PC flipping activity of ATP10 for their membrane recruitment and membrane tubulation. This suggests that lipid flipping promotes membrane bending. Localization of the yeast PS flippase Drs2 to Golgi and endosomes was also shown to be required for vesicle formation from these organelles[19–21]. Therefore, it was proposed that P4-ATPases induce membrane curvature by lipid flipping, perhaps by creating an imbalance in the number of lipids in the membrane bilayers[17]. Thus, TAT-5-mediated PE flipping could increase the abundance of PE in the cytosolic leaflet of sorting endosomes, which induces membrane curvature towards the cytosol, a prerequisite for endosomal tubulation. Thus, the PE flipping activity of TAT-5 could promote endosomal trafficking.

If TAT-5 promotes membrane curvature for sorting nexins lacking a BAR domain, then it would be predicted that TAT-5 would not be required for cargo of SNX-BARs like SNX-1 and SNX-6, but would be required for trafficking by SNX-PX or SNX-FERM proteins that lack BAR domains, like SNX-3 and SNX-27. Consistently, the TAT-5 ortholog ATP9A does not control endosomal trafficking of the SNX1 cargo Shiga toxin B in HeLa cells[15,22], but is required for the trafficking of the glucose transporter 1 (GLUT1)[15], which is a cargo of SNX27[23], which has no BAR domain[24,25]. In contrast, TAT-5 only regulates Wntless trafficking, which is predominantly trafficked by SNX-3[1,26], when retromer trafficking is also disrupted[3]. As SNX-3 has no BAR domain [18], this suggests that SNX-3 can still promote Wntless recycling independent of TAT-5. Thus, TAT-5 could promote membrane curvature for multiple endosomal trafficking pathways lacking BAR domain proteins, but is not likely to be an essential component of these pathways.

MON-2, PAD-1 and their mammalian orthologs are also required for the trafficking of Wntless redundantly with retromer like TAT-5[3]. These results suggest that TAT-5 could also be mediator of the MON-2 and PAD-1 trafficking pathway. Intriguingly, we saw enlarged late endosomes after loss of PAD-1, MON-2 and TAT-5 strongly suggesting a similar function during endosomal trafficking. To test whether TAT-5 could function in the same trafficking pathway as MON-2 and PAD-1, we first need to identify the cargo trafficked by the TAT-5, PAD-1 and MON-2 complex (see list of potential cargoes in 5.3.). This suggests that the endosomal tubulation function of TAT-5 could promote many endosomal trafficking pathways.

If TAT-5 flipping activity promotes the tubulation of endosomes, then TAT-5 could be required for its own trafficking. This ultimately means that the regulation of TAT-5 trafficking may be required to control protein trafficking from endosomes and that TAT-5 could regulate the trafficking of another unidentified MV release inhibitor. Thus, by examining how TAT-5 activity is regulated to control MV release, we also gained knowledge about the regulatory mechanisms of endocytic recycling.

6.4. Identifying more regulators of TAT-5 activity and microvesicle release

Our study identified a multitude of TAT-5 trafficking regulators and one potential TAT-5 activator, identifying the first set of proteins that regulate this essential flippase. However, it is likely that more TAT-5 regulators exist that have not yet been identified. Using our degron-based screening technique to identify genes that inhibit MV release, Birgit Karmann screened 133 candidate genes involved in membrane trafficking, lipid biogenesis and lipid transporters[27]. Expanding the screen could result in the identification of more TAT-5 regulators and MV release inhibitors. We would prioritize the lethal/sterile set (~1,200 genes), since all proteins we have found to inhibit MV release are lethal or sterile (discussed in chapter 3). Thus, continued screening for MV release inhibitors is likely to uncover more proteins required for TAT-5 PE flipping activity. This will ultimately help us to understand the mechanisms that control PE asymmetry and shed light on the inhibitory pathways of MV budding.

Furthermore, screening for regulators of TAT-5 trafficking could also reveal proteins involved in MV budding. For example, we readily observed TAT-5 mistrafficking phenotypes after *snx-1, snx-3,* or *snx-6* RNAi, but there was no increase in MV release until we made double mutants. Thus, screening GFP::TAT-5 localization in our original candidate set or the lethal/sterile set could reveal regulators of TAT-5 trafficking and MV release that were overlooked in the original screen. Alternatively, we could screen for increased MV release in a sensitized *snx-1, snx-3* or *mon-2* mutant background. This would allow the identification of redundant regulators of MV release.

In addition to identifying how TAT-5 is activated, identifying how TAT-5 is inactivated may open the possibility to spatiotemporally control TAT-5 activity. Furthermore, identifying new proteins that promote MV release is of great interest. However, screening for proteins that activate MV budding is technically challenging. Not many EVs were seen outside the cells of *C. elegans* embryos using EM[28], probably because of rapid uptake after their release[29,30]. One strategy to identify MV release activators would be to use double RNAi knockdown, where one RNAi depletes *pad-1* to increase MV release and the second would target a potential ectocytosis activator. If a protein activates MV release, its knockdown would lead to reduced MV budding in a *pad-1* RNAi background, as we previously observed for ESCRT subunits and RAB-11 in a *tat-5* RNAi background[28]. Thus, identifying proteins that induce MV release may reveal proteins that inhibit TAT-5 flippase activity and will help us to understand the mechanisms of MV release.

Ultimately, once we have identified the set of proteins that control TAT-5 PE flipping activity, we gain understanding of the activity regulation of this essential flippase and also identify mechanisms that inhibit or induce MV release *in vivo*. Since TAT-5 and the regulators we identified are conserved in animals[31], the knowledge that we gain about its regulation in *C. elegans* is likely to be transferable to humans. Our studies provide us with tools to visualize and experimentally control the formation of MVs not just in the worm, but also in mammals, which may allow us in the future to observe the release, fate and signaling potential of different populations of MVs in a certain tissue at a particular time.

6.5. Outlook

The increased EV release observed from the several *C. elegans* mutants is similar to the increased EV release reported from mammalian cells during several diseases[27,28,32]. For example, cancer cells have increased EV production and these EVs are enriched with cargo that function in cancer spreading and metastasis formation[33,34]. During neuroinflammation, increased amounts of EVs in the blood and cerebrospinal fluid were found in multiple sclerosis (MS) patients and these EVs are thought to be involved in spreading pro-inflammatory signals and disrupting the blood brain barrier[32,35]. However, the mechanisms that inhibit EV release from healthy cells and promote disease-related EV release are largely unclear.

Our identification of conserved disease-related genes in the inhibition of EV release can uncover the mechanisms and functions of disease-related EV budding. For example, a single mutation at a highly conserved region in the human RME-8 (Asn855Ser) was identified in familial Parkinson's disease[36], suggesting that RME-8 disruption is involved in Parkinson's pathogenesis. α-synuclein is released in EVs from neuron cell culture that causes cytotoxicity, which is proposed to be involved in pathologies of Parkinson's disease[37], but whether increased production of α-synuclein-loaded EVs have a role in Parkinson's disease pathology is still unclear. In combination with our data from *C. elegans,* we propose that the EV inhibitory function of RME-8 could have a role in pathologies of familial Parkinson. Thus, it should be tested whether more EVs are found in the spinal fluid of familial Parkinson's patients. Thus, we believe that the identified EV inhibitors in *C. elegans* will help to identify and study the function of disease-related EVs in mammals.

EVs are of broad interest to produce cell-specific vesicles to carry drugs to recipient cells[38–40]. However, robust EV production with sufficient quantities from patient cells is still a challenge[38]. We show that the knockdown of conserved EV release inhibitors like PAD-1 dramatically increases EV formation. Thus, it should be tested whether EV release is increased when PAD-1 orthologs DOPEY1 and/or DOPEY2 are depleted. If EV release is increased after DOPEY1/2 knockdown, then this strategy could be used to enhance EV release from cultured patient cells, allowing their use for biomarker studies or to create patient-matched EV-based drug delivery vehicles. Thus, our set of EV inhibitors may also help to boost EV extraction in the clinic, further emphasizing the value of basic cell biology research.

6.6. References

1. Harterink, M. *et al.* A SNX3-dependent retromer pathway mediates retrograde transport of the Wnt sorting receptor Wntless and is required for Wnt secretion. *Nat. Cell Biol.* **13**, 914–923 (2011).
2. Lorenowicz, M. J. *et al.* Inhibition of late endosomal maturation restores Wnt secretion in Caenorhabditis elegans vps-29 retromer mutants. *Cell. Signal.* **26**, 19–31 (2014).
3. McGough, I. J. *et al.* SNX3-retromer requires an evolutionary conserved MON2:DOPEY2:ATP9A complex to mediate Wntless sorting and Wnt secretion. *Nat. Commun.* **9**, 3737 (2018).
4. Cui, Y. *et al.* Retromer has a selective function in cargo sorting via endosome transport carriers. *J. Cell Biol.* **218**, 615–631 (2019).
5. Berezikov, E. Homologous gene targeting in Caenorhabditis elegans by biolistic transformation. *Nucleic Acids Res.* **32**, e40 (2004).
6. Praitis, V., Casey, E., Collar, D. & Austin, J. Creation of low-copy integrated transgenic lines in Caenorhabditis elegans. *Genetics* **157**, 1217–1226 (2001).
7. Frøkjær-Jensen, C. *et al.* Single-copy insertion of transgenes in Caenorhabditis elegans. *Nat. Genet.* **40**, 1375–1383 (2008).
8. McMahon, H. T. & Boucrot, E. Membrane curvature at a glance. *J. Cell Sci.* **128**, 1065–1070 (2015).
9. Van Meer, G., Voelker, D. R. & Feigenson, G. W. Membrane lipids: Where they are and how they behave. *Nat. Rev. Mol. Cell Biol.* **9**, 112–124 (2008).
10. Hou, S., Johnson, S. E. & Zhao, M. A One-Step Staining Probe for Phosphatidylethanolamine. *ChemBioChem* **16**, 1955–1960 (2015).
11. Iwamoto, K. *et al.* Curvature-dependent recognition of ethanolamine phospholipids by duramycin and cinnamycin. *Biophys. J.* **93**, 1608–1619 (2007).
12. Hullin-Matsuda, F., Makino, A., Murate, M. & Kobayashi, T. Probing phosphoethanolamine-containing lipids in membranes with duramycin/cinnamycin and aegerolysin proteins. *Biochimie* **130**, 81–90 (2016).
13. Emoto, K. *et al.* Redistribution of phosphatidylethanolamine at the cleavage furrow of dividing cells during cytokinesis. *Proc. Natl. Acad. Sci. U. S. A.* **93**, 12867–12872 (1996).
14. Dalton, L. E., Bean, B. D. M., Davey, M. & Conibear, E. Quantitative high-content imaging identifies novel regulators of Neo1 trafficking at endosomes. *Mol. Biol. Cell* **28**, 1539–1550 (2017).
15. Tanaka, Y. *et al.* The phospholipid flippase ATP9A is required for the recycling pathway from the endosomes to the plasma membrane. *Mol. Biol. Cell* **27**, 3883–3893 (2016).
16. Nothwehr, S. F., Roberts, C. J. & Stevens, T. H. Membrane protein retention in the yeast Golgi apparatus: dipeptidyl aminopeptidase A is retained by a cytoplasmic signal containing aromatic residues. *J. Cell Biol.* **121**, 1197–209 (1993).
17. Takada, N. *et al.* Phospholipid-flipping activity of P4- ATP ase drives membrane curvature.

EMBO J. **37**, (2018).
18. Salzer, U., Kostan, J. & Djinović-Carugo, K. Deciphering the BAR code of membrane modulators. *Cellular and Molecular Life Sciences* **74**, 2413–2438 (2017).
19. Liu, K., Hua, Z., Nepute, J. A. & Graham, T. R. Yeast P4-ATPases Drs2p and Dnf1p are essential cargos of the NPFXD/Sla1p endocytic pathway. *Mol. Biol. Cell* **18**, 487–500 (2007).
20. Furuta, N., Fujimura-Kamada, K., Saito, K., Yamamoto, T. & Tanaka, K. Endocytic Recycling in Yeast Is Regulated by Putative Phospholipid Translocases and the Ypt31p/32p–Rcy1p Pathway. *Mol. Biol. Cell* **18**, 295–312 (2007).
21. Hanamatsu, H., Fujimura-Kamada, K., Yamamoto, T., Furuta, N. & Tanaka, K. Interaction of the phospholipid flippase Drs2p with the F-box protein Rcy1p plays an important role in early endosome to trans-Golgi network vesicle transport in yeast. *J. Biochem.* **155**, 51–62 (2014).
22. Bujny, M. V., Popoff, V., Johannes, L. & Cullen, P. J. The retromer component sorting nexin-1 is required for efficient retrograde transport of Shiga toxin from early endosome to the trans Golgi network. *J. Cell Sci.* **120**, 2010–2021 (2007).
23. Steinberg, F. *et al.* A global analysis of SNX27–retromer assembly and cargo specificity reveals a function in glucose and metal ion transport. *Nat. Cell Biol.* **15**, 461–471 (2013).
24. Carlton, J., Bujny, M., Rutherford, A. & Cullen, P. Sorting nexins - Unifying trends and new perspectives. *Traffic* **6**, 75–82 (2005).
25. Liu, J.-J. Retromer-Mediated Protein Sorting and Vesicular Trafficking. *J. Genet. Genomics* **43**, 165–177 (2016).
26. Zhang, P., Wu, Y., Belenkaya, T. Y. & Lin, X. SNX3 controls Wingless/Wnt secretion through regulating retromer-dependent recycling of Wntless. *Cell Res.* **21**, 1677–1690 (2011).
27. Beer, K. B. *et al.* Extracellular vesicle budding is inhibited by redundant regulators of TAT-5 flippase localization and phospholipid asymmetry. *Proc. Natl. Acad. Sci.* **115**, E1127–E1136 (2018).
28. Wehman, A. M., Poggioli, C., Schweinsberg, P., Grant, B. D. & Nance, J. The P4-ATPase TAT-5 inhibits the budding of extracellular vesicles in C. elegans embryos. *Curr. Biol.* **21**, 1951–1959 (2011).
29. Abels, E. R. & Breakefield, X. O. Introduction to Extracellular Vesicles: Biogenesis, RNA Cargo Selection, Content, Release, and Uptake. *Cellular and Molecular Neurobiology* **36**, 301–312 (2016).
30. König, J., Frankel, E. B., Audhya, A. & Müller-Reichert, T. Membrane remodeling during embryonic abscission in *Caenorhabditis elegans*. *J. Cell Biol.* **216**, 1277–1286 (2017).
31. van der Mark, V. A., Oude Elferink, R. P. J. & Paulusma, C. C. P4 ATPases: Flippases in health and disease. *Int. J. Mol. Sci.* **14**, 7897–7922 (2013).
32. Budnik, V., Ruiz-Cañada, C. & Wendler, F. Extracellular vesicles round off communication in the nervous system. *Nat. Rev. Neurosci.* **17**, 160–172 (2016).
33. Al-Nedawi, K. *et al.* Intercellular transfer of the oncogenic receptor EGFRvIII by microvesicles derived from tumour cells. *Nat. Cell Biol.* **10**, 619–624 (2008).
34. Ciardiello, C. *et al.* Focus on extracellular vesicles: New frontiers of cell-to-cell communication in cancer. *Int. J. Mol. Sci.* **17**, 175 (2016).
35. Verderio, C. *et al.* Myeloid microvesicles are a marker and therapeutic target for neuroinflammation. *Ann. Neurol.* **72**, 610–624 (2012).
36. Vilariño-Güell, C. *et al.* DNAJC13 mutations in Parkinson disease. *Hum. Mol. Genet.* **23**, 1794–801 (2014).
37. Emmanouilidou, E. *et al.* Cell-produced α-synuclein is secreted in a calcium-dependent manner by exosomes and impacts neuronal survival. *J. Neurosci.* **30**, 6838–6851 (2010).
38. Ohno, S. I., Drummen, G. P. C. & Kuroda, M. Focus on extracellular vesicles: Development of extracellular vesicle-based therapeutic systems. *International Journal of Molecular Sciences* **17**, 172 (2016).
39. van Dommelen, S. M. *et al.* Microvesicles and exosomes: Opportunities for cell-derived membrane vesicles in drug delivery. *J. Control. Release* **161**, 635–644 (2012).
40. Lakhal, S. & Wood, M. J. A. Exosome nanotechnology: An emerging paradigm shift in drug delivery. *BioEssays* **33**, 737–741 (2011).

Abbreviations

AB	Anterior blastomere
ADAM	A disintegrin and metalloprotease
AEX	ABoc, expulsion (defecation) defective
AID	Auxin-inducible degradation
ALP	Alkaline phosphatase
AMAN	α Mannosidase
ANY	Antagonist to Neo1 in yeast
Ape	Aminopeptidase
APP	Amyloid precursor protein
ARF	Adenosine diphosphate ribosylation factor
ARL	ARF-like
ARMMs	ARRDC1-mediated microvesicles
Arp	Actin-related protein
ARRDC1	Arrestin domain-containing protein
ASB	Antibody staining buffer
ATG	Autophagy-related protein
ATP	Adenosine triphosphate
ATPase	Adenosine triphosphatase
BAR	Bin Amphiphysin Rvs
BEC	Beclin
BiP	Binding immunoglobulin protein
BSA	Bovine serum albumin
BWM	Body wall muscle
Capu	Cappuccino
Cas	CRISPR-associated
CAV	Caveolin
CD	Cell Death
CDC	Cell Division Control
cDNA	coding DNA
C. elegans	*Caenorhabditis elegans*
Cfs	CDC50 suppressor
CG	Cortical granules
CHC	Clathrin Heavy Chain
CI-MPR	Cation-Independent Mannose 6-Phosphate Receptor
COP	Coat protein complex
CPY	Carboxypeptidase Y

CRSPR	Clustered Regularly Interspaced Short Palindromic Repeats
ctrl	Control
DABCO	1,4-diazabicyclo[2.2.2]octane
DAPI	4‘,6-diamidino-2-phenylindole
DCB	Dimerizing and Cyp5 Binding
Del	Deletion
DEPC	Diethyl pyrocarbonate
DIC	Differential interference contrast
DMT	Divalent Metal Transporter
DNA	Deoxyribonucleic acid
Dnf	Drs2 Neo1 family
Dop	Dopey
DPAP A	Dipeptidyl aminopeptidase A
Drs	Deficiency in Ribosomal Structures
DTC	Distal tip cell
DYN	Dynamin
EC	Excretory Canal
ECL	Enhanced Chemiluminescence
ECM	Embryonic Culture Medium
ECS	Elongin B/C-Cul2/Cul5-SOCS-box
EDTA	Ethylenediaminetetraacetic acid
EEA	Early endosome antigen
EG	Excretory Glands
EGFP	Enhanced GFP
EGL	Egg laying defective
EGF	Epidermal Growth Factor
EGFR	Epidermal Growth Factor Receptor
EM	Electron microscopy
EMS	Endomesodermal precursor
Emb	Embryonic lethal
ER	Endoplasmic reticulum
ERM	Ezrin/Radixin/Moesin
ESCRT	Endosomal sorting complex required for transport
et al.	et alia
EV	Extracellular Vesicles
F	Filial-Generation
FB	Fibrous Bodies

FERM	Protein 4.1/Ezrin/Radixin/Moesin
FGT	Facilitated Glucose Transporter
FIM	Fluorescence intensity manager
FYVE	Fab1, YOTB, Vac1 and EEA1
Gag	Group-specific antigen
GAPDH	Glyceraldehyde 3-phosphate dehydrogenase
GDP	Guanosine diphosphate
GEF	Guanosine triphosphate exchange factor
GFP	Green Fluorescent Protein
Gga	Golgi-localized, Gamma-adaptin ear homology, Arf-binding protein
GLUT	Glucose Transporter
GPCR	G protein-coupled receptor
Grp78	78-kDa glucose-regulated protein
GTP	Guanosine triphosphate
HEPES	4-(2-hydroxyethyl)-1-piperazineethanesulfonic acid
HIV	Human immunodeficiency virus
HRS	Hepatocyte growth factor-regulated tyrosine kinase substrate
HRP	Horseradish peroxidase
HSP	Heat Shock Protein
HUS	Homology Upstream of Sec7
i.e.	id est
IHC	Immunohistochemistry
IGFR	Insulin Growth Factor Receptor
ILV	Intraluminal Vesicle
ILP	Insulin-Like Protein
Ins	Insertion
INT	Intestine
IPLA	Intracellular phospholipase A
KLC	Kinesin light chain
L	Larval stage
LEM	Ligand Effect Modulator
Let	Lethal
LMP	lysosome-associated membrane protein homolog
LST	Lateral Signaling Target
mCh	monomeric Cherry
MIG	abnormal cell migration
MO	Membranous Organelles

MON	Monensin sensitivity
Mrh	Membrane protein related to Hsp30p
mRNA	Messenger RNA
MosSci	mos1-mediated single copy insertion
MS	Multiple Sclerosis
MV	Microvesicle
MVB	Multivesicular Body
MVB-12	multivesicular body sorting factor 12
Nat. Commun.	Nature Communications
N	Number
NEB	New England Biolabs
Neo	Neomycin-resistance
NGM	Normal growth media
NMY	Non-muscular Myosin
NR	Nerve Ring
P	Posterior cell
PA	Phosphatidic acid
PAA	Polyacrylamide
PAD	Patterning defective
PBS	Phosphate-buffered saline
PC	Phosphatidylcholine
PCR	Polymerase Chain Reaction
PDZ	post synaptic density protein (PSD95), Drosophila disc large tumor suppressor (Dlg1), and zonula occludens-1 protein (zo-1)
PE	Phosphatidylethanolamine
PH	Plekstrin Homology
PI	Phosphoinositide
PI3K	Phosphatidylinositol-three-Kinase
PIxP	Phosphatidylinositol-x-Phosphate
$PIxP_2$	Phosphatidylinositol-x-bisphosphate
PIP2	Phosphoinositide-bisphosphate
PIPES	Piperazine-N,N′-bis(2-ethanesulfonic acid)
PIE	Pharynx and intestine in excess
PL	Phospholipid
PLA	Phospholipase A
PLC	Phospholipase C
PM	Plasma membrane

PNAS	Proceedings of the National Academy of Sciences
PS	Phosphatidylserine
PX	Phox
RAB	Ras-related in brain
RAL	Ras-related GTPase homolog
RME	Receptor-mediated Endocytosis
RNA	Ribonucleic acid
RNAi	Ribonucleic acid interference
RUSH	Retention using selective hooks
S. cerevisiae	*Saccharomyces cerevisiae*
SCRM	Scramblase
SDS	Sodium Dodecyl Sulfate
S.E.M.	Standard Error of the Mean
sgRNA	single guide RNA
SH	Src homology
SLC	Soluble carrier
SM	Sphingomyelin
aSMase	acid Sphingomyelinase
nSMase	neutral Sphingomyelinase
SNARE	Soluble N-ethylmaleimide-sensitive factor attachment receptor
Snc	Synaptobrevin homolog
SNX	Sorting nexin
SOCS	Suppressor of cytokine signaling
SP	Signal peptidase
Spir	Spire
SQV	Squashed vulva
Sso	Supressor of Sec One
Ste	Sterile
SYX	Syntaxin
TAT	Transbilayer amphipath transporters
TBS	Tris-buffered saline
TBST	Tris-buffer saline with Tween20
TEM	Transmission electron microscopy
Tfn	Transferrin
TGN	Trans golgi network
TIR	Transport inhibitor response
Tlc	Telomerase component

Tlg	T-snare affecting a Late Golgi compartment
TM	Transmembrane
TSG	Tumor susceptibility gene
UNC	Uncoordinated
UVRAG	Ultraviolet radiation resistance-associated gene protein
V-ATPase	Vacuolar-type H^+ ATPase
VAMP	Vesicle-associated membrane protein
VF	Vacuole Formation
VPS	Vacuolar protein sorting
WASH	Wiskott-Aldrich syndrome protein homolog to SCAR
WASP	Wiskott-Aldrich syndrome protein
WNT	Wingless-related integration site
WT	Wild type
XKR	XK-related protein
YPT	Yeast protein two
YSL	*ypt-51* synthetic lethal
ZF	Zinc finger
ZIF	Zinc finger-interacting protein

Acknowledgements

Many people contributed to this thesis, to whom I would like to express my deepest gratitude:

First of all, I want to thank my supervisor Dr. Ann Wehman, who gave me the opportunity to do this thesis in her lab and who taught me everything I needed to know to come this far. I thank her for her constant encouragement and support and for all the valuable scientific inputs. I very much appreciated that she encouraged me to present my work at so many conferences. Special thanks also go to her for critically proof reading this manuscript.

I also thank my thesis committee team Prof. Dr. Antje Gohla and Dr. Eric Lambie for their great support and discussions, which helped me to successfully finish my thesis.

Many thanks go to the whole team of the Wehman lab. I thank Dr. Ahmad Fazeli for all his helpful scientific advises and for proof reading my thesis. I also thank our former and excellent technicians Theresa Henninger and Anne Haberberger for their great help in the lab. I absolutely enjoyed working with you the past years.

During the time of my thesis, I was lucky to work with many talented students. I especially thank the interns Kenneth Kuhn, Jennifer Rivas-Castillo, Alida Melse and Jona Causemann who helped significantly to collect the data for my papers and this thesis.

I also thank all the other students who have ever been to the Wehman lab for creating such a warm and productive atmosphere and that they spiced up every day, tuning these years to an unforgettable experience.

I thank my friends for being my all-time cheerleaders and for reminding me of what is really important. I especially thank Felix for proof reading.

My deepest gratitude goes to Martin who always encourages me to go on and for knowing when it is time to remind me about life beyond lab.

In the end, I want to gratefully thank my family who blessed me with love and always believed in me and supported me ever since.

Curriculum Vitae

Katharina Beate Beer
Born 07.05.1988 in Greiz, Germany

Education

Since 11/2014	PhD thesis “Identification and Characterization of TAT-5 regulators that control Microvesicle budding”. Primary Supervisor: Dr. Ann M. Wehman, Graduate School of Life Sciences (GSLS), University of Würzburg
2011 – 2013	Master of Science in *Diversity and Evolution* “Functional analysis of FGF-pathway genes in *Tribolium castaneum”*. Supervisor: Prof. Dr. Reinhard Schröder, University of Rostock
2008 – 2011	Bachelor of Science in *Biological Sciences* “Temperature effects on growth of an arctic diatom after incubation in the dark”. Supervisor: PD Dr. Rhena Schuman, University of Rostock
1998 – 2007	Abitur. Integrierte Gesamtschule (IGS) „Grete Unrein“ in Jena

Awards

2018	Talk award at the Rudolf-Virchow-Center Retreat; Bad Brückenau, Germany
	Travel grant from the GSLS for the International Meeting of the German Society for Cell Biology (DGZ) in Leipzig, Germany
2017	Best poster prize at the “FEBS-EMBO Advanced Lecture Course: Molecular Architecture, Dynamics and Function of Bio membranes”; Cargése, France
2016	Outstanding Abstract Award for exceptional research presented at the 5th annual meeting of the International Society of Extracellular Vesicles (ISEV) in Rotterdam, Netherlands
2015	Travel grant from the GSLS for the 20th International *C. elegans* Meeting in Los Angeles, USA

Presentations

2018	K. B. Beer, Wehman A. M. “How to find the needle in the hay-stack: Degron-tagging to label membrane-wrapped structures” **Talk Award:** Rudolf-Virchow-Center Retreat; Bad Brückenau, Germany

K. B. Beer, Wehman A. M.
"Retrograde trafficking proteins control lipid flippase activity to inhibit Extracellular vesicle budding"
Talk: International Meeting of the German Society for Cell Biology (DGZ); Leipzig, Germany

K. B. Beer, Fazeli G., Nance J.F., Stigloher C., Wehman A. M.
"Retromer-associated proteins and PAD-1 control TAT-5 flippase activity to inhibit extracellular vesicle budding"
Poster: 77th Annual Meeting of the Society for Developmental Biology; Portland, USA

2017 K. B. Beer, Wehman A. M.
"Retromer-associated proteins and PAD-1 control TAT-5 to inhibit microvesicle budding"
Talk: Rudolf-Virchow-Center Retreat; Bad Brückenau, Germany

K. B. Beer, Rivas-Castillo J., Kuhn K., Fazeli G., Nance J.F., Stigloher C., Wehman A. M.
"PAD-1 activates TAT-5 to prevent extracellular vesicle release in *C. elegans* embryos"
Poster: EMBO/EMBL Symposium: Molecular and Cell Biology of Membranes, Heidelberg

K. B. Beer, Rivas-Castillo J., Kuhn K., Fazeli G., Nance J.F., Stigloher C., Wehman A. M.
"Retromer and PAD-1 regulate TAT-5 activity to inhibit membrane budding"
Poster and Award Talk: FEBS-EMBO Advanced Lecture Course: Molecular Architecture, Dynamics and Function of Biomembranes"; Cargése, France

2016 K. B. Beer, Stigloher C., Wehman A. M.
"PAD-1 activates TAT-5 to prevent Extracellular Vesicle release in *C. elegans* embryos"
Award and Talk: 5th Annual ISEV Meeting; Rotterdam, Netherlands
Poster: European Worm Meeting; Berlin, Germany

K. B. Beer, Wehman A. M.
"Regulation of a lipid flippase to prevent extracellular vesicle release in *C. elegans*"
Talk: 11th International GSLS Student Symposium "EUREKA!"; Würzburg, Germany

K. B. Beer, Stigloher C., Wehman A. M.
"PAD-1 prevents extracellular vesicle budding in *C. elegans* embryos"
Poster: 13th International PhD Student Symposium "Horizons in Molecular Biology"; Göttingen, Germany

2015 K. B. Beer, Stigloher C., Wehman A. M.
"PAD-1 prevents extracellular vesicle budding in *C. elegans* embryos"
Talk: Rudolf-Virchow-Center Retreat; Bad Staffelstein, Germany
Poster: 10th International GSLS Student Symposium "EUREKA!"; Würzburg, Germany
Poster: 20th International *C. elegans* Meeting; Los Angeles, USA
Poster: International Meeting of the DGZ; Köln, Germany

Publication List

K. B. Beer, Fazeli G., Judasova K., Irmisch L., Causemann J., Mansfeld J., Wehman A. M.: Degron-tagged reporters probe membrane topology and enable the specific labelling of membrane-wrapped structures. (2019) **Nature Communications**, 10(1):3490

K. B. Beer, Rivas-Castillo J., Kuhn K., Fazeli G., Karmann B., Nance J. F., Stigloher C., Wehman A. M.:
Extracellular vesicle budding is inhibited by redundant regulators of TAT-5 flippase localization and phospholipid asymmetry. (2018) **PNAS**.115(6):E1127-E1136.

K. B. Beer, Wehman A. M.:
Mechanisms and functions of extracellular vesicle release *in vivo* – What we can learn from flies and worms. (2017) **Cell Adhesion and Migration**, 11(2):135-150

Sharma R., K. Beer, Iwanov K., Schmöhl F., Beckmann P. I., Schröder R.:
The single *fgf* receptor gene in the beetle *Tribolium castaneum* codes for two isoforms that integrate FGF8- and Branchless-dependent signals. (2015) **Developmental Biology**, 402(2):264-275

Date, Place Signature

Affidavit

I hereby confirm that my thesis entitled "Identification and characterization of TAT-5 interactors that regulate extracellular vesicle budding" is the result of my own work. I did not receive any help or support from commercial consultants. All sources and / or materials applied are listed and specified in the thesis.

Furthermore, I confirm that this thesis has not yet been submitted as part of another examination process neither in identical nor in similar form.

Place, Date Signature

Eidesstattliche Erklärung

Hiermit erkläre ich an Eides statt, die Dissertation "Identifizierung und Charakterisierung von TAT-5 Interaktoren, welche die Ausschüttung von Extrazellulären Vesikeln regulieren" eigenständig, d.h. insbesondere selbständig und ohne Hilfe eines kommerziellen Promotionsberaters, angefertigt und keine anderen als die von mir angegebenen Quellen und Hilfsmittel verwendet zu haben.

Ich erkläre außerdem, dass die Dissertation weder in gleicher noch in ähnlicher Form bereits in einem anderen Prüfungsverfahren vorgelegen hat.

Ort, Datum Unterschrift